Swansea University
Prifysgol Abertawe

Nonlinear Model Updating in Structural Dynamics

This dissertation is submitted
in fulfilment of the requirement for the degree of
Doctor of Philosophy

Javad Taghipour

Supervisors:
Prof. Hamed Haddad Khodaparast
Prof. Michael I. Friswell

Faculty of Science and Engineering
Swansea University

College of Engineering

October 2021

To my lovely wife, Azam

and

my beloved parents

Abstract

Identification of nonlinear structural dynamics has received a significant attention during last decades. Yet, there are many aspects of the identification methods of nonlinear structural models to be improved. The main objective of this study is to introduce novel identification approaches for nonlinear structures. The first step in identifying nonlinear structural elements is to detect their exact location. Hence, the first section of this study focuses on the localization of nonlinear elements in structural dynamics utilizing base excitation measured data. To this end, a localization approach is used to find the location of nonlinear electromagnetic restoring force applied to the tip of a cantilever beam.

Inferring the exact location of nonlinear elements, identification methods are utilized to identify and characterize the mathematical model of nonlinear structures. However, various sources of noise and error may affect the accuracy of the identified model. Therefore, in the second part of the thesis, the effect of various sources of inaccuracy on the results of nonlinear model identification is investigated. It is shown that measurement noise, expansion error, modelling error, and neglecting the effect of higher harmonics may lead to an erroneously identified model.

An optimization-based framework for the identification of nonlinear systems is proposed in this work in order to avoid the bottlenecks mentioned above. The introduced method is applied to a test rig composed of a base-excited cantilever beam subjected to an electromagnetic force at the tip. According to the nonlinear response of the system, four different functions are assumed as candidate models for the unknown nonlinear electromagnetic force. The measured response is compared with the reconstructed response using various models and the most appropriate mathematical model is selected.

Utilizing optimization-based identification method to characterize complex mathematical models with large number of unknown parameters would be computationally expensive. Therefore, this study introduces a harmonic-balance-based parameter estimation method for the identification of nonlinear structures in the presence of multi-harmonic response and force. For this purpose, a method with two different approaches are introduced: Analytical Harmonic-Balance-based (AHB) approach and the Alternating Frequency/Time approach using Harmonic Balance (AFTHB). The method is applied to five simulated examples of nonlinear systems to highlight different features of the method. The method can be applied to all forms of both smooth and non-smooth nonlinear functions. The computational cost is relatively low since a dictionary of candidate basis functions is avoided. The results illustrate that

neglecting higher harmonics, particularly in systems with multi-harmonic response and force, may lead to an inaccurate identified model. The AFTHB approach benefits from including significant harmonics of the response and force. Applying this method leads to accurate algebraic equations for each harmonic, including the effect of higher harmonics without truncated error. In the last part of this study, the AFTHB method is applied to two experimental case studies and identifies the nonlinear mathematical model of the structures. The first case is composed of a cantilever beam with a nonlinear electromagnetic restoring force applied to the tip which is excited by a multi-harmonic external force. In the second experimental case study, a configuration of linear springs applies a geometric nonlinear restoring force to the tip of a cantilever beam resulting in internal resonance in the dynamics of the system. The good performance of the AFTHB approach in estimating the unknown parameters of the structure is illustrated by the results of identification.

Keywords: Structural Dynamics, Nonlinear Model updating, Measurement Noise, Modelling Error, Optimization, System Identification, Harmonic Balance Method

If you DON'T have a bar on access, include the declarations below

Declarations

This work has not previously been accepted in substance for any degree and is not being concurrently submitted in candidature for any degree.

Signed..... [redacted] .....

Date.....02/08/2021.....

This thesis is the result of my own investigations, except where otherwise stated. Other sources are acknowledged by footnotes giving explicit references. A bibliography is appended.

Signed..... [redacted] .....

Date.....02/08/2021.....

I hereby give consent for my thesis, if accepted, to be available for photocopying and for inter-library loan, and for the title and summary to be made available to outside organisations.

Signed..... [redacted] .....

Date.....02/08/2021.....

The University's ethical procedures have been followed and, where appropriate, that ethical approval has been granted.

Signed..... [redacted] .....

Date.....02/08/2021.....

Table of contents

Acknowledgements

First of all, I am sincerely thankful to my first supervisor, Prof. Hamed Haddad Khodaparast whose support and encouragement has been invaluable throughout this study. It would be out of my reach to complete my study without his deep knowledge, extensive experience and thoughtful guidance in the past few years. I cannot be grateful enough to him for all his personal supports and friendly relationship that made my PhD life an incredible experience.

My deepest gratitude goes to my second supervisor Prof. Michael I. Friswell for the continuous support and his patience, motivation, and immense knowledge. His guidance helped me in all the time of research and writing of this thesis. His advices and recommendation in the meetings and conversations were vital in inspiring me to think outside the box and form comprehensive perspectives towards engineering problems.

I would like to thank Dr Hassan Jalali for his great advices and involvement in my work. I am also in debt with Dr Alex Shaw for his technical support during my PhD. His immense knowledge and experience in experimental studies was a great help to me. Also, I would like to thank Dr Xing Wang for his valuable advice regarding my research.

I would like to say a special thank you to my friends and colleagues that have made my study and life in Swansea a wonderful time. To Dr Hadi Madinei who gave his continuous invaluable supports to me since the very first day of my life in Swansea. To Dr Nidhal Jamia for all the fun and challenge we had with the experiments in the lab. To Dr Sajad Kiani, Dr German Martinez-Ayuso, Dr Farzad Mohebbi, Dr Darren Williams, Dr Sanjay Komala Sheshachala, Kensley Balla, Dr Chen Wang, Dr Huaiyuan Gu, Dr Jiaying Zhang, Dr Davide Balatti, Dr Kayalvizhi Lakshmanan, and Dr Tanmoy Chatterjee for all their help and friendship.

In the most important place, I am extremely grateful to my wonderful wife, Azam, who has patiently supported and encouraged me throughout my study. Words cannot express my gratitude to my supportive parents and my dearest brothers who were there for me every time I needed.

I really appreciate the financial support from the College of Engineering at Swansea University through the PhD scholarship in support of EPSRC project EP/P01271X/1.

List of figures

List of tables

Chapter 1

Background

1.1 Introduction

In this chapter, a brief theoretical background and a brief explanation of Finite element method (FEM) and modal analysis are provided. Then, System Equivalent Reduction-Expansion Process (SEREP) and Craig-Bampton reduction/expansion methods are described in detail. Modified complex averaging (MCXA) technique and harmonic balance method (HBM) are also described in this chapter.

1.2 Finite Element Method

There are various methods for investigating the behaviour of the mechanical structures. One of the most popular and useful methods used to study the behaviour of different engineering structures is the finite element method (FEM), ([1]-[3]). The finite element method is a numerical approach used to find approximate solutions of various engineering problems by discretising the continuous structures into simple finite sub-regions (elements). These elements are shaped by some selected points (Nodes) which are connected to each other by lines or surfaces, depending on the dimension of sub-region. These elements can take any geometric shape which gives the possibility of computing the approximate behaviour of the structure at each node in relation with other nodal points. Each element is described using shape functions depending on the dimensions (geometry of the structure) and the number of degrees of freedom of the element and the accuracy of the approximation. The finite element method requires the following conditions of continuous solution over each element, the continuity of the solution and forces of adjacent elements to be satisfied. Given the geometry of the elements and selecting the proper shape functions, the matrix form of the governing equations of each element is obtained using the appropriate theory. Then, the global matrix equation of the structure is obtained by assembling

the matrix equation of individual elements. Solving the global matrix equation of the system gives the approximate solution to study the static/dynamic behaviour of the system.

Although the finite element modelling of a structure is a widespread method to investigate the behaviour of engineering structures, there are several sources of inaccuracy leading to error in the results obtained from finite element models. These sources of error can be categorised into three categories:

- The FE-based errors come from the finite element method,
- The errors come from applying the numerical methods to solve the equations
- The uncertainty-based errors.

The FE-based errors are the inevitable inaccuracies due to the approximations of discretising the continuous structures into the finite sub-regions. These errors can be reduced by improving the mesh quality of the elements and selecting the appropriate element shape functions.
Different numerical methods are used to solve the finite element equations. Numerical methods are based on approximations and normally produce some level of inaccuracies due to various numerical operations such as truncation, integration, and accumulated round-off error. More details can be found in [4].

The second category includes the errors come from the uncertainties either in the model of the structure (e.g. uncertainty in the modelling of the mechanical joints) or in the parameters of the model (e.g. variabilities in the material properties). The inaccuracies resulted from the uncertainties of the structure parameters can be reduced by utilizing experimental data along with various model updating methods.

1.3 Modal Parameters

Every individual structure is defined using its intrinsic characteristics called Modal Parameters. Determining the modal parameters of a structure is the first step in mathematical modelling of the dynamics of the structure. These parameters include:

- *Natural frequency* or resonant frequency is a characteristic of a structure that shows the frequency (or frequencies) at which a structure tends to oscillate. If a structure is excited by a force near its natural frequency, the amplitude of vibration of the structure is resonated and the phenomenon is called *resonance*.
- *Damping ratio* determines how the transient (free) vibration of a structure is mitigated. The mechanisms of the structural damping are not precisely recognized. Besides, the level of damping ratio of engineering structures is usually very low. Hence, identifying its exact value is more difficult than natural frequencies.

- *Mode shape* defines the geometric shape of the structure in free vibration at its natural frequencies.

The process during which the modal parameters are identified is called Modal Analysis. There are two different types of modal analysis: theoretical modal analysis and experimental modal analysis. Experimental modal analysis is described in Section 1.5. Here, it is briefly described how to find the modal parameters through the theoretical modal analysis. Finding the modal parameters of an undamped system is different from a damped system.

Undamped system - A simple mass-spring multi-degree-of-freedom system is considered. The governing equation in matrix form is given by the following equation.

$$\mathbf{M}\ddot{\mathbf{x}} + \mathbf{K}\mathbf{x} = \mathbf{f}(t) \tag{1.1}$$

where $\mathbf{M}$ and $\mathbf{K}$ denote the mass and stiffness matrices, respectively, and $\mathbf{f}(t)$ is the force vector applying to the structure. Considering the undamped free vibration of the structure and assuming a harmonic response for the structure in the form

$$\mathbf{x}(t) = \mathbf{X}e^{j\omega t}, \quad j = \sqrt{-1}, \tag{1.2}$$

the structural eigenproblem is written as

$$\mathbf{K}\phi_i = \lambda_i \mathbf{M}\phi_i, \quad \lambda_i = \omega_i^2, \tag{1.3}$$

where λ_i and ϕ_i denote the eigenvalue and the eigenvector of the ith mode of the system, respectively. ω_i is the ith natural frequency of the system. The eigenparameters are defined by solving the eigenproblem of Eq. (1.3). Using the mass and stiffness matrices, the undamped eigenvalues and accordingly the undamped natural frequencies of the structure are defined,

$$\det\left|\mathbf{K} - \lambda_i \mathbf{M}\right| = 0, \tag{1.4}$$

Then, using the eigenvalues obtained from Eq. (1.4), the eigenvectors (mode shapes) of the structure can be found by solving the eigenproblem of Eq. (1.3). Having the eigenvectors, and using the orthogonality of the eigenvectors with respect to mass gives the following equation,

$$\mathbf{\Phi}^T\mathbf{M}\mathbf{\Phi} = \mathbf{I}, \quad \mathbf{\Phi}^T\mathbf{K}\mathbf{\Phi} = \mathbf{\Lambda} = \mathbf{diag}\left[\omega^2\right], \tag{1.5}$$

where $\mathbf{I}$ denotes the identity matrix, $\mathbf{\Lambda}$ is a diagonal matrix including the eigenvalues (squared natural frequencies) of the structure, and $\mathbf{\Phi}$ represents the matrix of eigenvectors. There are a multitude of built-in functions in different software which are able to find the modal parameters of the structures

using their mass, damping, and stiffness matrices. Defining the physical coordinates of the structure as a multiplication of mode shapes $\mathbf{\Phi}$ and the generalized coordinates $\mathbf{q}$

$$\mathbf{x} = \mathbf{\Phi q}, \tag{1.6}$$

and premultiplying Eq. (1.1) by $\mathbf{\Phi}^T$, the undamped equation of motion of the system can be decoupled as

$$\mathbf{I}\ddot{\mathbf{q}} + \mathbf{\Lambda q} = \mathbf{\Phi}^T\mathbf{f}(t), \tag{1.7}$$

By this, a complex multi-degree-of-freedom system is simplified to a number of single-degree-of-freedom systems.

Damped Systems - Identifying the modal damping of engineering structures is more complicated. The equation of motion of a damped structure is written as

$$\mathbf{M}\ddot{\mathbf{x}} + \mathbf{C}\dot{\mathbf{x}} + \mathbf{K}\mathbf{x} = \mathbf{f}(t) \tag{1.8}$$

where $\mathbf{C}$ denotes the damping matrix. In general, damping of a system can be categorized into two classes: proportional damping and non-proportional damping. The proportional damping is a special case of the general damping expression which is valid under certain conditions, [5]. Using Eq. (1.6) and premultiplying Eq. (1.8) $\mathbf{\Phi}^T$, the damped equation of motion is rewritten as

$$\mathbf{I}\ddot{\mathbf{q}} + \mathbf{\Phi}^T\mathbf{C}\mathbf{\Phi}\dot{\mathbf{q}} + \mathbf{\Lambda q} = \mathbf{\Phi}^T\mathbf{f}(t). \tag{1.9}$$

If $\mathbf{\Phi}^T\mathbf{C}\mathbf{\Phi}$ results in a diagonal matrix, the damping of the system can be assumed as a linear combination of mass and stiffness of the system, or one of them. This type of damping is called *Rayleigh damping* or *proportional damping* and is defined as

$$\mathbf{C} = \alpha\mathbf{M} + \beta\mathbf{K}, \tag{1.10}$$

where α and β are the real scalar coefficients of the proportional damping. Substituting the proportional damping of Eq. (1.10) into Eq. (1.8), the governing equation of the system will be treated similar to an undamped system. Then, the modal parameters are defined in a similar manner. In this case, the damping ratios of the system is obtained as, Friswell and Mottershead [6],

$$\zeta_i = \frac{\alpha}{2\omega_i} + \frac{\beta\omega_i}{2}, \tag{1.11}$$

$\mathbf{\Gamma} = \mathbf{\Phi}^T\mathbf{C}\mathbf{\Phi}$ is a diagonal matrix containing the damping ratios of Eq. (1.11). More details on different types of proportional damping can be found in [7].

It is shown by experimental analysis (e.g. [8]) that many of the real-life structures possess complex modes and do not satisfy the criterion for the proportional damping assumption. The damping for such structures is *non-proportional damping*. Indeed, if $\mathbf{\Phi}^T\mathbf{C}\mathbf{\Phi}$ is not diagonal, the mode shapes of the structure will acquire complex values instead of real values. Therefore, the damping of the system is not of the type of proportional damping. Adhikari [9] introduced an index for non-proportionality of damping based on a specific normalization of the complex mode shapes. In case of the structures with non-proportional damping, the natural frequencies and mode shapes of the system are obtained from the modal analysis of the undamped system. The reader is referred to Friswell and Mottershead [6] and Ewins [10] for more details on theoretical and experimental modal analysis.

1.4 Frequency Response Function

There are various ways of illustrating the dynamic behaviour of a mechanical structure. One way is to show the behaviour of the system using a transfer function as the ratio of the response of the system to the input in the frequency domain. This ratio is called the Frequency Response Function (FRF) which is obtained using the Fourier transforms of the input and output of a dynamic system. For a dynamical system defined using a linear mathematical equation of motion, the FRF can be calculated exploiting the mass, damping, and stiffness matrices. For example, the following governing equation is given for the case of a general linear system subjected to a harmonic external force.

$$\mathbf{M}\ddot{\mathbf{x}} + \mathbf{C}\dot{\mathbf{x}} + \mathbf{K}\mathbf{x} = \mathbf{F}e^{j\omega t} \tag{1.12}$$

A harmonic response is assumed for this system as

$$\mathbf{x}(t) = \mathbf{X}e^{j\omega t}, \tag{1.13}$$

Substituting the assumed response function of Eq. (1.13) into Eq. (1.12), and balancing the coefficients of $e^{j\omega t}$ on both sides of the equation, the equation of motion of the system is obtained in the frequency domain.

$$\left(-\mathbf{M}\omega^2 + j\omega\mathbf{C} + \mathbf{K}\right)\mathbf{X} = \mathbf{F}, \tag{1.14}$$

where $\mathbf{X}$ and $\mathbf{F}$ denote the complex amplitude of the displacement and force, respectively. For a single-degree-of-freedom system, FRF is defined as the ratio of the response amplitude to the force amplitude. However, for a multi-degree-of-freedom system the FRF is not calculated simply as the ratio

between $\mathbf{X}(\omega)$ and $\mathbf{F}(\omega)$. The FRF for such system is defined as

$$\mathbf{H}(\omega) = \mathbf{B}^{-1}(\omega) = \left(-\mathbf{M}\omega^2 + j\omega\mathbf{C} + \mathbf{K}\right)^{-1}, \tag{1.15}$$

where $\mathbf{B}(\omega)$ is defined as dynamic stiffness of the system. In practical cases, usually the exact model of the system is not available, particularly in the early stages of the design of a structure. Therefore, it is required to obtain the FRFs of the structure using the experimental measurements. Unfortunately, calculating the FRFs using the input and output signals is not as straightforward as Eq. (1.15). In other words, the FRFs of a dynamical system are not obtained by simply dividing the Fast Fourier Transform (FFT) of the response and force signals. Indeed, the FRFs of the dynamical systems are calculated using auto-spectral densities and cross-spectral densities, Friswell and Mottershead [6]. There are two estimators to find the FRF of a system: H1 estimator and H2 estimator, [6].

$$\begin{aligned} H_{ij}(\omega) &= \frac{S_{xf_{ij}}(\omega)}{S_{ff_{jj}}(\omega)}, \quad \text{H1 estimator} \\ H_{ij}(\omega) &= \frac{S_{xx_{ii}}(\omega)}{S_{fx_{ji}}(\omega)}, \quad \text{H2 estimator} \end{aligned} \tag{1.16}$$

where H_{ij} denotes the transfer function of the i^{th} row and j^{th} column of the FRF matrix. $S_{xx_{ii}}$ and $S_{ff_{jj}}$ are the auto-spectral densities of the response and force signals, respectively, obtained as

$$S_{xx_{ii}} = X_i(\omega)\bar{X}_i(\omega), \quad S_{ff_{jj}} = F_j(\omega)\bar{F}_j(\omega), \tag{1.17}$$

where $X_i(\omega)$ and $F_j(\omega)$ are the FFTs of the time domain signals of the measured/simulated response and force, respectively at DoFs i and j. The overbar sign denotes their complex conjugates. The cross-spectral densities of the response and force signals are defined respectively as

$$S_{xf_{ij}} = X_i(\omega)\bar{F}_j(\omega), \quad S_{fx_{ji}} = F_j(\omega)\bar{X}_i(\omega), \tag{1.18}$$

Selecting one of these estimators depends on whether the objective is to reduce the effect of the noise from the input or output signal. If it is aimed to minimize the effect of noise in the input (force) signal, the H2 estimator is used to find the FRF. On the other hand, in case of noisy response, the H1 estimator is used to reduce the effect of noise in the calculated FRF. If both input and output signals are clear of any noise, there will not be any difference between the results of the two estimators. In addition, to minimize the effect of noise in practical cases, the measurements obtained from several tests are used to average the spectral densities. In case of using only one measurement, without any averaging, the two estimators will give the same FRFs.

In the experimental studies, the response of the system is usually measured in terms of acceleration. However, having the response in one form of acceleration, velocity, or displacement, the other forms of the response can be simply calculated. For example, the displacement of the system is obtained by dividing the acceleration signal by $-\omega^2$. There are different types of FRFs depending on the type of the measured response used for calculating the FRFs. The FRFs obtained using the measured acceleration signal is called Inertance (or Accelerance). Using the measured velocity signals gives the FRFs as Mobility of the system. If the displacement signal is used to find the FRFs of a dynamical system, it is referred to as system Receptance (or Admittance).

1.5 Experimental Modal Analysis

One way to introduce the dynamics of a structure is to describe it using its modal characteristics. The natural frequency, damping ratio, and mode shape are the modal parameters giving the fundamental information about the mechanical structures. The process during which these characteristics are identified is called modal analysis in the technical literature ([6],-[10]-[12]). The theoretical modal analysis identifies the modal parameters of the structures using the model obtained from prior-knowledge of the structure and its material properties. As there are various sources of error in modelling the structures, the theoretical modal analysis is usually inaccurate and there is a gap between the resultant modal parameters and actual ones. On the other hand, experimental modal analysis estimates the modal characteristics of a structure using vibration tests.

Depending on the number of excitation and measurement points, there are usually three types of modal tests: single-input single-output (SISO), single-input multi-output (SIMO), and multi-input multi-output (MIMO). To perform modal analysis on a structure, usually SISO and SIMO tests are used. However, the following advantages can be gained by a MIMO test, [13]:

- to distribute the energy more evenly over the structure
- to excite more modes of interest in a desired frequency range
- to avoid inconsistencies in the measured FRFs due to moving the force transducers and accelerometers to the required locations
- to have more consistent time invariant data set and minimize the effect of noise and nonlinear issues.

Depending on whether the measured experimental data is in the time or frequency domain, there are various methods in the literature that can be used to analyse the test data to derive the modal parameters [12]. The methods working with time-domain experimental data include, but are not limited

to, the Least-Squares Complex Exponential method (LSCE) [14], the Ibrahim Time Domain method (ITD) [15, 16], the Stochastic Subspace Identification method (SSI) [17], the Eigen System Realisation Algorithm (ERA) [18], and the Polyreference Complex Exponential method (PRCE) [19, 20]. The first three methods are for the SIMO modal analysis, while the last two methods work for MIMO tests. Indeed, PRCE is an extension of the LSCE to MIMO applications. Least-Squares Frequency Domain method (LSFD) [14], the Global Rational Fraction Polynomial method (GRFP) [21, 22], and the Identification of Structural System Parameters method (ISSPA) [23] are some of the methods introduced for the case of modal analysis using frequency domain test data.

However there is no unique correct way to carry out vibration testing for modal analysis, doing these types of tests requires various considerations to be taken. There are extensive explanations on different aspects of the modal vibration tests. Regarding the test set-up, care should be taken of the support of the structure, as well as the support of the excitation system (shaker) and the attachment of the excitation system to the structure (e.g. stinger bolted to the structure). The support of the structure should be defined so that it does not adversely affect the properties of the structure. Most importantly, the structure support should be defined so that the installation and experimental measurement is repeatable. Although the support of the excitation system is not as important as the support of the structure, the ground transmission between the excitation systems should be avoided. Shaker is attached to the structure using a slender rod referred to as stinger. The length and the diameter (thickness) of the stinger should be selected carefully regarding the structure under test and the type of vibration test to avoid additional constraint on the structure. As well as the support of the structure and the shaker, the attachment of the shaker to the structure should keep the restraint on the structure at the minimum possible level.

There are various excitation methods for modal testing. In terms of the excitation mechanism used for the test, these methods can be categorized into two parts: the impact excitation via a hammer; and excitation using a shaker via a stinger. The selection of the appropriate excitation method depends on different factors such as the structure under test, the boundary conditions, the purpose of the test, and the level of excitation.

The measurement of the vibration test is carried out by force and response sensors. The measured data is then converted to the desired format in the time or frequency domain using the data acquisition system. There are various types of force transducers and response (acceleration, velocity, or displacement) sensors which can be selected regarding the type of the structure, the purpose of the test, and the sensitivity level required for the test. There are also different data acquisition systems that can be used for vibration tests.

1.6 Reduction-Expansion Methods

In practice, it is almost impossible to measure all the coordinates of mechanical structures. It can be due to difficult access to some parts of the structure or because of insufficient measuring equipment. Hence, some degrees of freedom remain unmeasured. In this case, there are two possible options to deal with the spatially incomplete measurements. The first option is to project the unmeasured coordinates onto the measured DOFs and use a reduced order model (Reduction). The second one is to use the measured responses to estimate the response at the unmeasured coordinates (Expansion). In the first case, the model is truncated, and in the later one, the measurement is expanded to all degrees of freedom of the structure.

1.6.1 System Equivalent Reduction-Expansion Process (SEREP)

One of the most useful methods to reduce or expand finite element models is the System Equivalent Reduction-Expansion Process (SEREP), [24, 25]. The equation of motion of the system is considered as in the form of Eq. (1.8). It is assumed that the system has total p degrees of freedom of which m DOFs are measured and the remaining $u = p - m$ coordinates are unmeasured. Separating the measured and unmeasured coordinates and rearranging the equation of motion, Eq. (1.8), gives

$$\begin{bmatrix} \mathbf{M}_{mm} & \mathbf{M}_{mu} \\ \mathbf{M}_{um} & \mathbf{M}_{uu} \end{bmatrix} \begin{Bmatrix} \ddot{\mathbf{x}}_m \\ \ddot{\mathbf{x}}_u \end{Bmatrix} + \begin{bmatrix} \mathbf{C}_{mm} & \mathbf{C}_{mu} \\ \mathbf{C}_{um} & \mathbf{C}_{uu} \end{bmatrix} \begin{Bmatrix} \dot{\mathbf{x}}_m \\ \dot{\mathbf{x}}_u \end{Bmatrix} + \begin{bmatrix} \mathbf{K}_{mm} & \mathbf{K}_{mu} \\ \mathbf{K}_{um} & \mathbf{K}_{uu} \end{bmatrix} \begin{Bmatrix} \mathbf{x}_m \\ \mathbf{x}_u \end{Bmatrix} = \begin{Bmatrix} \mathbf{F}_m \\ \mathbf{0} \end{Bmatrix} \tag{1.19}$$

where subscripts p, m, and u denote respectively the total number of DOFs, the number of measured DOFs, and the number of unmeasured DOFs, respectively. The mass normalized eigenvectors of the eigen-problem of Eq. (1.19) is considered as $\mathbf{\Phi} = [\mathbf{\Phi}_{pm} \;\; \mathbf{\Phi}_{pu}]$, in which the eigenvector of the measured and unmeasured coordinates are separated. The vector of the response is written in terms of eigenvectors and generalized coordinates.

$$\begin{Bmatrix} \mathbf{x}_m \\ \mathbf{x}_u \end{Bmatrix} = \begin{bmatrix} \mathbf{\Phi}_{mm} & \mathbf{\Phi}_{mu} \\ \mathbf{\Phi}_{um} & \mathbf{\Phi}_{uu} \end{bmatrix} \begin{Bmatrix} \mathbf{z}_m \\ \mathbf{z}_u \end{Bmatrix}. \tag{1.20}$$

Substituting Eq. (1.20) into Eq. (1.19) and pre-multiplying by $\mathbf{\Phi}^T = [\mathbf{\Phi}_{pm} \;\; \mathbf{\Phi}_{pu}]^T$, the equation of motion is rewritten in terms of modal coordinates.

$$\begin{aligned} \mathbf{\Phi}^T \begin{bmatrix} \mathbf{M}_{mm} & \mathbf{M}_{mu} \\ \mathbf{M}_{um} & \mathbf{M}_{uu} \end{bmatrix} \mathbf{\Phi} \begin{Bmatrix} \ddot{\mathbf{z}}_m \\ \ddot{\mathbf{z}}_u \end{Bmatrix} + \mathbf{\Phi}^T \begin{bmatrix} \mathbf{C}_{mm} & \mathbf{C}_{mu} \\ \mathbf{C}_{um} & \mathbf{C}_{uu} \end{bmatrix} \mathbf{\Phi} \begin{Bmatrix} \dot{\mathbf{z}}_m \\ \dot{\mathbf{z}}_u \end{Bmatrix} \\ + \mathbf{\Phi}^T \begin{bmatrix} \mathbf{K}_{mm} & \mathbf{K}_{mu} \\ \mathbf{K}_{um} & \mathbf{K}_{uu} \end{bmatrix} \mathbf{\Phi} \begin{Bmatrix} \mathbf{z}_m \\ \mathbf{z}_u \end{Bmatrix} = \mathbf{\Phi}^T \begin{Bmatrix} \mathbf{F}_m \\ \mathbf{0} \end{Bmatrix} \end{aligned} \tag{1.21}$$

The transformation matrix $\mathbf{T}$ is introduced as [25]

$$\mathbf{T} = \mathbf{\Phi}_{pm}\mathbf{\Phi}_{mm}^{-1} = \begin{Bmatrix} \mathbf{\Phi}_{mm} \\ \mathbf{\Phi}_{um} \end{Bmatrix} \mathbf{\Phi}_{mm}^{-1}, \tag{1.22}$$

The mass, damping, and stiffness matrices are respectively transformed to the identity $\mathbf{I}$, modal damping $\mathbf{\Gamma}$, and eigenvalue matrices $\mathbf{\Lambda}$, resulting the following equation.

$$\begin{bmatrix} \mathbf{I}_{mm} & \mathbf{0} \\ \mathbf{0} & \mathbf{I}_{uu} \end{bmatrix} \begin{Bmatrix} \ddot{\mathbf{z}}_m \\ \ddot{\mathbf{z}}_u \end{Bmatrix} + \begin{bmatrix} \mathbf{\Lambda}_{mm} & \mathbf{0} \\ \mathbf{0} & \mathbf{\Lambda}_{uu} \end{bmatrix} \begin{Bmatrix} \dot{\mathbf{z}}_m \\ \dot{\mathbf{z}}_u \end{Bmatrix} + \begin{bmatrix} \mathbf{\Gamma}_{mm} & \mathbf{0} \\ \mathbf{0} & \mathbf{\Gamma}_{uu} \end{bmatrix} \begin{Bmatrix} \mathbf{z}_m \\ \mathbf{z}_u \end{Bmatrix} = \mathbf{\Phi}^T \begin{Bmatrix} \mathbf{F}_m \\ \mathbf{0} \end{Bmatrix} \tag{1.23}$$

Assuming $\mathbf{z}_u = 0$, the vector of generalized coordinates is truncated to the measured DOFs, giving the equation of motion at the measured coordinates as

$$\mathbf{I}_{mm}\ddot{\mathbf{z}}_m + \mathbf{\Lambda}_{mm}\ddot{\mathbf{z}}_m + \mathbf{\Gamma}_{mm}\ddot{\mathbf{z}}_m = \mathbf{\Phi}_{pm}^T\mathbf{F}_m \tag{1.24}$$

Using the truncation assumption and from Eq. (1.20), $\mathbf{x}_m = \mathbf{\Phi}_{mm}\mathbf{z}_m$ is given. Substituting $\mathbf{z}_m = \mathbf{\Phi}_{mm}^{-1}\mathbf{x}_m$ into Eq. (1.24) and pre-multiplying by ${\mathbf{\Phi}_{mm}^{-1}}^T$ gives

$$\begin{aligned} {\mathbf{\Phi}_{mm}^{-1}}^T\mathbf{\Phi}_{pm}^T\mathbf{M}_{mm}\mathbf{\Phi}_{pm}\mathbf{\Phi}_{mm}^{-1}\ddot{\mathbf{x}}_m + {\mathbf{\Phi}_{mm}^{-1}}^T\mathbf{\Phi}_{pm}^T\mathbf{C}_{mm}\mathbf{\Phi}_{pm}\mathbf{\Phi}_{mm}^{-1}\dot{\mathbf{x}}_m \\ + {\mathbf{\Phi}_{mm}^{-1}}^T\mathbf{\Phi}_{pm}^T\mathbf{K}_{mm}\mathbf{\Phi}_{pm}\mathbf{\Phi}_{mm}^{-1}\mathbf{x}_m = {\mathbf{\Phi}_{mm}^{-1}}^T\mathbf{\Phi}_{pm}^T\mathbf{F}_m, \end{aligned} \tag{1.25}$$

Substituting Eq. (1.22) into Eq. (1.25), the truncated equation of motion of the reduced order model is obtained

$$\mathbf{M}_r\ddot{\mathbf{x}}_m + \mathbf{C}_r\dot{\mathbf{x}}_m + \mathbf{K}_r\mathbf{x}_m + = \mathbf{F}_r, \tag{1.26}$$

where $\mathbf{M}_r = \mathbf{T}^T\mathbf{M}\mathbf{T}$, $\mathbf{C}_r = \mathbf{T}^T\mathbf{C}\mathbf{T}$, $\mathbf{K}_r = \mathbf{T}^T\mathbf{K}\mathbf{T}$, and $\mathbf{F}_r = \mathbf{T}^T\mathbf{F}$ denote the truncated mass, damping, and spring matrices and the force vector of the reduced order model. The following equation is used to expand the measured coordinates and estimate the response or force at the unmeasured DOFs, [24, 25].

$$\begin{Bmatrix} \mathbf{x}_m \\ \mathbf{x}_u \end{Bmatrix} = \mathbf{T}\mathbf{x}_m, \tag{1.27}$$

1.6.2 Craig-Bampton Method

In Craig-Bampton method [26], the coordinates of the structure under study are partitioned into the boundary and interior coordinates. Boundary degrees of freedom (DOFs) represent the shared DOFs with adjacent structures or subjected to external loadings. The remaining degrees of freedom are referred to as interior DOFs. The general equation of motion of the structure under study is partitioned into

boundary and interior coordinates.

$$\begin{bmatrix} \mathbf{M}_{bb} & \mathbf{M}_{bi} \\ \mathbf{M}_{ib} & \mathbf{M}_{ii} \end{bmatrix} \begin{Bmatrix} \ddot{\mathbf{x}}_b \\ \ddot{\mathbf{x}}_i \end{Bmatrix} + \begin{bmatrix} \mathbf{C}_{bb} & \mathbf{C}_{bi} \\ \mathbf{C}_{ib} & \mathbf{C}_{ii} \end{bmatrix} \begin{Bmatrix} \dot{\mathbf{x}}_b \\ \dot{\mathbf{x}}_i \end{Bmatrix} + \begin{bmatrix} \mathbf{K}_{bb} & \mathbf{K}_{bi} \\ \mathbf{K}_{ib} & \mathbf{K}_{ii} \end{bmatrix} \begin{Bmatrix} \mathbf{x}_b \\ \mathbf{x}_i \end{Bmatrix} = \begin{Bmatrix} \mathbf{f}_b \\ \mathbf{0} \end{Bmatrix} \tag{1.28}$$

where $\mathbf{M}$, $\mathbf{C}$, $\mathbf{K}$ are respectively the mass, damping, and stiffness matrices, $\mathbf{x}$ is displacement, and $\mathbf{f}_b$ is the external force applied to the structure. The subscripts b and i denote the boundary and interior coordinates, respectively. The Craig-Bampton transformation matrix is created as [26]

$$\mathbf{T}_{CB} = \begin{bmatrix} \mathbf{I}_{bb} & \mathbf{0}_{bi} \\ \mathbf{\Psi}_{ib} & \mathbf{\Phi}_{ii} \end{bmatrix} \begin{Bmatrix} \mathbf{x}_b \\ \eta_i \end{Bmatrix} \tag{1.29}$$

where

$$\begin{Bmatrix} \mathbf{x}_b \\ \mathbf{x}_i \end{Bmatrix} = \mathbf{T}_{CB} \begin{Bmatrix} \mathbf{x}_b \\ \eta_i \end{Bmatrix} \tag{1.30}$$

$\mathbf{\Psi}_{ib}$ and $\mathbf{\Phi}_{ii}$ are respectively constrained modes and fixed interface vibrations modes of the structure, $\mathbf{I}$ denotes the identity matrix, and η_i is the vector of generalized coordinates associated with the interior degrees of freedom. To obtain a constraint mode, the interior coordinates of the structures are constrained and a unit displacement is applied to one of the boundary coordinates. The static deformation resulted from such loading condition is referred to as constraint mode.

$$\mathbf{\Psi}_{ib} = -\mathbf{K}_{ii}^T \mathbf{K}_{ib}, \tag{1.31}$$

Fixed interface vibration modes, on the other hand, are resulted from solving the undamped eigenvalue problem of the structure constrained at its boundary coordinates.

$$\left(\mathbf{K}_{ii} - \omega_{i,j}^2 \mathbf{M}_{ii}\right) \phi_{i,j} = \mathbf{0}, \quad j = 1, \cdots, k, \tag{1.32}$$

where $\omega_{i,j}$ and $\phi_{i,j}$ denote the jth eigenfrequency and fixed interface vibration mode, respectively. Care should be taken to compute sufficient number k of modes to obtain an adequate model. However, typically the required number of k is small. The transformation matrix $\mathbf{T}_{CB}$ is used to obtain the truncated equation of motion

$$\begin{bmatrix} \hat{\mathbf{M}}_{bb} & \hat{\mathbf{M}}_{bk} \\ \hat{\mathbf{M}}_{kb} & \mathbf{I}_{kk} \end{bmatrix} \begin{Bmatrix} \ddot{\mathbf{x}}_b \\ \ddot{\eta}_i \end{Bmatrix} + \begin{bmatrix} \hat{\mathbf{C}}_{bb} & \hat{\mathbf{C}}_{bi} \\ \hat{\mathbf{C}}_{ib} & \zeta_{ii} \end{bmatrix} \begin{Bmatrix} \dot{\mathbf{x}}_b \\ \dot{\eta}_i \end{Bmatrix} + \begin{bmatrix} \hat{\mathbf{K}}_{bb} & \mathbf{0}_{bi} \\ \mathbf{0}_{ib} & \mathbf{\Lambda}_{ii} \end{bmatrix} \begin{Bmatrix} \mathbf{x}_b \\ \eta_i \end{Bmatrix} = \begin{Bmatrix} \mathbf{f}_b \\ \mathbf{0} \end{Bmatrix} \tag{1.33}$$

The truncated mass, damping, and stiffness matrices are obtained, respectively, as

$$\begin{aligned}
\hat{\mathbf{M}} &= \hat{\mathbf{T}}_{CB}^T \hat{\mathbf{M}} \hat{\mathbf{T}}_{CB} = \begin{bmatrix} \hat{\mathbf{M}}_{bb} & \hat{\mathbf{M}}_{bk} \\ \hat{\mathbf{M}}_{kb} & \mathbf{I}_{kk} \end{bmatrix}, \\
\hat{\mathbf{C}} &= \hat{\mathbf{T}}_{CB}^T \hat{\mathbf{C}} \hat{\mathbf{T}}_{CB} = \begin{bmatrix} \hat{\mathbf{C}}_{bb} & \hat{\mathbf{C}}_{bi} \\ \hat{\mathbf{C}}_{ib} & \zeta_{ii} \end{bmatrix}, \\
\hat{\mathbf{K}} &= \hat{\mathbf{T}}_{CB}^T \hat{\mathbf{K}} \hat{\mathbf{T}}_{CB} = \begin{bmatrix} \hat{\mathbf{K}}_{bb} & \mathbf{0}_{bi} \\ \mathbf{0}_{ib} & \mathbf{\Lambda}_{ii} \end{bmatrix},
\end{aligned} \tag{1.34}$$

where

$$\begin{aligned}
\hat{\mathbf{M}}_{bb} &= \mathbf{M}_{bb} - \mathbf{M}_{bi}\mathbf{K}_{ii}^{-1}\mathbf{K}_{ib} - \mathbf{K}_{bi}\mathbf{K}_{ii}^{-1}\mathbf{M}_{ib} + \mathbf{K}_{bi}\mathbf{K}_{ii}^{-1}\mathbf{M}_{ii}\mathbf{K}_{ii}^{-1}\mathbf{K}_{ib}, \\
\hat{\mathbf{M}}_{bk} &= \left(\mathbf{K}_{bi}\mathbf{K}_{ii}^{-1}\mathbf{M}_{ii} + \mathbf{M}_{bi}\right)\mathbf{\Phi}_{ik} = \hat{\mathbf{M}}_{kb}^T, \\
\hat{\mathbf{C}}_{bb} &= \mathbf{C}_{bb} - \mathbf{C}_{bi}\mathbf{K}_{ii}^{-1}\mathbf{K}_{ib} - \mathbf{K}_{bi}\mathbf{K}_{ii}^{-1}\mathbf{C}_{ib} + \mathbf{K}_{bi}\mathbf{K}_{ii}^{-1}\mathbf{C}_{ii}\mathbf{K}_{ii}^{-1}\mathbf{K}_{ib}, \\
\hat{\mathbf{C}}_{bk} &= \left(\mathbf{K}_{bi}\mathbf{K}_{ii}^{-1}\mathbf{C}_{ii} + \mathbf{C}_{bi}\right)\mathbf{\Phi}_{ik} = \hat{\mathbf{C}}_{kb}^T, \\
\zeta_{kk} &= \mathbf{\Phi}_{ik}^T\mathbf{C}_{ii}\mathbf{\Phi}_{ik}, \\
\hat{\mathbf{K}}_{bb} &= \mathbf{K}_{bb} - \mathbf{K}_{bi}\mathbf{K}_{ii}^{-1}\mathbf{K}_{ib}
\end{aligned} \tag{1.35}$$

$\mathbf{\Lambda}_{kk}$ is the eigenfrequency matrix obtained from Eq. (1.32).

1.7 Nonlinear Vibration Analysis Methods

A general equation of motion of a nonlinear dynamic system is considered.

$$\mathbf{M}\ddot{\mathbf{x}} + \mathbf{C}\dot{\mathbf{x}} + \mathbf{K}\mathbf{x} + \mathbf{f}_n(x, \dot{x}) = \mathbf{F}(t), \tag{1.36}$$

where $\mathbf{M}$, $\mathbf{C}$, $\mathbf{K}$ denote respectively the mass, damping, and stiffness matrices of the nonlinear system, $\mathbf{f}_n(x, \dot{x})$ is the nonlinear restoring force, and $\mathbf{F}(t)$ is the vector of the external force. There are different methods in the literature proposed for solving the equation of motion of nonlinear structures, ([27]-[33]). In this section, the two methods which are used in the investigations of the present thesis are explained: the modified complex averaging technique (MCXA), and the harmonic balance method (HBM). These methods are utilized to obtain the steady state dynamics of the system when the response of the system is assumed to be periodic.

1.7.1 Modified Complex Averaging Technique (MCXA)

A dynamical system subject to harmonic external force is considered. In case of periodic response, the modified complex averaging technique (MCXA) is utilized to obtain the steady state dynamics of the

system, [32, 33]. In order to use this technique, the response $x_i(t)$ of the ith degree of freedom of the system is approximated using the sum of the static response $x_{i,0}$ and N_H harmonics of the response $x_{i,n}(t)$,

$$x_i(t) = x_{i,0} + \sum_{n=1}^{N_H} x_{i,n}(t), \quad i = 1, \cdots, N_i, \tag{1.37}$$

where N_i is the number of degrees of freedom of the system. Defining new complex variables on each harmonic

$$\psi_{i,n} = \dot{x}_{i,n} + jn\omega x_{i,n} = \varphi_{i,n} e^{jn\omega t}, \quad \bar{\psi}_{i,n} = \dot{x}_{i,n} - jn\omega x_{i,n} = \bar{\varphi}_{i,n} e^{-jn\omega t}, \tag{1.38}$$

where ω is the excitation frequency, $\varphi_{i,n}$ is a complex valued variable and the overbar denotes the complex conjugate. The displacement $x_{i,n}(t)$ and its derivatives $\dot{x}_{i,n}(t)$ and $\ddot{x}_{i,n}(t)$ can be derived for each harmonic of every degree of freedom as below.

$$\begin{aligned} x_{i,n} &= \frac{1}{2jn\omega}\left(\varphi_{i,n} e^{jn\omega t} - \bar{\varphi}_{i,n} e^{-jn\omega t}\right), \\ \dot{x}_{i,n} &= \frac{1}{2}\left(\varphi_{i,n} e^{jn\omega t} + \bar{\varphi}_{i,n} e^{-jn\omega t}\right), \\ \ddot{x}_{i,n} &= \frac{1}{2}\left(\dot{\varphi}_{i,n} e^{jn\omega t} + \dot{\bar{\varphi}}_{i,n} e^{-jn\omega t}\right) + \frac{jn\omega}{2}\left(\varphi_{i,n} e^{jn\omega t} - \bar{\varphi}_{i,n} e^{-jn\omega t}\right), \end{aligned} \tag{1.39}$$

Substituting Eqs. (1.38) and (1.39) into the governing equation of the system and averaging over each harmonic, $N_i \times N_H$ new first order differential equations are obtained in terms of the new complex variables $\varphi_{i,n}$. The complex variables $\varphi_{i,n}$ are separated into real and imaginary parts.

$$\varphi_{i,n} = y_{2[(i-1)N_H+n]-1} + j y_{2[(i-1)N_H+n]}, \quad i = 1, \cdots, N_i, \tag{1.40}$$

Substituting Eq. (1.40) into the equation of motion of the system and treating real and imaginary parts separately, $2 \times N_i \times N_H$ first order differential equations are derived in the general form as below

$$\dot{\mathbf{Y}} = R(\mathbf{Y}), \tag{1.41}$$

where $\mathbf{Y} = [y_1\ y_2\ \cdots\ y_{2N_iN_H}]^T$ is the unknown vector and $\dot{\mathbf{Y}} = [\dot{y}_1\ \dot{y}_2\ \cdots\ \dot{y}_{2N_iN_H}]^T$ is the derivative of $\mathbf{Y}$. For the case of steady state dynamics, eliminating the time derivatives $\dot{\mathbf{Y}} = [\dot{y}_1\ \dot{y}_2\ \cdots\ \dot{y}_{2N_iN_H}]^T$ results in algebraic equations in the form

$$R(\mathbf{Y}) = 0, \tag{1.42}$$

For nonlinear systems, it would be difficult or in many cases impossible to find an explicit analytic solution. Hence, in this study, the pseudo arc-length continuation method has been used to solve the nonlinear Eq. (1.42) and compute unknown variables y_k, $k = 1, \cdots, 2 \times N_i \times N_H$, by which amplitude

of each harmonic can be determined.

$$X_i^n = \sqrt{\left(\frac{y^2_{2[(i-1)N_H+n]-1} + y^2_{2[(i-1)N_H+n]}}{n\omega}\right)}, \tag{1.43}$$

A MATLAB code for the pseudo arc-length continuation method has been developed to obtain the steady state response in the frequency domain. Stability analysis of the steady state solution of the nonlinear system is also performed using Lyapunov's first method of stability analysis and simple linearization of Eq. (1.42) around its equilibrium points by considering the eigenvalues of the Jacobian matrix.

1.7.2 Harmonic Balance Method

The Harmonic Balance Method (HBM) is a method used for quantitative analysis of nonlinear systems with periodic response, [28, 29]. Considering the equation of motion of Eq. (1.37), and considering the system behaves with periodic response, the dynamic response of the system is assumed as a harmonic response in the form of Fourier series with definite number of terms.

$$x_i(t) = x_0 + \sum_{n=1}^{H} \left(a_n(t)\sin(n\omega t) + b_n(t)\cos(n\omega t)\right), \tag{1.44}$$

where $x_i(t)$ is the response of the ith degree-of-freedom of the system, x_0 denotes the static displacement of the ith oscillator, H is the number of harmonics considered in the dynamic response of the system, and a_n, b_n are respectively the slowly varying sine and cosine coefficients of the nth harmonic of the response. In the case of steady state dynamic analysis, a_n, b_n are considered as constant parameters. The assumed response of Eq. (1.44) is substituted into the equation of motion Eq. (1.37) of the nonlinear system. Balancing the two sides of the resulting equation for the coefficient x_0 of the static displacement and the coefficients a_n, b_n of sin and cos terms of the H harmonics of the response, $(2H+1)$ algebraic equations are obtained.

$$R_j(x_0, a_n, b_n) = 0, \quad n = 1, \cdots, H, \quad j = 1, \cdots, (2H+1), \tag{1.45}$$

Solving the nonlinear algebraic equations of Eq. (1.45), the unknown coefficients x_0, a_n, b_n of the assumed harmonic response Eq. (1.44) of the dynamic system is obtained.

As explained above, both MCXA and HBM are used to find the steady state response of dynamical systems with periodic behaviour. It can be shown that in spite of different formulation of both techniques, application of MCXA and HBM leads to the same conclusion. However, the simplicity of the MCXA

technique in applying to higher order smooth nonlinearities is considered as the advantage of this method with respect to the HBM.

On the other hand, the accuracy of these methods in predicting the dynamics of the system under study strongly relies on the number of harmonics taken into account, particularly in case of strongly nonlinear systems. Therefore, both methods are difficult to use in dealing with the cases including a large number of harmonics or non-smooth nonlinearities. Indeed, contribution of the large number of harmonics to the dynamics of the system results in high computational costs and using MCXA and HBM would be cumbersome. Besides, MCXA and HBM cannot predict non-periodic or chaotic behaviours. Therefore, instead of MCXA or HBM, numerical integration methods such as Runge-Kutta or Newmark method are used in case of systems with high content of harmonics, or systems with non-periodic or chaotic responses.

1.8 Thesis Outline

Chapter 1 provides theoretical background required for understanding the thesis. Finite element method (FEM) and modal analysis are briefly explained. Then, SEREP expansion method is described in detail. Modified complex averaging (MCXA) technique and harmonic balance method (HBM) are also explained for the investigation of steady state dynamics of nonlinear structures.

Chapter 2 gives a literature review on nonlinear localization methods and various identification approaches for structural dynamics. Identification methods from different categories such as modal-base approaches, time/frequency/time-frequency domain methods, and linearization methods are reviewed in addition to localization approaches. A discussion on parametric and non-parametric identification methods is given in this chapter. Also, the equivalent dynamic stiffness mapping (EDSM) technique is also described in detail.

Chapter 3 focuses on the localization of nonlinear elements in structural dynamics utilizing base excitation measured data. To this end, a symmetric configuration of permanent magnets and electro-magnets are designed to provide nonlinear restoring force at the tip of a cantilever beam. The cantilever is mounted on a shaker bed and excited by base motion of the shaker with constant amplitude of acceleration. The underlying linear model of the nonlinear system is updated exploiting the results obtained from very low-amplitude excitation. Then, the localization approach is used to find the location of nonlinearity.

Chapter 4 aims to investigate the effect of various sources of inaccuracy on the results of nonlinear model identification. To this end, the equivalent dynamic stiffness mapping (EDSM) technique is chosen as a well-developed identification method in nonlinear structural dynamics. Then, the sensitivity of the EDSM technique is investigated with respect to measurement noise and different sources of inaccuracy

such as expansion error, modelling error, and the error due to neglecting higher harmonics. Finally, an optimization-based framework is used to identify the model of a cantilever using experimental data. This framework helps to avoid the effect of various sources of error and measurement noise.

Chapter 5 proposes an optimization-based framework for identification of nonlinear systems. The introduced method is applied to a test rig composed of a base-excited cantilever beam subjected to an electromagnetic force at the tip. Mathematical model of the nonlinear structure is identified for four different models of nonlinear electromagnetic restoring force. It is observed that nonlinear force up to the fifth order nonlinear stiffness and a linear damping is producing an excellent agreement between the measured nonlinear responses and predictions.

Chapter 6 introduces a parameter estimation method for identification of nonlinear structures in the presence of multi-harmonic response and force. For this purpose, a method with two different approaches is introduced: Analytical Harmonic-Balance-based (AHB) approach and the Alternating Frequency/Time approach using Harmonic Balance (AFTHB). The method is applied to five simulated examples of nonlinear systems to highlight different features of the method. The results illustrate that neglecting higher harmonics, particularly in systems with multi-harmonic response and force, may lead to inaccurate identified model.

Chapter 7 applies the AFTHB method to two experimental case studies and identifies the nonlinear mathematical model of the structures. The performance of the AFTHB approach in estimating the unknown parameters of the structure is illustrated by the results of identification.

Chapter 8 gives the conclusions of the present study and provides suggestion for future work.

1.9 Thesis Contribution

The main contributions of this thesis are threefold:

- Investigating the sensitivity of the nonlinear identification methods to various sources of inaccuracy; this study is carried out and described in Chapter 4.
- Developing an optimisation-based method for nonlinear model identification in structural dynamics. The method is described in Chapter 5.
- Developing an identification method with two different approaches known as the AHB and AFTHB approaches. The method and the study on its application to various types of nonlinearities are given in Chapter 6. Also, the application of the AFTHB approach is demonstrated in experimental case studies. The results are discussed in Chapter 7.

Each of the above points is elaborated below.

In this thesis, the sensitivity of the nonlinear identification methods is investigated to various sources of inaccuracy. To do this, the effect of accumulated error due to using linear expansion methods such as SEREP in estimating the response at unmeasured coordinates is studied on the results of nonlinear model identification. In addition, it is shown that the presence of noisy measurement makes it difficult to identify the model of nonlinear systems. Modelling error and the error introduced by neglecting higher harmonics in nonlinear structures are other sources of inaccuracy that may affect the outcome of the identification methods.

To minimize the error introduced by using the expansion methods in estimating the response at unmeasured coordinates, an optimization-based framework is developed in this study. The optimization process benefits from a gradient-based algorithm utilizing the *fmincon* function in MATLAB. To minimize the implicit regularization in the optimization process, and to avoid missing the global optimal of the problem, different initial conditions which are distributed over the variation range of optimization parameters are used for the optimization process.

Another contribution of this thesis is to develop an identification method with two different approaches for identifying nonlinear structures: the Analytical Harmonic-Balance-based (AHB) approach and the Alternating Frequency/Time approach using Harmonic Balance (AFTHB). These two approaches use the harmonic balance method and utilize the measured steady state harmonic response of nonlinear structures to identify their model. The main novelty of the proposed method is that it considers all significant harmonics of the response and force signal in nonlinear structures. In addition, the method is applicable to a wide range of smooth and non-smooth complex nonlinearities. Also, the method can be used for complicated multi-DoF systems with relatively low computational costs and high accuracy. The application of the proposed AFTHB approach on two nonlinear experimental case studies is demonstrated in Chapter 7.

1.10 Research Outcome

The research outcome of this thesis is listed as below:

1. **J. Taghipour**, H.H. Khodaparast, M.I. Friswell, A.D. Shaw, H. Jalali, N. Jamia, *Harmonic-Balance-Based Parameter Estimation of Nonlinear Structures in the Presence of Multi-Harmonic Response and Force*, Mechanical Systems and Signal Processing, 162 (2022), 108057.

2. **J. Taghipour**, H.H. Khodaparast, M.I. Friswell, H. Jalali, H. Madinei, N. Jamia, *On the Sensitivity of the Equivalent Dynamic Stiffness Mapping Technique to Measurement Noise and Modelling Error*, Applied Mathematical Modelling, (2021) 89, pp. 225-248.

3. **J. Taghipour**, H.H. Khodaparast, H. Madinei, H. Jalali, *Detection of Localized Nonlinearity in Dynamical Systems Using Base Excitation Experimental Results*, Journal of Theoretical and Applied Vibration and Acoustics, (2020) 6(1), pp. 35-50.

4. **J. Taghipour**, H.H. Khodaparast, M.I. Friswell, H. Jalali, *An Optimization-Based Framework for Nonlinear Model Selection and Identification*, Vibration, (2019) 2(4), pp. 311-331.

5. **J. Taghipour**, H.H. Khodaparast, *Identification of localised nonlinearities in structural dynamics*, 2nd International Conference on Advances in Aerospace Structures, Systems and Technology, May 2019, London.

6. **J. Taghipour**, H.H. Khodaparast, M.I. Friswell, H. Jalali, H. Madinei, X. Wang, *Localisation, characterisation and identification of localised nonlinearity in structural dynamics using base excitation frequency response functions*, PROCEEDINGS OF ISMA2018 AND USD2018, 2127-2138.

7. N. Jamia, H. Jalali, **J. Taghipour**, M.I. Friswell, H.H. Khodaparast, *An Equivalent Model of a Nonlinear Bolted Flange Joint*, Mechanical Systems and Signal Processing, 153 (2021), 107507.

8. N. Jamia, H. Jalali, **J. Taghipour**, M.I. Friswell, H.H. Khodaparast, *Dynamic Analysis of Bolted Joints: Detailed and Equivalent Modelling*, Nonlinear Structures & Systems, (2021) Volume 1, pp. 215-221. Conference Proceedings of the Society for Experimental Mechanics Series, Springer.

9. N. Jamia, **J. Taghipour**, H. Jalali, M.I. Friswell, H.H. Khodaparast, A.D. Shaw, *Numerical and Experimental Investigations of Nonlinearities in Bolted Joints*, 29th Biennial Conference on Noise and Vibration Engineering, ISMA2020At: 7-9 September 2020, Leuven, Belgium.

10. H. Jalali, **J. Taghipour**, H. Madinei, H.H. Khodaparast, M.I. Friswell, *Uncertainty Modelling and Identification in Structural Joint Contact Interfaces*, 7th International Conference on Computational Methods in Structural Dynamics and Earthquake Engineering, June 2019, Greece.

1.11 Closure

This chapter provided some theoretical backgrounds including Finite Element method and modal analysis. Two of the most commonly used expansion/reduction methods including the system equivalent reduction-expansion process (SEREP) and the Craig-Bampton Method have been described in detail in this chapter. The complex averaging technique (CXA) and the harmonic balance method (HBM) have been explained in this chapter as two of analytical nonlinear vibration analysis methods. The thesis outline and the research outcome of the present study were given at the end of this chapter.

Chapter 2

Literature Review

2.1 Introduction

Nowadays, researchers try to utilize the characteristics of nonlinear phenomena to increase the performance of the modern devices and structures. Hence, there are ever-increasing demands for applications of nonlinear structures in industry. For example, nonlinear energy harvesting and nonlinear vibration control are two fields of study that have attracted the most attention during recent years. On the other hand, utilizing the capabilities of nonlinear structures requires the structure to be well-understood. In addition, numerical models are widely used to design and predict the behavior of the engineering structures. Therefore, having an exact model of nonlinear structures is essential in structural dynamics. Since linear models fail to predict the complicated responses such as multi-harmonic responses, quasi-periodic responses, chaotic behavior, or jump phenomena, nonlinear model identification methods are required.

Prior to the identification of nonlinear elements in dynamical structures, the nonlinearities should be characterized to determine if they are localized or non-localized. The exact location of localized nonlinearities should then be determined. This chapter provides a literature review on linear and nonlinear model identification and localization methods. The research gaps are identified through the literature review and the objectives of the thesis are introduced in this chapter, accordingly.

2.2 Localization of Structural Nonlinearity

Almost all engineering structures have nonlinearities arising from various sources such as nonlinear material, geometry, or joints. Of these structures, many have weak nonlinearities so that they can be properly linearized using conventional theories. However, on the other hand, in many applications the nonlinearity is too strong to be neglected. Hence, in order to have an accurate prediction of the behaviour of the system, the nonlinear model has to be identified and characterized. There have been numerous

studies on nonlinear identification techniques, mostly relying on the assumption of the pre-known location of the nonlinearity. However, when there is insufficient information about the linearity or nonlinearity of the system, a prerequisite for identifying nonlinear elements is to detect the existence of nonlinearities and determine their exact location in engineering structures. These localization methods are used also in other applications such as structural health monitoring to detect the location of cracks or unexpected flaws. Accordingly, many localization approaches have been presented in recent decades ([34]-[41]). In general, all localization methods are based on the comparison between an analytical model of the structure and the experimental data.

In practice, usually it is not possible to measure the response at all coordinates of the structure. For instance, measuring the response of the system in the vicinity of joints is too difficult, or when a relatively large structure is tested, there may not be enough equipment to measure all of the required coordinates. Lin and Ewins [36] developed a method based on correlating an analytical model with experimental data to locate the localized nonlinear elements in dynamical structures. The method presented in their study does not require complete measurement at all coordinates, and modelling error is considered in this method. They applied the aforementioned method on both numerical and experimental studies to demonstrate its performance.

Investigating the nonlinear localization approaches based on domain decomposition, Cresta et al. [37] proposed two strategies and applied them to analyse the post-buckling behaviour of long slender structures. They carried out a comparative study on the performance of different methods based on the convergence results. Ondra et al. [38] introduced an approach based on the Hilbert transform in the frequency domain and artificial neural networks to detect and identify structural nonlinearities. In this method, training data required for the artificial neural network is created using the frequency response function described by the Hilbert transform. To this end, assumptions on the possible types of nonlinearities and corresponding parameter ranges are required. In [39], Koyuncu et al. utilized cascaded optimization and neural networks in order to localize and identify the nonlinear elements of dynamical structures. Possible locations of nonlinearities, possible nonlinear forms, and possible range of parameters' values are selected for the structure considering the physics of the problem. Of course, this requires experience and good engineering insight to avoid any errors in localization of structural nonlinearity. The assumed possibilities are then used to produce training data using a finite element model of the structure. Cascaded optimization and neural networks employ this data set to find, detect and characterize the nonlinearities of the system. The approach introduced in their study require assumptions or pre-knowledge about the location and type of nonlinearities, as well as the range of parameter values, which may affect the results of localization and identification of the nonlinear elements.

Developing a localization technique to detect the location of localized nonlinearities based on incomplete measurements, Wang et al. [40] tried to eliminate the limitation on the complete measurement

for nonlinear localization. The method presented in their study does not require the type of nonlinearity to be assumed or pre-known. Many of the nonlinear localization and identification methods use the frequency response of the system. Also, they usually utilize the data obtained from force excited vibrational tests, as it is easier to find the frequency response function in single-input-multi-output tests. Özer and Özgüven [41] presented a localization method to detect localized structural nonlinearities using sinusoidal vibration test data.

2.3 Nonlinear Identification Methods

In contrast to linear model updating which is a well-developed and matured field of study, the nonlinear identification of structural dynamics is an ongoing research area attracting a great deal of attention. Refs. ([34],[42]-[45]) give comprehensive reviews on nonlinear identification methods and the developments in this field. There are a multitude of criteria to categorize the structural identification methods. One criterion is according to the type of measured data used for identification. In general, all linear and nonlinear identification methods can be listed in two categories: modal-based methods and response-based methods. In modal-based methods, the experimentally measured modal parameters of the system are used to identify the model of the system. On the other hand, the response-based methods utilize the measured response of the system either in the time domain, the frequency domain, or the hybrid time-frequency domain. The following subsections give a brief literature review of identification methods categorized in the aforementioned categories.

2.3.1 Modal-Based Approaches

The modal parameters and how they define basic information of the dynamic behaviour of mechanical structures was discussed in Section 1.3. Modal analysis is a well-developed approach for identifying linear structures. It has also been taken up through recent decades by researchers in structural dynamics for the application of nonlinear structures. There are linear and nonlinear identification methods based on the measured modal properties of the system. Linear modal identification methods are completely mature ([6], [10]-[12]). Although there are a lot of research activities in this field of study, nonlinear modal identification is considered as relatively new in structural dynamics.

CONCERTO is a code presented by Carrella and Ewins [46] for identifying nonlinear structures using the measured response of the system to the excitation. CONCERTO estimates the isolated nonlinear response of the system utilizing the assumption of single-harmonic response. The application of COCERTO was illustrated in Refs. [46] and [47]. Wright et al. [48] proposed the nonlinear resonant decay method (NLRDM) to identify structural nonlinearities. NLRDM is capable of identifying structures exploiting multiple-mode measurements, in contrast to CONCERTO and other single-mode based

methods such as the method introduced by Link et al. [49]. The applicability of NLRDM was shown in the identification of different complex nonlinear structures ([50]-[54]).

Conventional modal approaches, which are mainly used for linear structure identification, can also be applied to the structures with weak nonlinearities. However, it may lead to inaccurate model to apply the traditional linear modal methods to essentially nonlinear structures. Therefore, the concept of Nonlinear Normal Modes (NNM) [55, 56] is used as the basis for many identification approaches. First, nonlinear phase resonance was extended from linear phase resonance testing to utilize the concept of NNM in nonlinear identification ([57]-[62]). Renson et al. [63] exploited the robustness of the NNM backbone curve to develop an identification method.

2.3.2 Time-domain methods

The time-domain identification methods exploit the time history of the measured force and response to identify the nonlinear model of the structure. Crawley and Aubert [64] proposed the so called force-state mapping technique to identify the nonlinear structural elements using the time-domain experimental data. An application of force-state mapping is found in [65] for identifying the nonlinear model of structural joints. Kerschen et al. [66] investigated the performance of the restoring force surface method in identifying nonlinear structural elements of a cantilever beam. In this regard, they considered the vibrations of a clamped beam with two different types of nonlinearities. Firstly, a cantilever beam was considered with a piecewise linear stiffness, and secondly, a bilinear stiffness was taken into account. Their method requires the displacement, velocity, acceleration and force at all degrees of freedom to be measured in the time domain.

A number of linear and nonlinear time-domain identification methods have been developed based on time-series analysis. Box and Jenkins [67] introduced a linear approach using auto-regressive moving average (ARMA) models. Nonlinear ARMA with eXogeneous input (NARMAX), which is possibly the most reliable and widely-used extension of ARMA for nonlinear structures, was proposed by Leontaritis and Billings [68, 69]. NARMAX provides the possibility to consider a noise model within the identified model of the structure. However, finding a stable recursive procedure which is suitable for the noise model may sometimes be a significant problem. Billings et al. [70] designed correlation tests to evaluate the validity of the identified models using NARMAX. To control the complexity of the model, Korenberg et al. [71] introduced a development of NARMAX by proposing an orthogonal estimation algorithm to estimate the model parameters in a sequential manner. However, the orthogonal estimator cannot be applied to nonlinear-in-the-parameter models such as neural networks [72].

Feldman [73] exploited the capability of the modern Hilbert Vibration Decomposition approach to introduce a nonparametric identification method to characterize the nonlinear elastic force functions and backbone curves of asymmetric nonlinear vibration structures. The method presented by Feldman

does not require a priori information about the system structure or its parameters. In [74], Feldman demonstrated the identification of a nonlinear structure utilizing a Hilbert transform (HT) method by exploiting the time-domain response and force data obtained from free and forced vibration tests. Feldman proposed that the accuracy of the identification of the time-frequency distribution of a signal of the response of a time-varying nonlinear system can significantly be improved by using HT processing along with Hilbert vibration decomposition and congruent functions. Worden and Hensman [75] surveyed the benefits and limitations of using the Bayesian approach for identification of nonlinear structural systems. This approach is not limited to any assumption regarding the type and parameters of the system nonlinearity.

Green [76] introduced a novel Bayesian identification method to estimate the nonlinear structural dynamics using the Markov-chain Monte Carlo Data Annealing. Using training data in identifying the nonlinear structures is another approach of model identification exploiting the time-domain experimental data. Green et al. [76] developed a Bayesian identification approach to characterize structural systems using the training data obtained from vibration tests. Using the Hilbert Transform (HT), Feldman and Braun [78] proposed two identification approaches based two different signal processing approaches: signal demodulation and signal decomposition. Lenaerts et al. [79] used the updating technique of proper orthogonal decomposition to study the test system of the companion paper [80].

Masri and Caughy [81] introduced a nonparametric identification method to describe the properties of the system in terms of orthogonal functions. In the so called force-state mapping method, the measured response and applied force signals in the time domain are exploited to determine the force transmission characteristics of a nonlinear structure or sub-structure in terms of its mechanical state. Then, the transmitted force is plotted in a three-dimensional mapping versus displacement and velocity in order to determine a surface called the force-state map that identifies the nonlinear characteristics of the system. Al-Hadid and Wright [82] compared the use of orthogonal and ordinary polynomials in the curve-fitting process of the force-state mapping technique. They showed multiple advantages of the ordinary polynomial approach, such as improved accuracy and enabling the usage of special functions to model non-polynomial types of nonlinearity. They also modified the method to detect the location of discrete nonlinear elements within lumped parameter systems.

Yasuda et al. [83] presented a technique to identify nonlinear multi-degree-of-freedom systems. The method requires the nonlinear elements of the system to be assumed using polynomial functions and unknown parameters. The measured response and applied force in the time domain are used to express the quantities and nonlinear functions in a Fourier series. The unknown parameters are determined by applying the harmonic balance method. Feldman [84] utilized the Hilbert transform to present a technique for identification of nonlinear systems. His method is able to identify instantaneous modal

parameters of the system exploiting the time-domain measured data obtained from free vibration analysis and forced vibration tests with various types of excitation.

Marchesiello et al. [85] investigated the effect of nonphysical poles on the time-domain subspace identification (TNSI) approach proposed by Marchesiello and Garibaldi [86]. They carried out an experimental study to identify the localized nonlinear elements of a multi-degree-of-freedom system. Marchesiello and Garibaldi [87] investigated the applicability of the TNSI method in identifying non-smooth structural nonlinearities. Narayanan et al. [88] introduced a multiple-trial time-domain harmonic-balanced based method using multiple test data to reduce the error due to single data identification.

2.3.3 Frequency Domain Methods

One deficiency in using the conventional methods, such as H1 and H2, to estimate the frequency response function of a nonlinear system is that such methods are not able to eliminate the effect of nonlinearities in the system and subsequently predict the underlying linear system accurately. To solve this problem, Richards and Singh [89] presented a spectral identification method based on the "reverse path" formulation to identify multi-degree of freedom nonlinear systems using multi-input multi-output data. For this purpose, broad-band Gaussian random excitation is applied to obtain the nonlinear response of the system. In this approach, the nonlinear elements are considered as feedback forces on the underlying linear system. The application of this method can be found in Refs. ([80]-[93]). Kerschen and Golinval [80] utilized the aforementioned method to introduce a two-step identification approach to generate an accurate finite element model of nonlinear structures. In their proposed approach, frequency response functions of the underlying linear system resulting from the Conditioned Reverse Path (CRP) method are correlated with the analytical FRFs to update the linear parameters of the system. CRP was used in [90] to identify and investigate the behaviour of a cantilever beam with a geometric nonlinearity.

Noël and Kerschen [94, 95] introduced a frequency-domain method to identify nonlinear systems. In this subspace-based technique, the nonlinearity of the system is considered as a feedback force applied to the underlying linear system and is identified utilizing the frequency domain data. Hill et al. [96] studied the behaviour of a two-degree-of-freedom system subjected to an external force utilizing the backbone curves of the system. They presented a method to find the backbone curves of the system using the second order normal form technique. Renson et al. [63] developed a method to extract the backbone curve of the underlying conservative system. They adapted control-based continuation to track the locus where the response and the excitation are in quadrature. Londoño et al. [97] introduced a method to identify systems with discrete nonlinearities by exciting the structure at a single resonant frequency making the structure vibrate with large displacement where significant effects of nonlinearities are assured. In this method, assuming a form of nonlinearity, the system backbone curves are used to

identify the linear and nonlinear parameters of the system. The backbone curves are estimated using measured decay data.

Arslan et al. [98] compared the performance of two frequency-domain identification methods using experimental data from a test rig to identify its nonlinear element. Carrella and Ewins [46] introduced a single-DOF modal analysis frequency domain identification method based on the principle of linearization that exploits the measured frequency response functions (FRFs) to identify the nonlinear elements of the dynamical systems. Wang et al. [99] developed a strategy to update the finite element model of nonlinear structures. In order to avoid the ill-conditioning caused by the Laplace operator, Yang and Sanada [100] introduced a frequency domain subspace identification using the w-operator. Adams and Allemang [101] introduced a frequency domain nonlinear identification method which utilizes the internal nonlinear feedback in a closed loop to estimate the parameters of the nonlinear model of the structure.

Using the Volterra series [102], which is a widely-used functional series, is another approach to nonlinear structural dynamics identification in the frequency domain. However, the large number of unknown parameters to be identified in Volterra identification can be considered as the main shortcoming of this approach. Representing a dynamical system using a Volterra series and exploiting the associated linear equations (ALEs), Feijoo et al. [103] showed that dealing with the associated frequency response functions (AFRFs) in the frequency domain is easier than the higher-order frequency response functions (HOFRFs). The Wiener series is defined as an orthogonal basis of the Volterra series. In [104], da Silva et al. utilized Wiener series and Kautz filters to introduce an identification approach for estimating nonlinear systems. By estimating the HOFRFs of a breathing crack modelled by a bilinear nonlinearity, Chatterjee [105] showed the capability of multi-dimensional kernels of Volterra series in estimating the HOFRFs. Peng et al. [106] and [107] used the nonlinear output frequency-response functions (NOFRFs) [106, 109], which is a Volterra-based concept, to introduce linear and nonlinear identification algorithms, respectively. Lang and Billings [110] exploited the capability of NOFRFs to investigate the energy transfer properties of non-linear systems in the frequency domain.

2.3.4 Time-Frequency Methods

Having measured input data is an important part of conventional identification methods. To avoid the necessity of input data measurement, Haroon et al. [111] took advantage of both time and frequency domain techniques to identify the nonlinear elements of structures in the absence of measured input data. Time domain data is used to find a proper assumption for the form of the nonlinearity, and the assumed nonlinear form is used with frequency domain data to find an appropriate model to predict the linear and nonlinear response of the system. Prawin and Rao [112] presented a time-frequency identification method using a Volterra series approximation to estimate the nonlinear model of structural dynamical systems.

Some identification methods have been dually presented in both the time and frequency domains [113]. Adams and Allemang [101] introduced the nonlinear identification through feedback of the outputs (NIFO) method in the frequency domain which is the dual of the restoring force surface (RFS) method presented by Masry and Coughy [81] in the time domain. This method determines the parameters of nonlinear models by exploiting internal feedback considered as nonlinear elements. Marchesiello and Garibaldi [114] proposed a time-domain subspace identification (TNSI) method of nonlinear oscillating systems considering the nonlinear elements of the structures as internal feedback forces. Despite the very simple formulation of this method, finding numerically stable solutions requires special care to be taken to avoid ill-conditioning in the problem. Hence, they proposed a numerically robust implementation of a time-domain algorithm applicable to nonlinear mechanical systems introduced by Lacy and Bernstein [115]. Likewise, Noël and Kerschen [95] considered the nonlinearities as feedback forces applied to the underlying linear system and introduced a subspace-based identification method (FNSI) utilizing frequency domain measured data. Noël et al. [113] utilized two subspace nonlinear identification methods formulated in the time and frequency domains, called TNSI and FNSI, in order to identify a strongly nonlinear satellite structure. Another duality can be seen in the conditioned reverse path (CRP) identification method presented by Richards and Singh [89] and its alternative time domain decorrelation technique, referred to as the orthogonalised reverse path (ORP) method, introduced by Muhamad et al. [93]. Kerschen et al. [116] compared the Restoring Force Surface (RFS) method, which is a time domain approach, and the frequency domain Conditioned Reverse Path (CRP) method, for the identification of nonlinear structures.

To conquer the difficulties caused by single harmonic excitation, multi-harmonic excitation was suggested by Narayanan et al. [117] to identify the parameters of nonlinear structures using a hybrid time-frequency approach. Feldman [118, 119] introduced time-frequency domain identification based on Hilbert vibration decomposition (HVD). The empirical mode decomposition (EMD) is method used to decompose multicomponent signals and to identify nonlinear systems in the frequency domain, [120].

2.3.5 Linearization Methods

There are many nonlinear identification methods based on linearizing the nonlinear system. However, linearization is often not a good approach in identifying nonlinear structures. Noel and Kerschen [43] backed this statement by providing two reasons. First, the linearized models of nonlinear structures cannot be interpolated, as they just work for only a specific set of parameters. Second, as they are linearized models, they are not capable of predicting the nonlinear behaviour such as jumps, modal interactions, and harmonics. In spite of the weaknesses of linearization-based methods, they are still popular as they benefit from the link with well-developed linear techniques ([6]-[12],[121, 122]). Other

than this, industry is not yet willing to accept the intrinsically nonlinear methods in practice and is still relying on standard linear models.

Some authors introduced identification methods using harmonic excitation measurements. They based their methods on the assumption that the system is oscillating only with the fundamental excitation frequency [41, 125]. Özer et al. [123] introduced a method based on a describing function approach for identifying nonlinear structural elements. They used the Sherman–Morrison matrix to isolate the nonlinearity of the system. The Equivalent Dynamic Stiffness Mapping technique was proposed by Wang and Zheng [125] for the identification of nonlinear structural elements in dynamical systems using steady-state primary harmonic frequency response functions (FRF). There is no need for the type and parameters of the nonlinearity to be pre-known in this method, however having knowledge of the type of nonlinear element leads to a better parameter estimation and identification of the system.

There are several methods in the literature that try to find the best linear approximations (BLA) that describe the behavior of nonlinear structures. Schoukens at al. [126] developed a method based on using random test data for identifying nonlinear systems. Some applications of the BLA-based linearization methods can be found in Refs. ([127]-[130]). Some other works utilized the concept of time-varying linear models to identify the dynamic behavior of nonlinear structures ([131]-[133]).

2.4 Parametric vs Non-parametric Identification

In another type of classification, nonlinear identification methods can be categorized into two main classes: non-parametric ([134]-[135]) and parametric ([136]-[149]). The latter group can be divided into two sub-classes: methods with a model selection stage ([136]-[145]) and methods using an assumed model for the nonlinear system ([146]-[149]). Despite the efforts in developing nonlinear identification methods, there is not yet any identification method that can be generally applied to an extensive range of nonlinear systems. Indeed, the methods from each of the two categories have their own advantages and disadvantages. Most importantly, nonparametric methods do not require prior knowledge or assumptions for the type of nonlinearities, which is an advantage over parametric approaches. However, the high computational cost is a common drawback of nonparametric methods. The time-domain method of force-state mapping (FSM) [81, 134] is a commonly used non-parametric nonlinear identification method in structural dynamics. Despite the simple formulation and its non-parametric nature, the high computational costs of FSM limit the applications of this method to the simple practical structures with few degrees of freedom.

To avoid the necessity for surface fitting, which makes FSM computationally expensive, Karaağaçlı and Özgüven [135] developed a frequency-domain non-parametric identification method by determining a describing surface of nonlinearity exploiting response-controlled stepped-sine measured data. This

method is shown to have good performance in identifying systems with relatively simple nonlinearities. The method has the advantage of characterizing the systems with nonlinearity as a function of frequency. However, the method has convergence problems for more complex structures with non-smooth nonlinearities. To overcome this problem, Karaağaçlı and Özgüven suggested applying parametric curve fitting to the extracted non-parametric surfaces or using higher order finite differences to obtain the describing surface rather than first-order finite differences. Although this may solve the convergence issue and even increase the accuracy of the result, it will increase the complexity of the method.

Selecting an appropriate model that truly represents the structure is very important. Various model selection algorithms have been introduced in the literature, including forward, backward, and exhaustive search methods ([136]-[139]). Although these methods are applicable to linear in the parameters nonlinear models, they cannot be used for other nonlinear systems. Some identification methods utilize a dictionary of basis functions ([125],[140]-[143]) to select the type of nonlinearity rather than using prior assumptions for the type of nonlinear force. Although this approach is able to consider a wide range of nonlinear functions in the candidate pool, it has high computational costs, and some nonlinearities are difficult to represent with suitable basis functions. Fuentes et al. [141] introduced a Bayesian-based equation discovery method to overcome these problems by setting to zero all parameters of the basis functions not related to the model using a sparsity-inducing prior within a Relevance Vector Machine (RVM) framework. However, the selection of the basis functions is difficult, and various statistical methods have been investigated. Brunton et al. [142] used a manual selection of a threshold that gives an appropriate set of basis vectors for each problem, although the bias induced by the implicit regularization is a limitation. Ben Abdessalem et al. [143] investigated the performance of various approximate Bayesian computations for the purpose of model selection. Their method exploits a predefined dictionary of candidate nonlinear models, but possible combinations of candidate models are missed. In addition, due to the recursive numerical simulation required to select the appropriate model, their method has a high computational cost. Considering the limitations of model selection, an empirical approach (i.e. expert engineer) to make a proper estimate for the type of nonlinearity based on the experimental observation is still a reliable option for nonlinear model identification methods. Exploiting engineering insight avoids the high computational costs of an extensive dictionary of candidate basis functions. This approach forms the basic assumption for a large number of parametric identification methods ([146]-[149]). Although using incorrect nonlinear functions as the assumed type of nonlinear force may lead to inaccurate model identification, using this approach significantly reduces the computational costs. Furthermore, this approach ensures that the selected mathematical model for the nonlinear structure under study is physically meaningful.

Methods of non-parametric model identification and parameter estimation of assumed models are both important in the analysis of nonlinear systems. For many systems, such as nonlinear springs or

frictional contact interfaces, it is straightforward to estimate the nature of the model and the important part in characterizing nonlinear model identification. For instance, there are well known models such as the Coulomb friction model, the Lu-Gre model, the Dahl model, the Valanis model, the Iwan model, and the Maxwell slip model, which are usually used in modelling contact interfaces. Using an appropriate identification approach that leads to physically justifiable parameters for these models is also important in structural dynamics.

Accurate knowledge of the properties of the underlying linear system of the nonlinear structure is another important issue. Updating the underlying linear model of nonlinear structures exploiting experimental data obtained from very low-amplitude excitation tests is a practical approach and widely used ([147]-[149]). However, this approach may not be applicable to systems with non-smooth nonlinearities such as Coulomb friction. Some identification methods characterize the mathematical model of nonlinear structures without knowledge of the underlying linear system. The physics of the underlying linear system may be modelled and the parameters estimated or updated during the nonlinear identification process.

Guisquet and Amabili [149] presented a procedure to characterize the nonlinear damping and stiffness parameters of a single-degree-of-freedom model using large-amplitude experimental data obtained from a continuous system excited by a harmonic force. They based the parameter estimation of the presented procedure on the harmonic balance method in which they approximate the nonlinear model using a Fourier expansion with different truncation orders. The procedure requires the type and location of the nonlinearities to be known a-priori and the underlying linear system to be updated.

2.5 Equivalent Dynamic Stiffness Mapping Technique

The equivalent dynamic stiffness mapping (EDSM) technique presented by Wang and Zheng [125] is used in this thesis to investigate the effect of different sources of inaccuracy on the results of identification. Hence this method is explained in detail in this section.

This method exploits the experimental data obtained from harmonic excitation in frequency domain to identify the unknown internal forces of structures. The method benefits from the concept of dynamic stiffness. The dynamic stiffness is introduced as the inverse of transfer function obtained using measured displacement, [137]. The dynamic stiffness includes the inertia, damping and stiffness of a linear system. The equivalent dynamic stiffness in the EDSM technique utilizes the same concept to linearize the unknown nonlinear force. The approach is based on mapping a curve/surface to the equivalent dynamic stiffness of the unknown linear/nonlinear internal forces obtained from measured force and response. To this end, some candidate basis functions are selected. Then, the equivalent stiffness and damping of the candidate basis functions are utilized to map a mathematical model to the experimental data. The

governing equation of a general nonlinear dynamical system can be considered as,

$$\mathbf{M}\ddot{\mathbf{x}} + \mathbf{C}\dot{\mathbf{x}} + \mathbf{K}\mathbf{x} + \mathbf{f}_{nl}(\mathbf{x}, \dot{\mathbf{x}}) = \mathbf{F}(t) \tag{2.1}$$

where $\mathbf{M}$, $\mathbf{C}$ and $\mathbf{K}$ are mass, damping and stiffness matrices, respectively. $\mathbf{F}(t)$, $\mathbf{x}(t)$ and $\mathbf{f}_{nl}(\mathbf{x}, \dot{\mathbf{x}})$ are respectively the applied force, response and nonlinear restoring force vectors. The external applied force is considered to be harmonic, i.e. $\mathbf{F}(t) = \mathbf{F}_{ex}e^{j\omega t}$. In addition, in many practical engineering applications, the sub-harmonics and super-harmonics of the response of the structure are mitigated so that the response can be assumed to be dominated by its primary harmonic. Therefore, the EDSM technique utilizes this assumption and considers a single-harmonic response, as $\mathbf{x}(t) = \mathbf{X}e^{j\omega t}$. Also, the EDSM technique assumes the nonlinear force could be expanded in a Fourier series considering only the primary harmonic, as $\mathbf{f}_{nl}(\mathbf{x}, \dot{\mathbf{x}}) = \mathbf{F}_{NL}e^{j\omega t}$. This is a key for this approach, as it utilizes this assumption to obtain the equivalent dynamic stiffness of linear/nonlinear basis functions using the Fourier Integral. By substituting the assumed force and response vectors into Eq. (2.1) one obtains,

$$\mathbf{F}_{NL} = \mathbf{F}_{ex} - \left(\mathbf{K} + j\omega\mathbf{C} - \omega^2\mathbf{M}\right)\mathbf{X}, \tag{2.2}$$

where $\mathbf{F}_{ex}$ and $\mathbf{X}$ are the vectors of the external force and the response of the system in the frequency domain and $j = \sqrt{-1}$. As the type of nonlinearity is unknown, it is assumed to be composed of both nonlinear stiffness and nonlinear damping as

$$\mathbf{F}_{NL} = \mathbf{D}_{eq}\mathbf{X} = \left(\mathbf{K}_{eq} + j\omega\mathbf{C}_{eq}\right), \tag{2.3}$$

where $\mathbf{K}_{eq}$ and $\mathbf{C}_{eq}$ denote, respectively, the equivalent stiffness and damping elements of the nonlinear internal force. The unknown Equivalent Dynamic Stiffness $\mathbf{D}_{eq}$ of the internal force is defined as the ratio of the nonlinear internal force to the displacement response of the system in the frequency domain. However, as the total number of unknowns in $\mathbf{D}_{eq}$ is more than the number of equations in Eq. (2.3), it cannot be solved as a system of linear equations. Indeed, the elements of $\mathbf{D}_{eq}$ at which there is no nonlinear element should be zero. In addition, $\mathbf{D}_{eq}$ is a symmetric matrix, and thus, in case of ungrounded (connected) nonlinearities between two DOFs i and j, $D_{eq_{ij}} = D_{eq_{ji}}$. Therefore, instead of solving Eq. (2.3) as a system of equations to find the matrix $\mathbf{D}_{eq}$, it is solved individually for each nonlinear element.

It is taken for granted that prior to the characterization of the nonlinear element, the exact location of the nonlinearity, i.e. whether it is grounded or ungrounded and the involved DOFs, has been determined. Accordingly, for grounded nonlinearities, in which only one degree of freedom is involved, the equivalent

Table 2.1: Different types of internal forces and their ideal equivalent dynamic stiffness.

Type of internal force	Exact internal force	Ideal Equivalent Dynamic Stiffness
Linear stiffness	$f_{NL} = kx$	$D_{eq} = k$
Viscous damping	$f_{NL} = c\dot{x}$	$D_{eq} = j\omega c$
Quadratic stiffness	$f_{NL} = kx\|x\|$	$D_{eq} = \frac{8}{3\pi}k\|X\|$
Quadratic stiffness	$f_{NL} = kx\|\dot{x}\|$	$D_{eq} = \frac{4}{3\pi}k\omega\|X\|$
Cubic stiffness	$f_{NL} = kx^3$	$D_{eq} = \frac{3}{4}k\|X\|^2$
Quadratic damping	$f_{NL} = c\dot{x}\|\dot{x}\|$	$D_{eq} = j\frac{8}{3\pi}c\omega^2\|X\|$
Quadratic damping	$f_{NL} = c\dot{x}\|x\|$	$D_{eq} = j\frac{4}{3\pi}c\omega\|X\|$
Cubic damping	$f_{NL} = c\dot{x}^3$	$D_{eq} = j\frac{3}{4}c\omega^3\|X\|^2$
Coulomb friction	$f_{NL} = \mu N\text{sign}(\dot{x})$	$D_{eq} = \frac{4j(\mu N)}{\pi\|X}$

dynamics stiffness $\mathbf{D}_{ii}$, is obtained as

$$D_{ii} = \frac{f_{N_i}}{X_i}, \tag{2.4}$$

The real and imaginary parts of the equivalent dynamics stiffness give the equivalent nonlinear stiffness $k_{eq_{ii}}$ and equivalent nonlinear damping $c_{eq_{ii}}$ of the nonlinear internal force,

$$k_{eq_{ii}} = \Re\left(D_{ii}\right), \quad c_{eq_{ii}} = \frac{\Im\left(D_{ii}\right)}{\omega}, \tag{2.5}$$

For the case of ungrounded (connected) nonlinearities the relations of Eqs. (2.4) and (2.5) become

$$D_{ij} = \frac{f_{N_i}}{X_i - X_j}, \quad k_{eq_{ij}} = \Re\left(D_{ij}\right), \quad c_{eq_{ij}} = \frac{\Im\left(D_{ij}\right)}{\omega}, \tag{2.6}$$

where D_{ij}, $k_{eq_{ij}}$, and $c_{eq_{ij}}$ are the element of dynamic stiffness, equivalent nonlinear stiffness, and equivalent nonlinear damping between DOF-i and DOF-j. Then, candidate basis functions are used to fit a curve/surface to the equivalent stiffness and damping data points obtained from Eqs. (2.5) and (2.6). To this end, Fourier Integrals of the candidate basis functions form the analytical equivalent dynamic stiffness of the assumed nonlinear force. Table 2.1 includes different types of linear and nonlinear internal forces and their ideal equivalent dynamic stiffness obtained using Fourier Integral [125]. Comparing the experimentally measured equivalent dynamic stiffness of Eqs. (2.4) and (2.6) with the analytical equivalent dynamic stiffness obtained from Fourier Integral of basis functions, unknown parameters of the mathematical model of the nonlinear internal force are estimated.

It is worth mentioning that the EDSM technique is based on some assumptions and has some limitations:

- As the identification procedure of the described method utilizes deterministic FRFs, the method requires steady state responses. Therefore, it should be ensured that the steady state response is measured and used in the calculations.
- All of the coordinates are required to be known. If some DOFs are not measured, they should be estimated utilizing an expansion method (e.g. SEREP) that may result in some inaccuracy.
- The method is based on the assumption that the primary harmonic is dominant and all other harmonics of the response are neglected.
- In practical systems, particularly in multi-DOF systems with strong nonlinearities and a flexible structure, there may be ill-conditioning problems in calculating the equivalent dynamic stiffness.

2.6 Motivation

This chapter gives an overview of the nonlinear identification methods, the strengths and weaknesses of the introduced methods, and also the research gap in the field of model identification in structural dynamics. The literature review reveals the lack of enough research work focused on the effect of various sources of inaccuracy on the outcome of the identification process. To have an identified model of nonlinear structures, it is important to understand not only the structure itself, but also the factors affecting the accuracy of the identified model. Indeed, recognizing the sources of error helps to know the reason of possible inaccuracy in the identification results. Another lack in the literature of structural identification methods is related to an approach that deals with high number of complex nonlinearities with high accuracy and relatively low computational costs. The methods in the literature suffer either from high computational costs [81, 134], complexity of application [149], incapable of dealing with complex nonlinearities [143, 135], or some limitations such as the implicit regularization bias [142] or neglecting higher harmonics [125]. The model selection, its complexity, and relatively high computational cost resulted by model selection procedures is another problem that many of identification methods encounter with. In addition, using a pool of candidate basis functions leads to ignore some possible nonlinear functions out of the candidate pool. Therefore, this is a necessity in structural dynamics to develop an identification method that can give a simplicity of application and deals with different types of smooth and non-smooth nonlinearities in various MDOF nonlinear systems with low computational costs and high accuracy. The objectives of the current thesis are based on the aforementioned research gap and are described in the following section.

2.7 Thesis Objective

Identification of nonlinear structural dynamics has received a significant attention during last decades. Yet, there are many aspects of the identification methods of nonlinear structural models to be improved. For example, in spite of a vast majority of research works dedicated to modelling the jointed structures, the dynamic behavior in the joint contact interfaces is not still well-understood. Another lack in the nonlinear identification is dealing with different sources of inaccuracy such as expansion error and neglecting higher harmonics.

The main objective of this study is to introduce novel identification approaches for nonlinear structures. The very first step in identification process of structural nonlinear elements is to detect their exact location. It is shown in this study how to detect the location of a localized structural nonlinearity. Having the exact location of nonlinear elements, identification methods are utilized to identify and characterize the mathematical model of nonlinear structures. However, there are various sources of noise and error that may affect the accuracy of the identified model. For example, it is common in practice to have incomplete measurement due to lack of enough equipment or difficulty in accessing some parts of structures such as joint interfaces. Therefore, various expansion methods are exploited to estimate the response of the structure at unmeasured coordinates. Using linear expansion methods such as SEREP to estimate unmeasured response of nonlinear systems may result in error in the estimated response, and eventually leads to inaccurate mathematical model. Other than this, sources of inaccuracy include, but not limited to, measurement noise, modelling error, and neglecting higher harmonics. In this study, the sensitivity of identification methods is investigated to measurement noise and different sources of error.

According to the significance of various sources of inaccuracy in the results of identification process, one may aim to avoid these types of error. To this end, one solution is developing an optimization-based framework for identification of nonlinear structures. To avoid the expansion error, the necessity of estimating the unmeasured coordinates using expansion methods should be removed. Also, the accuracy of the method should not be dependant to considering all the contributing harmonics to the response of the system. Developing such a method to achieve the aforementioned objectives is aimed in this study.

Although optimization-based identification method is always an option for structural dynamics, utilizing such methods to characterize the mathematical models with large number of unknown parameters would be computationally expensive. Besides, identifying the mathematical model using only the primary harmonic (i.e. neglecting higher harmonics) in the structures with multi-harmonic response and force may lead to erroneous results. Therefore, it is aimed in this study to introduce a parameter estimation method for identification of nonlinear structures in the presence of multi-harmonic response and force. For this purpose, a method with two different approaches is introduced: Analytical Harmonic-Balance-based (AHB) approach and the Alternating Frequency/Time approach using Harmonic Balance (AFTHB). The AHB approach is based on expanding the nonlinear functions in frequency domain utilizing analytical

methods such as Fourier Integral (FI), Complex Averaging (CXA) technique or Harmonic Balance Method (HBM). This approach exploits the measured data in the frequency domain. In AFTHB approach, on the other hand, the nonlinear functions are expanded in the frequency domain by calculating the Fourier Transform of the measured time response. It is shown that AHB approach is very accurate in theory if all significant harmonics of force and response are taken into account. Nevertheless, it is often cumbersome to include all significant harmonics of the response in the analytical expansion of nonlinear functions. Besides, it would be difficult to use AHB for the structures with complex forms of nonlinearities such as Coulomb friction and also for multi-DoF nonlinear systems. Therefore, the AFTHB approach is developed based on the corresponding method used for harmonic balance. The proposed method is based on the following assumptions:

- The method requires the nonlinear functions to describe the nonlinear restoring forces in the model to be known a-priori. Engineering insight to know the appropriate type of nonlinearity in the system is essential to guarantee the accuracy of the identified nonlinear model.
- The underlying linear model of the structure is updated using the experimental data obtained from very low-amplitude excitation tests prior to the nonlinear identification process. Keeping the excitation amplitude at a very low level assures the nonlinearities of the structure are not excited. However, the proposed method is also able to estimate the parameters of the underlying linear model during the nonlinear identification process.

According to the discussion made in this section, the optimization-based method introduced in Chapter 5 and the methods proposed in Chapter 6 are categorized as parametric methods that require a-priori assumptions of the type and location of the nonlinearities.

2.8 Closure

In this chapter, a literature review on different identification methods has been provided. In addition, a discussion was made on the comparison between parametric and non-parametric approaches. The Equivalent Dynamic Stiffness Mapping (EDSM) technique was described in this chapter as a method that is used in the present work. At the end of this chapter, the objectives of the present thesis have been explained.

Chapter 3

Localization of Structural Nonlinearity Using Base Excitation Tests

3.1 Introduction

Almost all engineering structures have nonlinearities coming from various sources such as nonlinear material, geometry, or joints. Of these structures, many can be properly linearized using conventional theories, as their nonlinearities are weak enough to be ignored. However, on the other hand, in many applications the nonlinearity is stronger than to be neglected. Hence, in order to have an accurate prediction of the behaviour of the system, the nonlinear model required to be identified and characterized.

This chapter is focused on localization of structural nonlinearities utilizing the experimental data. To this end, a localization process is developed based on the method introduced by Wang et al. [40] to detect the exact location of nonlinear structural elements utilizing the experimental results obtained from base excitation vibration tests. The localization process is applied to a nonlinear system composed of a cantilever beam subjected to an electromagnetic nonlinear force at the tip. For this purpose, base motion of the shaker bed is used as base excitation of the cantilever beam. A combination of two pairs of electromagnets and permanent magnets generates a nonlinear force which is applied to the tip of the cantilever beam. A symmetric configuration is designed with permanent magnets attached to the free end of the cantilever beam, while a pair of electromagnets is placed on the two sides of the permanent magnets. A base motion with constant amplitude of acceleration is utilized to excite the cantilever beam. The responses obtained from low-amplitude base motion are exploited to update the underlying linear

system. There are many well-developed linear model updating methods in the literature, [6, 10, 150], to be used for this purpose. Using the updated model of the underlying linear system along with the nonlinear response of the structure resulting from high-amplitude excitation, the exact location of the nonlinear element is detected using the developed localization process based on the method introduced by Wang et al. [40].

3.2 Numerical Case Study

A stainless steel cantilever beam shown in Figure 3.1 with the length 0.30 m, width 30 mm, and thickness 1.5 mm has been considered for numerical simulation. The modulus of elasticity and the density of the beam are taken as $E = 205$ GPa and $\rho = 7800$ kg/m^3, respectively.

The equation of motion of the system of cantilever beam of Figure 3.1 is derived using the finite element method.

$$\mathbf{M}\ddot{\mathbf{w}} + \mathbf{C}\dot{\mathbf{w}} + \mathbf{K}\mathbf{w} + \mathbf{f}_{NL}\left(\mathbf{w}, \dot{\mathbf{w}}\right) = \mathbf{f}_b(t) \tag{3.1}$$

where $\mathbf{M}$, $\mathbf{C}$, and $\mathbf{K}$ denote, respectively, the mass, damping, and stiffness matrices of the underlying linear system of the structure, $\mathbf{w}$, $\dot{\mathbf{w}}$, and $\ddot{\mathbf{w}}$ are the relative displacement of the beam with respect to the base motion and its time derivatives, respectively, $\mathbf{f}_{NL}$ is the nonlinear internal force which is assumed to be a linear-cubic stiffness, and $\mathbf{f}_b(t)$ is the equivalent force vector of the base excitation which is applied to the structure. The mass and stiffness matrices of two-node linear Euler-Bernoulli beam elements are [3],

$$\mathbf{M}_e = \frac{\rho A L_e}{420}\begin{bmatrix} 156 & 22L_e & 54 & -13L_e \\ 22L_e & 4L_e^2 & 13L_e & -3L_e^2 \\ 54 & 13L_e & 156 & -22L_e \\ -13L_e & -3L_e^2 & -22L_e & 4L_e^2 \end{bmatrix} \tag{3.2}$$

and

$$\mathbf{K}_e = \frac{EI}{L_e^3}\begin{bmatrix} 12 & 6L_e & -12 & 6L_e \\ 6L_e & 4L_e^2 & -6L_e & 2L_e^2 \\ -12 & -6L_e & 12 & -6L_e \\ 6L_e & 2L_e^2 & -6L_e & 4L_e^2 \end{bmatrix} \tag{3.3}$$

Calculating the global mass and stiffness matrices using Eqs. (3.2) and (3.3), and considering proportional damping for the cantilever beam, the damping matrix can be written as,

$$\mathbf{C} = \alpha\mathbf{M} + \beta\mathbf{K} \tag{3.4}$$

where α and β are proportional damping coefficients. In this example,

$$\alpha = 2.5 \times 10^{-1}, \quad \beta = 2.5^{-5}. \tag{3.5}$$

Point masses $p_m = 6, 6, 6, 8$ g are located at positions $x_m = l/6, 3l/6, 5l/6, l$, respectively, where l is the length of the beam. The tip of the beam is attached to a grounded nonlinear spring. The nonlinear spring is assumed to have a linear-cubic stiffness creating the nonlinear restoring force as

$$F_N = k_l w(l,t) + k_N w^3(l,t), \tag{3.6}$$

where

$$k_l = 20 \ \frac{N}{m}, \quad k_N = 3.5 \times 10^5 \ \frac{N}{m^3}. \tag{3.7}$$

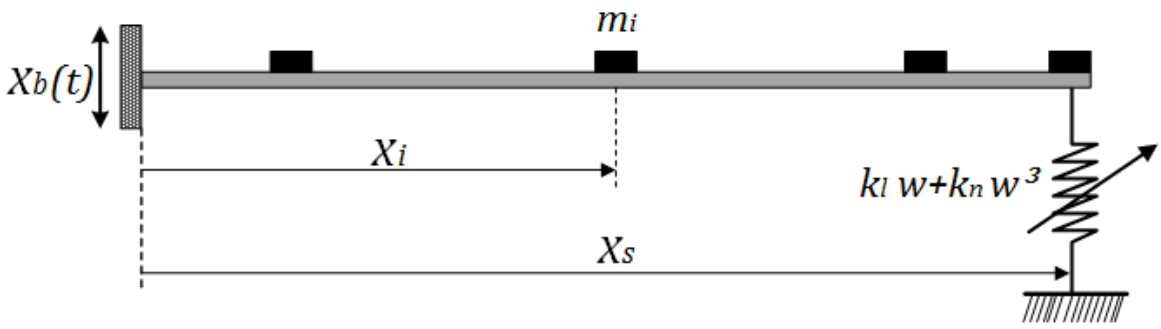

Figure 3.1: Base excitation of a cantilever beam with a nonlinear force at the tip.

The finite element model of the system is obtained utilizing 6 two-node Euler-Bernoulli beam elements. It is assumed that the measurement is spatially incomplete so that the responses of the beam are measured only at DOFs 1, 5, and 9 (having distances 5, 15, and 25 cm from the clamped end of the beam, respectively).

3.3 Experiment Case Study

In this section, the experimental set-up is presented. The structure under study, the excitation mechanism, the measurement equipment, and the attachments are explained. Then, the assumed mathematical model of the experimental set-up is given.

3.3.1 Experimental Set-up

The experimental setup considered in this study and its finite element schematic are shown in Figure 3.2. The main structure in this setup is a steel cantilever beam. A pair of permanent magnets are attached

Table 3.1: Geometry and material properties of the experimental setup.

Parameters (unit)	value
Length of cantilever beam, l (m)	0.3
Width of cantilever beam, d (m)	0.03
Thickness of cantilever beam, t (m)	0.0015
Density of cantilever beam, ρ $\left(\frac{\text{kg}}{\text{m}^3}\right)$	7800
Modulus of elasticity of the cantilever beam, E (GPa)	193
Mass of each accelerometer (g)	8
Each permanent magnet mass, m_p (g)	4
Permanent magnet pull strength, *N42* Neodymium magnets (kgf)	2
Electromagnet pull strength (kgf)	25
Applied voltage to electromagnets, V (V)	20
Initial gap between electromagnets and permanent magnets (cm)	6

to the tip of the beam and two electromagnets are located symmetrically on both sides of the permanent magnets, as shown in Figure 3.2. At the equilibrium position of the cantilever beam, symmetric 6-cm gaps exist between the two pairs of permanent and electromagnets. Attractive magnetic forces are created in the electromagnets by applying a voltage level of 20 V to the two electromagnets. These two pairs of permanent magnets and electromagnets generate a nonlinear electromagnetic restoring force which is applied to the tip of the cantilever beam. The cantilever beam is attached to the shaker bed and is excited by the base motion of the shaker with constant acceleration. Stepped-sine excitation is utilized to measure the nonlinear response of the structure. The displacement of the shaker bed is measured using an accelerometer attached to the shaker, while three other accelerometers are used to measure the translational degrees of freedom 1, 5, and 9, shown in the schematic in Figure 3.2. These accelerometers have masses of 8 g and attached to the beam as shown in Figure 3.2. Table 3.1 contains the geometry and material properties of the experimental setup. The pull strength of a permanent magnet and electromagnet in Table 3.1 is the highest possible holding power of a magnet, measured in kgf (kilogram force) or lbf (pound force), [151].

The following section derives a nonlinear mathematical model for the cantilever beam system in Figure 3.2.

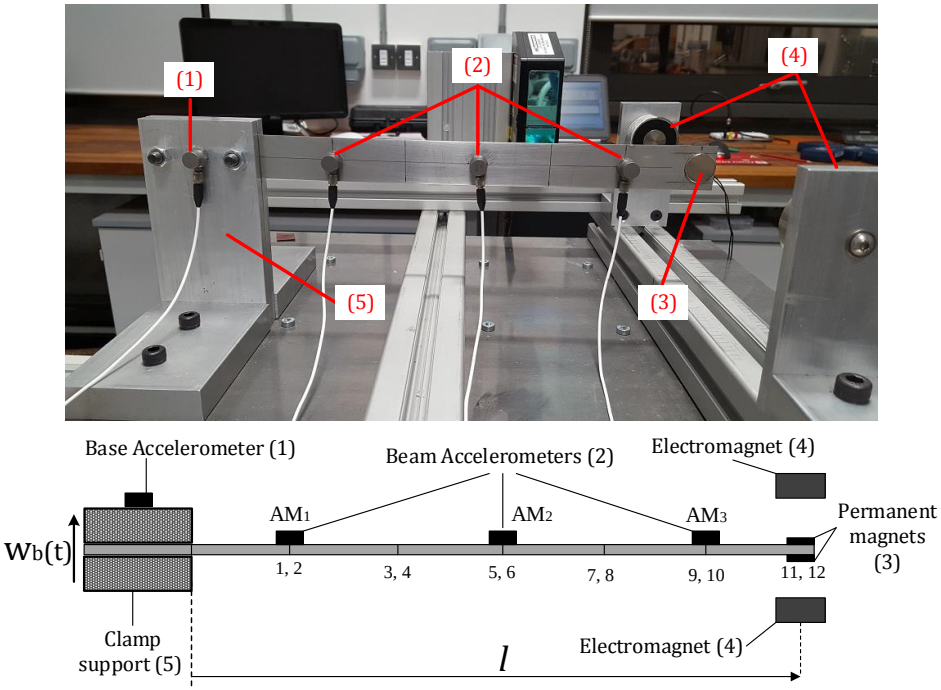

Figure 3.2: Test-rig assembly and its finite element schematic.

3.3.2 Mathematical Model

Considering a cantilever beam with Young's modulus E, density ρ, length L, width d, and thickness h, subjected to base excitation, the finite element model of the structure shown in Figure 3.2 can be obtained as Eq. (3.1) using Euler-Bernoulli beam theory. The mass and stiffness matrices of two-node linear Euler-Bernoulli beam elements are obtained as Eqs. (3.2) and (3.3).

Calculating the global mass and stiffness matrices using element matrices of mass and stiffness, proportional damping is considered for the cantilever beam as in Eq. (3.4).

Another important issue is to consider the effect of the aluminium L-shaped clamp to which the cantilever beam is attached. In fact, the beam under investigation is clamped between two short thick aluminium beams. These two aluminium support beams act like two very stiff springs attached to the base of the steel beam. Although the clamp is very stiff and will not undergo large deflections, it is not completely rigid. The high stiffness of the clamp may cause significant changes in the frequency response of the system, particularly in the frequencies of the resonances and anti-resonances of the system. Therefore, the effect of the very high stiffness of the clamp is simulated by a linear spring between the shaker bed and the base of cantilever. This linear spring represents the bending stiffness of the L-shaped clamp. It is worth noting that the deflection of the L-shaped clamp is in the same direction of the motion of the beam and rotational motion of the clamped support is in torsional direction of the beam (as seen in Figure 3.3). Because the torsional motion of the beam is not considered in this study, there is no need for a rotational spring representing torsional degree of freedom of the beam. All bolted joints assumed to be rigidly connected in this model. Furthermore, the equivalent masses of two aluminium support beams are taken into account as an additional mass. Figure 3.3 illustrates the equivalent system of the beam subject to the motion of shaker bed. The torsional deflection of the L-shaped clamp is assumed to be negligible; the beam does not have any rotation at the base. Hence, the assumed mode shapes of the cantilever are used to simulate the dynamics of the beam. Equivalent mass m_b and linear stiffness k_b of the aluminium beams can be estimated by the following equations, [137].

$$m_b = \frac{33}{144}\left(\rho_{Al} V_{Al_b}\right), \quad k_b = \frac{3 E_{Al} I_{Al_b}}{L_{Al_b}^3}, \tag{3.8}$$

where ρ_{Al} and E_{Al} are density and modulus of elasticity of aluminium, respectively. V_{Al_b}, I_{Al_b}, and L_{Al_b} denote, respectively, the volume, the second moment of area, and the length of each aluminium support beam.

As explained in Section 3.3.1, the excitation method used in this study is base excitation. In other words, there is no explicit force vector applied on the structure. In fact, the base movement is transferred to the structure and makes it oscillate. The equivalent force of base excitation applied on the structure

is [10],

$$\mathbf{f}_b(t) = -\ddot{z}_b \mathbf{M}\mathbf{g}, \tag{3.9}$$

where $\mathbf{f}_b(t)$ denotes the equivalent force vector of base motion transferred to the structure, $\mathbf{M}$ is the mass matrix of the system, $\ddot{z}_b$ is the base acceleration in the time domain, and $\mathbf{g}$ is the force coordinator vector defined as,

$$g_i = \begin{cases} 1, & \text{if } z_i \text{ and } z_b \text{ are in the same direction,} \\ 0, & \text{if they are not in the same direction.} \end{cases} \tag{3.10}$$

where z_i denotes the displacement at DoF-i.

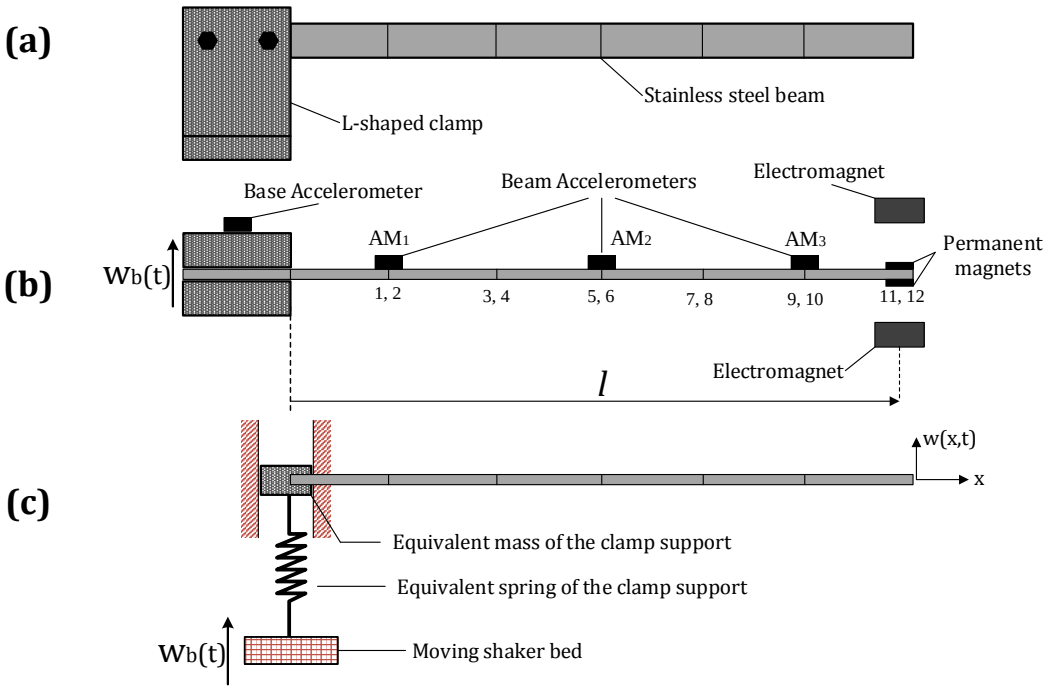

Figure 3.3: Schematic view of the experimental test-rig including side view (a) and top view (b) of the beam attached to the shaker bed; (c) the equivalent model of the system of shaker bed and cantilever beam.

3.4 Localization

In this study, the localization process introduced by Wang et al. [40] is developed for vibration tests with base excitation. This method is based on the comparison between the responses of the underlying linear system and the nonlinear system. Therefore, two types of vibration tests are required. One is the low amplitude excitation test which is used to update the model of the underlying linear system, and the other one is a high amplitude excitation test giving the nonlinear dynamics of the system required for the localization process.

Hence, the localization process is described below:

1. ***Linear model updating***: For both localization and identification of mechanical structures, an accurate model of the underlying linear system is required. Consequently, having any modelling error may lead to inaccuracy in the result of the localization or identification process. Hence, in order to reduce the modelling error to the lowest possible amount, the measured linear response of the system, obtained from low-amplitude excitation test, is used to update the preliminary model of the underlying linear system prior to start the localization process. To this end, there are a variety of linear model updating methods developed in the literature [6, 10, 150]. In this study, sensitivity-based linear model updating method presented by Mottershead et al. [6, 10, 150] is exploited to update the underlying linear model of the structure. For more details, one may refer to Ref. [6, 10, 150]. The updated underlying linear model is obtained as

$$\mathbf{M}\ddot{\mathbf{w}}(t) + \mathbf{C}\dot{\mathbf{w}}(t) + \mathbf{K}\mathbf{w}(t) = 0, \tag{3.11}$$

   where $\mathbf{M}$, $\mathbf{C}$, and $\mathbf{K}$ are updated mass, damping and stiffness matrices, respectively.

2. ***Data selection***: It is not necessary to take into account all of the data over the whole frequency span. Indeed, in order to accelerate the localization process, data selection is carried out to discard any unnecessary data. The localization process is based on the difference between the response of the nonlinear structure and its underlying linear system under the same excitation. Therefore, a high-amplitude excitation signal is applied to the structure to measure the nonlinear response of the system. On the other hand, having the updated underlying linear system, the measured high-amplitude excitation signal is applied to the system of Eq. (3.11) to simulate the linear response of the system. The deviation vector ε_{nl} of the measured nonlinear response from the simulated linear response is defined as

$$\varepsilon_{nl} = \mathbf{w}_{nl}^{ex}(\omega) - \mathbf{w}_{l}^{sim}(\omega), \tag{3.12}$$

where ω denotes the frequency of the harmonic excitation. $\mathbf{w}_{nl}^{ex}(\omega)$ and $\mathbf{w}_{l}^{sim}(\omega)$ are, respectively, the measured nonlinear response of the nonlinear structure and the simulated linear response of the underlying linear system in the frequency domain under the same high-amplitude excitation. ε_{nl} is measured in the frequency domain over a range of excitation frequency in which the nonlinear behaviour of the structure is measured. The frequency range may include some frequencies at which the different between the nonlinear response and the response of the underlying linear system is not significant. The measured data at these frequencies are discarded to reduce the computational costs. To do this, a criterion is chosen to select the measured data for the localization process. The criterion is defined to guarantee that the effect of the nonlinearity on the dynamics of the structure is significant enough and is

$$\left\|\varepsilon_{nl}\right\|_{\infty} > \delta_c \tag{3.13}$$

where $||\square||_{\infty}$ represents the infinity norm, and δ_c is the threshold for the defined criterion. To minimize the effect of measurement noise and modelling error, δ_c is taken as [152],

$$\delta_c = \left\|\mathbf{w}_{nl}^{ex}\right\| \times (2 \sim 5\%), \tag{3.14}$$

where $||\square||$ denotes the Euclidean norm.

3. ***Nonlinear force assessment***: The method does not require complete spatial measurement at all coordinates. However, the effect of unmeasured degrees of freedom are considered in this method. Accordingly, the coordinates of the system are categorized into measured and unmeasured regions:

$$\mathbf{w} = \begin{Bmatrix} \mathbf{w}_m \\ \mathbf{w}_u \end{Bmatrix}, \tag{3.15}$$

where the indices m, u represent the measured and unmeasured DOFs, respectively. The measured degrees of freedom are expanded by the SEREP expansion method to predict the response of the system at unmeasured coordinates. However, since SEREP is a linear method, using this method for nonlinear systems may lead to some error in the results. This problem will be addressed in Chapter 4 of the thesis, and the error that results from the application of the linear SEREP method to expand the measured response of the nonlinear systems will be investigated. The unmeasured DOFs are projected onto the measured region using the Craig-Bampton reduction method, Section 1.6.2. Consequently, through a series of simple mathematics [36], the reduced nonlinear force (RNF) is calculated as a summation of measured nonlinear forces and the projection

of unmeasured nonlinear forces onto the measured region.

$$\mathbf{F}_{reduced} = \mathbf{F}_{eq_H} - \left(\mathbf{D}_{mm} - \mathbf{D}_{mk}\mathbf{D}_{kk}^{-1}\mathbf{D}_{km}\right)\mathbf{w}_m, \tag{3.16}$$

where $\mathbf{F}_{eq_H}$ denotes the force vector equivalent to the high-amplitude base excitation. $\mathbf{D}_{mm}$, $\mathbf{D}_{mk}$, $\mathbf{D}_{kk}$, $\mathbf{D}_{km}$ are dynamic stiffness sub-matrices computed using truncated mass, damping, and stiffness matrices obtained from Craig-Bampton method, Section 1.6.2.

$$\mathbf{D} = -\omega^2\mathbf{M} + j\omega\mathbf{C} + \mathbf{K}, \tag{3.17}$$

The index of the reduced nonlinear force is calculated as a summation of the amplitudes of the RNFs at the measured DOFs over a range of measured frequencies,

$$\mathbf{I}_{\mathbf{F}^*_{reduced}} = \sum_{\omega_i} |\mathbf{F}^*_{reduced}(\omega_i|\,, \tag{3.18}$$

The suspect region for the location of the nonlinearity is determined using the resulting RNFs, the index of the RNFs, and the phase of the RNFs. Consequently, the preliminary decision for the location of the nonlinear elements is made by minimizing the residual J_{err},

$$\mathbf{F}_{suspect} = \text{ArgMin}\left\|J_{err}\right\|, \tag{3.19}$$

where

$$J_{err} = \left[\boldsymbol{\Psi}_{um}^T\mathbf{B}_u \;\; \mathbf{B}_m\right]\mathbf{F}_{suspect} - \mathbf{F}_{reduced}, \tag{3.20}$$

and $\mathbf{B}_u$ and $\mathbf{B}_m$ are the input matrices for the unmeasured and measured DOFs in the suspect region, respectively. $\boldsymbol{\Psi}_{um}$ denotes the matrix of constraint modes in the Craig-Bampton reduction method, Section 1.6.2.

4. ***Verification***: Finally, the result of the location is verified by comparing the nonlinear forces for the suspected region with the reduced nonlinear forces for the measured region

$$\left\|J_{err}\right\| \ll \left\|\mathbf{F}_{reduced}\right\|, \tag{3.21}$$

The criterion of Eq. (3.21) is required to be satisfied for the results of localization process to be valid.

3.5 Results and Discussion

3.5.1 Numerical Case Study

Using direct time integration in MATLAB, the time responses of the system of Figure 3.1 were obtained. To obtain the steady state response, the computation is performed for 300 cycles with a time step of 1/1000 of each cycle. To ensure the transient response has completely decayed, the first 250 cycles of computation at each frequency are discarded. Utilizing the Fourier Transform in MATLAB, the steady state response of the system is obtained in the frequency domain.

Figure 3.4 illustrates the measured frequency domain steady state responses of the beam at the three measured points. The response is shown as the ratio of the displacement with respect to the amplitude of the base acceleration. Applying low amplitude base excitation led to the underlying linear system to be excited, without exciting the nonlinearity of the system, as shown in Figure 3.4 in blue color. The high amplitude sweep-up stepped-sine excitation resulted in nonlinear behaviour of the system, shown by red circles in Figure 3.4.

The localization process is applied to the simulated data and resulted in the reduced nonlinear forces of three measured DOFs shown in Figure 3.5(a). As it can be seen in Figure 3.4, there's a considerable difference between the response amplitude of the linear and nonlinear behaviour of the beam within the frequency span of [11.5-14.75] (Hz). Therefore, the data within the frequency range of [11.5-14.75] (Hz) was selected during the data selection step.

Figure 3.6 shows the index of the RNFs of the measured DOFs. The magnitude of the indices of three measured DOFs indicates that the nonlinearity of the system may be closer to node 5 (i.e. DOF 9). However, there's a possibility of existence of more than one nonlinearity.

Looking at the phase diagram of the RNFs, one can see the same phase at DOFs 1 and 9, and π rad of phase difference at DOF 5 with respect to DOFs 1 and 9. Then, it can be concluded that all of these RNFs at DOFs 1, 5, and 9 are produced by a nonlinearity at an unmeasured DOF. Therefore, DOFs 1, 5, and 9 are discarded from suspect region. Therefore, the RNFs are calculated at DOFs 3, 7, and 11, as the suspected region, using the linear constraint modes of the Craig-Bampton reduction method [86]. The indices of calculated RNFs, depicted in Figure 3.7, indicates the existence of a nonlinear element at DOF-11.

Figure 3.8 illustrates the indices of RNF at DOFs 1, 5, 9, and 11 with direct measurement at DOF 11. This shows that the nonlinear element is truly located at DOF 11, which in accordance with the result of preliminary location decision.

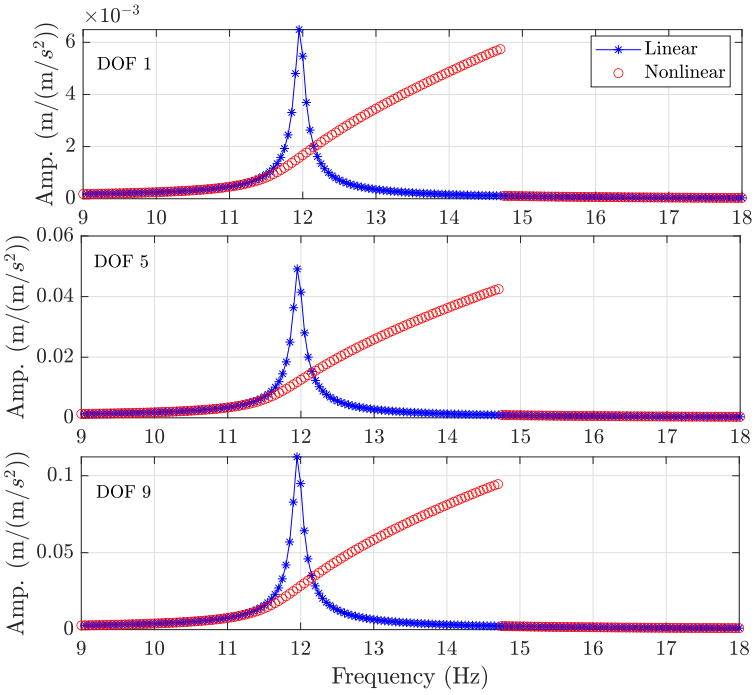

Figure 3.4: Frequency-response amplitude at DOFs 1, 5, and 9; Blue line-star: Linear response (low amplitude excitation), red circles: Nonlinear response (high-amplitude excitation).

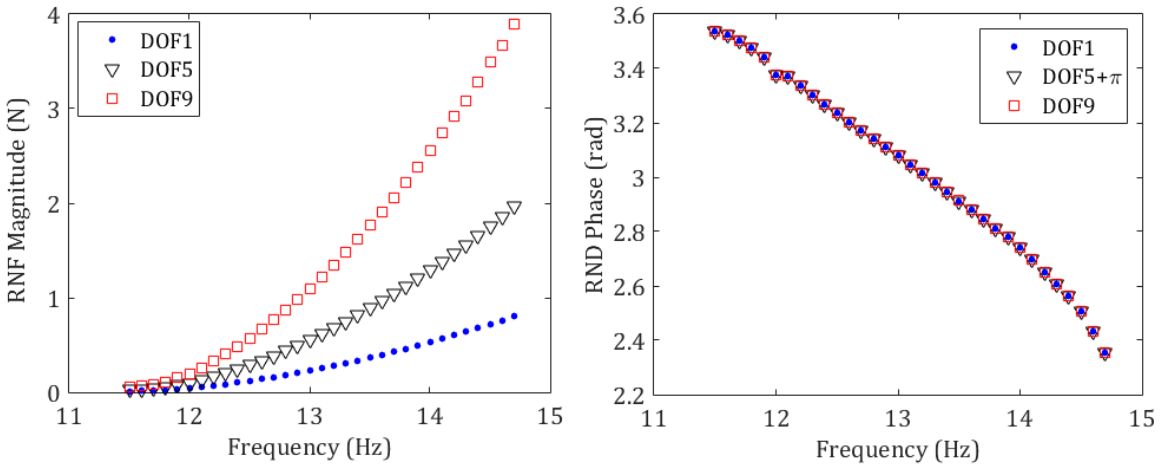

Figure 3.5: (a) Magnitude and (b) phase of the reduced nonlinear forces at the measured DOFs of the cantilever beam.

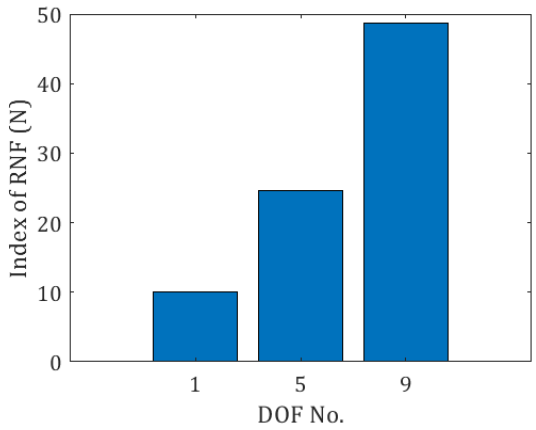

Figure 3.6: Indices of reduced nonlinear forces at measured DOFs 1, 5, and 9.

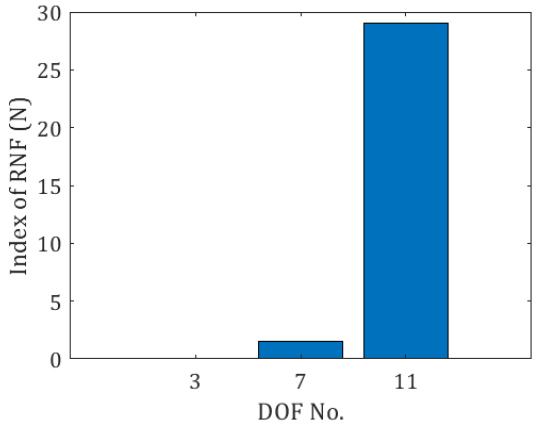

Figure 3.7: Indices of RNFs in the suspect region.

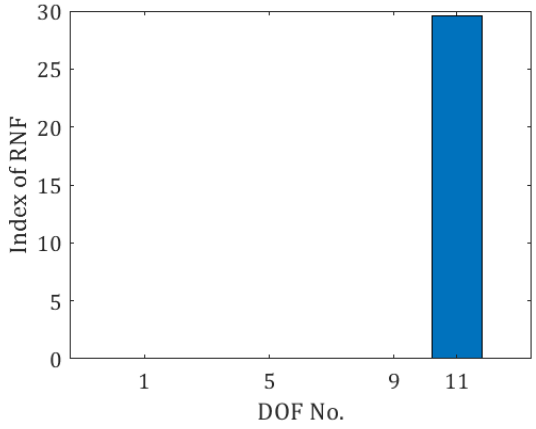

Figure 3.8: Indices of reduced nonlinear force including direct measurement at DOF11.

Table 3.2: Fixed and updated parameters of the underlying linear model.

	Description of Parameters (units)		Parameter values	
			Initial Values	Updated Values
Fixed Parameters	Mass of the accelerometers	m_a (kg)	0.008	–
	Mass of the permanent magnets	m_p (kg)	0.004	–
	Linear mass density of the beam	ρA $\left(\frac{\text{kg}}{\text{m}}\right)$	0.368	–
	Length of the beam	L (m)	0.3	–
Updated Parameters	Proportional damping coefficient	α $\left(\frac{\text{N.s}}{\text{m.kg}}\right)$	0.2	0.294
	Proportional damping coefficient	β (s)	1×10^{-5}	1.33×10^{-5}
	Flexural stiffness of the beam	EI $\left(\text{N.m}^2\right)$	1.741	1.64
	Equivalent stiffness of the clamp	k_b $\left(\frac{\text{N}}{\text{m}}\right)$	8.256×10^5	5.5×10^5
	Equivalent mass of the clamp support	m_b (kg)	0.1016	0.103

3.5.2 Experimental Case Study

The section gives the results and discussion for an experimental case study. First, a comparison is given between the numerically simulated response obtained using the updated linear model of the system and the experimentally measured linear response obtained from a low-amplitude test. After illustrating the results of the localization process, the application of the localization procedure on the present nonlinear structure is discussed.

As explained, in order to perform the localization process of the present study, two different sets of vibration tests are carried out; low amplitude and high amplitude tests. For the case of low amplitude vibration test, the shaker bed moves with constant acceleration with amplitude equal to 2% of the gravitational acceleration g. The excitation level for the high-amplitude test is sufficient to excite the nonlinearity of the structure. In this study, the base motion with a constant acceleration amplitude equal to 8% of the gravitational acceleration is used to measure the nonlinear response of the cantilever beam.

In order to minimize the effect of modelling error in the results of localization process, the underlying linear model of the structure is required to be updated using the measured data obtained from very low-amplitude vibration test. In this study, three parameters of the system (the flexural stiffness EI, base stiffness k_b, and the base mass m_b) are updated using the sensitivity-based updating method [126] and the first three natural frequencies. Then, experimentally measured damping ratio of the linear response of the system along with the sensitivity-based updating method for damping ratio is exploited to update the proportional damping coefficients α and β. Table 3.2 gives the values of all parameters of the structure considered in updating the underlying linear model.

The updating process has been repeated for 20 iterations. The values of updated parameters EI, k_b and m_b are shown in Figure 3.9 during the updating process. As illustrated in Figure 3.10, the updated numerical model is capable of predicting accurately the experimentally measured natural frequencies.

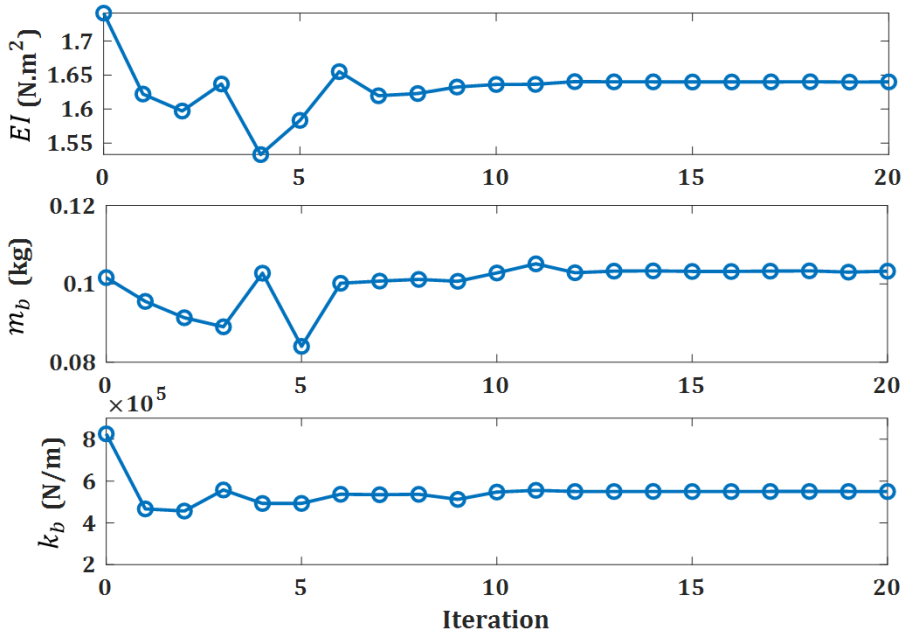

Figure 3.9: The parameters updated in the process of linear model updating.

The numerical linear frequency response of the structure is simulated exploiting the updated parameters of the underlying linear model. Figure 3.11 illustrates the numerically simulated frequency response in comparison with the measured dynamics of the structure at DOF1 within the frequency range (0-200) Hz, which includes the first three natural frequencies. The experimental results within the frequency range of 80 to 120 Hz shows inaccuracy in the measurement. This is due to insufficient samples for averaging the experimental measurement. Indeed, by taking a larger number of measurements and accordingly more samples for averaging the response, the effect of noise in the measured data will be reduced, and the experimental results will be cleaner. It is observed that the anti-resonance frequencies can be accurately predicted by the updated model, as well as the resonance frequencies. Here it should be mentioned that the updating process does not utilize the anti-resonance frequencies. As a result, the numerically updated results being in an excellent accordance with experimentally measured at both resonance and anti-resonance frequencies verifies the validity of the updated linear model. Figure 3.12 gives a comparison between the low-amplitude experimental and updated numerical linear responses at the vicinity of the first resonance, taking the effect of nonlinear electromagnetic force into consideration both in experimental and numerical results.

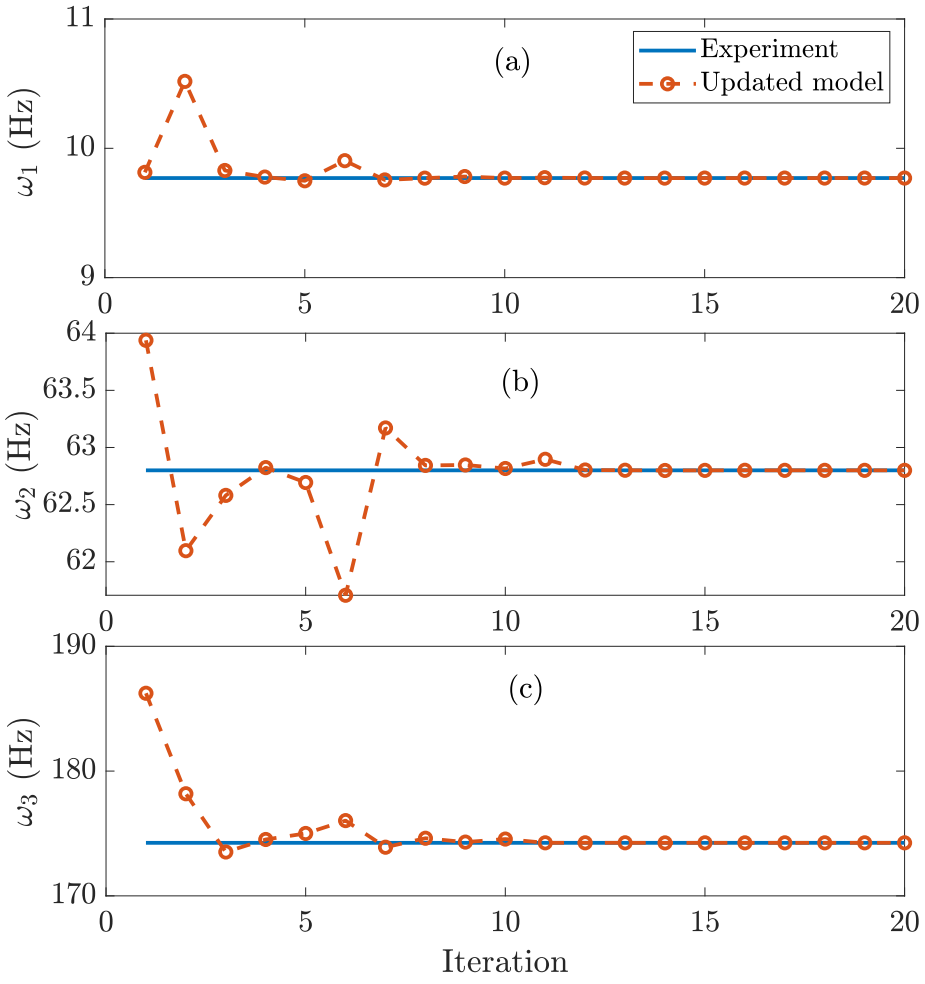

Figure 3.10: The numerical natural frequencies obtained using the updated linear model versus the experimentally measured ones.

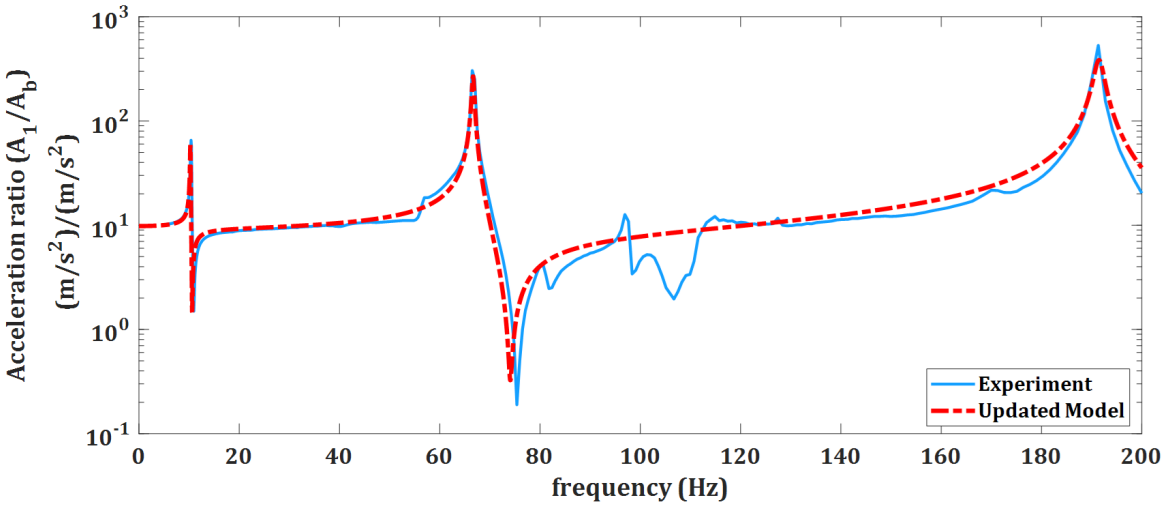

Figure 3.11: The experimentally measured frequency response compared with the updated numerical frequency response of the cantilever beam at DOF1. This figure shows the ratio of the amplitudes of accelerations as the frequency response of the structure.

After updating the linear finite element model, this linear model is used to detect the exact location of the nonlinear element of the structure. Utilizing the updated linear model and the experimental data from the high amplitude tests, the reduced nonlinear forces of the system are obtained according to the localization process. To this end, the structure is subjected to a constant acceleration base excitation with a large amplitude of 0.08 g. The high-amplitude constant acceleration of the movement of the shaker bed is shown in Figure 3.13 for the frequency span of 8.9 Hz to 11 Hz. It is worth mentioning that the interaction between the shaker and the dynamics of the system in the vicinity of the natural frequency may lead to a variation in the excitation level. Hence, a closed-loop (controlled) stepped-sine vibration test is performed in order to control the excitation signal. Forward and backward sweeps may be required to obtain all stable solutions of the system, particularly in the region of multi-solution response. However, taking the upper branch of the nonlinear response (with larger amplitude) into consideration guarantees the nonlinearity of the dynamic response to be considered in the calculation. This is because the bigger the difference between nonlinear and linear responses, the better the results of localization process. However, the system of the present study has a softening nonlinearity. Therefore, only the backward sweep (sweep-down) test, which provides the upper branch of the response, is sufficient. The amplitude of the excitation is required to be large as it makes sure the system shows nonlinear dynamic response. Figure 3.14 illustrates the response-frequency diagram of the nonlinear dynamics of the system, including amplitudes and phases at three DOFs 1, 5, and 9 which are related to the translational displacement of the points respectively with distances 5, 15, and 25 cm from the fixed end of the cantilever beam. The localization process is carried out using the measured nonlinear responses of the structure for the purpose of detecting the exact location of the unknown nonlinear restoring force.

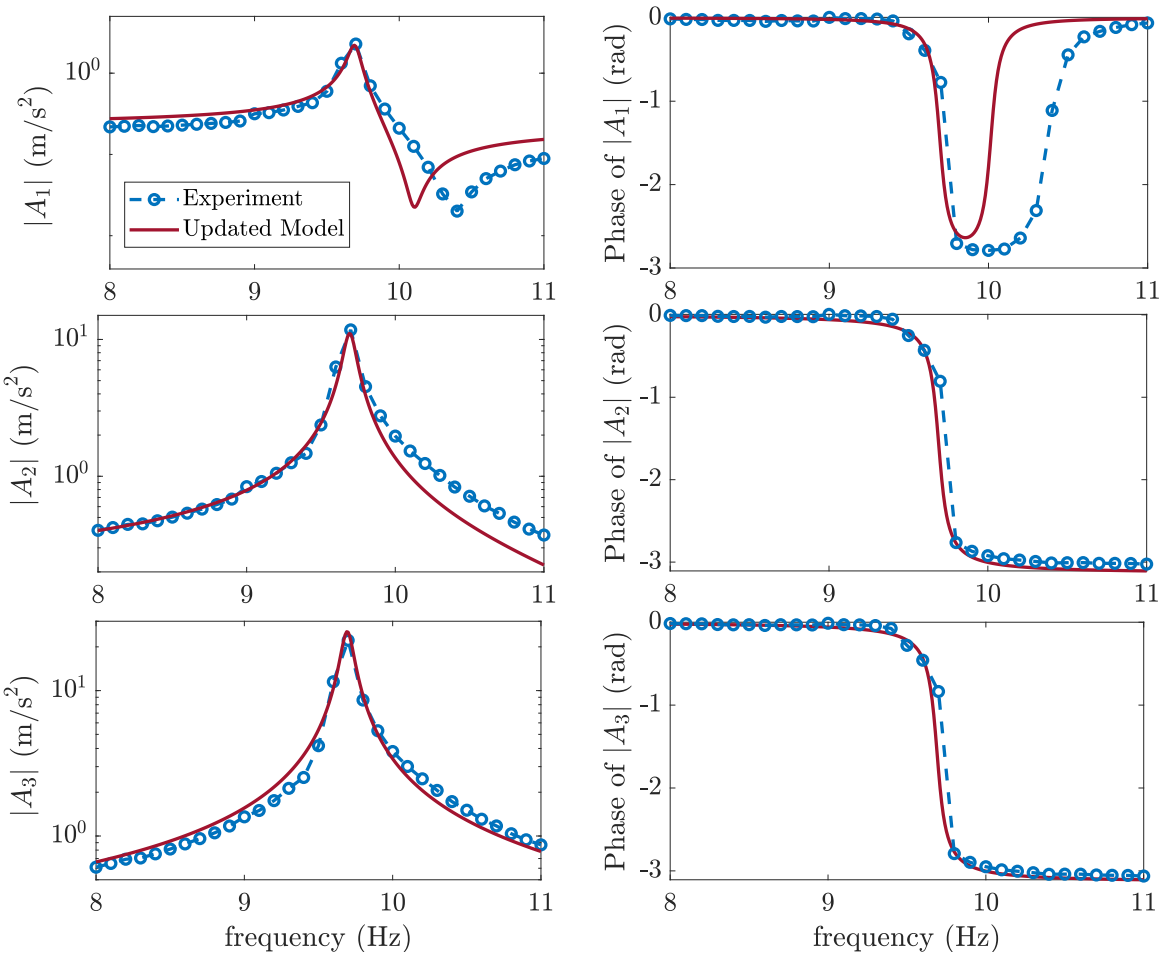

Figure 3.12: The updated linear response in comparison with the measured dynamics of the nonlinear structure obtained from low amplitude vibration test. A_i $(i = 1, 2, 3)$ denotes the amplitude of the accelerations measured respectively by three accelerometers.

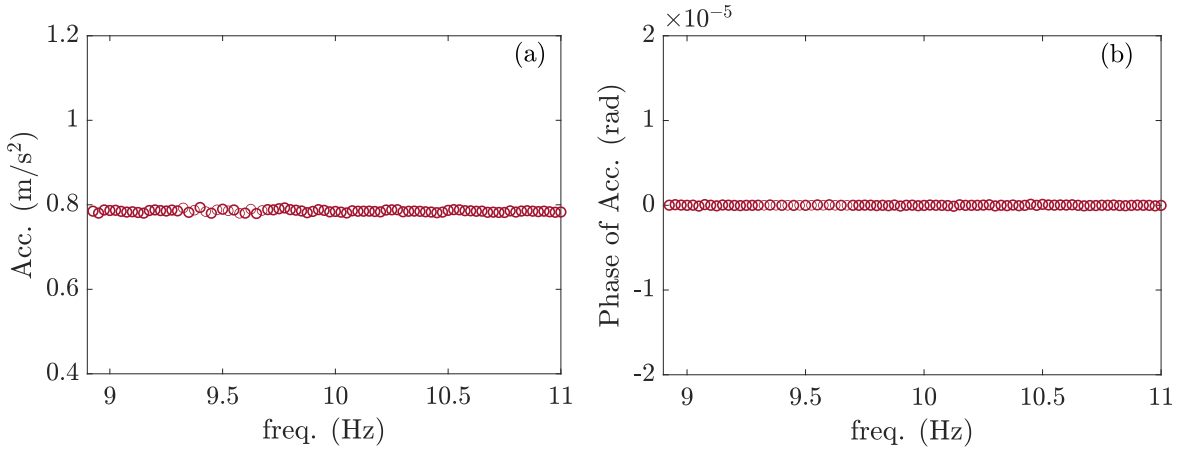

Figure 3.13: Controlled constant acceleration base motion; (a) amplitude, (b) phase.

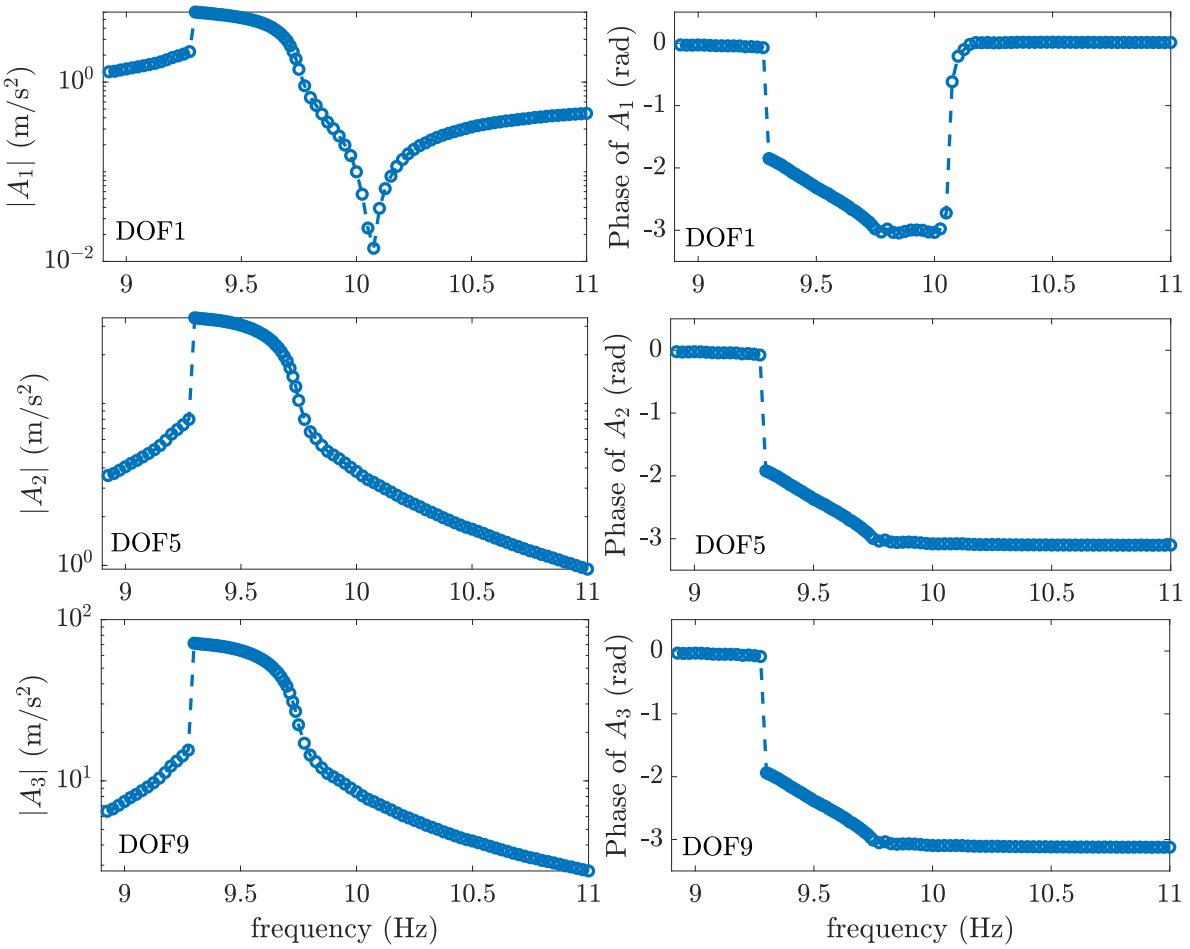

Figure 3.14: The measured nonlinear dynamics of the system captured using high amplitude vibration test. $|A_1|$, $|A_2|$, and $|A_3|$ represent the amplitude of the accelerations respectively measured by three accelerometers.

The localization is carried out using the measured nonlinear responses, according to the process explained in Section 3.4. Figure 3.15 illustrates the magnitude and phase of the reduced nonlinear force at the measured DOFs. The indices of the reduced nonlinear force for measured DOFs 1, 5, and 9 are shown in Figure 3.16, demonstrating that the nonlinear element is located at or close to DOF 9. On the other hand, Figure 3.15 illustrates a phase difference of 180 degrees between DOFs 5 and 9, while the index of the nonlinear force of DOF 9 is shown in Figure 3.16 to be much greater than the one of DOF 5. Therefore, it can be concluded that there is no ungrounded (connected) nonlinear element between DOFs 5 and 9. Conclusively, DOFs 1 and 5 can be discarded from suspect region of nonlinearity. Besides, DOF3 located between DOFs 1 and 5 can be discarded from suspect region. As a result, DOFs 7, 9, and 11 are considered as suspect DOFs. The nonlinear force has been calculated for the suspect region. Looking at the indices of nonlinear forces in suspect region, Figure 3.17, one can interpret that the nonlinear element may be at both DOFs 9 and 11. However, looking at the difference between indices of nonlinear forces of two DOFs, the nonlinear force can be considered as a localized grounded nonlinearity at DOF 11. Using the results of the localization process, the type of nonlinearity can be identified via different identification methods.

This chapter addressed the localization of localized structural nonlinearities located at nodal points of the FE model of the structure. The method is also able to detect the location of multiple localized nonlinearities located at different locations. Besides, if the nonlinearity is located at a location between two nodes, this can be interpreted using the magnitude and phase of the RNFs of the two DoFs adjacent to the location of nonlinearity. In fact, if the FE method is used for modelling, the forces/moments and the displacements are all defined at nodes and it is not possible to identify nonlinearity in the element. In other words, in FE modelling, a nonlinearity inside an element will be represented by force-displacement relationships at nodes. In this case, to detect the exact location of a nonlinear element, a finer mesh of the structure is required so that the location of nonlinearity is located at a nodal point.

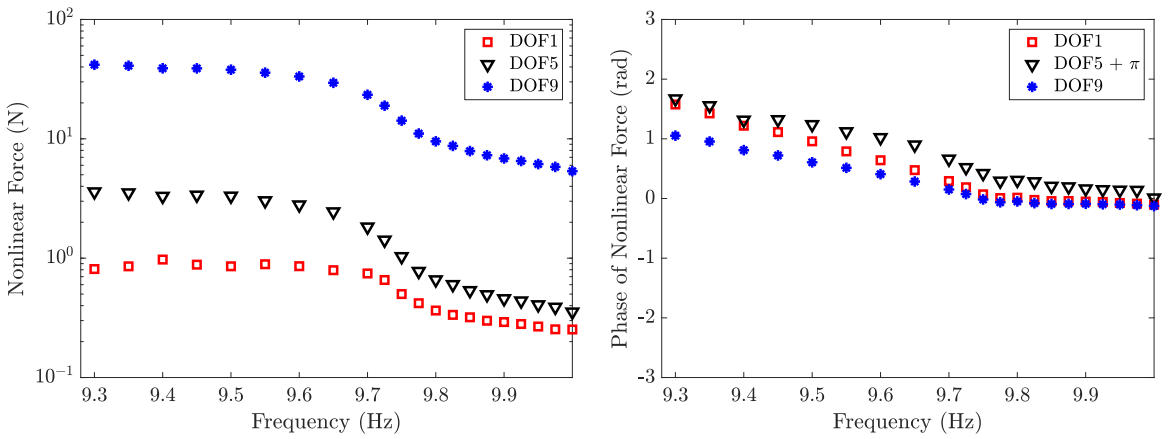

Figure 3.15: Magnitude and phase of the reduced nonlinear force at the measured degrees of freedom.

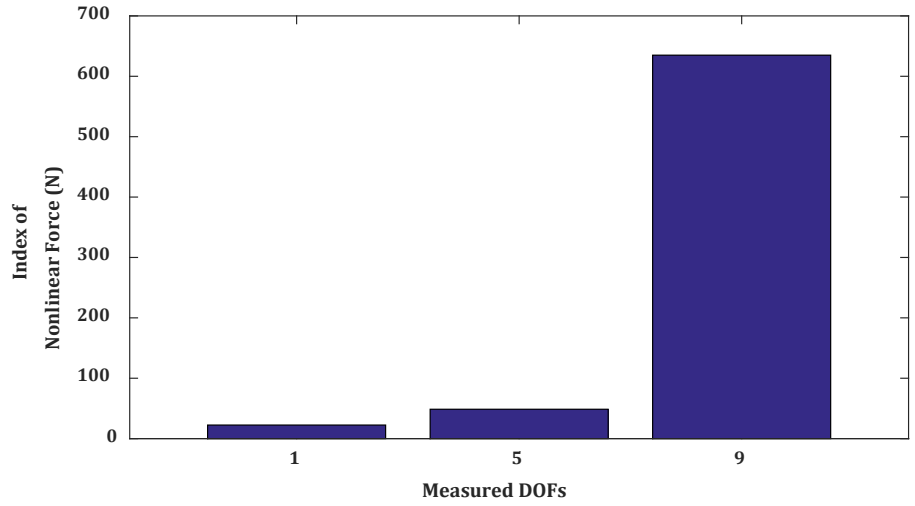

Figure 3.16: Indices of the nonlinear forces at the measured DOFs.

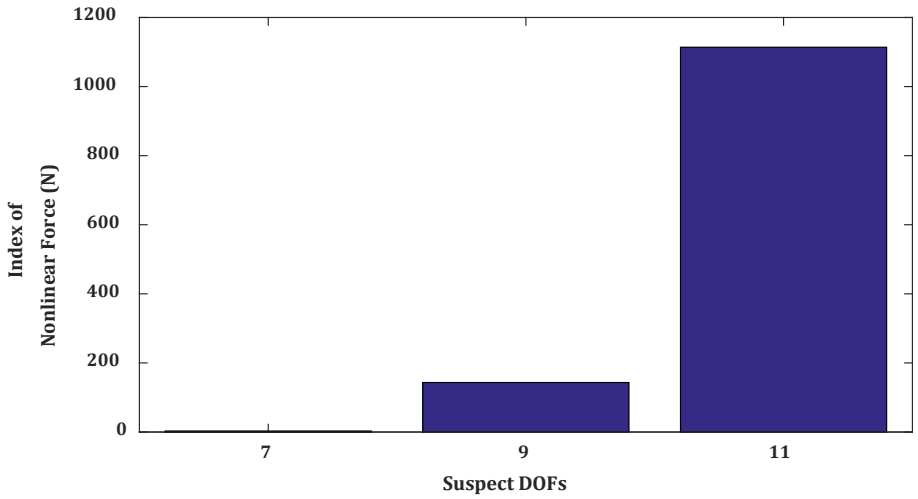

Figure 3.17: Indices of the nonlinear forces at the suspect DOFs.

3.6 Closure

The study carried out in this chapter has aimed to detect the location of localized nonlinearity in structural dynamics using base excitation experiments. To this end, a localization method has been employed to detect the localized nonlinear elements of two nonlinear systems: a numerical case study composed of a cantilever beam with a nonlinear restoring force at the tip, and an experimental case study in which an electromagnetic nonlinear force is applied to the tip of a cantilever. In the experimental set-up, a symmetric configuration of two pairs of electromagnets and permanent magnets generates

a nonlinear force which is applied to the tip of the cantilever beam. For the purpose of localization, two types of vibration tests have been carried out. Low-amplitude test results were used to update the model of the underlying linear system of the structure, while the results of the high-amplitude test are required for the localization process itself. The results of the localization demonstrate the capability of the method utilized to detect the location of nonlinear elements in both the numerical and experimental cases under study.

Chapter 4

On the Sensitivity of the Identification Methods to Measurement Noise and Modelling Error

4.1 Introduction

Nonlinear behaviour is very likely to occur in most practical structures due to the effects of material properties, structural joints and boundary conditions. However, in many applications, the nonlinearity is small enough so that the structure is analysed using linear theories. On the other hand, there are unknown strong nonlinearities in many structures making it difficult to predict accurately the dynamic behaviour of the structures using linear analysis. Therefore, an appropriate nonlinear model is required to investigate the dynamics of the system. As a consequence, identification (localization, characterization and quantification) of such nonlinearities has received significant attention over recent decades.

Unlike the numerical simulation of theoretical problems, the experimental study of practical structures is never free of noise. As the model of underlying linear system is an essential requirement in the identification of nonlinear systems and investigation of their dynamics, having an accurate linear model of the underlying linear system is very important. On the other hand, the presence of nonlinearity in the system yields modelling errors in the updating of the linear model. Furthermore, the complexity of the structure, insufficient sensors, and the high cost of experiments, often make it impossible to have complete measurements at all coordinates of the nonlinear system. Therefore, due to the existence of

noise and modelling errors, an additional error may occur in the estimation of the responses at the unmeasured coordinates.

The response of nonlinear systems is usually a multi-harmonic (including sub- or super-harmonics) behaviour. In many problems, the sub- or super-harmonics of the response are significant and cannot be neglected. Therefore, considering only primary harmonic of the response may be errorsome. The aforementioned noise and errors may lead to errors in the results of the identification methods. The study in this chapter is focused on the investigation of the sensitivity of the Equivalent Dynamic Stiffness Mapping technique (EDSM) [125] to experimental noise and various types of errors and showing the advantages of an optimisation based approach in the presence of measurement noise.

In this chapter, both theoretical and experimental studies are carried out to analyse the sensitivity of the EDSM technique to noise and error. In this regard, the accuracy of the application of the EDSM technique is verified using numerical simulation of a nonlinear discrete multi-degree-of-freedom (MDOF) system and a nonlinear cantilever beam. Steady state responses of numerical simulations are obtained by utilizing the Modified Complex Averaging (MCXA) technique [32, 33] and numerical arc-length continuation. Considering various types of noise and error, the sensitivity of the EDSM technique is studied using both theoretical results of both discrete and continuous nonlinear systems. It is concluded that contaminated data used for the identification may lead to errors in the results of the EDSM identification. Then, an optimization-based framework is utilized to identify the nonlinear system of the cantilever beam. By using the optimization method, one may reduce the inaccuracy arising from the aforementioned sources of noise and errors. The nonlinear response of the system obtained from the optimization method and the EDSM technique are compared with the simulated response of the system. It is shown that by using the optimization method, the use of an expansion method and consideration of the higher harmonics of the response are not required. Finally, a brief conclusion of the study is presented.

4.2 Mathematical Modelling

In this section, the mathematical models of two numerical cases are presented: a nonlinear three-DOF discrete system, and a cantilever with a nonlinear restoring force. Then, the accuracy of the semi-analytic Modified Complex-Averaging (MCXA) technique and the EDSM method, respectively, in estimating the steady state response of nonlinear dynamic systems and identifying nonlinear systems is verified. For this purpose, the steady state dynamic response of two systems is considered. To find the steady state response of the numerical case studies, the semi-analytic MCXA method is used along with the numerical arc-length continuation method. Direct numerical integration in MATLAB is also used to obtain the response of the numerical systems. The Equivalent Dynamic Stiffness Mapping (EDSM)

Table 4.1: Values for the parameters of the system shown in Figure 4.1.

Parameters (unit)	value	Parameters (unit)	value	Parameters (unit)	value
m_1(kg)	1	$c_{23}(\frac{\text{N.s}}{\text{m}})$	0.25	$k_{l_{23}}(\frac{\text{N}}{\text{m}})$	30
m_2(kg)	2	$c_3(\frac{\text{N.s}}{\text{m}})$	0.15	$k_{n_{23}}(\frac{\text{N}}{\text{m}^3})$	300
m_3(kg)	1.5	$k_{l_1}(\frac{\text{N}}{\text{m}})$	25	$k_{l_3}(\frac{\text{N}}{\text{m}})$	30
$c_1(\frac{\text{N.s}}{\text{m}})$	0.1	$k_{n_1}(\frac{\text{N}}{\text{m}^3})$	400	$k_{n_3}(\frac{\text{N}}{\text{m}^3})$	500
$c_{12}(\frac{\text{N.s}}{\text{m}})$	0.2	$k_{l_{12}}(\frac{\text{N}}{\text{m}})$	50	F(N)	1.5

technique is used to identify the assumed unknown nonlinear forces of the considered systems. Refer to Chapter 1 for detailed description of MCXA and EDSM techniques.

4.2.1 MDOF Mass-Spring System

The first system is a 3DOF mass-spring system shown in Figure 4.1,

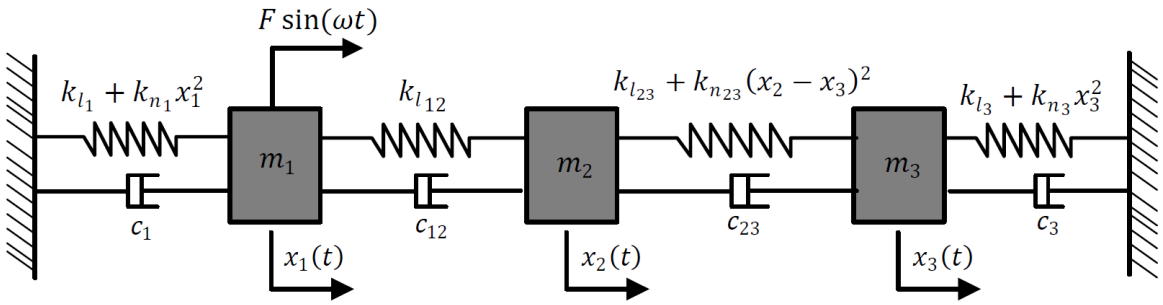

Figure 4.1: Three-DOF discrete nonlinear system.

The governing equations of the system is derived using Newton's second law as

$$\begin{aligned} m_1\ddot{x}_1 + c_1\dot{x}_1 + k_{l_1}x_1 + k_{n_1}x_1^3 + c_{12}(\dot{x}_1 - \dot{x}_2) + k_{l_{12}}(x_1 - x_2) &= F\sin(\omega t) \\ m_2\ddot{x}_2 + c_{12}(\dot{x}_2 - \dot{x}_1) + k_{l_{12}}(x_2 - x_1) + c_{23}(\dot{x}_2 - \dot{x}_3) + k_{l_{23}}(x_2 - x_3) + k_{n_{23}}(x_2 - x_3)^3 &= 0 \\ m_3\ddot{x}_3 + c_3\dot{x}_3 + k_{l_3}x_3 + k_{n_3}x_3^3 + c_{23}(\dot{x}_3 - \dot{x}_2) + k_{l_{23}}(x_3 - x_2) + k_{n_{23}}(x_3 - x_2)^3 &= 0, \end{aligned} \tag{4.1}$$

where m_1, m_2 and m_3 are the masses of the oscillators, c_1, c_{12}, c_{23}, c_3 are damping coefficients, $k_{l_1}, k_{l_{12}}, k_{l_{23}}, k_{l_3}$ are linear stiffnesses and $k_{n_1}, k_{n_{23}}, k_{n_3}$ denote the coefficients of nonlinear cubic stiffness. A harmonic external force with an amplitude of F and excitation frequency of ω is applied to the first degree of freedom. Table 4.1 contains the values given to the parameters of the system of Eq. (4.1) used for numerical simulations in this study.

It is assumed that all parameters are known except $c_1, c_3, k_{l_1}, k_{n_1}, k_{n_{23}}, k_{l_3}, k_{n_3}$. Accordingly, the mass, damping and stiffness matrices and the vector of nonlinear forces for the system shown in Figure 4.1 is defined as,

$$
\begin{aligned}
M = \begin{bmatrix} m_1 & 0 & 0 \\ 0 & m_2 & 0 \\ 0 & 0 & m_3 \end{bmatrix}, \quad C = \begin{bmatrix} c_{12} & -c_{12} & 0 \\ -c_{12} & c_{12}+c_{23} & -c_{23} \\ 0 & -c_{23} & c_{23} \end{bmatrix} \\
K = \begin{bmatrix} k_{l_{12}} & -k_{l_{12}} & 0 \\ -k_{l_{12}} & k_{l_{12}}+k_{l_{23}} & -k_{l_{23}} \\ 0 & -k_{l_{23}} & k_{l_{23}} \end{bmatrix} \\
f_{NL} = \begin{bmatrix} c_1\dot{x}_1 + k_{l_1}x_1 + k_{n_1}x_1^3 \\ k_{n_{23}}(x_2 - x_3)^3 \\ c_3\dot{x}_3 + k_{l_3}x_3 + k_{n_3}x_3^3 + k_{n_{23}}(x_3 - x_2)^3 \end{bmatrix} \\
f_{(t)} = \begin{bmatrix} F\sin(\omega t) \\ 0 \\ 0 \end{bmatrix}
\end{aligned}
\tag{4.2}
$$

The nonlinear force f_{NL} in Eq. (4.2) includes both linear and nonlinear parts. The reason is to show the performance and accuracy of the EDSM technique in the absence of any source of inaccuracy. In fact, the aim is to show that the EDSM technique is able to predict both linear and nonlinear parts very accurately if there is no source of error. Therefore, Eq. (4.1) is rearranged in matrix form so that the vector of nonlinear force f_{NL} includes only unknown parameters, which are identified using the Equivalent Dynamic Stiffness Mapping technique.

4.2.2 Nonlinear Cantilever Beam

A nonlinear stainless-steel cantilever beam subject to an external harmonic force is considered as the second system studied in this chapter. The beam is assumed to have the geometry and material properties given in Table 4.2. As shown in Figure 4.2, a nonlinear restoring force is applied to the tip of the beam through a grounded nonlinear attachment including a nonlinear spring (a linear and a cubic stiffness) and a linear dashpot. The nonlinear restoring force and parameters are given as

$$
f_{NL} = c_l\dot{w}(l,t) + k_l w(l,t) + k_N w^3(l,t), \tag{4.3}
$$

where

$$
c_l = 0.004\ \frac{\text{N.s}}{\text{m}}, \quad k_l = 20\ \frac{\text{N}}{\text{m}}, \quad k_N = 1\times 10^5\ \frac{\text{N}}{\text{m}^3}. \tag{4.4}
$$

Table 4.2: Geometry and material properties of the beam shown in Figure 4.2.

Properties (unit)	value
Length, l (m)	0.30
Width, d (mm)	30
Thickness, h (mm)	1.5
Modulus of Elasticity, E (GPa)	205
Density, ρ ($\frac{\text{kg}}{\text{m}^3}$)	7800
Damping coefficient per length, γ ($\frac{\text{kg}}{\text{m.s}}$)	0.2

and $w(l,t)$ denotes the deflection of the beam at the tip. Harmonic point force $F_{ex}(t) = f\sin(\omega t)$ excitation is used to excite the beam. In the configuration of the beam in Figure 4.2, there are four point masses $p_m = 6, 6, 6, 8$g respectively located at positions $x_m = [l/6, 3l/6, 5l/6, l]$ from the clamped end of the beam, where l is the beam length. Tip mass represents the mass of bolts and nuts used to attach spring and dashpot to the beam. The three other masses represent the mass of accelerometers used to measure the response of the beam.

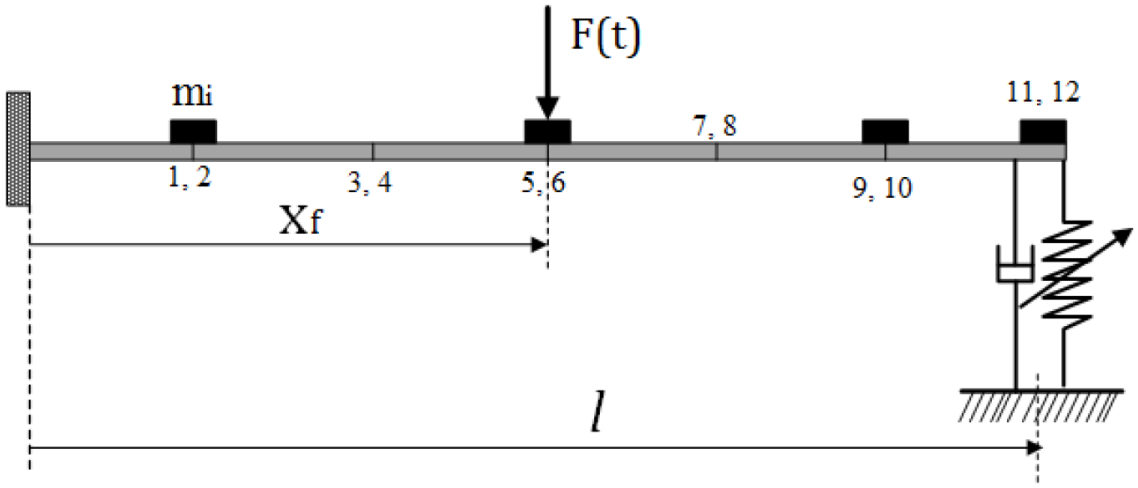

Figure 4.2: Schematic of the cantilever beam with a grounded nonlinear restoring force at the tip.

According to Euler-Bernoulli beam theory [3] and utilizing the Finite Element method and six two-node linear Euler-Bernoulli beam elements, the given nonlinear structure is governed by following equation in matrix form

$$\mathbf{M}\ddot{\mathbf{w}}(t) + \mathbf{C}\dot{\mathbf{w}}(t) + \mathbf{K}\mathbf{w}(t) + \mathbf{f}_{NL}(\mathbf{w}, \dot{\mathbf{w}}) = \mathbf{f}_{ex}(t), \tag{4.5}$$

where $\mathbf{M}, \mathbf{C}, \mathbf{K}$ denote the global mass, damping, and stiffness matrices, respectively. $\mathbf{w}(t)$ is the time response of the beam at instant time t. The vectors of displacement and its time derivatives are shown by $\mathbf{w}(t), \dot{\mathbf{w}}(t)$, and $\ddot{\mathbf{w}}(t)$, respectively. $\mathbf{f}_{NL}(\mathbf{w}, \dot{\mathbf{w}})$ is the unknown nonlinear internal force of the system.

4.3 Numerical Simulation and Results

In this section, numerical simulation is carried out to obtain the dynamic response of the two case studies introduced in Section 4.2. First the simulated response of the 3DOF system is used to verify the accuracy of the MCXA technique in predicting the nonlinear dynamics of the system. Then, the results of the cantilever beam are exploited to verify the accuracy of the EDSM technique in identification of the nonlinear system in the absence of any type of measurement noise or modelling error. Then, some of the simulated nonlinear dynamic responses of the two case studies are presented.

4.3.1 Verification of the MCXA Technique

In order to verify the accuracy of the MCXA method, the 3DOF system of Figure 4.1 is considered. The steady state dynamics of the system of Eq. (4.1) with parameters of Table 4.1 is obtained using the MCXA technique and the Runge Kutta direct integration method in MATLAB. Then, the results of the two methods are compared.

To simulate the response of the system using MCXA, the first three harmonics of the response are considered. Figures 4.3 and 4.4 illustrates the amplitude-frequency and phase-frequency diagrams of the first three harmonics of the steady state dynamics of the system. $|X_{H_i}|$ and φ_{H_i} in Figures 4.3 and 4.4 denote, respectively, the amplitude and phase of i-th harmonic of the steady state response. Stable and unstable branches of the steady state response are shown by blue and red lines, respectively. The stability of the steady state response of the system was investigated using Lyapunov's first method of stability analysis.

Figure 4.5 illustrates the comparison between the first and third harmonics of the steady state dynamics of the 3DOF system obtained using the MCXA technique and ODE integration in MATLAB. Although there is a good compatibility between the results obtained by the MCXA technique and the results estimated using ODE integration, ODE direct integration is not capable of estimating the unstable solutions, as expected. In addition, the ability of ODE integration to predict all of the stable solutions, particularly the ones with limited stability range, depends on proper selection of initial conditions. On the other hand, increasing the accuracy of direct integration to estimate the stable solutions may lead to significant increases in computational costs. In contrast, the MCXA technique is able to predict all stable and unstable solutions with significantly lower computational costs.

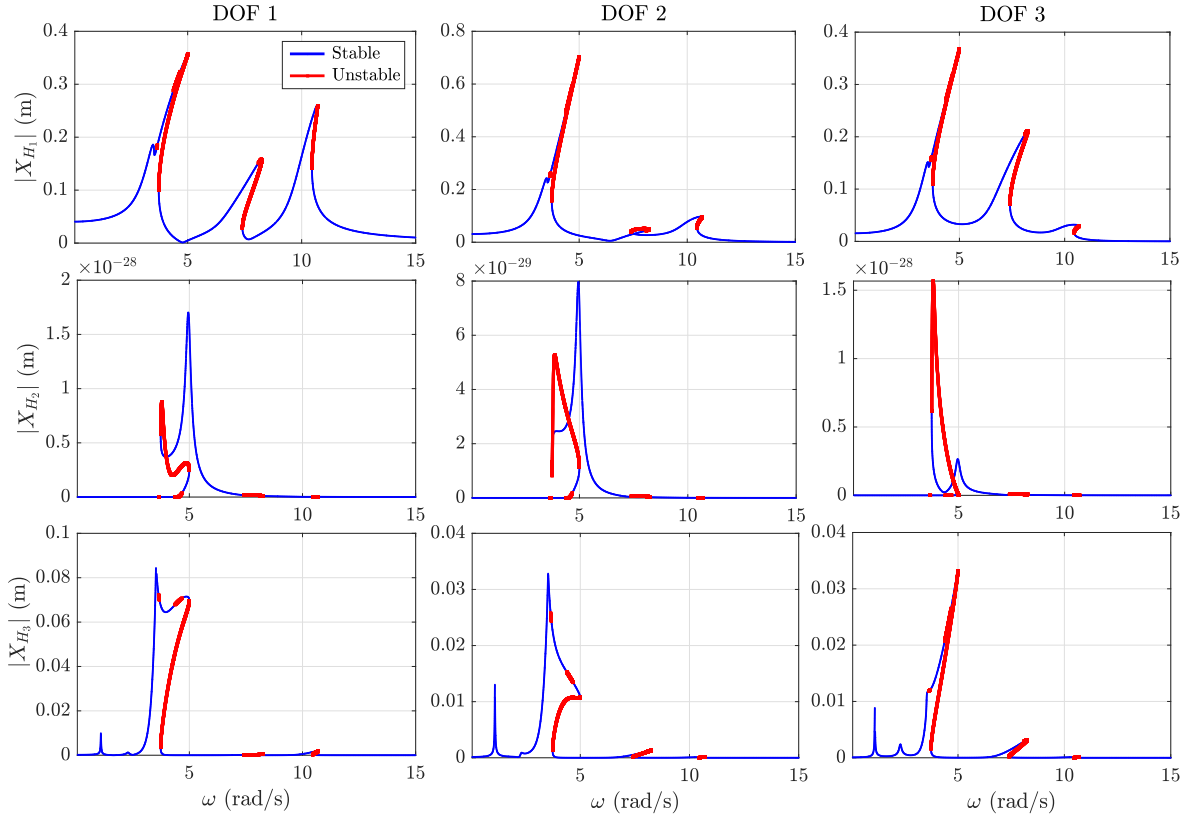

Figure 4.3: Amplitude–frequency diagram of the first three harmonics of the steady state response of the 3DOF system. Blue lines denote the stable branches and red lines represent the unstable branches.

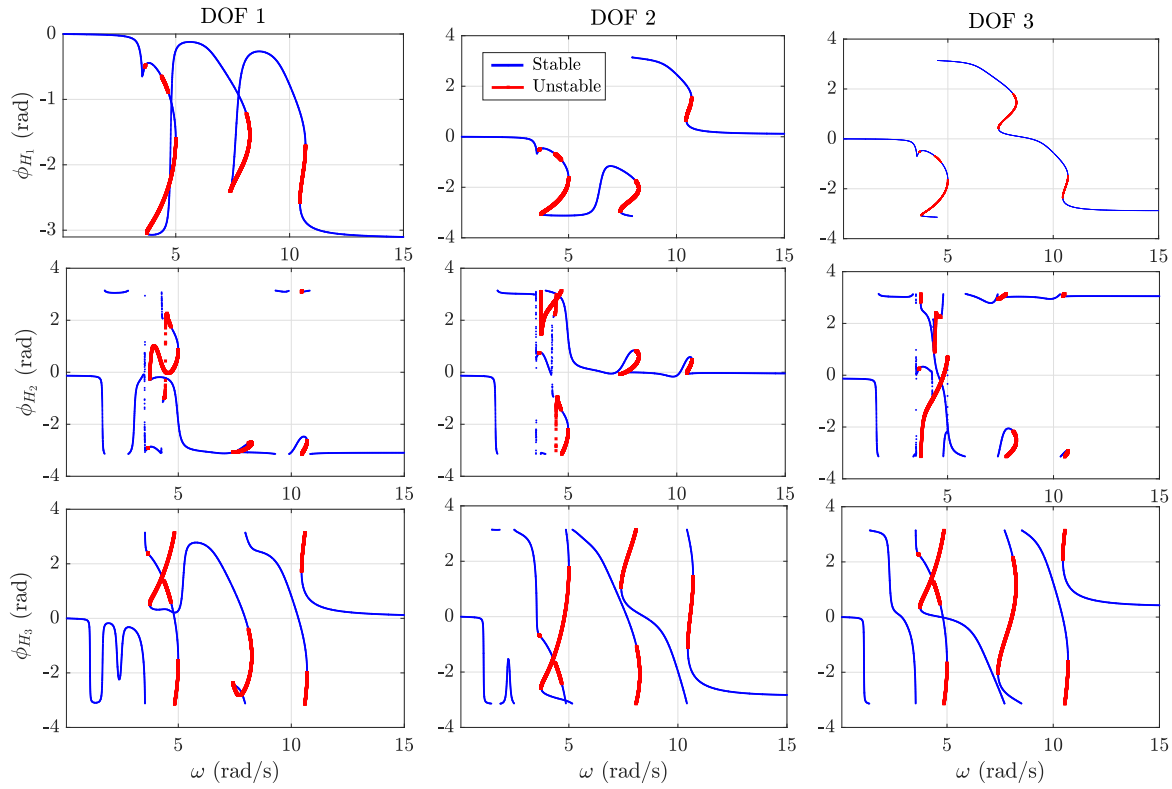

Figure 4.4: Phase–frequency diagram of the first three harmonics of the steady state response of the 3DOF system. Blue lines denote the stable branches and red lines represent the unstable branches.

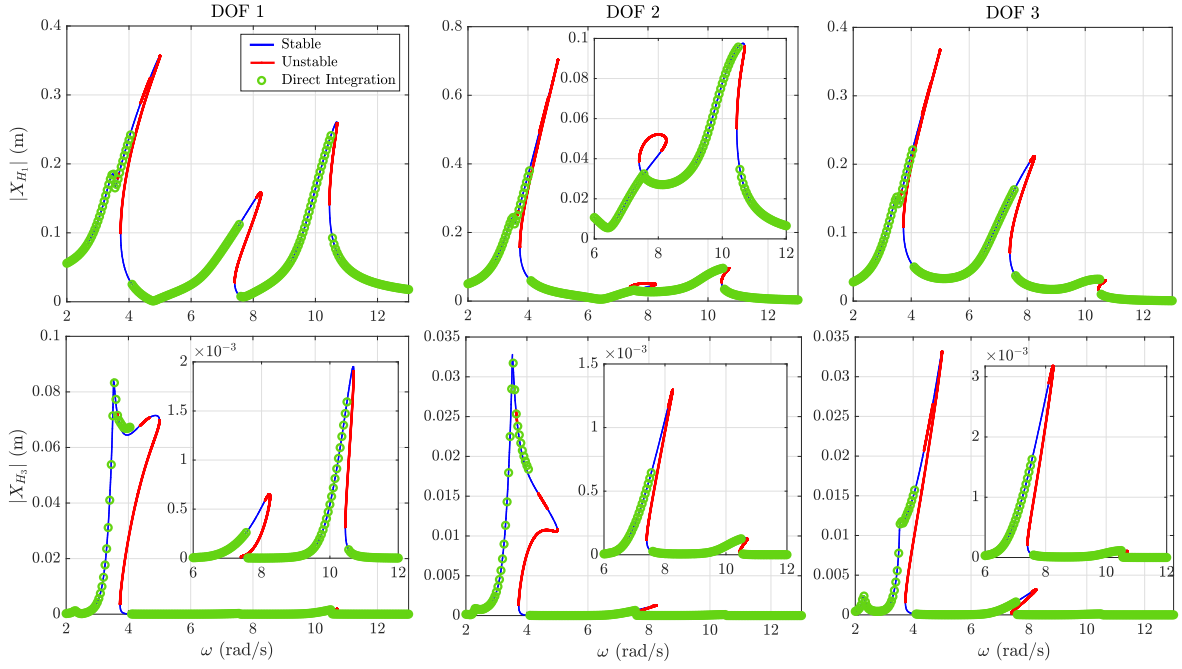

Figure 4.5: Comparison between the first and third harmonics of the steady state response of the 3DOF system obtained by the MCXA technique and ODE integration.

Figure 4.6 shows the comparison between the time history of the steady state response of the 3DOF system at $\omega = 3.5$ rad/s obtained using the MCXA technique and ODE integration. Figure 4.6(a) illustrates the multi-harmonic response of the system, while Figures 4.6(b) and 4.6(c) demonstrate, respectively, the first and third harmonics of the response. The results show a good compliance between the two different methods. However, since the MCXA technique is able to obtain both stable and unstable branches of the response, and also has a much lower computational cost than ODE integration, the MCXA technique is used here in this study.

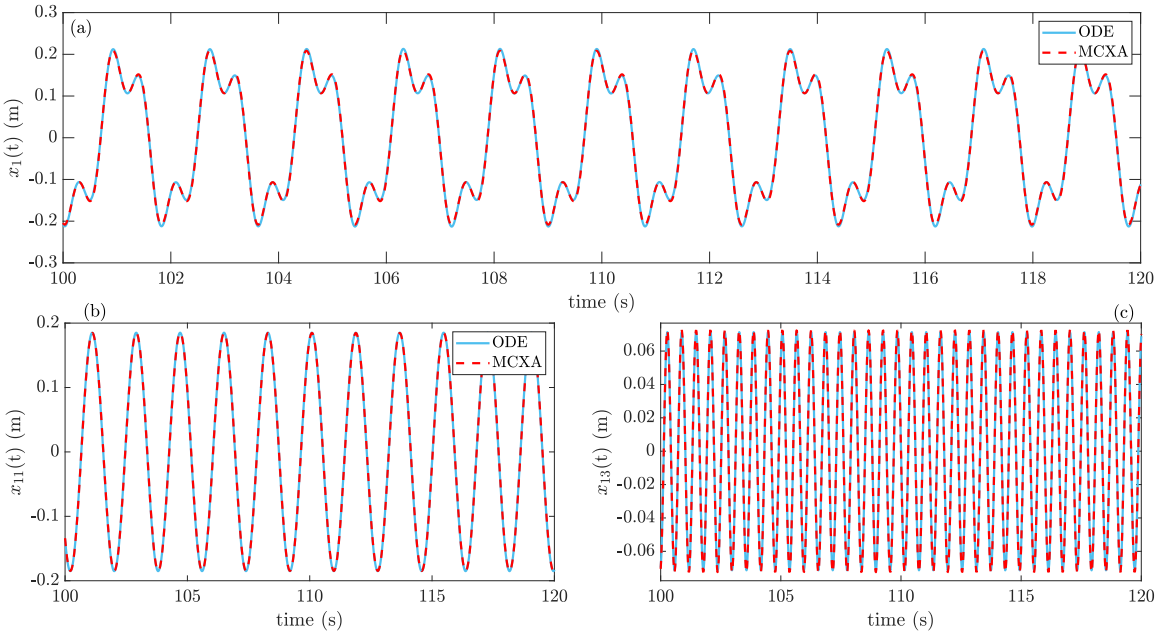

Figure 4.6: Comparison between the time history of the first degree of freedom of the 3DOF system obtained using MCXA and ODE integration. (a) Multi-harmonic response; (b) primary harmonic; (c) third harmonic.

4.3.2 Verification of the EDSM Technique

In this section, the accuracy of the EDSM method is verified in the absence of any noise and error. For this purpose, the steady state dynamics of the two example nonlinear systems are obtained using the MCXA technique and arc-length continuation. The nonlinear forces of the two systems are identified using the EDSM technique.

4.3.2.1 Discrete MDOF Nonlinear System

The three-DOF nonlinear discrete system of Eq. (4.1) is used to verify the accuracy of the EDSM technique. The EDSM technique is used to identify various types of unknown internal forces including linear and nonlinear stiffness and linear damping, for both grounded and ungrounded cases.

For the purpose of verification, it is assumed that the response includes only the primary harmonic and simulation is performed accordingly. The effect of higher harmonics in the results of the identification is discussed later in the chapter. Using the MCXA technique, described in Section 1.7.1, the steady state response of the system of Eq. (4.1) is obtained. Figure 4.7 gives the amplitude and phase of the response of the system, where the blue lines denote the stable responses and red lines show the unstable branches of the response of the system. The stability of the steady state response of the system was investigated using Lyapunov's first method of stability analysis.

Once the frequency domain response of the system has been obtained, the Equivalent Dynamic Stiffness Mapping technique is applied to identify the unknown internal forces of the system. The ideal equivalent dynamic stiffness of different types of internal forces are given in Table 4.1. Accordingly, a linear spring and a cubic stiffness spring are shown respectively as a constant and a quadratic in the plot of the real part of the equivalent dynamic stiffness versus the amplitude of the response. On the other hand, linear damping is given as a constant in the plot of the imaginary part of the equivalent dynamic stiffness versus the amplitude of the response.

Figure 4.8 shows the real part of the equivalent dynamic stiffness in terms of the frequency domain amplitude of the response of the system. From the plot of the real part of D_{eq} the linear stiffness is identified as a constant, while the nonlinear part would be identified as a variation with respect to the amplitude of the response. Figure 4.8(a) shows the grounded stiffness is composed of a linear and a nonlinear part which is attached to DOF 1. The ungrounded (connected) nonlinear stiffness between DOFs 2 and 3 is shown in Figure 4.8(b). The grounded nonlinear stiffness attached to DOF 3 is shown in Figure 4.8(c). The imaginary parts of the equivalent dynamic stiffness identify the equivalent damping coefficients of the nonlinear internal force, as shown in Figure 4.9. The grounded equivalent damping coefficients of DOFs 1 and 3 are linear in Figures 4.9(a) and 4.9(b), respectively.

4.3.2.2 Cantilever Beam

In order to investigate the capability of the EDSM identification technique in identifying the nonlinearities of continuous systems, a theoretical case study is carried out in this section on the cantilever beam described in Section 4.2. In order to verify the accuracy of the EDSM technique in the absence of all sources of inaccuracy, it assumed that there is no noise in the simulated data or modelling error in the underlying linear model. In addition, for the sake of simplicity, it is assumed that the response is free of higher harmonics. As the EDSM technique requires the response of the system to be given (simulated/measured) at all coordinates, in order to avoid any expansion error due to the estimation of unmeasured coordinates, the simulated response at all coordinates are utilized in the EDSM identification process. However, particularly for continuous systems, it is not possible to have complete measurements at all coordinates in practical applications.

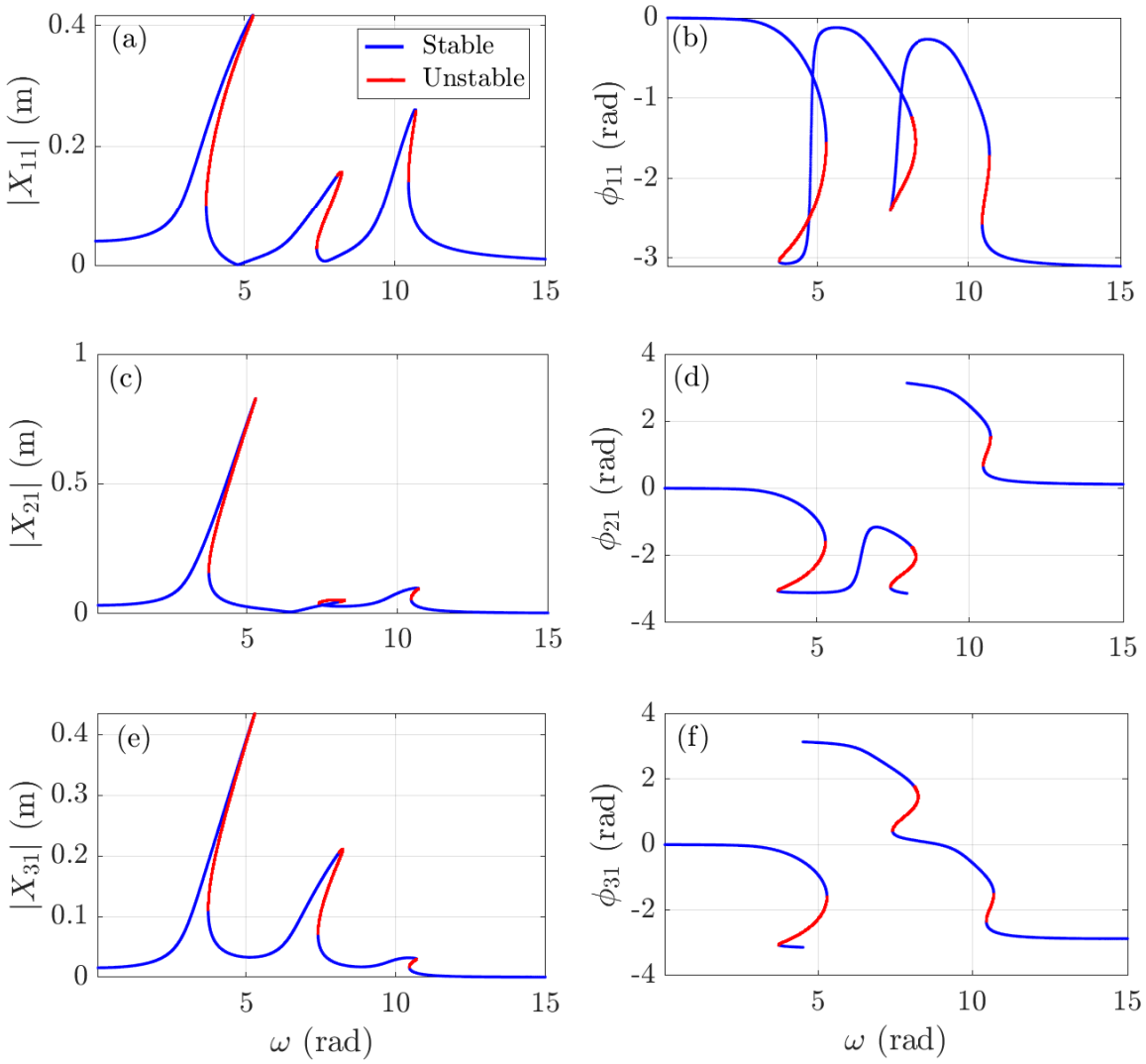

Figure 4.7: (a, c, e) Amplitude-frequency response and (b, d, f) Phase of the 1st, 2nd , and 3rd oscillators of the nonlinear discrete system, respectively.

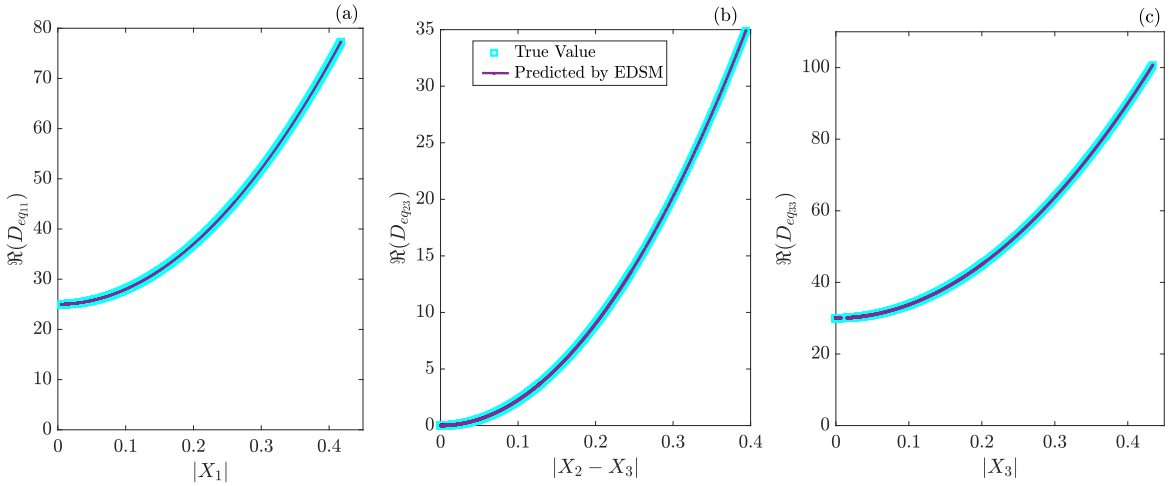

Figure 4.8: The real parts of the dynamic stiffness demonstrate the stiffness of nonlinear internal force of the system. (a) grounded nonlinear cubic stiffness including linear part at DOF1; (b) ungrounded nonlinear stiffness between DOFs 2 and 3; (c) grounded nonlinear stiffness including linear part connected to DOF 3.

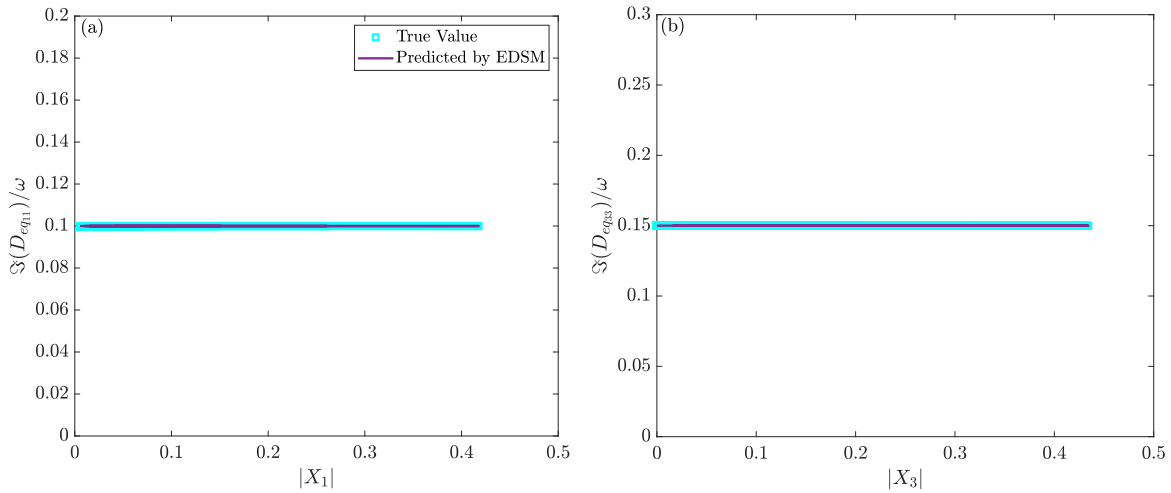

Figure 4.9: The imaginary parts of the dynamic stiffness identify the unknown linear damping at (a) DOF1 and (b) DOF 3.

The steady state dynamics of the cantilever beam is simulated by developing a code in MATLAB using the MCXA technique [32, 33] and are-length continuation method. Different force amplitudes are applied to the beam in order to obtain the linear and nonlinear responses of the system. Figure 4.10(a) illustrates the underlying linear and nonlinear responses of the system at DOF 11, the coordinate where the nonlinear restoring force is applied, for $F = 1$ N. To obtain the underlying linear system, the nonlinear element is neglected in the simulation. Figure 4.10(b) shows the nonlinear response of the cantilever beam in the vicinity of first natural frequency for different values of force amplitude F.

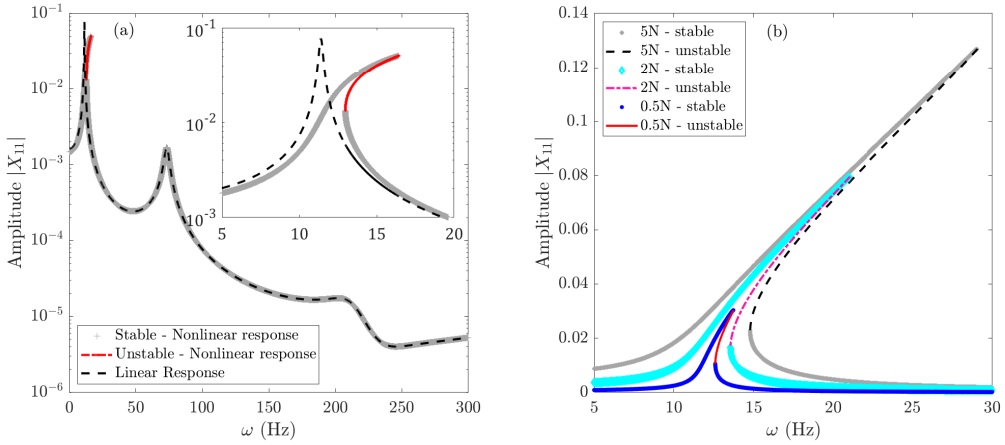

Figure 4.10: (a) Amplitude-frequency response of the underlying linear and nonlinear system of the cantilever beam for F=1 N; (b) amplitude-frequency response of the system for different force amplitudes.

From the nonlinear response of the system at all degrees of freedom, the Equivalent Dynamic Stiffness Mapping (EDSM) technique is used to identify the nonlinear element. Figures 4.11(a) and 4.11(b) respectively illustrate the comparison between the estimated and true values of the equivalent stiffness and damping of the nonlinear restoring force applied to the cantilever beam. Due to the Fourier Integral used to find the equations of motion in the frequency domain, the cubic nonlinear stiffness is given by a quadratic in Figure 4.11(a), with the constant 20N/m indicating the linear part of the stiffness. The nonlinear internal force also includes linear damping with $c_l = 0.004$ N.s/m, and the identification gives an accurate constant value equal to the linear damping coefficient, see Figure 4.11(b). As demonstrated, the EDSM technique is capable of accurately predicting the unknown nonlinear force, without any noise or error.

4.3.3 Sensitivity to Error and Noise

Using the numerical simulation of both discrete and continuous nonlinear systems, the capability of the EDSM technique for the identification of nonlinearities has been investigated in the absence of noise and error. It is easy to avoid modelling errors and noise in simulated data, but in practical systems and

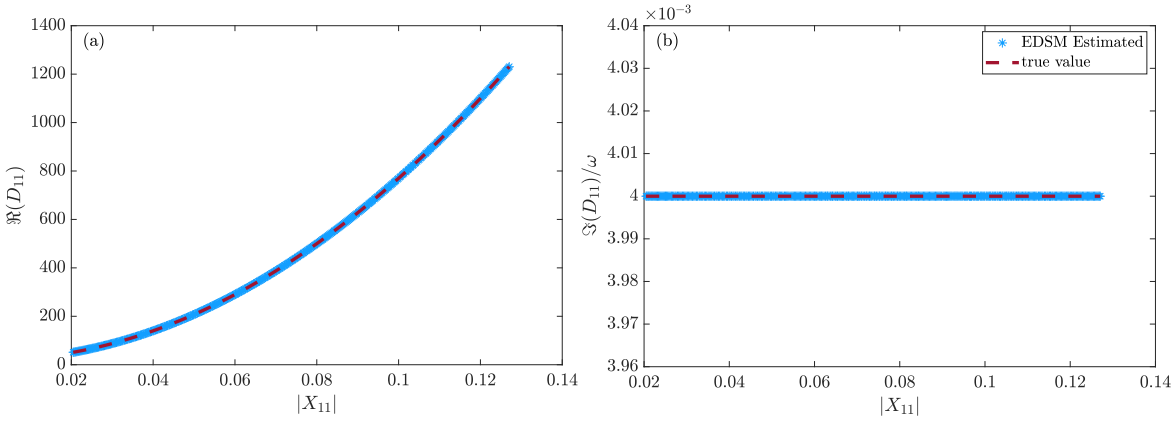

Figure 4.11: (a) Equivalent nonlinear stiffness, obtained from the real part of the equivalent dynamic stiffness, in comparison with the true value; (b) comparison of the estimated and true value of damping of the nonlinear restoring force.

in experimental study, measurement noise is inevitable. Therefore, having noise in the measured data makes it difficult to accurately identify the unknown elements/parameters and may lead to inaccuracy in the results of the identification.

In addition, many of the nonlinear identification methods require the underlying linear model to be properly updated in advance. However, since even the low amplitude response of a nonlinear system is not exactly same as the response of its underlying linear system, updating the underlying linear system using the measured response of the nonlinear system is unlikely to be free of error. This modelling error will also result in incorrect identification.

Incomplete measurement in experimental studies is considered as another source of error in the EDSM technique. Indeed, in practical systems, it is almost always impossible to have complete measurements due to insufficient equipment or sensors, or the difficulty in placing sensors. As the EDSM technique requires the responses of the system at all coordinates to be determined (measured or estimated), expansion methods are used to estimate the response at unmeasured DOFs, and this may create errors in the estimated data to be used in the EDSM technique.

The other source of error in the identification of nonlinear elements of dynamic structures is neglecting the presence of higher harmonics in the dynamics of the structure. Indeed, in many nonlinear structures the effect of higher harmonics in the response is too significant to be neglected. Therefore, utilizing only the primary harmonic of the response in the identification process, as many of the identification methods do, may result in considerable error with respect to the magnitude of higher harmonics in the response.

In this section, the numerical simulations of the previously introduced continuous and discrete systems of the nonlinear cantilever beam and three-DOF Duffing oscillator are used to investigate the

sensitivity of the EDSM technique to noise and various types of error such as expansion error, modelling error, and the error due to neglecting the higher harmonics in the response of nonlinear systems.

4.3.3.1 The Effect of Expansion Error

Expansion methods such as System Equivalent Reduction Expansion Process (SEREP) [6], which is explained in Section 1.6.1, are used to estimate the response of the system at unmeasured coordinates. For a system with p measured DOFs and q unmeasured DOFs, the unmeasured response is estimated using the SEREP method as

$$\begin{Bmatrix} \mathbf{X}_m \\ \mathbf{X}_u \end{Bmatrix} = \mathbf{T}\mathbf{X}_m \tag{4.6}$$

where $[\mathbf{X}_m]_{p\times 1}$ and $[\mathbf{X}_u]_{q\times 1}$ are respectively the measured response and estimated response at unmeasured coordinates, $[\mathbf{T}]_{n\times p}$ denotes the transform matrix of the SEREP method, and n is the number of total degrees of freedom. Subscripts m and u denote the measured and unmeasured responses, respectively. Since such expansion methods are usually based on the linear systems, using them for nonlinear systems may lead to some error in the estimated response. Therefore, the estimated response at unmeasured coordinates is slightly deviated from the actual unmeasured response, $\mathbf{X}_u = \mathbf{X}_u^a + \delta\mathbf{X}_u$. $\mathbf{X}_u^a$ is the actual response at unmeasured DOFs and $\delta\mathbf{X}_u$ denotes the error of estimating the response at unmeasured DOFs using SEREP. Nonlinear force may be obtained using the estimated response as

$$\begin{aligned} \mathbf{F}_{NL} = \mathbf{F}_{ex} - \left(\mathbf{K} + j\omega\mathbf{C} - \omega^2\mathbf{M}\right)\left(\begin{Bmatrix} \mathbf{X}_m \\ \mathbf{X}_u^a \end{Bmatrix} + \begin{Bmatrix} \mathbf{0} \\ \delta\mathbf{X}_u \end{Bmatrix}\right), \\ \mathbf{F}_{NL} = \mathbf{F}_{NL}^a + \delta\mathbf{F}_{NL} \end{aligned} \tag{4.7}$$

where $\mathbf{F}_{NL}^a$ denotes the vector of actual nonlinear force and $\delta\mathbf{F}_{NL}$ is the vector of error in the identified nonlinear force arising from the use of SEREP method to estimate the response at unmeasured coordinates.

$$\delta\mathbf{F}_{NL} = -\left(\mathbf{K} + j\omega\mathbf{C} - \omega^2\mathbf{M}\right)\begin{Bmatrix} \mathbf{0} \\ \delta\mathbf{X}_u \end{Bmatrix} \tag{4.8}$$

To study the effect of expansion error, it is assumed that the measurements on the beam are carried out on only three degrees of freedom (DOFs 1, 5, 9) using three simulated accelerometers shown in Figure 4.2. Hence, the responses of the measured coordinates are expanded using the SEREP expansion method to predict the response at unmeasured DOFs. Figure 4.12(a) shows the measured and estimated responses for the translational coordinates of the system under 1N harmonic excitation force in the neighbourhood of first natural frequency. The expansion error from the SEREP expansion is given in

Figure 4.12(b). The maximum expansion error for the translational DOFs is 1.5% at DOF11. The EDSM technique is then applied to the simulated (DOFs 1, 5, 9) and estimated (other DOFs) steady state response of the system obtained for different amplitudes of external force, F, to identify the unknown nonlinear elements.

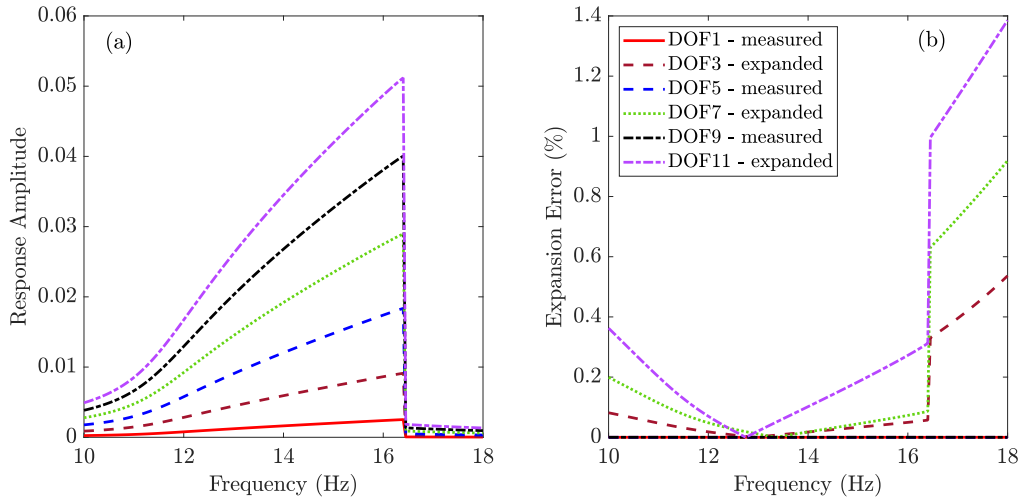

Figure 4.12: (a) Estimation of the translational responses of the system at unmeasured DOFs using the measured data and SEREP expansion. (b) The expansion error (%) for translational DOFs.

Applying the SEREP expansion method to the incomplete measurement, identified stiffness and damping gives the results shown in Figure 4.13. To fit a curve to the EDSM data, a constant function for the linear damping and a quadratic curve for the nonlinear cubic stiffness are assumed. The identified nonlinear force is given as,

$$\begin{gathered} f_{NL} = c_l \dot{w}(l,t) + k_l w(l,t) + k_N w^3(l,t), \\ c_l = 0.0435 \ \frac{\text{N.s}}{\text{m}}, \quad k_l = 40 \ \frac{\text{N}}{\text{m}}, \quad k_N = 7.3 \times 10^4 \ \frac{\text{N}}{\text{m}^3}. \end{gathered} \tag{4.9}$$

The error caused by the expansion has led to errors of 987%, 100%, and 27% in the identification of c_l,k_l, and k_N, respectively.

The identification process has been performed using different numbers of coordinates of the simulated response of the system to study the effect of expansion error in the final results of the identification. Figure 4.14 demonstrates how increasing the number of measured/simulated coordinates may decrease the level of error in the results of the identification.

The main purpose of the identification of nonlinear systems is to generate an accurate mathematical model so that it can predict the behaviour of the system precisely. Figure 4.15 shows a comparison between the simulated response of the nonlinear system and the response regenerated using the identified

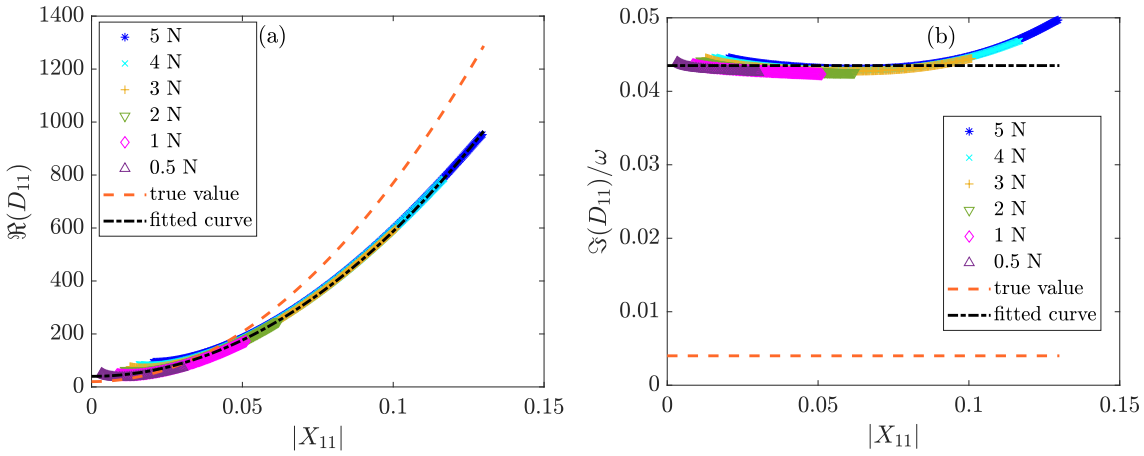

Figure 4.13: Errors in the identified stiffness (a) and damping (b) due to using SEREP expansion to estimate the response at unmeasured DOFs. The response was simulated/measured only at three DOFs: 1, 5, and 9.

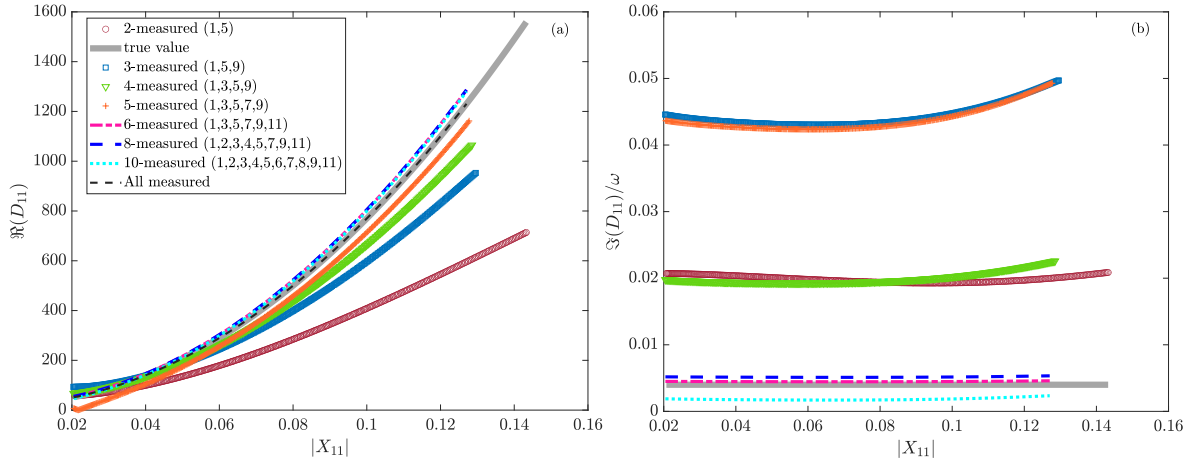

Figure 4.14: Identification of the unknown nonlinear force using the simulated response at different numbers of degrees of freedom. The response of the system was obtained for $F = 4$N.

nonlinear force of Eq. (4.9). It is observed that the identified parameters are not able to regenerate exactly the simulated response.

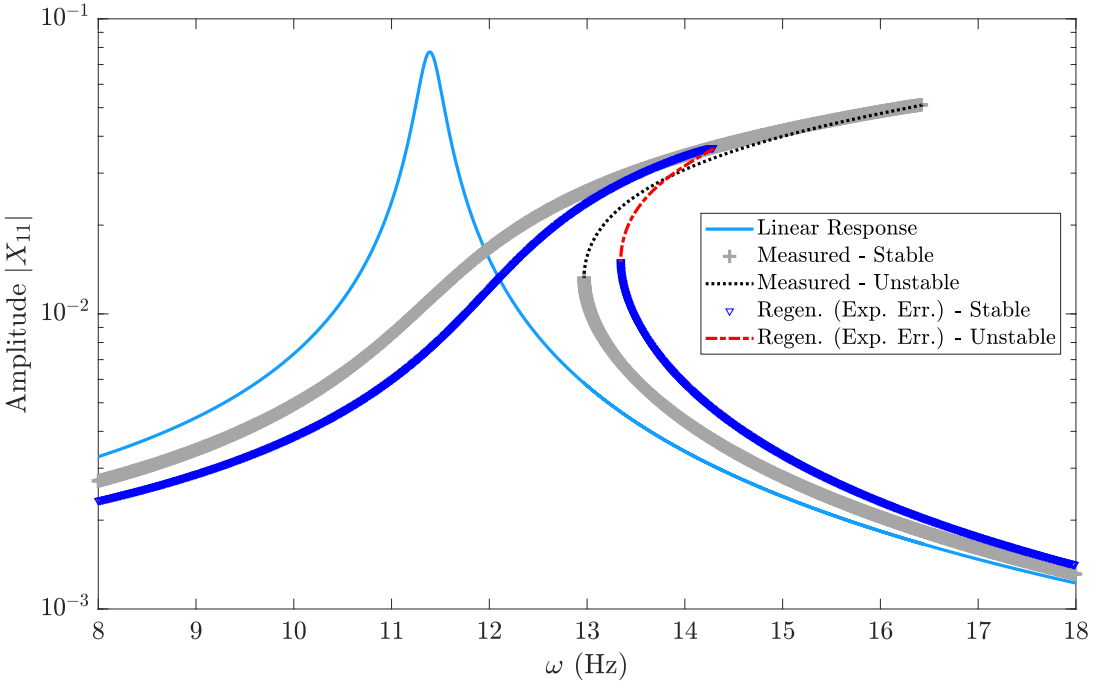

Figure 4.15: Comparison of the simulated response of the nonlinear system with the response regenerated using the identified parameters of Eq. (4.9), considering the effect of expansion error.

4.3.3.2 The Effect of Modelling Error

Other than the error due to the expansion of the incomplete measured responses, modelling error may result in considerable error in the identified parameters. Modelling error comes from updating the underlying linear system and it may arise from contaminated data or using the low amplitude nonlinear response to identify the underlying linear model. Having modelling error in the updated underlying linear model is shown by deviation from actual values of the linear system as

$$\mathbf{M} = \mathbf{M}^a + \delta\mathbf{M}, \quad \mathbf{C} = \mathbf{C}^a + \delta\mathbf{C}, \quad \mathbf{K} = \mathbf{K}^a + \delta\mathbf{K}, \tag{4.10}$$

where $\mathbf{M}$, $\mathbf{C}$, and $\mathbf{K}$ are respectively updated mass, damping, and stiffness matrices. Superscript a and δ denote the actual value and error of each identified matrix, respectively. Using an inaccurate underlying

linear model may lead to inaccurate nonlinear force as

$$\mathbf{F}_{NL} = \mathbf{F}_{ex} - \left(\mathbf{K}^a + \delta\mathbf{K} + j\omega\left(\mathbf{C}^a + \delta\mathbf{C}\right) - \omega^2\left(\mathbf{M}^a + \delta\mathbf{M}\right)\right)\left(\begin{Bmatrix}\mathbf{W}_m\\ \mathbf{W}_u^a\end{Bmatrix} + \begin{Bmatrix}\mathbf{0}\\ \delta\mathbf{W}_u\end{Bmatrix}\right), \qquad \mathbf{F}_{NL} = \mathbf{F}_{NL}^a + \delta\mathbf{F}_{NL} \tag{4.11}$$

where $\mathbf{F}_{NL}^a$ denotes the vector of actual nonlinear force and $\delta\mathbf{F}_{NL}$ is the vector of error in the identified nonlinear force arising from the use of SEREP method to estimate the response at unmeasured coordinates and modelling error in updating the underlying linear system.

$$\begin{aligned}\delta\mathbf{F}_{NL} = &-\left(\mathbf{K}^a + j\omega\mathbf{C}^a - \omega^2\mathbf{M}^a\right)\begin{Bmatrix}\mathbf{0}\\ \delta\mathbf{W}_u\end{Bmatrix}\\ &-\left(\delta\mathbf{K} + j\omega\delta\mathbf{C} - \omega^2\delta\mathbf{M}\right)\left(\begin{Bmatrix}\mathbf{W}_m\\ \mathbf{W}_u^a\end{Bmatrix} + \begin{Bmatrix}\mathbf{0}\\ \delta\mathbf{W}_u\end{Bmatrix}\right)\end{aligned} \tag{4.12}$$

A usual way to update the underlying linear system is using the response of the nonlinear system excited by a very low-amplitude external force. Although the effect of nonlinear force on the response of the system decreases by reducing the amplitude of excitation force, one cannot get rid of it in practical systems. In other words, one of the most significant sources of modelling error is the difference between the response of the true (pure linear) underlying linear system and the linear response obtained from a low amplitude excitation test of the nonlinear system. In addition, using a low-amplitude excitation results in a higher contribution of noise and error in the measured response, and leads to bigger errors in the measured data. A low amplitude excitation of 0.01 N was applied to both the underlying linear system and the nonlinear system of Figure 4.2 and the responses are shown in Figure 4.16. Such differences in the responses may cause errors in updating the modal parameters of the underlying linear system (i.e. natural frequency, damping ratio, and mode shape). As the updated underlying linear model of the nonlinear system is used for both expansion and identification, the existence of modelling errors may lead to additional errors in both the expansion and the identification of the system.

Here it is assumed that a complete measurement has been performed and there is no expansion error in the identification process. Figure 4.17 demonstrates the identification of the unknown internal stiffness and damping considering two levels of modelling error (+5%,+10%) in the parameters of the underlying linear system (E, ρ, γ). Applying 5% and 10% modelling error to the parameters of the underlying linear system resulted in 5% and 9% errors in the identification of the nonlinear stiffnesses, respectively. The errors for the identified linear stiffnesses were 5% and 12.5%. Furthermore, EDSM was not capable of estimating the linear damping. The identified nonlinear forces for two levels of modelling error were obtained as,

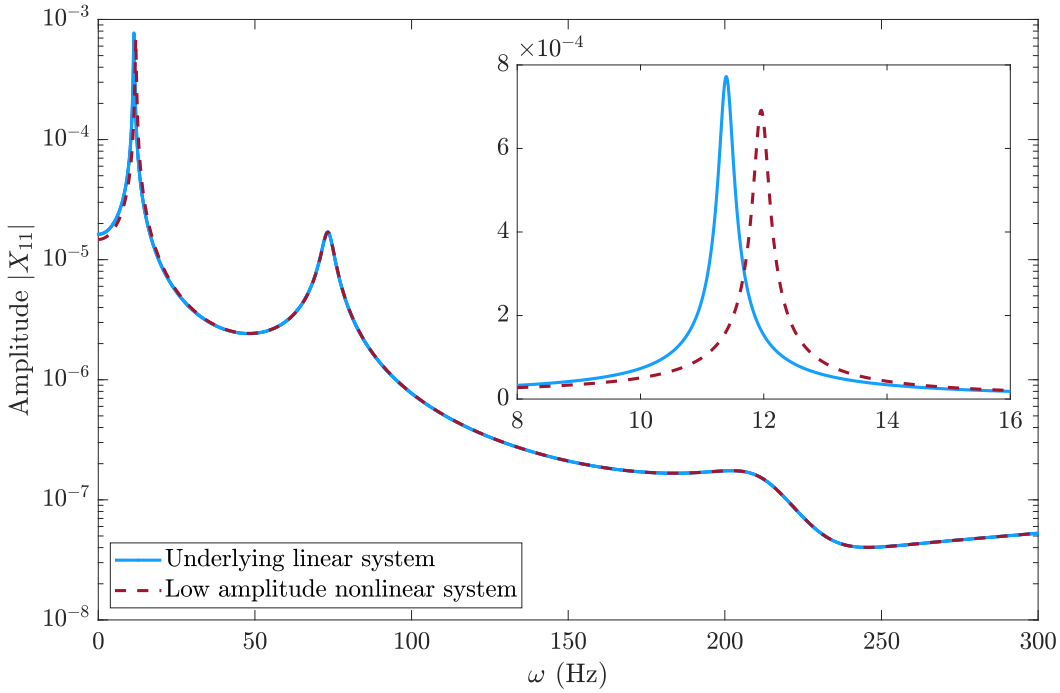

Figure 4.16: Difference between a purely linear system and the response of a nonlinear system with a very low amplitude excitation.

$$F_N = c_l \dot{w}(l,t) + c_N \dot{w}(l,t) w^2(l,t) + k_l w(l,t) + k_N w^3(l,t), \tag{4.13}$$

with identified parameters for modelling error of +5%

$$c_l = 0.0034 \ \frac{\text{N.s}}{\text{m}}, \quad c_N = 0.325 \ \frac{\text{N.s}}{\text{m}^3}, \quad k_l = 19 \ \frac{\text{N}}{\text{m}}, \quad k_N = 1.05 \times 10^5 \ \frac{\text{N}}{\text{m}^3}. \tag{4.14}$$

and identified parameters for modelling error of +10%

$$c_l = 0.0028 \ \frac{\text{N.s}}{\text{m}}, \quad c_N = 0.675 \ \frac{\text{N.s}}{\text{m}^3}, \quad k_l = 17.5 \ \frac{\text{N}}{\text{m}}, \quad k_N = 1.09 \times 10^5 \ \frac{\text{N}}{\text{m}^3}. \tag{4.15}$$

4.3.3.3 The Effect of Noise

Figures 4.18 and 4.19 show the effect of noise in the measured data on the results of the identification. In order to investigate the effect of noise, four different levels (0.5,1,2,5 %) of normally distributed noise have been applied to the response of the system. Incomplete measurements are assumed and there is no modelling error. In fact, a combination of expansion error and noise effects are shown in Figures 4.18 and 4.19. It is observed in Figure 4.18 that increasing the noise level in the response of the system may

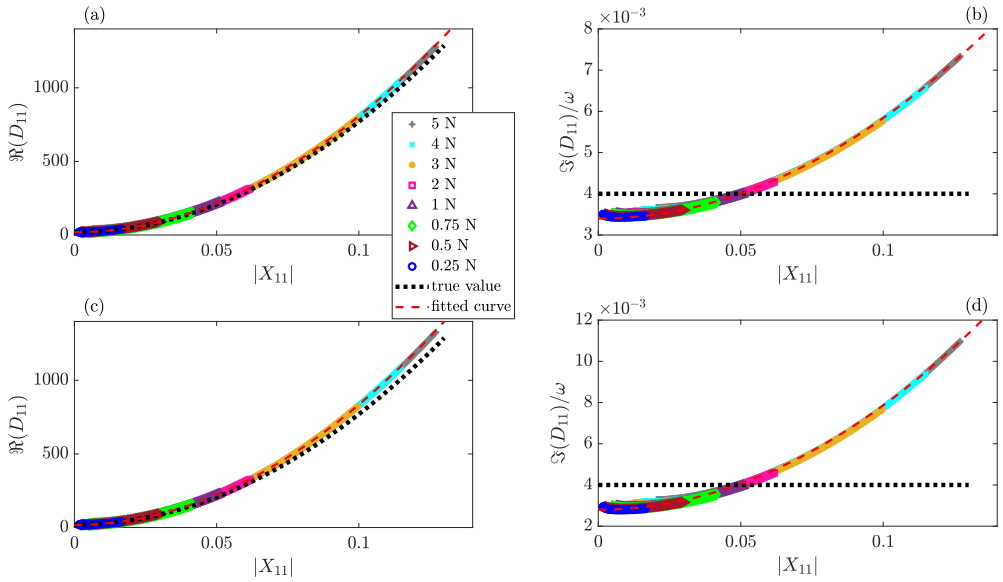

Figure 4.17: The effect of modelling error on the identification of nonlinear force of the system using the EDSM method. (a & b) modelling error of +5% (c & d) modelling error of +10%.

make it difficult to fit a reasonable curve to the EDSM data points, and therefore, it would be difficult to identify the nonlinear internal force. Note that, in practice, the noise is not likely to be normally distributed.

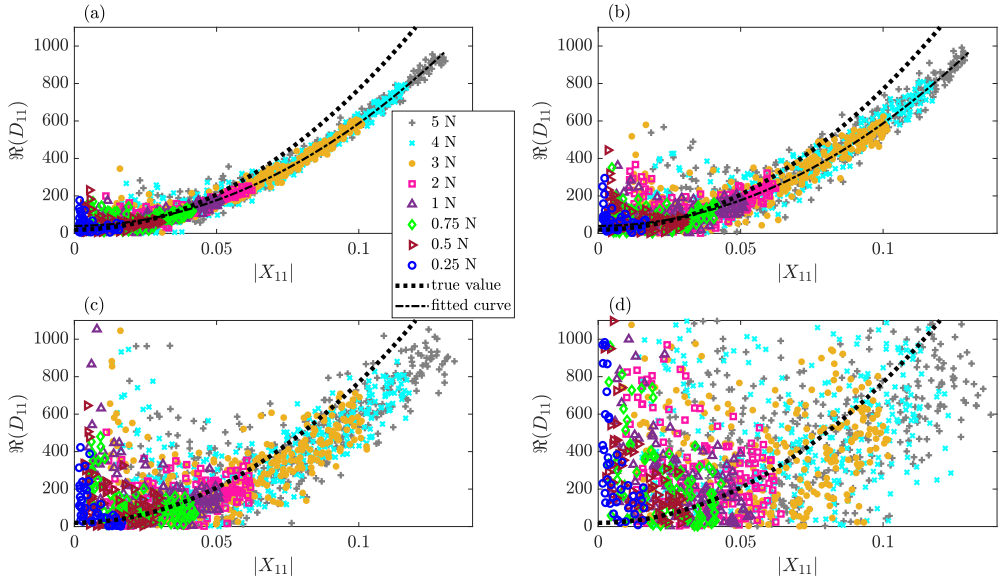

Figure 4.18: Identification of stiffness with different noise levels. (a) 0.5%, (b) 1%, (c) 2%, (d) 5%.

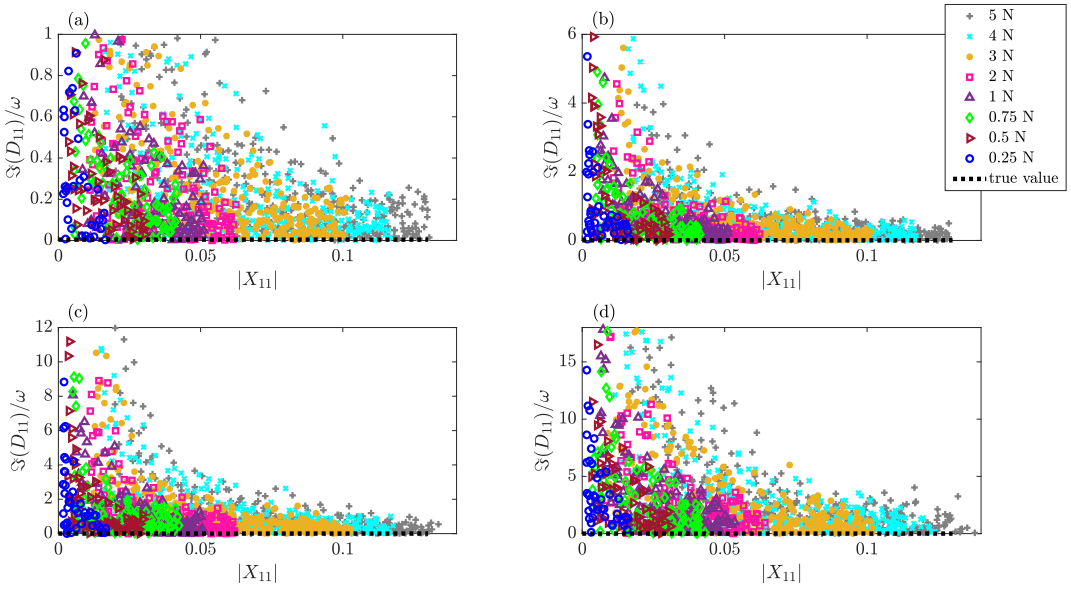

Figure 4.19: Identification of damping with different noise levels. (a) 0.5%, (b) 1%, (c) 2%, (d) 5%.

4.3.3.4 The Effect of Higher Harmonics

One of the most important problems to be considered in the analysis of nonlinear systems is the participation of the higher harmonics in the response of the system. Although the primary harmonic is dominant in many nonlinear systems and higher harmonics can be neglected during the analysis, neglecting higher harmonics in cases where they play a significant role in the behaviour of the system may lead to considerable errors in the results of the analysis. In this section, the effect of higher harmonics on the results of identification of nonlinear elements of dynamical systems is investigated. To this end, the 3-DOF discrete system of Figure 4.1 is considered.

The simulated steady state dynamics of the system shown in Figure 4.7 was obtained neglecting the higher harmonics in the response, and the parameters were identified in Figures 4.8 and 4.9 based on this assumption. However, higher harmonics usually play significant role in the dynamics of nonlinear systems. The simulation data was used to identify the unknown nonlinear elements of the system, and the response was assumed to include only the primary harmonic. Therefore, neglecting higher harmonics in the identification process would not lead to an effective identification. In this section, the higher harmonics are considered in the response of the system and it is assumed that the simulation/measurement includes higher harmonics in addition to the primary harmonics in the steady state response of the system.

Figure 4.20 illustrates the amplitude and phase of the primary harmonic of the response of the nonlinear system in the frequency domain, with and without the presence of higher harmonics in the simulation. $|X_{11}|$, $|X_{21}|$, and $|X_{31}|$ in Figure 4.20 denote the amplitudes of the primary harmonics of three degree of freedom of the system of Figure 4.1, respectively. φ_{11}, φ_{21}, and φ_{31} represent the phases

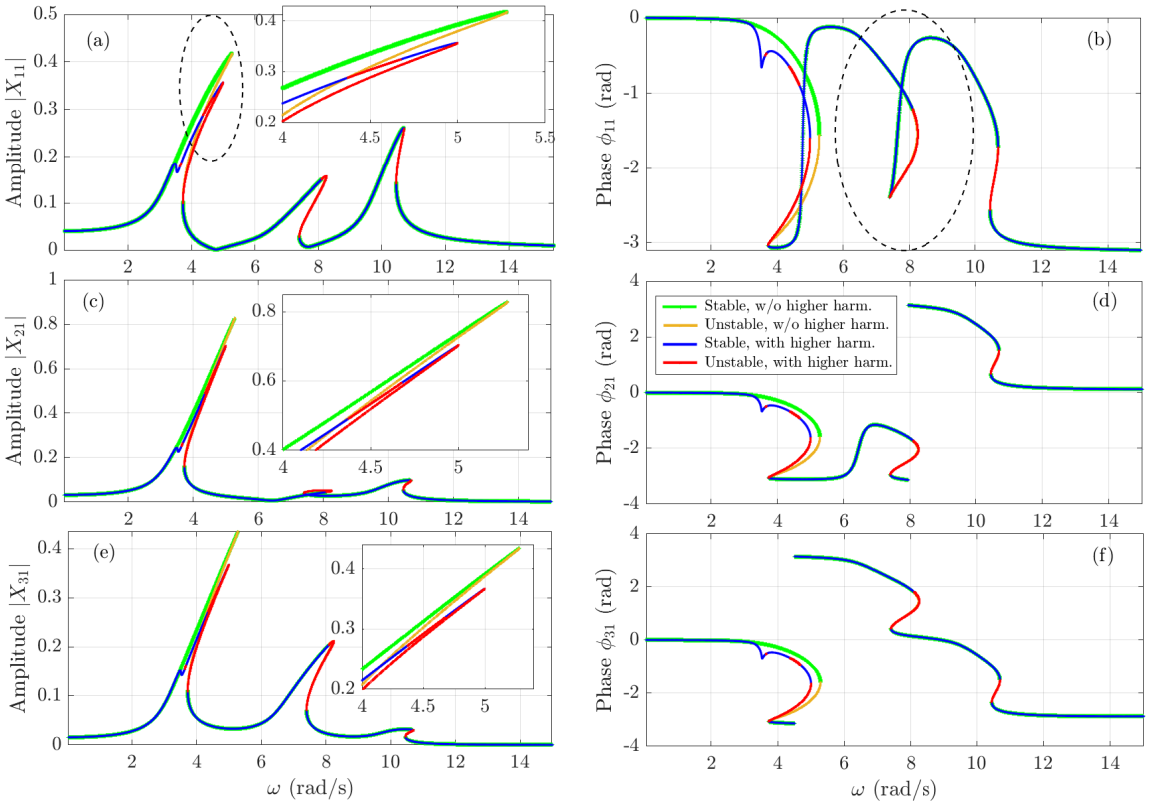

Figure 4.20: Comparison of the primary harmonic of the nonlinear response of the three-DOF discrete system with and without considering higher harmonics in the simulation.

of the primary harmonic of the steady state response of the 3DOF system. As shown, the presence of higher harmonics makes the most difference for the first resonant frequency of the response. And among all three degrees of freedom, DOF 1 has been affected more than two other DOFs. The amplitude and phase of the first three harmonics of the response of the nonlinear system of Eq. (4.1) is shown in Figure 4.3. The phase of the response of each degree of freedom is the same for all harmonics. As shown, due to the presence of the cubic nonlinearity in the system, the amplitude of the second harmonic is zero as expected. However, the third harmonic of the response mainly appears in the vicinity of the first resonant frequency, and its amplitude is small in the neighbourhood of the second and third resonances. The maximum ratio between the amplitude of the third harmonics of the response of DOF 1 and the amplitude of its primary harmonic is 0.5 at $\omega = 3.53$ rad, while this ratio is 0.14 at $\omega = 3.53$ rad for DOF 2 and 0.09 at $\omega = 5$ rad for DOF 3. All of these peak points occur within the neighbourhood of the first resonance, $\omega = 2 \sim 6$ rad.

Accordingly, neglecting the higher harmonics in the response of the system in the vicinity of first resonant frequency has the biggest effect in generating errors in the identification. In other words, implementing the identification process using only the primary harmonic of the response within the frequency range of the second and third resonances, as illustrated in Figures 4.21 and 4.22, may not lead to significant errors in the results, as the higher harmonics cannot be observed strongly in the response in that region. Figures 4.21 and 4.22 demonstrate the results of the identification of the unknown parameters using the primary harmonic of the response of the system within the region of the second and third resonances, respectively. Apparently, due to the small participation of the higher harmonics in these regions, the magnitude of the error in the identification is not significant. In contrast, if the identification is performed using only the primary harmonic of the response in the vicinity of the first resonance, neglecting higher harmonics will result in significant errors in the identification results, see Figure 4.23. In Figures 4.21-4.23, $|X_{11}|$, $|X_{21}|$, and $|X_{31}|$ are, respectively, the amplitudes of the primary harmonics of three degrees of freedom of the system of Figure 4.1. $D_{eq_{11}}$, $D_{eq_{23}}$, $D_{eq_{33}}$ denote the equivalent dynamic stiffness, respectively, for the grounded nonlinear element attached to DOF 1, the ungrounded nonlinear force between DOFs 2 and 3, and the grounded nonlinear element attached to DOF 3.

4.3.4 Identification Using Optimization

According to the discussion in Section 4.3, one may conclude that there are many sources of inaccuracy affecting the results of identification methods, particularly for the EDSM technique. To avoid such sources of inaccuracy, or at least to reduce their effects on the results of identification, an optimization-based framework is used to identify nonlinear structures. The optimization-based framework is presented in details in Chapter 5. In this section, the nonlinear system of the cantilever beam of Figure 4.2 is

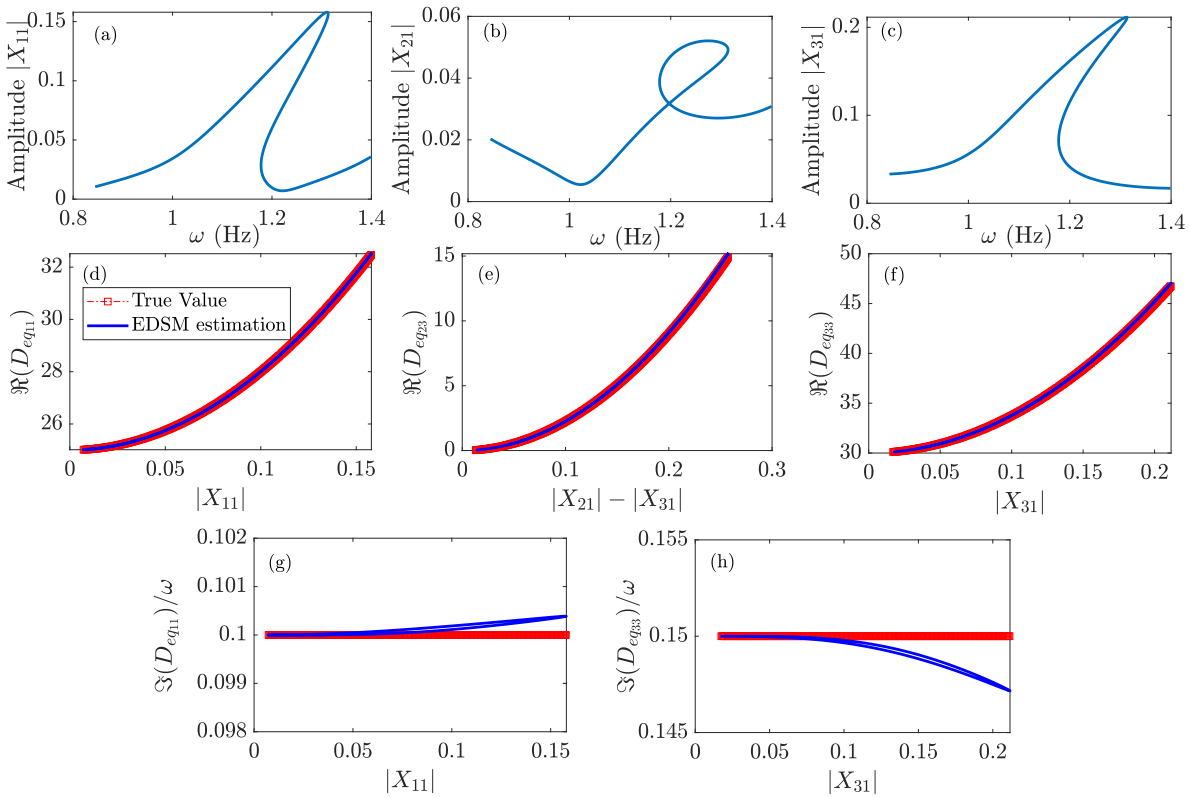

Figure 4.21: The primary harmonic of the amplitude-frequency responses of three oscillator in the neighbourhood of second resonance used in the EDSM identification; (d, e, f) Comparison of true EDSM-estimated nonlinear stiffnesses and linear damping (g and h).

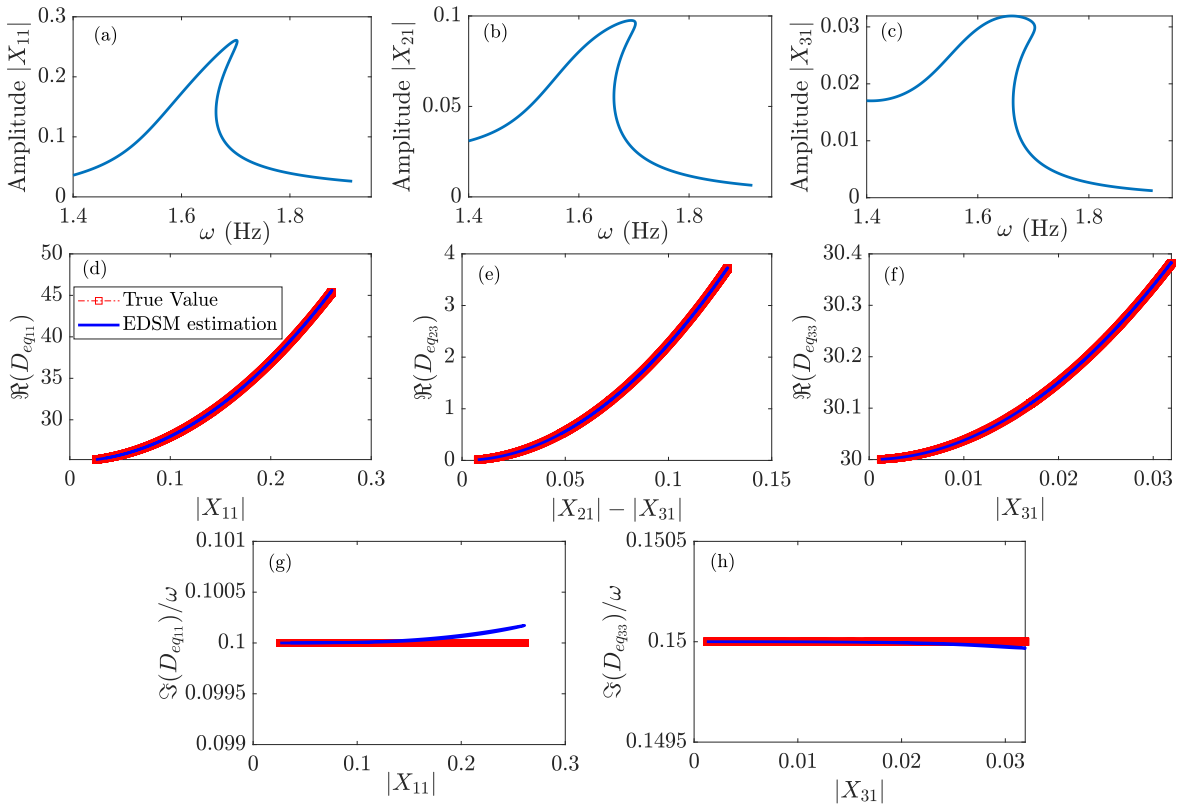

Figure 4.22: (a, b, c) The primary harmonic of the amplitude-frequency responses of three oscillator in the neighbourhood of third resonance used in the EDSM identification; (d, e, f) Comparison of true EDSM-estimated nonlinear stiffnesses and linear damping (g and h).

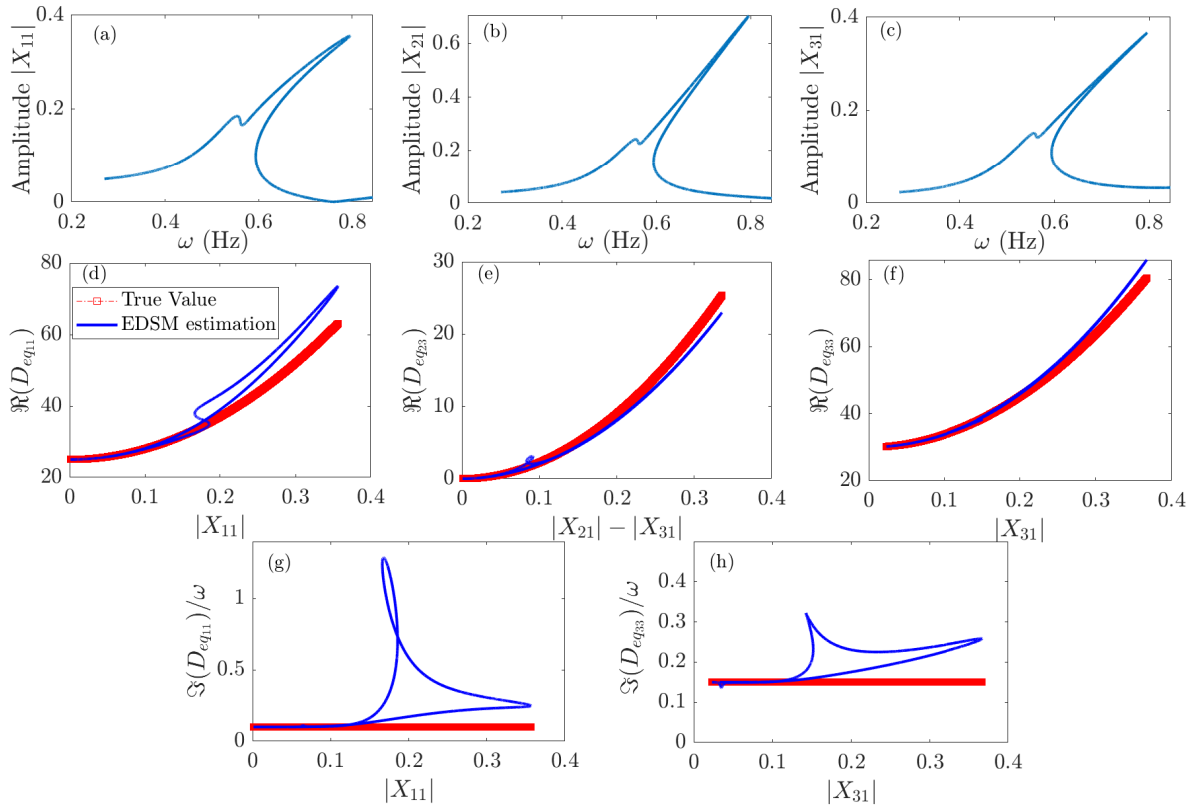

Figure 4.23: (a, b, c) The primary harmonic of the amplitude-frequency responses of three oscillator in the neighbourhood of first resonance used in the EDSM identification; (d, e, f) Comparison of true EDSM-estimated nonlinear stiffnesses and linear damping (g and h).

identified utilizing the framework proposed in Chapter 5. For this purpose, following assumptions and considerations are taken into account:

- Only the inaccuracy due to expansion method is considered. All other sources of inaccuracy (i.e. noise and modelling error) are neglected.
- The identified nonlinear force obtained from the EDSM method are considered as the initial estimate for the unknown parameters of the nonlinear force in the optimization process.
- The objective function is defined so that the difference between the measured/simulated and estimated nonlinear response are minimized.

$$J = \min \left(\sum_{i=1}^{N_f} | \log \left(\|X_m(\Omega_i)\|_2 \right) - \log \left(\|X_a(\Omega_i)\|_2 \right) | \right), \tag{4.16}$$

  where X_m and X_a are respectively the experimental/simulated response and the estimated response of the system in the frequency domain.
- Considering the response of the system in the vicinity of the resonance may improve the efficiency of the optimization process.
- In nonlinear systems, multiple solutions for the response may occur (more than one stable solution). In such cases, the most significant stable branch of the response is considered within the range of the multiple solutions.
- The unstable solution of the numerical estimation is neglected, as it is almost impossible to measure the unstable solution in an experiment.

To compare the result of the optimization-based framework with the result of the EDSM technique, the identified nonlinear force of the cantilever beam given by Eq. (4.9) is considered as the initial estimate for the optimization process. It is assumed that the response of the cantilever beam is measured at only the three DOFs 1, 5, and 9. Figure 4.24 shows the simulated response at DOF 9 of the beam under the excitation force amplitude of $F = 1$ **N** and compares it with the regenerated response obtained using the identified nonlinear force from the EDSM technique. As mentioned above, the unstable and the lower stable branch of the response are neglected. The optimization method aims to minimize the difference between the simulated/measured and the estimated response. As a spatially complete measurement is not required in the optimization-based framework, it is not necessary to use an expansion method in order to estimate the response at unmeasured DOFs. Therefore, the measured response at only one of the measured DOFs (e.g. DOF 9) is used for the optimization process. The optimized parameters of the nonlinear force are obtained using the optimization process exploiting the identified parameters of

Table 4.3: Optimized parameters of the nonlinear force of the cantilever beam.

Parameters (unit)	True Value	Identified by EDSM		Optimized	
		Value	Error (%)	Value	Error (%)
$c_l \frac{\text{N.s}}{\text{m}}$	0.004	0.0435	987	0.00427	6.75
$k_l \frac{\text{N}}{\text{m}}$	20	40	100	21.586	19.93
$k_N \frac{\text{N}}{\text{m}^3}$	1×10^5	7.3×10^4	-27	9.355×10^4	-6.45

Eq. (4.9) as the initial estimate. Table 4.3 gives a comparison between the true values of the parameters of the nonlinear force and the identified values obtained from the EDSM and optimization methods.

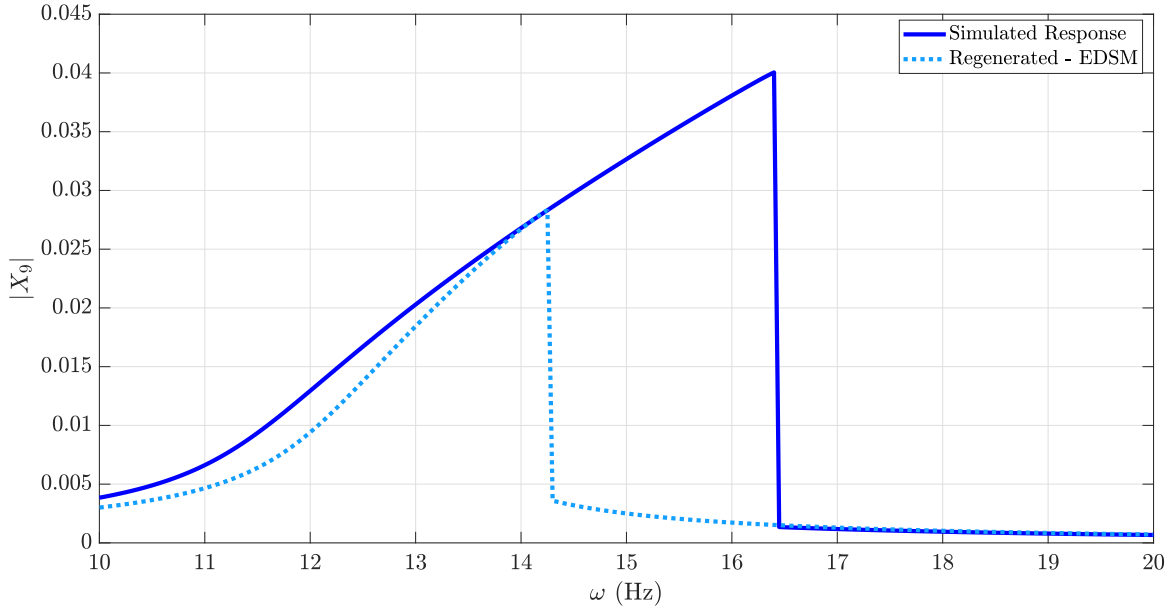

Figure 4.24: Simulated/measured response at DOF 9 compared with the regenerated response obtained from the nonlinear model identified using EDSM technique.

As it can be seen, the accuracy of the identified values of the parameters have been significantly improved. However, as the cubic stiffness is dominant in dynamics of the system at the vicinity of the resonant frequency, the linear stiffness has not been optimized to a very accurate value. The optimized parameters are used to regenerate the nonlinear response of the cantilever beam. Figure 4.25 compares the simulated nonlinear response with the numerically regenerated ones obtained from the nonlinear models identified using the EDSM technique and the optimization method. The identified nonlinear model obtained from optimization method is shown to be more accurate than the identified model of the EDSM technique.

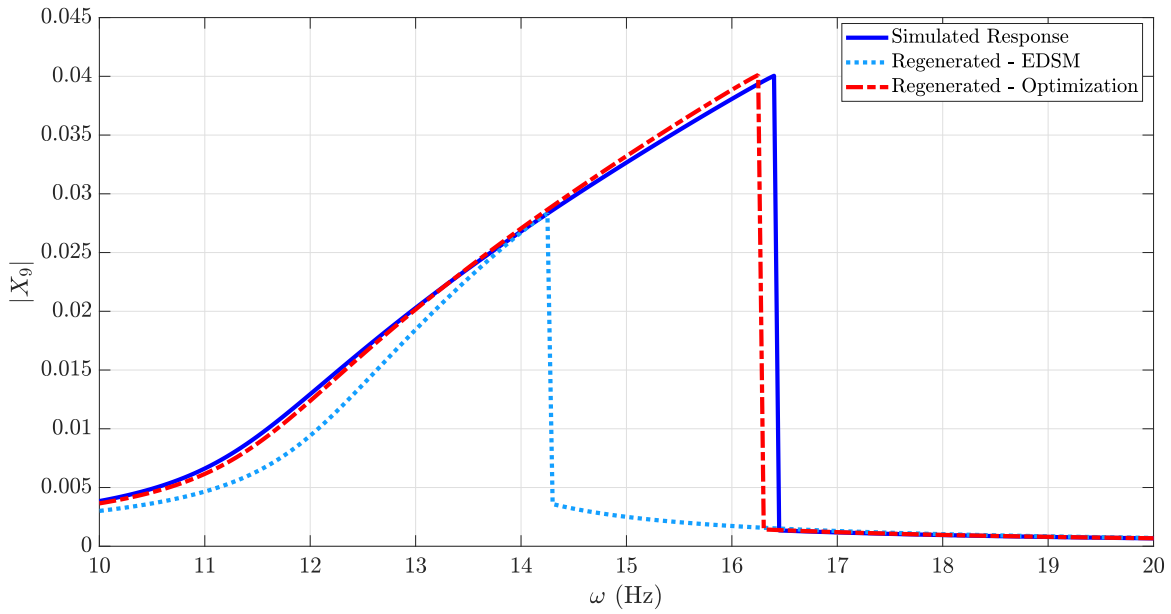

Figure 4.25: Simulated/measured response at DOF 9 compared with the regenerated response obtained from nonlinear models identified using the EDSM technique and the optimization-based framework.

To verify the reliability of the model identified using the optimization-based framework, the simulated/measured responses of the system at three measured, namely DOFs 1, 5, and 9, are compared with the regenerated response using the optimized parameters. Figure 4.26 illustrates the comparison between the simulated and regenerated response at DOFs 1, 5, and 9. Although the optimization was performed using only DOF 9, the identified model is capable of estimating the response at the other degrees of freedom.

4.4 Closure

This chapter has investigated the sensitivity of the identification using the Equivalent Dynamic Stiffness Mapping (EDSM) technique to noise in measured data and various types of error such as expansion error, modelling error, and the error due to neglecting the higher harmonics in the response of nonlinear systems. For this purpose, a theoretical study has identified the structural nonlinearities of two nonlinear systems (a discrete three-DOF Duffing system and a cantilever beam with a nonlinear restoring force applied to the tip of the beam) considering the presence of all the aforementioned sources of inaccuracy (noise and error). First, the accuracy of the EDSM technique in the identification of nonlinear elements has been verified by applying the method to two example nonlinear systems. Afterwards, numerical simulation of the two systems has been performed in MATLAB and the simulated data has been used to investigate the effect of the presence of noise in the simulated/measured data, expansion error in the

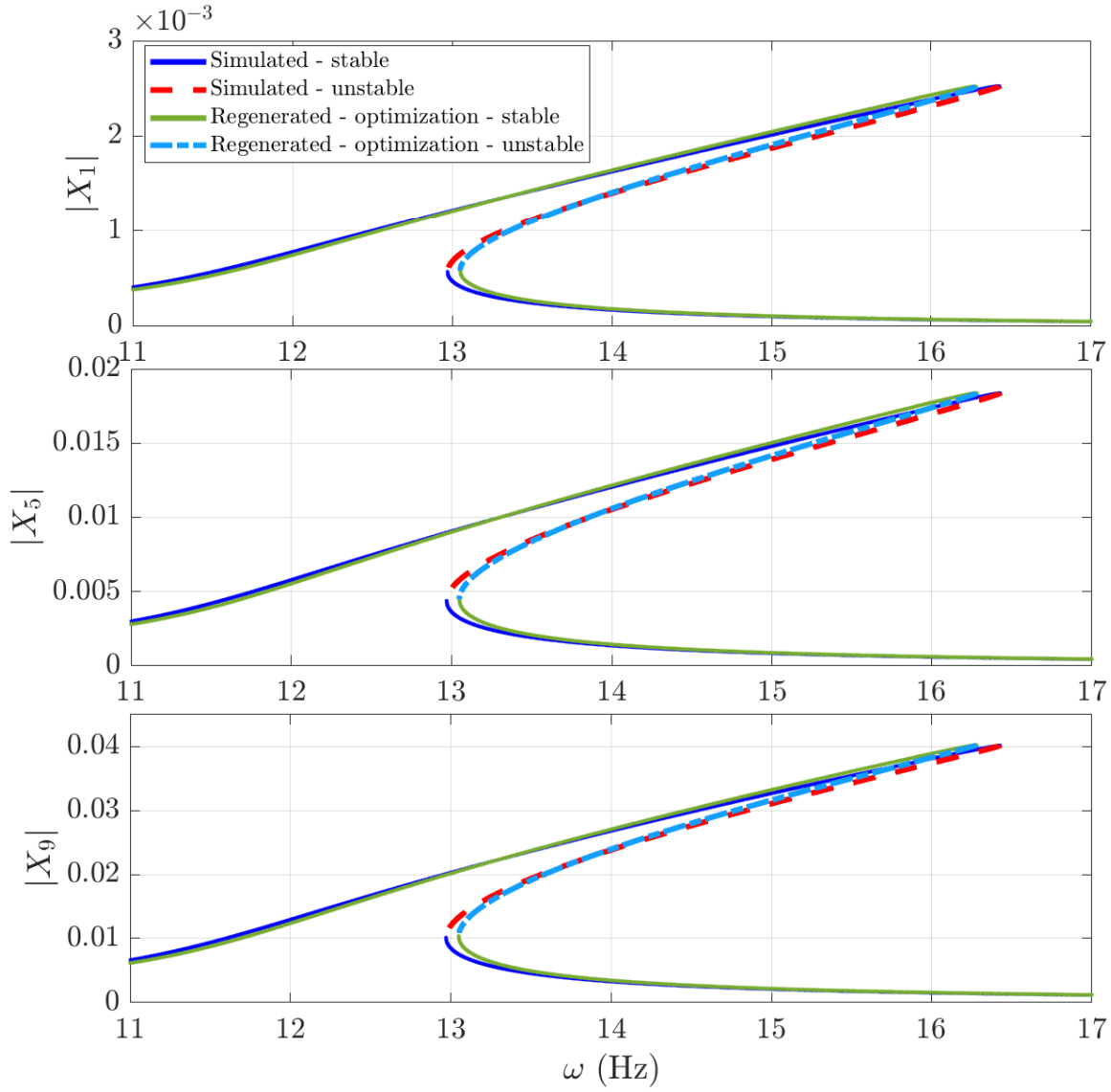

Figure 4.26: Comparison between the simulated/measured response at DOFs 1, 5, and 9 and the regenerated response obtained from nonlinear model identified using the optimization method.

estimation of the unmeasured coordinates, modelling error in the updated underlying linear model, and the error due to neglecting the higher harmonics in the nonlinear response of the system, on the outcome of the identification process. The nonlinear response of the system has been regenerated using the identified parameters with the presence of the sources of error and the generated response was compared with the simulated response in the absence of any noise or error. According to the results, although the EDSM technique is capable of identifying accurately the nonlinear elements in the absence of any source of inaccuracy, it has been demonstrated that this method is very sensitive to sources of inaccuracy and would result in significant errors in the model of the nonlinear system. Finally, the nonlinear force of the system with a cantilever beam was identified utilizing an optimization framework using the results of EDSM technique as the initial parameter estimate for the optimization process. Minimizing the difference between the measured/simulated and estimated nonlinear responses of the system at one of the measured coordinates was set as the objective function of the optimization process. The validity of the results of the optimization method was verified by comparing the response at other measured DOFs. Using the optimization method, one may avoid the inaccuracy resulting from expansion methods or the effect of higher harmonics. The comparison between the estimated and measured responses illustrates that the optimization method is able to identify the nonlinear system and regenerate the measured/simulated nonlinear response.

Chapter 5

An optimization-based framework for nonlinear model selection and identification

5.1 Introduction

Mathematical models have been increasingly used in nonlinear structural dynamics. However, the type of nonlinearity and the parameters of these nonlinear models need to be identified from experimental data. This is mainly due to the lack of knowledge about the mechanism of the nonlinearity in structures while in service. Therefore, there has been considerable attention in nonlinear model identification using vibration test data. To this end, the identified mathematical model should not only be capable of predicting the real-life behaviour of an unknown structure, but also must be physically meaningful. In other words, it is essential to ensure that any mathematical model developed through the process of identification is a valid physical model. Having a valid physical model in the identification process using experimental data will lead to more reliable and meaningful identified parameters.

This chapter proposes a framework using an optimization-based method for nonlinear system identification. The method assumes that the nonlinear force can be expanded using a Taylor series. This mathematical model consists of a linear part (first order term) that can be identified from well-known sensitivity-based model updating ([6]-[12],[127]) and, for the nonlinear part, the order of the nonlinearity increases sequentially, and an optimization-based method can be used to identify the parameters for each case. The proposed method is applied to a cantilever beam subjected to an electromagnetic force. The whole system is base excited, and thus a cantilever beam is clamped to the movable bed of a shaker.

Two permanent magnets attached to both sides of the tip of the beam along with two electromagnets located symmetrically on the two sides of the permanent magnets generate the nonlinear restoring force applied on the beam. The structure is excited by constant acceleration base motion of the shaker. First, the underlying linear system is updated using the linear response of the system obtained from low amplitude excitation. Afterwards, the nonlinear frequency response of the system measured from a high amplitude vibration test is used to estimate the coefficients of the nonlinear electromagnetic force. Four levels of nonlinearity for stiffness are assumed. It is observed that nonlinear force up to the fifth order nonlinear stiffness and a linear damping produces an excellent agreement between the measured nonlinear responses and predictions. Increasing the order of nonlinearity in stiffness and damping has not shown significant improvement in the optimization results.

5.2 Experimental set-up

The experimental set-up used for the study in this chapter is a cantilever beam subject to a nonlinear electromagnetic force at the tip of the beam. The set-up is described in Section 3.3.1 and shown in Figure 3.2. The dimensions and the material properties of the structure, and the properties of permanent magnets and electromagnets are given in Table 3.1.

As explained later in this chapter, two types of tests are required in the identification process of the present study; first a low amplitude test for measuring the linear response of the system being utilized in updating the underlying linear model, and second a high amplitude test for measuring the nonlinear response of the system to be used in the identification process. For the low amplitude test, the structure is excited by a constant acceleration excitation of amplitude $0.02g$, where g is the gravitational acceleration. Figure 3.12 illustrates the linear response of the structure excited by this low amplitude base motion. A_1, A_2, and A_3 denote the accelerations measured by accelerometers AM1, AM2, and AM3, respectively. In order to obtain a nonlinear response from the high amplitude test, the amplitude of the excitation has to be large enough to guarantee that the nonlinearity of the system is excited. In this study, the base of the structure (shaker bed) is excited by a constant acceleration of amplitude $0.08g$ to assure the nonlinear response of the system.

Figure 3.13 illustrates the constant acceleration base excitation for the frequency span of $f = [8.9 - 11]$ Hz. It is notable that the feedback of the response of the structure, particularly in the neighbourhood of the resonant frequency, may change the amplitude of the excitation. Therefore, in order to keep the amplitude of the desired excitation constant, a sine test is carried out at each frequency point to measure the steady state response of the system. As a result, all the experimental data measured from the sine tests at each frequency step are utilized to find the frequency response of the system. To obtain all stable branches of the nonlinear response, both sweep-up and sweep-down tests were carried out.

However, as the upper branch (with larger amplitude) is used in the optimization, only measuring the upper stable solution would be satisfactory. For this study, as is explained in Section 5.3 and also shown in the measured nonlinear response, the electromagnets provide softening nonlinearities. Therefore, a sweep-down stepped-sine test is carried out to measure the upper branch of the response. The excitation amplitude should be large enough to guarantee that the nonlinearity of the system is excited. The amplitudes and phases of the experimentally measured nonlinear response of the system at three points along the beam, 5, 15, and 25 cm away from the clamped end of the beam (which are equivalent to the locations of AM1, AM2, and AM3), are shown in Figure 3.14. The measured nonlinear responses are used to identify the unknown nonlinear restoring force of the system.

In the following section, a mathematical model is derived for the nonlinear system given by the experimental rig.

5.3 Mathematical model

In this section, the nonlinear force obtained from electromagnets explained in Section 5.2 is described by a mathematical model. To this end, a cantilever beam of length l, width d, thickness h, density ρ, and modulus of elasticity E is considered. Figure 3.3 illustrates the schematic of the cantilever beam model. The cantilever is subjected to an unknown nonlinear electromagnetic restoring force f_{NL} at the tip of the beam. The beam is mounted on a shaker base and is subject to base excitation.

The equation of motion of the system is derived using Lagrange's equation. Since the type of nonlinearity is unknown, a mathematical form is assumed for the nonlinear force to be considered in the model. This assumption is based on the physics of the problem and also measured nonlinear response of the system from experimental vibration tests. The attractive nonlinear force resulted by two symmetric electromagnets is generally given as [153, 154],

$$f_{NL} = -\left(\frac{c_s}{(d_0-\chi)^2} - \frac{c_s}{(d_0+\chi)^2}\right), \tag{5.1}$$

where χ denotes the displacement of the tip of the beam, d_0 is the gap between each electromagnet and the tip at equilibrium position, and c_s is a positive constant coefficient dependant on the voltage of the electromagnets. Using the Taylor expansion about the equilibrium position ($\chi = 0$), the nonlinear electromagnetic force of Eq. (5.1) is rewritten as

$$f_{NL} = -\left(\frac{4c_s\chi}{d_0^3} + \frac{8c_s\chi^3}{d_0^5} + \frac{12c_s\chi^5}{d_0^7} + \frac{16c_s\chi^7}{d_0^9} + \cdots\right), \tag{5.2}$$

Figure 5.1 compares the exact nonlinear electromagnetic function given in Eq. (5.1) with different orders of the Taylor series expansion of Eq. (5.2). The results show that the 7^{th} order Taylor series expansion gives a reasonably good approximation of the nonlinear function of Eq. (5.1).

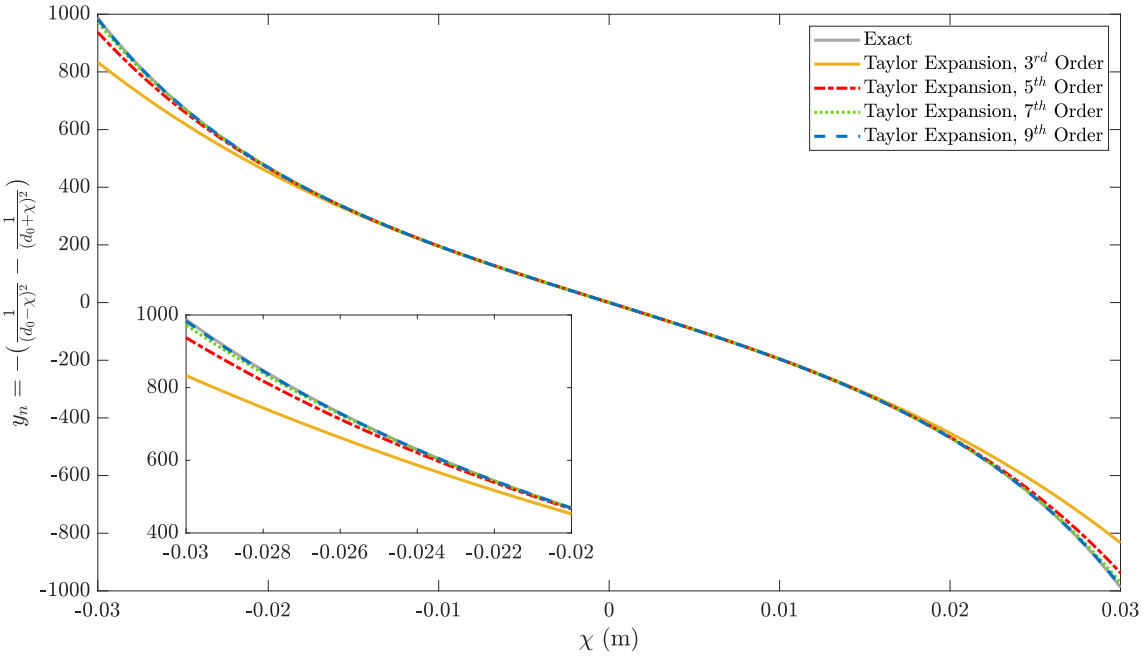

Figure 5.1: Comparison between the nonlinear electromagnetic force of Eq. (5.1) with different orders of its Taylor series expansion of Eq. (5.2), $d_0 = 0.06$.

The negative sign of the force indicates that attractive forces of two symmetric electromagnets generate softening nonlinearities in the system. Eq. (5.2) may be used as an appropriate assumption for the nonlinear force with coefficients only dependent on constants c_s and d_0. However, it is often very difficult to have a purely symmetric electromagnetic force in an experiment. Moreover, the model of Eq. (5.1) presented in [153] does not consider the damping effect of the electromagnetic force. Hence, in this study, a different framework will be considered to model the electromagnetic force. As shown in Eq. (5.2), the Taylor series expansion may be used to represent the nonlinear stiffness force created by the electromagnets. Care has been taken to ensure that the configuration is symmetric and therefore we may assume only the odd terms are included. The damping force can be also represented by a Taylor series expansion. Based on this, four possible models to represent the nonlinearity of electromagnetic force are shown in Table 5.1. As can be seen in the table, the order of stiffness and damping nonlinearity is increased gradually. The level of nonlinearity is increased until it does not improve the identification results, and then the model may be considered good enough to represent the nonlinear electromagnetic force.

Table 5.1: Possible models to represent electromagnetic force.

Model No.	Mathematical Formulation
Model I:	$f_{NL} = \lambda\dot{\chi} + k_l\chi + k_{n_3}\chi^3$
Model II:	$f_{NL} = \lambda\dot{\chi} + k_l\chi + k_{n_3}\chi^3 + k_{n_5}\chi^5$
Model III:	$f_{NL} = \lambda\dot{\chi} + k_l\chi + k_{n_2}\chi\lvert\chi\rvert + k_{n_3}\chi^3 + k_{n_5}\chi^5$
Model IV:	$f_{NL} = \lambda\dot{\chi} + \lambda_n\dot{\chi}\lvert\dot{\chi}\rvert + k_l\chi + k_{n_2}\chi\lvert\chi\rvert + k_{n_3}\chi^3 + k_{n_5}\chi^5$

In Table 5.1, λ, λ_n denote the linear and nonlinear damping coefficients, and $k_l, k_{n_2}, k_{n_3}, k_{n_5}$ indicate the linear stiffness, symmetric quadratic stiffness, cubic and fifth order stiffnesses, respectively. Note as the electromagnets are mounted on the movable bed of the shaker, as well as the beam, χ in the four models given in Table 5.1 should be the relative displacement of the tip of the beam.

As explained in Section 3.3.2, neglecting the effect of imperfect clamping affects the resonance and anti-resonance frequencies. Therefore, the effect of the imperfect clamping is considered in the model of the structure, as explained in Section 3.3.2. The equivalent mass and stiffness of the L-shaped aluminium clamp is given by Eq. (3.8).

Considering the assumed type of the nonlinearity and the effect of the clamp as a linear stiffness attached to the base of the beam, the governing equations of the system are derived using the Euler-Lagrange method. In this case, the equation of motion will be derived for case IV but the obtained solution for the nonlinear frequency response functions may be used for the three simpler models, i.e. Model I ($k_{n_5} = k_{n_2} = \lambda_n = 0$), Model II ($k_{n_2} = \lambda_n = 0$) and Model III ($\lambda_n = 0$). The kinetic and potential energy are given as follows

$$T = \frac{1}{2}\int_0^l \rho A \left(\frac{\partial w(x,t)}{\partial t}\right)^2 dx + \frac{1}{2}\sum_{n=1}^{N_p} M_n \left(\frac{\partial w(x,t)}{\partial t}\right)^2 \delta(x - x_n), \tag{5.3}$$

and

$$\begin{aligned} V = \frac{1}{2}\int_0^l EI \left(\frac{\partial^2 \left(w(x,t) - w_b(t)\right)}{\partial x^2}\right)^2 &+ \frac{1}{2}k_b \left(w(0,t) - w_b(t)\right)^2 + \frac{1}{2}k_l \left(w(l,t) - w_b(t)\right)^2 \\ &+ \frac{1}{3}k_{n_2} \left(w(0,t) - w_b(t)\right)^2 \left|w(0,t) - w_b(t)\right| \\ &+ \frac{1}{4}k_{n_3} \left(w(l,t) - w_b(t)\right)^4 + \frac{1}{6}k_{n_5} \left(w(l,t) - w_b(t)\right)^6, \end{aligned} \tag{5.4}$$

where $w(x,t)$ is the transverse vibration of the beam, x is the distance from the clamped end of the beam, $w_b(t)$ is the base motion of the shaker in transverse direction of the beam, M_n denotes all additional masses including accelerometers, permanent magnets attached to the tip, and the equivalent mass of the clamp support, and N_p is the total number of additional masses. Defining $z(x,t)$ as the relative

displacement of the beam with respect to the base motion $w_b(t)$ of the shaker bed

$$z(x,t) = w(x,t) - w_b(t), \tag{5.5}$$

the kinetic and potential energy can be rewritten as,

$$T = \frac{1}{2}\int_0^l \rho A \left(\frac{\partial\left(z(x,t)+w_b(t)\right)}{\partial t}\right)^2 dx + \frac{1}{2}\sum_{n=1}^{N_p} M_n \left(\frac{\partial\left(z(x,t)+w_b(t)\right)}{\partial t}\right)^2 \delta(x-x_n), \tag{5.6}$$

and

$$\begin{aligned} V = &\frac{1}{2}\int_0^l EI\left(\frac{\partial^2 z(x,t)}{\partial x^2}\right)^2 + \frac{1}{2}k_b z^2(0,t) + \frac{1}{2}k_l z^2(l,t) \\ &+\frac{1}{3}k_{n_2} z^2(l,t)|z(l,t)| + \frac{1}{4}k_{n_3} z^4(l,t) + \frac{1}{6}k_{n_5} z^6(l,t), \end{aligned} \tag{5.7}$$

Considering the proportional damping for the beam, Rayleigh's dissipation function of the system is also derived,

$$\begin{aligned} D = &\frac{1}{2}\int_0^l \left[\alpha\left(\frac{\partial z(x,t)}{\partial t}\right)^2 + \beta\left(\frac{\partial^3 z(x,t)}{\partial x^2 \partial t}\right)^2\right] dx \\ &+\frac{1}{2}\lambda\left(\frac{\partial z(l,t)}{\partial t}\right)^2 + \frac{1}{3}\lambda_n\left(\frac{\partial z(l,t)}{\partial t}\right)^2\left|\frac{\partial z(l,t)}{\partial t}\right|, \end{aligned} \tag{5.8}$$

where α, β are the proportional damping coefficients per length of the beam. Using Euler-Lagrange equation, along with the assumed mode method, the equation of motion of the system is derived. For this purpose, a solution is assumed for the response of the beam as

$$z(x,t) = \sum_{i=1}^{N_m} \phi_i(x) q_i(t), \tag{5.9}$$

where N_m represents the total number of modes used in the analysis, q_i denotes the i-th time variable modal coordinate, and ϕ_i is the i-th mode shape of the beam with the following boundary condition

$$\begin{aligned} \frac{\partial z}{\partial x} = 0, \quad \frac{\partial}{\partial x}\left(EI\frac{\partial^2 z}{\partial x^2}\right) = -k_b z(x,t), \quad at \quad x = 0 \\ EI\frac{\partial^2 z}{\partial x^2} = 0, \quad \frac{\partial}{\partial x}\left(EI\frac{\partial^2 z}{\partial x^2}\right) = 0, \quad at \quad x = l, \end{aligned} \tag{5.10}$$

In this study, a single-mode approximation of the system is utilized for the identification process. Therefore, the equations of motion are derived for this single-mode approximation. For the sake of brevity, the subscripts related to the first mode are neglected. In order to apply the assumed mode method, quadratic stiffness and damping energy terms of Eqs. (5.7) and (5.8) including absolute functions

can be approximated using the following series,

$$\begin{aligned}\frac{1}{3}k_{n_2}z^2|z| &= \frac{1}{3}k_{n_2}z\left(\left(\frac{2}{\pi}\right)z+\left(\frac{4}{\pi}\right)z\sum_{n=1}^{\infty}\left(\frac{(-1)^nT_{2n}(z)}{-1+4n^2}\right)\right)\\ &= k_{n_2}\left(\frac{1}{2}c_1z^2+\frac{1}{4}c_3z^4+\frac{1}{6}c_5z^6+\cdots\right),\\ \frac{1}{3}\lambda_n\dot{z}^2|\dot{z}| &= \frac{1}{3}\lambda_n\dot{z}\left(\left(\frac{2}{\pi}\right)\dot{z}+\left(\frac{4}{\pi}\right)\dot{z}\sum_{n=1}^{\infty}\left(\frac{(-1)^nT_{2n}(\dot{z})}{-1+4n^2}\right)\right)\\ &= \lambda_n\left(\frac{1}{2}e_1\dot{z}^2+\frac{1}{4}e_3\dot{z}^4+\frac{1}{6}e_5\dot{z}^6+\cdots\right),\end{aligned} \tag{5.11}$$

where c_1, c_3,c_5, $\cdots$ and e_1, e_3, e_5, $\cdots$ are the coefficients of the approximations of Eq. (5.11), and $T_n(z)$ is the Chebyshev polynomial of the first kind, for instance

$$T_{10}(z) = -1+50z^2-400z^4+1120z^6-1280z^8+512z^{10} \tag{5.12}$$

According to the expansion series of Eq. (5.11), the nonlinear function $y_n = z^2|z|$ can be expanded using a polynomial function of the form

$$y_n = z^2|z| = \sum_{i=1}^{N_o}c_iz^{2i} \tag{5.13}$$

where N_o denotes the order of polynomial expansion, and c_i are the coefficients of the polynomial expansion. Figure 5.2 compares the exact nonlinear function of Eq. (5.13) with various order numbers N_o of its polynomial expansion. The results show that the polynomial of order 6 ($N_o = 3$) can approximate the exact nonlinear function of Eq. (5.13) with reasonably good accuracy in the variation range of displacement.

Given the approximations of Eq. (5.11) for the quadratic stiffness and damping terms, substituting the assumed solution of Eq. (5.9) into Eqs. (5.6-5.8), and applying the Euler-Lagrange method, equation of motion is obtained as

$$\begin{aligned}&\left(\rho AR_1+\sum_{n=1}^{N-p}M_nR_{2_n}\right)\ddot{q}+\left(\alpha R_1+\beta R_3\right)q+EIR_3q+\lambda R_4q\\ &+\lambda_ng_{nl}\dot{q}+k_bR_4q+k_lR_5q+k_{n_2}h_{nl}(q)+k_{n_3}R_7q^3+k_{n_5}R_8q^5\\ &\qquad\qquad = -\left(\rho AR_0+\sum_{n=1}^{N-p}M_nR_{0_n}\right)\ddot{w}_b,\end{aligned} \tag{5.14}$$

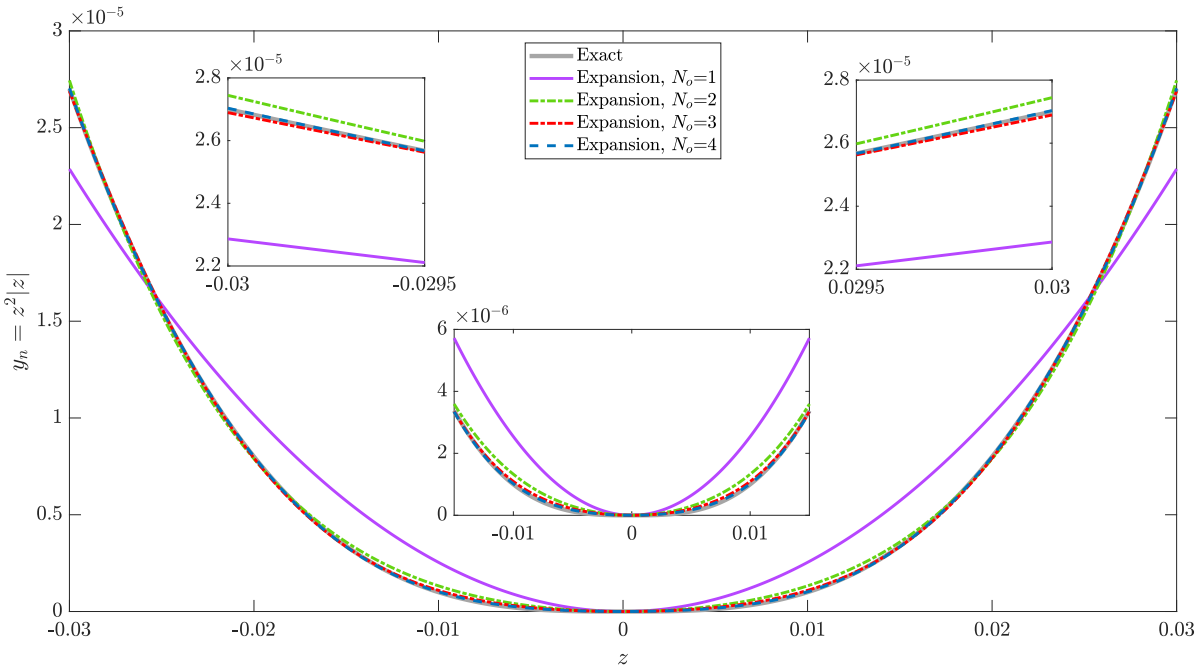

Figure 5.2: Comparison between the nonlinear function of Eq. (5.13) with different orders of its polynomial expansion.

where q denotes the time variable modal coordinate of first mode,

$$\begin{aligned} R_0 &= \int_0^l \phi_1 \, dx, \quad R_{0_n} = \phi_1\big|_{x_n}, \quad R_1 = \int_0^l \phi_1^2 \, dx, \\ R_{2_n} &= \phi_1^2\big|_{x_n}, \quad R_3 = \int_0^l \phi_1''^2 \, dx, \quad R_4 = \phi_1^2\big|_{x=0}, \\ R_5 &= \phi_1^2\big|_{x=l}, \quad R_7 = \phi_1^4\big|_{x=l}, \quad R_8 = \phi_1^6\big|_{x=l}, \end{aligned} \tag{5.15}$$

and

$$\begin{aligned} g_{nl}(\dot{q}) &= (e_1 R_4)\dot{q} + (e_3 R_7)\dot{q}^3 + (e_5 R_8)\dot{q}^5 + \cdots, \\ h_{nl}(q) &= (c_1 R_4)q + (c_3 R_7)q^3 + (c_5 R_8)q^5 + \cdots, \end{aligned} \tag{5.16}$$

There are many methods being able to solve the nonlinear differential equations of motion ([27]-[33]). Here in this study, the Harmonic Balance Method (HBM) is used to investigate the steady state dynamics of the system.

As the primary harmonic is dominant in the nonlinear response of the system, the higher harmonics are neglected in this chapter. Hence, in order to apply the HBM to the equations of motion Eq. (5.14) of the system, periodic time variable response $q(t)$ of the system is assumed as

$$q(t) = a(t)\sin(\Omega t) + b(t)\cos(\Omega t), \tag{5.17}$$

Slowly varying sine and cosine coefficients $a(t)$ and $b(t)$ are considered time-variant to study the transient response of the system. However, in this chapter only the steady-state behaviour is examined. Since the coefficients $a(t)$ and $b(t)$ are slowly-varying, $\ddot{a}$ and $\ddot{b}$ are neglected in the analysis. Accordingly, the time derivatives of the time variable $q(t)$ of the response are obtained as

$$\begin{aligned} \dot{q}(t) &= \left(\dot{b} + \Omega a\right)\cos(\omega t) + (\dot{a} - b\Omega)\sin(\omega t), \\ \ddot{q}(t) &= \Omega\,(2\dot{a} - b\Omega)\cos(\omega t) - \Omega\left(2\dot{b} + b\Omega\right)\sin(\omega t), \end{aligned} \tag{5.18}$$

Substituting Eqs. (5.17) and (5.18) into Eq. (5.14) and balancing the coefficients of $\sin(\omega t)$ and $\cos(\omega t)$, two differential equations are obtained as follows.

$$\begin{aligned} 2P_1\Omega\dot{a} + P_2\dot{b} &= P_1 b\Omega^2 - P_2 a\Omega - P_3 b - P_4 C_{g_{nl}} - P_5 C_{h_{nl}} - P_6 C_{q3} - P_7 C_{q5}, \\ P_2\dot{a} - 2P_1\Omega\dot{b} &= P_8 + P_1 a\Omega^2 + P_2 b\Omega - P_3 a - P_4 S_{g_{nl}} - P_5 S_{h_{nl}} - P_6 S_{q3} - P_7 S_{q5}, \end{aligned} \tag{5.19}$$

where

$$\begin{aligned} P_1 &= \rho A R_1 + \sum_{n=1}^{N_p} M_n R_{2_n}, \quad P_2 = \alpha R_1 + \beta R_3 + \lambda R_4, \\ P_3 &= k_b R_4 + EI R_3 + k_l R_4, \quad P_4 = \lambda_n, \quad P_5 = k_{n_2}, \quad P_6 = k_{n_3} R_7, \\ P_7 &= k_{n_5} R_8, \quad P_8 = -\left(\rho A R_0 + \sum_{n=1}^{N_p} M_n R_{0_n}\right) W_b, \\ C_{g_{nl}} &= (e_1 R_4)(\dot{b} + \Omega a) + (e_3 R_7) C_{qd3} + (e_5 R_8) C_{qd5} + \cdots, \\ S_{g_{nl}} &= (e_1 R_4)\,(\dot{a} - b\Omega) + (e_3 R_7) S_{qd3} + (e_5 R_8) S_{qd5} + \cdots, \\ C_{h_{nl}} &= (c_1 R_4) b + (c_3 R_7) C_{q3} + (c_5 R_8) C_{q5} + \cdots, \\ S_{h_{nl}} &= (c_1 R_4) a + (c_3 R_7) C_{q3} + (c_5 R_8) C_{q5} + \cdots, \end{aligned} \tag{5.20}$$

and

$$
\begin{aligned}
S_{q3} &= \frac{3}{4}a^3 + \frac{3}{2}ab^2, C_{q3} = \frac{3}{2}a^2b + \frac{3}{4}b^3,\\
S_{q5} &= \frac{5}{8}a^5 + \frac{15}{4}a^3b^2 + \frac{15}{8}ab^4, C_{q5} = \frac{15}{8}a^4b + \frac{15}{4}a^2b^3 + \frac{5}{8}b^5,\\
S_{qd3} &= \frac{3}{2}a^2\dot{a}\Omega^2 - \frac{3}{2}a^2b\Omega^3 + 3a\dot{a}\dot{b}\Omega - 3ab\dot{b}\Omega^2 + \frac{3}{4}\dot{a}^3\\
&\quad -\frac{9}{4}\dot{a}^2b\Omega + \frac{9}{4}\dot{a}b^2\Omega^2 + \frac{3}{2}\dot{a}\dot{b}^2 - \frac{3}{4}b^3\Omega^3 - \frac{3}{2}b\dot{b}^2\Omega,\\
C_{qd3} &= \frac{3}{4}a^3\Omega^3 + \frac{9}{4}a^2\dot{b}\Omega^2 + \frac{3}{2}a\dot{a}^2\Omega - 3a\dot{a}b\Omega^2 + \frac{3}{2}ab^2\Omega^3\\
&\quad +\frac{9}{4}a\dot{b}^2\Omega + \frac{3}{2}\dot{a}^2\dot{b} - 3\dot{a}b\dot{b}\Omega + \frac{3}{2}b^2\dot{b}\Omega^2 + \frac{3}{4}\dot{b}3,\\
S_{qd5} &= \frac{15}{8}a^4\dot{a}\Omega^4 - \frac{15}{8}a^4b\Omega^5 + \frac{15}{2}a^3\dot{a}\dot{b}\Omega^3 - \frac{15}{2}a^3b\dot{b}\Omega^4 + \frac{15}{4}a^2adota^3\Omega^2\\
&\quad -\frac{45}{4}a^2\dot{a}^2b\Omega^3 + \frac{45}{4}a^2\dot{a}b^2\Omega^4 + \frac{45}{4}a^2\dot{a}\dot{b}^2\Omega^2 - \frac{15}{4}a^2b^3\Omega^5\\
&\quad -\frac{45}{4}a^2b\dot{b}^2\Omega^3 + \frac{15}{2}a\dot{a}^3\dot{b}\Omega - \frac{45}{2}a\dot{a}^2b\dot{b}\Omega^2 + \frac{45}{2}a\dot{a}b^2\dot{b}\Omega^3\\
&\quad +\frac{15}{2}a\dot{a}\dot{b}^3\Omega - \frac{15}{2}ab^3\dot{b}\Omega^4 - \frac{15}{2}ab\dot{b}^3\Omega^2 + \frac{15}{8}\dot{a}^5 - \frac{25}{8}\dot{a}^4b\Omega\\
&\quad +\frac{25}{4}\dot{a}^3b^2\Omega^2 + \frac{15}{4}\dot{a}^3\dot{b}^2 - \frac{25}{4}\dot{a}^2b^3\Omega^3 - \frac{45}{4}\dot{a}^2b\dot{b}^2\Omega\\
&\quad +\frac{25}{8}\dot{a}b^4\Omega^4 + \frac{45}{4}\dot{a}b^2\dot{b}^2\Omega^2 + \frac{15}{8}\dot{a}\dot{b}^4 - \frac{5}{8}b^5\Omega^5 - \frac{15}{4}b^3\dot{b}^2\Omega^3 - \frac{15}{8}b\dot{b}^4\Omega,\\
C_{qd5} &= \frac{5}{8}a^5\Omega^5 + \frac{25}{8}a^4\dot{b}\Omega^4 + \frac{15}{4}a^3\dot{a}^2\Omega^3 - \frac{15}{2}a^3\dot{a}b\Omega^4 + \frac{15}{4}a^3b^2\Omega^5\\
&\quad +\frac{25}{4}a^3\dot{b}^2\Omega^3 + \frac{45}{4}a^2\dot{a}^2\dot{b}\Omega^2 - \frac{45}{2}a^2\dot{a}b\dot{b}\Omega^3 + \frac{45}{4}a^2b^2\dot{b}\Omega^4\\
&\quad +\frac{25}{4}a^2\dot{b}^3\Omega^2 + \frac{15}{8}a\dot{a}^4\Omega - \frac{15}{2}a\dot{a}^3b\Omega^2 + \frac{45}{4}a\dot{a}^2b^2\Omega^3\\
&\quad +\frac{45}{4}a\dot{a}^2\dot{b}^2\Omega - \frac{15}{2}a\dot{a}b^3\Omega^4 - \frac{45}{2}a\dot{a}b\dot{b}^2\Omega^2 + \frac{15}{8}ab^4\Omega^5\\
&\quad +\frac{45}{4}ab^2\dot{b}^2\Omega^3 + \frac{25}{8}a\dot{b}^4\Omega + \frac{15}{8}\dot{a}^4\dot{b} - \frac{15}{2}\dot{a}^3b\dot{b}\Omega\\
&\quad +\frac{45}{4}\dot{a}^2b^2\dot{b}\Omega^2 + \frac{15}{4}\dot{a}^2\dot{b}^3 - \frac{15}{2}\dot{a}b^3\dot{b}\Omega^3 - \frac{15}{2}\dot{a}b\dot{b}^3\Omega\\
&\quad +\frac{15}{8}b^4\dot{b}\Omega^4 + \frac{15}{4}b^2\dot{b}^3\Omega^2 + \frac{5}{8}\dot{b}^5
\end{aligned}
\tag{5.21}
$$

where W_b is the amplitude of the base acceleration $\ddot{w}_b$. In order to find the steady-state response of the system, the time-variant terms of Eq. (5.19) are set to zero. Consequently, the nonlinear differential equation of motion is transformed into two nonlinear algebraic equations as follows

$$
\begin{aligned}
P_1b\Omega^2 - P_2a\Omega - P_3b - P_4C_{g_{ss}} - P_5C_{h_{ss}} - P_6C_{q3} - P_7C_{q5} = 0,\\
P_8 + P_1a\Omega^2 + P_2b\Omega - P_3a - P_4S_{g_{ss}} - P_5S_{h_{ss}} - P_6S_{q3} - P_7S_{q5} = 0,
\end{aligned}
\tag{5.22}
$$

where

$$
\begin{aligned}
C_{g_{SS}} &= (e_1R_4)(\Omega a) + (e_3R_7)\left(\frac{3}{4}a^3\Omega^3 + \frac{3}{2}ab^2\Omega^3\right) \\
&+(e_5R_8)\left(\frac{5}{8}a^5\Omega^5 + \frac{15}{4}a^3b^2\Omega^5 + \frac{15}{8}ab^4\Omega^5\right) + \cdots, \\
S_{g_{SS}} &= (e_1R_4)(b\Omega) + (e_3R_7)\left(-\frac{3}{2}a^2b\Omega^3 - \frac{3}{4}b^3\Omega^3\right) \\
&+(e_5R_8)\left(-\frac{15}{8}a^4b\Omega^5 - \frac{15}{4}a^2b^3\Omega^5 - \frac{5}{8}b^5\Omega^5\right) + \cdots, \\
C_{h_{SS}} &= (c_1R_4)b + (c_3R_7)\left(\frac{3}{2}a^2b + \frac{3}{4}b^3\right) \\
&+(c_5R_8)\left(\frac{15}{8}a^4b + \frac{15}{4}a^2b^3 + \frac{5}{8}b^5\right) + \cdots, \\
S_{h_{SS}} &= (c_1R_4)a + (c_3R_7)\left(\frac{3}{4}a^3 + \frac{3}{2}ab^2\right) \\
&+(c_5R_8)\left(\frac{5}{8}a^5 + \frac{15}{4}a^3b^2 + \frac{15}{8}ab^4\right) + \cdots,
\end{aligned}
\tag{5.23}
$$

Different numerical methods are used to solve the nonlinear algebraic equations. Here, in this study, the resultant nonlinear algebraic equations of Eq. (5.22) are solved using the arc-length continuation method. The amplitude-frequency response of the system obtained from the numerical method is used in the optimization process to identify the nonlinear system. The following section explains the optimization process.

5.4 Nonlinear Identification

There are different methods introduced to identify the nonlinearities in the systems. One of the biggest weaknesses of most of these methods is accumulative error in the results of the identification process. Errors from various sources are accumulated in the identification process leading to a considerable error in the identified values of the parameters. Using the measured frequency domain data directly in the identification of parameters reduces such errors to the lowest possible. One significant error is when the low amplitude response of a nonlinear mechanical structure is used to update the underlying linear system. Although the effect of nonlinearity on the response of the system is at its lowest level for very low amplitude excitation, this effect cannot be eliminated from the measured response that affects the results of the updating procedure. Therefore, some modelling error appears in the underlying linear system.

In many practical engineering structures, it is not possible to have spatially complete measurements. On the other hand, some of the finite element based identification methods require all coordinates to be measured. Hence, various expansion methods, such as System Equivalent Reduction Expansion Process (SEREP), may be used to estimate the unmeasured coordinates, which may cause error in the final

results of the identification process. Avoiding expansion methods would eliminate the possible error in this process. The approach presented in this study aims to eliminate the aforementioned errors in the process of nonlinear identification.

The proposed method is composed of two main steps. In the first step, a linear model updating method is applied to the linear response of a low amplitude test. The resultant updated parameters are used as an appropriate initial guess for the underlying linear system. The updated parameters of the underlying linear system are then corrected in step two. By correcting the updated parameters obtained from the first step, the above-discussed error due to the effect of nonlinearity in the linear response of the system is cancelled.

The second step is to identify the underlying linear system and the nonlinear restoring force utilizing the updated linear model and nonlinear experimental response in an optimization process. The optimization process utilizes the gradient-based interior-point algorithm of the fmincon problem solver in MATLAB. To minimize the implicit regularization bias in the optimization process, and to avoid converging to a local optimal solution rather than finding the global optimal solution of the problem, different initial conditions which are distributed over the variation range of the optimization parameters are used for the optimization process. To model the unknown nonlinear force, a nonlinear form is assumed for the nonlinearity according to the experimental response. Here, good engineering insight is required to have an appropriate assumed model. Consequently, a numerical model is developed for the nonlinear system using the assumed nonlinear force with estimated linear parameters to be corrected and unknown nonlinear parameters to be estimated. Then, the optimized values of the system parameters are targeted by setting the inputs of the optimization process. To this end, an objective function defined by minimizing the difference between the experimental and analytical responses at the measured coordinates, [12], as

$$J = \min \left(\sum_{i=1}^{N_f} | \log \left(\| X_m(\Omega_i) \|_2 \right) - \log \left(\| X_a(\Omega_i) \|_2 \right) | \right), \tag{5.24}$$

where X_m and X_a denote respectively the experimental and numerical response of the system in the frequency domain at the measured points. Using the logarithmic scale in the objective function penalises large changes between optimized and experimental responses. Considering only measured coordinates in the identification procedure eliminates the need for a spatially complete measurement and the need to use expansion methods. Therefore, the associated error is eliminated from the calculations. N_f is the number of measured frequency lines considered in the optimization. Another input for the optimization process is the variation range of the parameters to be optimized. The optimized parameters are subjected to different constraints limiting the solution range of the objective function. For instance, the optimized parameters must have values within the allowable range. Therefore, a lower limit and an upper limit is

defined for every parameter. Also, the nonlinear algebraic equation of Eq. (5.22) is used as nonlinear equality conditions of the optimization process. In fact, the response obtained using the optimized parameters should satisfy the nonlinear algebraic equation of Eq. (5.22). Some data selection criteria may be applied on the frequency response before being used in the optimization process as described in the following:

- The first data selection is to narrow the frequency response to a range in which the effect of the nonlinearity is considerable. By applying this criterion, the calculation cost is reduced significantly, because there is no significant difference between the linear and the nonlinear responses in the region which is insensitive to the nonlinearity.
- The second is to neglect the unstable branches of the numerical solution which are not measured in the experimental tests.
- The third data selection criterion is to choose between the solutions in the multi-response regions. Having more than one solution at a single frequency line may cause the optimization process slow down or, in some cases, not to converge to a reasonable solution. In this case, usually the upper branch of solution (having the larger amplitude) is selected, because the effect of the nonlinearity is more significant compared to the lower branch. Of course, the selected branch must correspond to the experimentally measured response used for optimization. The lower branch of the response or responses at different excitation levels can be used to make sure that the results of the optimization are correct.

Applying all the constraints and criteria described above, the parameters of the assumed model of the nonlinear system are optimized. These values are used to estimate the linear (low amplitude test) and nonlinear response (high amplitude test) of the system. If an acceptable match is not observed between the experimentally measured response and the estimated response, the assumed form of the nonlinear force is revised, and the optimization process is repeated. This process is carried out until a good correlation between the experimental results and the analytical model is achieved.

5.5 Results and discussion

In this section, first the results of the linear model updating are presented and compared with the experimental linear response of the system. Afterwards, the results of the identification of the unknown nonlinear force of the system are discussed. In order to identify the structural model of the cantilever beam, first the underlying linear model is updated using linear updating methods ([6],[10]-[12]). For this purpose, the linear response of the nonlinear system is measured by exciting the structure with very low amplitude base excitation. The first three measured natural frequencies are used to update the

Table 5.2: Optimized parameters of the nonlinear force of the cantilever beam.

	Parameters		Parameter values (in SI units)	
	Description of parameters		Initial Values	Updated Values
Fixed Parameters	Mass of the accelerometers	m_a	0.008	–
	Mass of the permanent magnets	m_p	0.004	–
	Linear mass density of the beam	ρA	0.368	–
	Length of the beam	L	0.3	–
Updated parameters	Proportional damping coefficient	α	0.2	0.294
	Proportional damping coefficient	β	1×10^{-5}	1.33×10^{-5}
	Flexural stiffness of the beam	EI	1.741	1.64
	Equivalent stiffness of the clamp	k_b	8.256×10^5	5.5×10^5
	Equivalent mass of the clamp support	m_b	0.1016	0.103

underlying linear system. For this purpose, three parameters of the system are updated, the flexural stiffness EI, base stiffness k_b, and the base mass m_b. After updating three parameters using natural frequencies, the proportional damping coefficients α, β were updated. Table 5.2 gives all the values of the fixed and updated parameters of the system.

EI, k_b and m_b are updated using measured natural frequencies as shown in Figure 3.9. Figure 3.10 illustrates that after 20 iterations, the updated natural frequencies predicated by the numerical model are in excellent agreement with those obtained experimentally.

Having the updated parameters, the numerical linear frequency response is obtained using the updated linear model of the underlying linear structure. Figure 3.11 shows the experimental and updated linear frequency response of the system at the location of 1st accelerometer (AM1) for the frequency range containing the first three modes. A very important observation is that the updated model can estimate the anti-resonance frequencies. It is worth noting that the anti-resonance frequencies are not included in the updating method. Therefore, the good agreement between both resonance and anti-resonance frequencies shows the updated linear model is valid. The low-amplitude experimental and updated analytical linear responses are compared in Figure 3.12 in the neighbourhood of the first natural frequency in the presence of the nonlinear electromagnetic force.

Given the updated model of the underlying linear system, the nonlinear system is now identified. For this purpose, the nonlinear amplitude-frequency response of the system at the location of 3rd accelerometer (AM3) is used in optimization process to identify the nonlinear force. As expected from Eq. (5.2), the response of the system demonstrates a softening nonlinearity in the system. Having the updated underlying linear system, the measured nonlinear response of the system is utilized in the optimization process to estimate the unknown parameters of the nonlinear force of Model I given in

Table 5.1 as

$$\lambda = 0.005 \ \frac{\text{N.s}}{\text{m}}, \quad k_l = -2 \ \frac{\text{N}}{\text{m}}, \quad k_{n_3} = -1.7 \times 10^4 \ \frac{\text{N}}{\text{m}^3}, \tag{5.25}$$

Negative values of k_l and k_{n_3} indicate the softening nonlinearity due to the attractive electromagnetic force. The optimized parameters of the system are used to estimate the nonlinear response of the system. Then, the experimentally measured response is compared with the estimated response. Figure 5.3 illustrates the estimated response nearest the beam tip using Model I of Table 5.1 for the nonlinear force, and shows that the estimated nonlinear model is able to provide a fairly accurate prediction for the response of the nonlinear system.

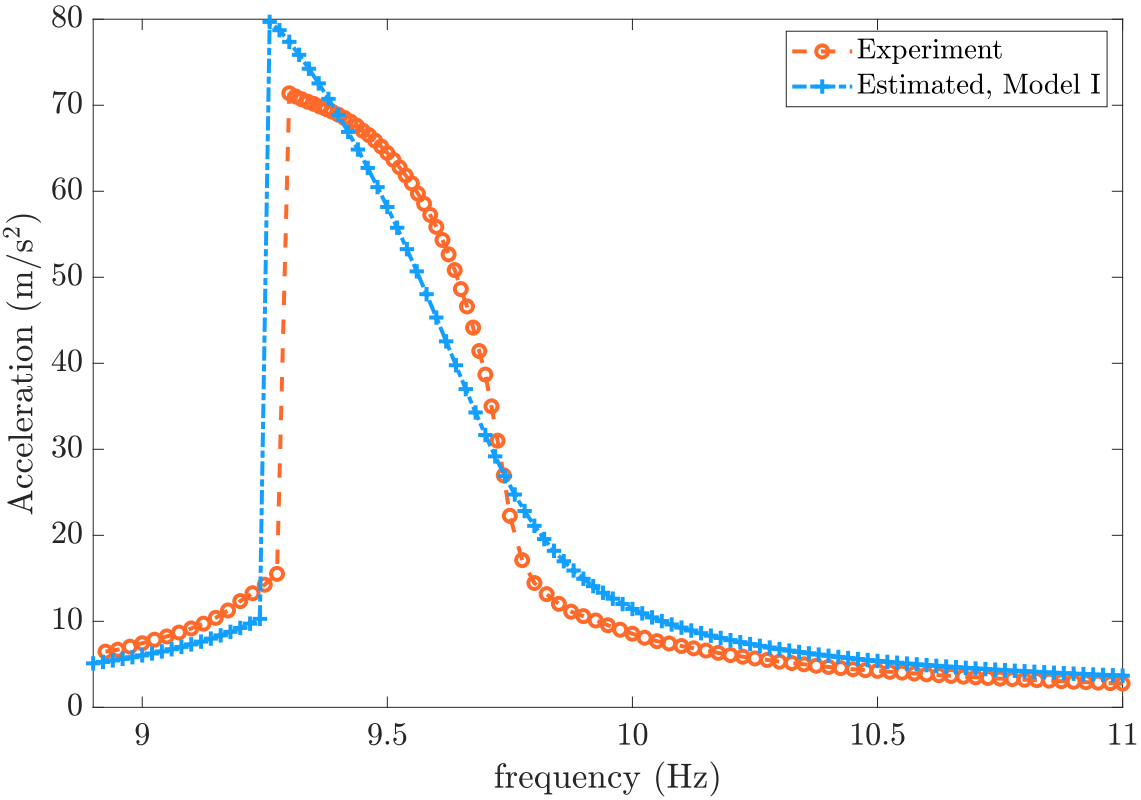

Figure 5.3: Comparison between the updated linear response and the measured response of the nonlinear system subject to low amplitude base excitation. A_1, A_2, and A_3 denote the accelerations measured by accelerometers AM1, AM2, and AM3, respectively.

Now, in order to increase the accuracy of the nonlinear model, Models II, III, and IV, introduced in Table 5.1, are used in the identification process. The optimization process is repeated for these models of the nonlinear force of Table 5.3 and the optimized values have been obtained. The optimized parameters are also presented in Table 5.3. Subsequently, the optimized parameters are used to estimate the nonlinear response of the system with the same excitation level. Figure 5.4 compares the measured nonlinear response, including amplitude and phase, at AM3 (25-cm away from the clamped end) with

Table 5.3: Optimized parameter values of different proposed models of nonlinear electromagnetic force given in Table 5.1

Model No.	Optimized Values					
	$\lambda \ \left(\frac{\text{N.s}}{\text{m}}\right)$	$\lambda_n \ \left(\frac{\text{N.s}}{\text{m}^2}\right)$	$k_l \ \left(\frac{\text{N}}{\text{m}}\right)$	$k_{n_2} \ \left(\frac{\text{N}}{\text{m}^2}\right)$	$k_{n_3} \ \left(\frac{\text{N}}{\text{m}^3}\right)$	$k_{n_5} \ \left(\frac{\text{N}}{\text{m}^5}\right)$
Model I	0.005	–	-2	–	-1.7×10^4	–
Model II	0.006	–	-1	–	-1.55×10^4	-5×10^6
Model III	0.0065	–	-2	1.25×10^3	-4.9×10^4	-9.8×10^6
Model IV	0.0075	0.0017	-2	1.225×10^3	-4.75×10^4	-9.65×10^6

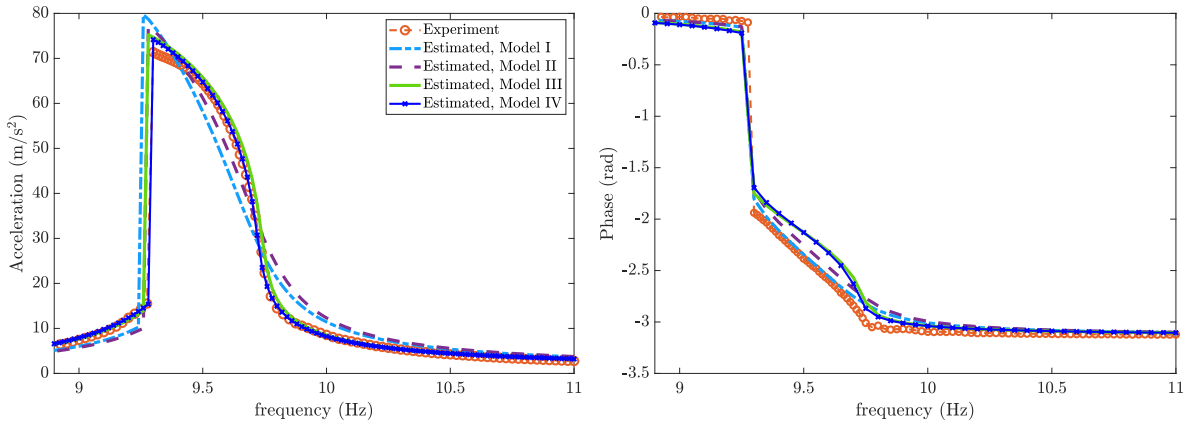

Figure 5.4: The comparison of the experimentally measured frequency response at the location of accelerometer AM3 (left (amplitude), right (phase)) with the estimated responses using the four assumed forms of the nonlinear force.

the estimated responses using all four assumed models of the nonlinear force. Figure 5.4 shows that the predictions from these four models are generally in good agreement with the experimental data. However, it can be seen that there is some improvement in the predictions from model III when compared to Model I, while there is very little difference in the predictions between Models III and IV. Based on this observation, one may conclude that because no noticeable change in the level of accuracy was achieved when the order of nonlinearity increased from Model III to Model IV, Model III should be considered as the identified model to represent the system.

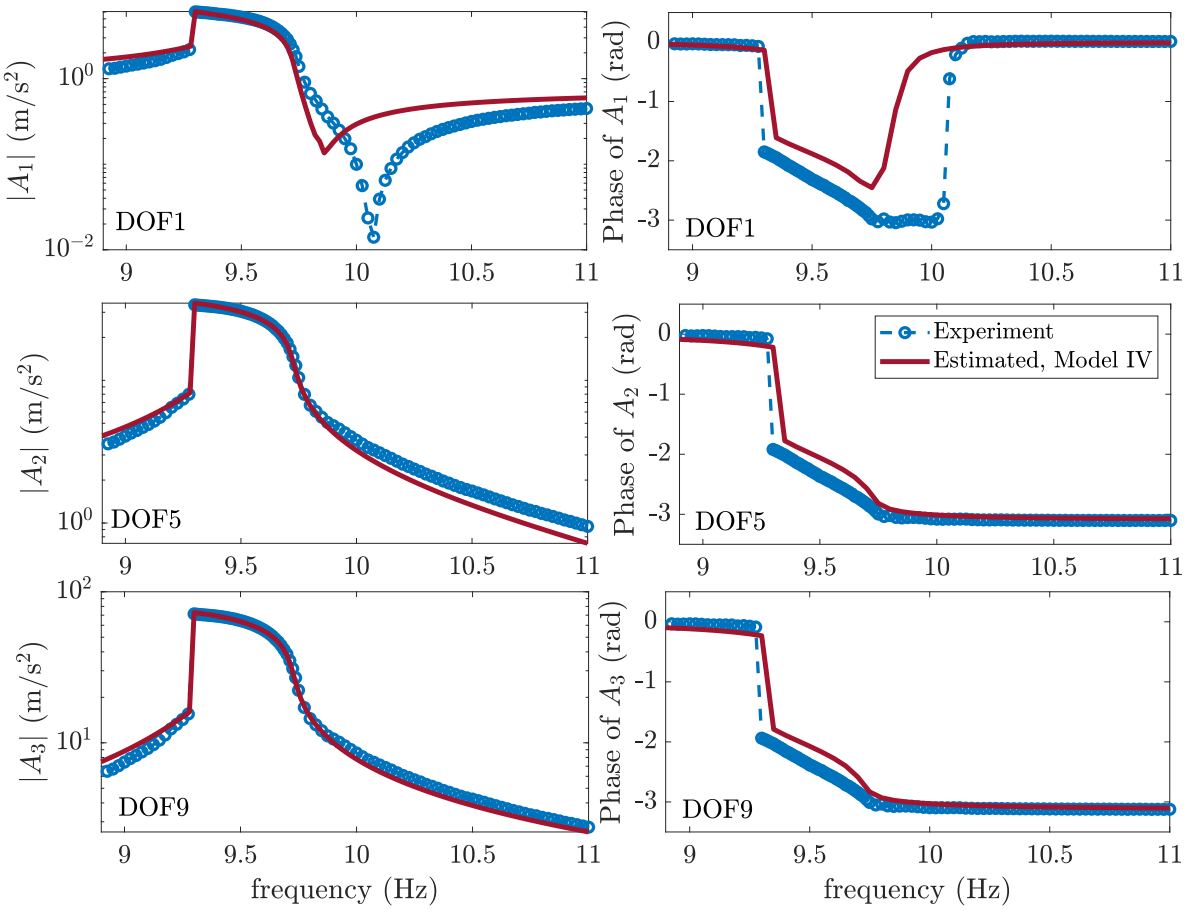

Figure 5.5: Comparison of the experimentally measured nonlinear responses and the numerically estimated responses using nonlinear Model IV. A_1, A_2, and A_3 denote the accelerations measured by accelerometers AM1, AM2, and AM3, respectively.

Another important problem in nonlinear system identification is assessing the validity of the model. To this end, the optimization process was only carried out using the response of only AM3. Therefore, in order to verify the validity of the results, the optimized parameters of model IV of the assumed nonlinear force are used to estimate the response of the nonlinear system at the three measured accelerometer locations, including both amplitude and phase of the acceleration. The estimated response is compared

with the experimental data in Figure 5.5. The results illustrate a good agreement between the measured and reconstructed response and confirms the validity of the identified model. In this study, the verification of the identified model is carried out by comparing the regenerated response with the measured response of the structure. A question that may arise here is why the nonlinear electromagnetic force is not measured directly in order to compare with the identified force. The answer is that in many practical applications, there are locations that are not accessible to measure displacement. Therefore, it is not possible to compare the exact nonlinear force at those locations. Similarly, for the case of nonlinear electromagnetic force in this study, it is not possible to measure the displacement at the tip of the beam. Hence, the accuracy of the identified model is verified by comparing the experimental response with its numerical estimation.

5.6 Closure

This chapter proposed a framework for nonlinear model identification. In this framework, the nonlinear element/force was represented by a Taylor series expansion. Based on the number of terms retained in the expansion, different possible models may be chosen. An optimization-based method can be used to identify the model parameters of the chosen models. The objective function of this optimization is the difference between the predicted nonlinear response and the experimental response. The predicted responses from the identified models are then compared with experimental results and one may determine how many terms should be retained in the Taylor series expansion. The proposed method is demonstrated on an experimental test case, where a nonlinear electromagnetic force is applied to the tip of a steel cantilever beam. First, the linear and nonlinear responses of the system were measured from low and high amplitude vibration tests, respectively. Euler Bernoulli beam theory is used to model the cantilever beam. The support of the beam is modelled with a spring and the effect of mass of support is also considered in the model. It was found that the linear model of the support is needed to predict the anti-resonances of the linear experimental responses. In the next step, four possible nonlinear models (using Taylor series expansion) were assumed for the electromagnetic force. The order of nonlinearity in the stiffness and damping terms were increased gradually in these models. The measured nonlinear responses were used in an optimization-based identification process to estimate the unknown parameters of these models. It has been demonstrated that a nonlinear model composed of linear damping and nonlinear stiffness (including linear, quadratic, cubic, and fifth-order terms) provides excellent agreement between the predicted responses and the corresponding measured responses. In addition, it is shown that adding a quadratic nonlinear damping to the assumed nonlinear model may not lead to a significant change in the results. The identified model is capable of predicting the experimental FRFs at points which are used in identification. This indicates the identified model is valid.

Chapter 6

Identification of Nonlinear Structural Systems via Harmonic Balance

6.1 Introduction

Most practical structures are nonlinear if excited with large forces. Many of these structures have weak nonlinear behaviour due to the nature of the structure or the working condition and can be approximated using conventional linear theories. However, linear theories are not applicable if the nonlinearity is significant in a dynamical system. In order to investigate the exact dynamics of structural systems, a very accurate mathematical model of the system is required. In addition, many practical systems require continuous monitoring to avoid any unexpected failure or damage in the system. Vibration based structural health monitoring (SHM) is a process to detect any damage by continuously observing any changes in the material or geometry of structure. In some cases, a mathematical model is used to predict the behaviour of the structure based on the practical measurement. In these cases, the accuracy of the model is vital. Thus, identification methods have been introduced in the literature.

It is usually impossible to measure all coordinates due to the complicated physics of the structure or a lack of measuring equipment, and hence unmeasured degrees of freedom need to be estimated using expansion methods. This may lead to error in the results of identification. Other than the inaccuracy coming from the expansion methods, there are various factors and different sources of noise or error affecting the results of the identification process. Practically, it is difficult to control the excitation force in experiments, and therefore the measured force and response signals usually include higher harmonics. There are experimental research works [131, 132] showing the high amplitude of the second harmonic of the force signal, although this does not usually result in a considerable higher harmonic response. Assuming that the response is dominated by only the primary harmonic may be acceptable for cases

in which higher harmonics have no significant contribution to the dynamics of the system. However, this assumption may result in significant errors in the identification of strongly nonlinear systems (e.g. systems with frictional contact interfaces). One of the most important sources of inaccuracy in the identification of nonlinear systems that has received less attention in the literature is neglecting the effect of higher harmonics, particularly where higher harmonics play a significant role in the response. Some research studies focused on the nonlinear vibration analysis considering the effect of higher harmonics [133], or investigated the effect of neglecting the higher harmonics on the results of the identification (refer to Chapter 4). Therefore, the objective of this study is to propose an identification method to consider the effect of significant harmonics of the multi-harmonic dynamics of the system. To this end, a method is introduced with two approaches: the Analytical Harmonic-Balance-based (AHB) approach and the Alternating Frequency/Time approach using Harmonic Balance (AFTHB). The AHB approach is based on expanding the nonlinear functions in the frequency domain utilizing analytical methods such as the Fourier Integral (FI), the Complex Averaging (CXA) technique [21, 22] or the Harmonic Balance Method (HBM) [19]. Indeed, this approach is an extended version of the EDSM technique [117] for multi-harmonic identification. This approach exploits the measured data in the frequency domain. In order to identify nonlinear systems using the AFTHB approach, the nonlinear functions are expanded in the frequency domain by calculating the Fourier Transform of the measured time response. It is shown that the AHB approach is very accurate in theory if all significant harmonics of force and response are taken into account. Nevertheless, it is often cumbersome to include all significant harmonics of the response in the analytical expansion of nonlinear functions. Besides, it would be difficult to use AHB for structures with complex forms of nonlinearities such as Coulomb friction and also for multi-degree of freedom nonlinear systems. Therefore, the AFTHB approach is developed based on the corresponding method used for harmonic balance [134, 135]. It should be noted that the AFTHB approach is different from well-known time-frequency methods such as the Wavelet and Hilbert Transforms. The great advantage of AFTHB is that it can be applied to any type of nonlinear functions, where there are significant harmonics in the response. It is worth noting that selecting the appropriate time step and sampling frequency is important to guarantee the accuracy of the results obtained by the AFTHB method. Nevertheless, there are many well-developed algorithms such as MATLAB ode solvers that automatically adjust the time steps during time marching.

This study develops a method with two different approaches to identify nonlinear dynamical systems exploiting multi-harmonic responses and force signals. Section 6.2 describes the theory of the method; the analytical (AHB) and the numerical alternating frequency/time (AFTHB) identification approaches are introduced. In Section 6.3, five simulated examples of nonlinear systems are considered and used to highlight different features of the method. Finally, Section 6.5 gives brief conclusions of the study.

6.2 Theory

The equation of motion of a general vibrating system subject to external forces is given by

$$\mathbf{M}\ddot{\mathbf{u}} + \mathbf{C}\dot{\mathbf{u}} + \mathbf{K}\mathbf{u} + \mathbf{f}_{NL}\left(\mathbf{u}, \dot{\mathbf{u}}\right) = \mathbf{f}_{ex}(t) \tag{6.1}$$

where $\mathbf{M},\ \mathbf{C},\ \mathbf{K} \in \mathbb{R}^{N_{eq}\times N_{eq}}$ denote the mass, damping, and stiffness matrices, respectively, and $\mathbb{R}$ represents real numbers. u is the vector of displacements, N_{eq} denotes the number of degrees of freedom of the system, $\mathbf{f}_{NL}\left(\mathbf{u}, \dot{\mathbf{u}}\right)$ represents the unknown linear/nonlinear restoring force, and $\mathbf{f}_{ex}(t)$ is the external force vector applied to the system. The nonlinear restoring force is assumed to be a combination of linear or nonlinear functions which is linear in the unknown parameters. Thus

$$\mathbf{f}_{NL} = \mathbf{A}\mathbf{g} = \begin{bmatrix} a_{1,1} & a_{1,2} & \cdots & a_{1,N_g} \\ a_{2,1} & a_{2,2} & \cdots & a_{2,N_g} \\ \vdots & \vdots & \ddots & \vdots \\ a_{N_{eq},1} & a_{N_{eq},2} & \cdots & a_{N_{eq},N_g} \end{bmatrix}_{N_{eq}\times N_g} \begin{Bmatrix} g_1 \\ g_2 \\ \vdots \\ g_{N_g} \end{Bmatrix}_{N_g\times 1}, \tag{6.2}$$

where $\mathbf{A} \in \mathbb{R}^{N_{eq}\times N_g}$ is the matrix of unknown parameters a_{ip} $(i = 1, \ldots, N_{eq},\ p = 1, \cdots, N_g)$ and $\mathbf{g} \in \mathbb{R}^{N_g\times 1}$ is the vector of assumed functions $g_p(\mathbf{u}, \dot{\mathbf{u}})$ of internal forces. N_g denotes the total number of functions assumed for the nonlinear restoring force. Determining the type of nonlinear functions requires precise engineering insight. Rearranging Eq. (6.1) and using Eq. (6.2), one can rewrite Eq. (6.1) in the following form in terms of the unknown nonlinear restoring forces,

$$\mathbf{A}\mathbf{g} = \mathbf{f}_{ex}(t) - \left(\mathbf{M}\ddot{\mathbf{u}} + \mathbf{C}\dot{\mathbf{u}} + \mathbf{K}\mathbf{u}\right), \tag{6.3}$$

In general, practical dynamical systems often experience multi-harmonic excitation from the external force including higher harmonics. Thus

$$\mathbf{f}_{ex}(t) = \sum_{m=1}^{N_f} \mathbf{F}_m \sin\left(m\omega t + \phi_m\right), \tag{6.4}$$

where N_f, $\mathbf{F}_m$, ω are respectively the number of force harmonics, the vector of force amplitudes for each harmonic, and the excitation frequency of the external force. ϕ_m denotes the phase of mth harmonic of the force signal. Accordingly, the oscillating system is most likely to have multi-harmonic dynamics. Hence, the steady state response of the system is assumed to be

$$u_i(t) = u_{i,0} + \sum_{n=1}^{N_H} u_{i,n}(t), \quad i = 1, \cdots, N_{eq}, \tag{6.5}$$

where N_H denotes the total number of harmonics which is not necessarily equal to N_f. $u_{i,0}$ denotes the static part and $u_{i,n}(t)$ is the n-th term of the dynamic response of the i-th degree of freedom (DOF),

$$\begin{aligned} u_{i,n}(t) &= \frac{1}{2j}\left(U_{i,n}e^{jH_n\omega t} - \bar{U}_{i,n}e^{-jH_n\omega t}\right), \\ \dot{u}_{i,n}(t) &= \frac{H_n\omega}{2}\left(U_{i,n}e^{jH_n\omega t} + \bar{U}_{i,n}e^{-jH_n\omega t}\right), \\ \ddot{u}_{i,n}(t) &= \frac{jH_n^2\omega^2}{2}\left(U_{i,n}e^{jH_n\omega t} - \bar{U}_{i,n}e^{-jH_n\omega t}\right), \end{aligned} \tag{6.6}$$

where overdot $\dot{\square}$ denotes differentiation with respect to time. $U_{i,n}$ and $\bar{U}_{i,n}$ are the complex amplitude of $u_{i,n}$ and its complex conjugate, respectively. H_n is the harmonic of the steady state dynamic response $u_{i,n}(t)$ which can be either sub- or super-harmonic of the excitation frequency ω. As the nonlinear functions $g_p(\mathbf{u}, \dot{\mathbf{u}})$ of the internal force are given as functions of the multi-harmonic responses of Eq. (6.5) and its derivatives, each function g_p itself can be assumed to be a multi-harmonic function with the form

$$g_p(\mathbf{u}, \dot{\mathbf{u}}) = v_{p,0} + \sum_{n=1}^{N_H} v_{p,n}(t), \quad p = 1, \cdots, N_{eq}, \tag{6.7}$$

where $v_{p,0}$ is the static response obtained as the mean value of the time response, and $v_{p,n}(t)$ is the n-th harmonic of the p-th function of the internal force,

$$v_{p,n}(t) = \frac{1}{2j}\left(V_{p,n}e^{jH_n\omega t} - \bar{V}_{p,n}e^{-jH_n\omega t}\right), \tag{6.8}$$

where $V_{p,n}$ is the complex amplitude of the H_n-th harmonic of the $p-th$ nonlinear function in the frequency domain, and $\bar{V}_{p,n}$ is its complex conjugate. Substituting Eqs. (6.5), (6.6) and (6.7) into Eq. (6.3), and averaging over each harmonic, $N_{eq} \times N_H$ algebraic equations are derived in the form below (N_H equations for every single equation of motion).

$$\mathbf{A}\mathbf{V}_n(\omega) = \mathbf{E}_n(\omega), \tag{6.9}$$

$\mathbf{E}_n \in \mathbb{C}^{N_{eq}\times 1}$ is the equivalent force defined as

$$\mathbf{E}_n(\omega) = \mathbf{F}_n - \left(-\mathbf{M}\left(H_n\omega\right)^2 + j\mathbf{C}H_n\omega + \mathbf{K}\right)\mathbf{U}_n, \quad n = 1, \cdots, N_H \tag{6.10}$$

where $\mathbb{C}$ represents complex numbers, $\mathbf{F}_n$ and $\mathbf{U}_n$ are, respectively, the vectors of the n-th harmonic of the force and response of the system in the frequency domain, and $V_n(\omega) \in \mathbb{C}^{N_g\times 1}$ is the vector of the amplitudes of the n-th harmonic of nonlinear functions $\mathbf{g}_p$ at excitation frequency ω.

$$\mathbf{V}_n(\omega) = \begin{bmatrix} V_{1,n} & \cdots & V_{p,n} & \cdots & V_{N_g,n} \end{bmatrix}^T, \quad n = 1, \cdots, N_H, \tag{6.11}$$

Afterwards, given the measured response $U_{i,n}$ and the external force signal in the frequency domain for N_ω frequency lines substituted in the transpose of Eq. (6.9), a system of linear algebraic equations is written in terms of the unknown matrix $\mathbf{A}$ with $N_{eq} \times N_g$ unknown parameters a_{ip}. The system of linear equation can be written for each harmonic as

$$\mathbf{B}_n \mathbf{A}^T = \mathbf{E}_n^*, \quad n = 1, \cdots, N_H, \tag{6.12}$$

where

$$\mathbf{B}_n(\omega) = \begin{bmatrix} \mathbf{V}_n(\omega_1) & \mathbf{V}_n(\omega_2) & \cdots & \mathbf{V}_n(\omega_{N_\omega - 1}) & \mathbf{V}_n(\omega_{N_\omega}) \end{bmatrix}^T, \quad n = 1, \cdots, N_H, \tag{6.13}$$

and

$$\mathbf{E}_n^* = \begin{bmatrix} \mathbf{E}_n(\omega_1) & \mathbf{E}_n(\omega_2) & \cdots & \mathbf{E}_n(\omega_{N_\omega - 1}) & \mathbf{E}_n(\omega_{N_\omega}) \end{bmatrix}^T, \quad n = 1, \cdots, N_H, \tag{6.14}$$

Then, the parameters may be estimated using two different approaches according to the number of harmonics of the response and the number of unknown parameters:

- If the number of harmonics of the response is equal or greater than the number of nonlinear functions ($H \geq N_g$), one can find the unknown parameters explicitly using an inverse method. In this way, the parameters may be estimated utilizing either the real or imaginary parts of Eq. (6.12) separately, or by using both, as

$$\mathbf{A}^T = pinv\left(\begin{bmatrix} \Re\left(\mathbf{B}_n\right) \\ \Im\left(\mathbf{B}_n\right) \end{bmatrix} \right) \begin{Bmatrix} \Re\left(\mathbf{E}_n^*\right) \\ \Im\left(\mathbf{E}_n^*\right) \end{Bmatrix}, \quad n = 1, \cdots, N_H, \tag{6.15}$$

  where $pinv\left(\square\right)$ is the pseudo-inverse of a matrix, $\Re$ and $\Im$ denote the real and imaginary parts, respectively.

- There may be some condition to make it difficult or infeasible to find the unknown parameters explicitly. For example, the number of unknown parameters may be so large with respect to the number of equations N_{eq}, or the number of measured frequency lines is not sufficient. Besides, the amplitude of the higher harmonics of the response may be too small to estimate the exact value of the parameters because of noise and ill-conditioning. In addition, the internal nonlinear force may be assumed such that the unknown parameters are inside the functions (e.g. as an exponent or argument of a function). In all these cases, the system is identified using an iterative optimization procedure. Standard methods and commercial software can be used to solve the optimization problem.

It is worth noting that the accuracy of the results of the identification process depends on the accuracy of the calculation of the frequency content of the signals (i.e. the FFTs). Therefore, selecting

an appropriate time step is required to measure the response, as well as a proper sampling rate to calculate the frequency content.

Now, two approaches are introduced to estimate the coefficient matrix $\mathbf{B}$ in the left hand side of Eq. (6.12).

6.2.1 Analytical Harmonic-Balance-Based (AHB) Approach

The analytical harmonic-balance-based (AHB) approach introduced in this section is based on exploiting the frequency domain data in order to determine the coefficient matrix $\mathbf{B}$. In this approach, an analytical method (e.g. the modified complex averaging technique (MCXA) or the Fourier integral) is used to find a multi-harmonic analytical expression to approximate the mathematical model of Eq. (6.3) in the frequency domain. In this study, MCXA is applied to the assumed model of Eq. (6.3). Refer to Section 1.7.1 for details of MCXA technique. Using Eq. (6.6), the amplitudes $\mathbf{V}_{p,n}$ of nonlinear functions of the internal force in the steady state dynamics can be written as functions of the complex amplitudes $U_{i,n}$ and their complex conjugate $\bar{U}_{i,n}$.

$$V_{p,n} = h\left(U_{i,n}, \bar{U}_{i,n}\right), \tag{6.16}$$

Then, Eq. (6.16) is used to shape the coefficient matrix $\mathbf{B}$ in Eq. (6.12). It is worth to note that:

- For the case of single harmonic approximation, this approach works the same as the Equivalent Dynamic Stiffness Mapping (EDSM) technique developed by Wang et al. [125]. In other words, the AHB approach is an extended version of the EDSM method for multi-harmonic identification.
- The AHB approach is applicable to nonlinear systems with smooth nonlinearities. In other words, as it is impossible to provide an exact multi-harmonic expression for non-smooth nonlinear functions such as Coulomb friction, the AHB approach may not be applicable for systems with such types of nonlinearities.
- The AHB approach is developed in this chapter to show that increasing the number of harmonics in the calculations will improve the accuracy of the identification results. In other words, by developing the AHB approach, it is shown that in case of systems with multi-harmonic response, neglecting higher harmonics in the identification process may result in considerable error.

6.2.2 Alternating Frequency/Time Approach Using Harmonic Balance (AFTHB)

In spite of the accuracy of the AHB approach described above, it is often cumbersome to apply to complicated models, especially in systems with a high number of DOFs and non-smooth nonlinearities.

Section 6.3 demonstrates that applying the AHB approach with higher harmonics would be very messy even for a cubic nonlinearity, although the results are shown to be very accurate. Therefore, an alternating frequency/time approach using harmonic balance (AFTHB) is proposed in this section. The proposed approach is based on a time-frequency transformation. The general vibrating system of Eq. (6.1) is considered. The measured steady state response of the system is assumed to be multi-harmonic with the form of Eq. (6.5). Also, each function g_p is assumed to be a multi-harmonic function with the form of Eq. (6.7), which its amplitudes $V_{p,n}$ are calculated numerically. Given the assumed type of nonlinearity and having measured the time response $u(t)$, nonlinear functions $g_p(u, \dot{u})$ of the internal force can be expanded numerically. Below is given the steps required to calculate the coefficient matrix $\mathbf{B}$.

- Calculate the time period $T = 2\pi/\omega$, and determine how many samples per cycle to use, as a power of 2. This really depends on how many harmonics are required to be taken into account, and can be relatively low (e.g. 32 or 64). Sample time points are obtained as $t_i = iT/N$, where N is the number of samples. Although increasing the number of samples improves the precision of the time response and hence the results of identification process, a very high number of samples may lead to significant increase in time required for the experimental and numerical study (computational cost). Therefore, an optimum sample number should be selected.

- Sample the nonlinear function $g(t_i)$ using the periodic response u of the system with time period T.

- Calculate the Fourier Transform (FT) of the sampled function $g_p(t_i)$. One should make sure the amplitude of the FT is correct. The FT gives the coefficient $V_{p,n}$ of the nonlinear function at each frequency.

$$V_{p,n}(\omega) = \mathcal{F}\left(g_p(t_i)\right), \tag{6.17}$$

  where $\mathcal{F}(\square)$ denotes the Fourier Transform.

- Shape the coefficient matrix $\mathbf{B}$ using the calculated frequency content $V_{p,n}$.

The great advantage is that this approach can be used for any nonlinear function. In addition, almost all of the significant harmonics of the function are immediately available. This approach also makes it feasible to consider the higher harmonics of the force.

In the following sections, several simulated and experimental case studies with different types of nonlinear elements are considered. For each case, the nonlinear mathematical model of the system is identified utilizing various methods including the EDSM technique (which works the same as the AHB approach with only the primary harmonic), the AHB approach with multi-harmonic approximations, and the AFTHB approach. The results are compared to investigate the applicability of the presented methods.

6.3 Simulated Case Studies

In this section, the proposed identification method with both AHB and AFTHB approaches is applied to four simulated case studies with different types and various numbers of nonlinear elements and excitation force. The objective of using these examples is to show the applicability of the proposed identification method with the time-frequency approach in single and multi-degree of freedom systems with different types of nonlinearity. The first case is a single-degree-of-freedom Duffing oscillator subject to a harmonic excitation force. The second case is the system of first case subject to multi-harmonic excitation. The third system is a single DOF (SDOF) mass-spring-damper system with Coulomb friction under harmonic excitation. The forth simulated case is a 2 DOF mass spring system with nonlinear damping and stiffness. The results of the identification of the unknown nonlinear restoring force are shown and discussed for each case study. As the last simulated case study, a multi-DoF system with various types of nonlinear elements is considered. The effect of noisy measurement and modelling error is studied on the identified model of this case study. Here in this study, first, it is assumed that the type of nonlinearity is known to investigate the accuracy of the proposed method in estimating the unknown parameter of a known nonlinear function. Also, the values of the unknown parameters estimated using the proposed approaches are compared with the EDSM technique to illustrate the effect of higher harmonics on the accuracy of the identification method. However, it is worth noting that the type of nonlinearity is not known in practical cases. Therefore, the type of nonlinearity should be assumed or selected using a model selection procedure or based on experienced engineering insight. Although having an experienced engineering insight is not necessary for assuming the type of nonlinearity, it will help the researcher narrow the possible candidate functions and significantly reduce the computational costs of the identification process. In Section 6.3.5, the effect of modelling error is investigated by assuming a different function rather than the exact nonlinear function.

6.3.1 Duffing Oscillator

Consider the equation of motion of a single degree of freedom Duffing oscillator, excited by a harmonic force, given by

$$m\ddot{u} + c\dot{u} + k_1 u + k_2 u^3 = F\sin(\omega t), \tag{6.18}$$

where the measured response is assumed to have the form of Eq. (6.5). Thus, the steady state response is defined using Eqs. (6.5) and (6.6). Here, the aim is to show the accuracy of the proposed AHB and AFTHB approaches in predicting the parameters of nonlinear structural elements, compared with the methods using only the primary harmonic such as the EDSM technique. Therefore, it is assumed that

the linear part of the SDOF system is known and the unknown nonlinear force in this system is

$$f_{NL} = k_2 u^3(t), \tag{6.19}$$

and the matrix of parameters and vector of nonlinear functions are respectively

$$\mathbf{A} = a = k_2, \quad \mathbf{g} = g(u, \dot{u}) = u^3, \tag{6.20}$$

Now the two approaches described above are applied to the Duffing oscillator system in order to find the unknown parameter k_2:

AHB Approach: The MCXA technique is applied to Eq. (6.18) in order to obtain the equation of motion in the frequency domain. To take account of the higher harmonics in the analysis, in this case, three harmonics of the response are considered. Substituting u_n, $\dot{u}_n$, $\ddot{u}_n$ $(n = 1, 2, 3)$ from Eq. (6.6) into the equation of motion of the system, averaging over the 1st, 2nd, and 3rd harmonics of the response, and performing a couple of simple mathematical manipulations, the following three algebraic equations are obtained. The process of derivation of equations in the frequency domain are given in Appendix A

$$\begin{aligned}
&\big(-m\omega^2 + cj\omega + k_l\big)U_1 + \frac{1}{4}k_n\big(3U_1^2\bar{U}_1 + 6U_1U_2\bar{U}_2 + 6U_1U_3\bar{U}_3 \\
&\qquad + 3\bar{U}_3U_2^2 - 3U_3\bar{U}_1^2 + 12U_0^2U_1 + 12jU_0U_2\bar{U}_1 + 12jU_0U_3\bar{U}_2\big) = F \\
&\big(-4m\omega^2 + 2cj\omega + k_l\big)U_2 + \frac{1}{4}k_n\big(3U_2^2\bar{U}_2 + 6U_2U_1\bar{U}_1 + 6U_2U_3\bar{U}_3 \\
&\qquad + 6U_1U_3\bar{U}_2 + 12U_0^2U_2 - 6jU_0U_1^2 + 12jU_0U_3\bar{U}_1\big) = 0 \\
&\big(-9m\omega^2 + 3cj\omega + k_l\big)U_3 + \frac{1}{4}k_n\big(-U_1^3 + 6U_3U_1\bar{U}_1 + 6U_3U_2\bar{U}_2 \\
&\qquad + 3U_3^2\bar{U}_3 + 3\bar{U}_1U_2^2 + 12U_0^2U_3 - 12jU_0U_1U_2\big) = 0,
\end{aligned} \tag{6.21}$$

The unknown parameter k_2 can be identified using each equation of Eq. (6.21). However, the small amplitude of the higher harmonics may lead to ill-conditioning. In this section, only the first equation, which is related to the primary harmonic of the system, is used to find k_2 as

$$k_2 = \frac{4\left(F - \left[-m\omega^2 + cj\omega + k_l\right]U_1\right)}{\left(3U_1^2\bar{U}_1 + 6U_1U_2\bar{U}_2 + 6U_1U_3\bar{U}_3 + 3\bar{U}_3U_2^2 - 3U_3\bar{U}_1^2 + 12U_0^2U_1 + 12jU_0U_2\bar{U}_1 + 12jU_0U_3\bar{U}_2\right)}, \tag{6.22}$$

Neglecting higher harmonics and utilizing only the primary harmonic of the response, k_2 is obtained as

$$k_2 = \frac{4\left(F - \left[-m\omega^2 + cj\omega + k_l\right]U_1\right)}{\left(3U_1^2\bar{U}_1\right)}/, \tag{6.23}$$

Table 6.1: Parameter values used in the simulation of the system of Eq. (6.18).

Parameters (unit)	m (kg)	c $\left(\frac{\text{N.s}}{\text{m}}\right)$	k_1 $\left(\frac{\text{N}}{\text{m}}\right)$	k_2 $\left(\frac{\text{N}}{\text{m}^3}\right)$	F (N)
Values	1	0.5	100	10^4	2

AFTHB Approach: Using this approach, the assumed nonlinear function is generated using time domain measured response u, $\dot{u}$as

$$g\left(u,\dot{u}\right)=u^3(t), \tag{6.24}$$

Then, the frequency content of the measured response $u(t)$ and the nonlinear function $g\left(u,\dot{u}\right)$ is calculated using the Fourier Transform (FFT). Accordingly, the multi-harmonic response $u(t)$ and the function $g\left(u,\dot{u}\right)$ are expanded based on their calculated frequency contents U_n, $\bar{U}_n$ and V_n, $\bar{V}_n$, respectively. The number of nonlinear functions in this case is $N_g=1$. Therefore, the equation of motion averaged (balanced) over the primary harmonic of $u(t)$ and $g\left(u,\dot{u}\right)$ is sufficient to estimate the unknown parameter k_2. Substituting the expansion of Eq. (6.24) into Eq. (6.18) and averaging over the primary harmonic, gives

$$\left(-m\omega^2+jc\omega+k_1\right)U_1+k_2V_1=F_1, \tag{6.25}$$

and parameter k_2 is obtained as

$$k_2=\frac{\left(F_1-\left(-m\omega^2+jc\omega+k_1\right)U_1\right)}{V_1}, \tag{6.26}$$

It is worth noting that as V_1 includes almost all significant harmonics participating in the response of the system as it is calculated numerically utilizing the time domain signal containing significant harmonics of the response and force. However, the precision of the approximation of V_1 can be increased by selecting enough and appropriate time step and sampling frequency. The numerical simulation of the dynamics of the Duffing oscillator of Eq. (6.18) is performed using direct ODE integration in MATLAB to obtain the steady state response of the system for different frequency lines. The parameter values used for the numerical simulation are given in Table 6.1.

Also, the response of the system is obtained utilizing the MCXA technique to investigate the accuracy of the numerical simulation (ODE, FFT). Figure 6.1 illustrates the steady state response of the system obtained using two different methods, namely the semi-analytic MCXA technique and numerical integration in MATLAB. A comparison between the generated nonlinear function $g(u,\dot{u})$ using numerical simulation and the nonlinear function obtained using the MCXA technique is shown in Figure 6.1. There is a good compatibility between the results obtained using two methods.

The variation of the identified parameter using different methods is given in Figures 6.3 and 6.4, in terms of excitation frequency ω and the primary harmonic displacement amplitude $|U_1|$. As shown, using

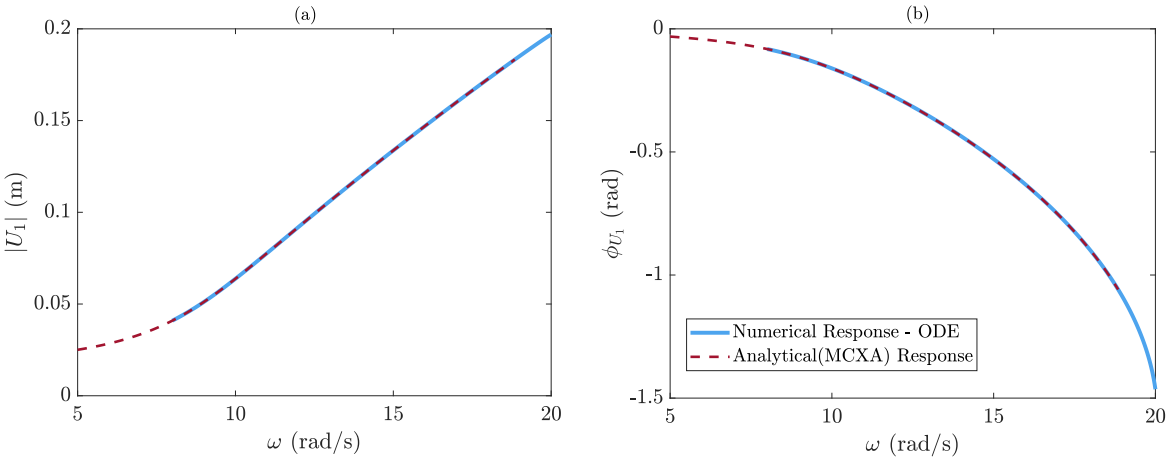

Figure 6.1: Comparison between the steady state response of the system obtained using the MCXA technique and numerical simulation.

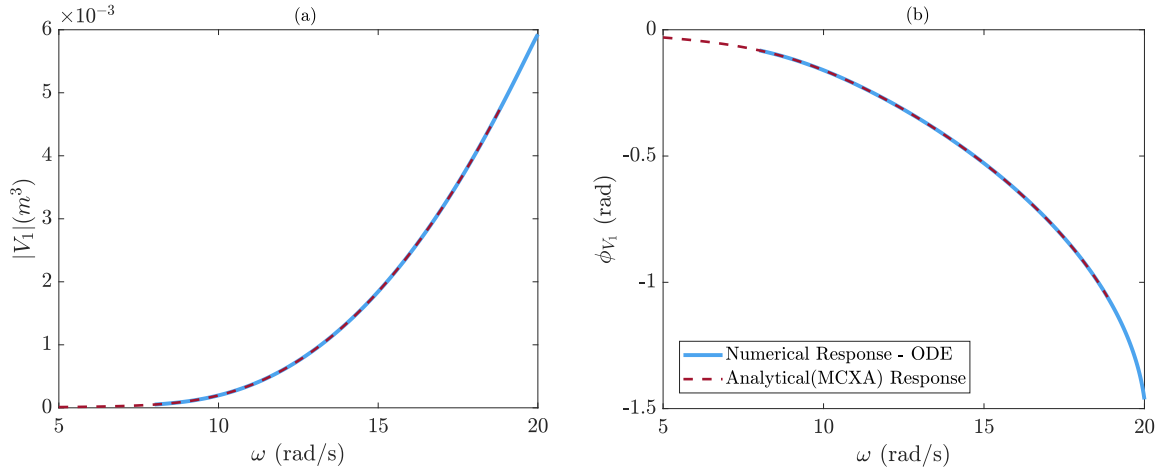

Figure 6.2: Comparison between the amplitude of the nonlinear function obtained using the MCXA technique and numerical simulation.

the EDSM technique and identifying the parameter exploiting only the primary harmonic would lead up to a 3.5% error in the estimated value. Considering three harmonics in the calculation will significantly improve the accuracy of the results and reduce the error below 0.01%. The results of the AHB approach can be even more accurate if more harmonics are considered. However, it would be complicated and burdensome. Nevertheless, the most accurate value of k_2 (with errors of less than 0.002%) has been identified using the AFTHB approach in which almost all of the significant harmonics of the response are taken into account. In addition, the results demonstrate that, as assumed in the definition of the nonlinear internal force, k_2 is a constant parameter and does not vary with ω and $|U_1|$.

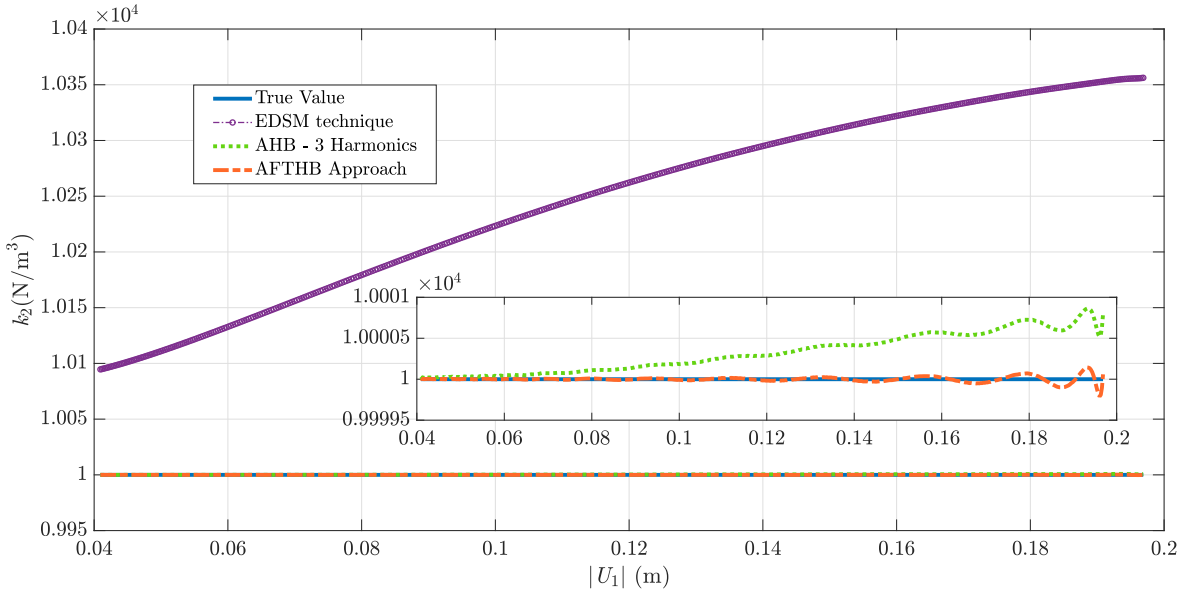

Figure 6.3: Identified value of parameter k_2 with respect to the magnitude of the amplitude of first harmonic of the response.

6.3.2 Duffing Oscillator under Multi-Harmonic Excitation

Consider Duffing oscillator system of Eq. (6.18), excited by a multi-harmonic force including primary and third harmonic, governed by

$$m\ddot{u} + c\dot{u} + k_1 u + k_2 u^3 = F_1 \sin(\omega t) + F_2 \sin(\omega t + \phi), \tag{6.27}$$

Table 6.2 includes the parameter values used for the simulation of the steady state dynamics of the system of Eq. (6.29). Numerical simulations of the nonlinear response are compared with the steady state nonlinear response obtained using the analytical MCXA technique. The first five harmonics of the response have been considered to investigate the steady state dynamics of the system using the MCXA technique. Figure 6.5 illustrates the amplitude and phase of the primary, third and fifth harmonics of

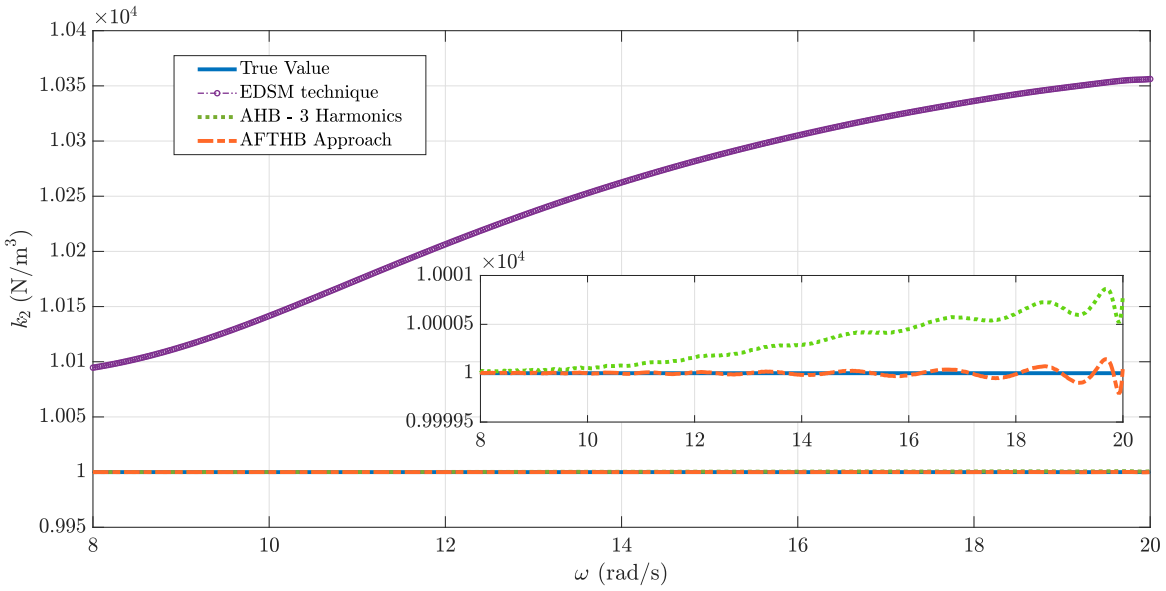

Figure 6.4: Identified value of parameter k_2 with respect to the excitation frequency.

Table 6.2: Parameter values used in the simulation of the system of Eq. (6.18).

Parameters (unit)	m (kg)	c $\left(\frac{\text{N.s}}{\text{m}}\right)$	k_1 $\left(\frac{\text{N}}{\text{m}}\right)$	k_2 $\left(\frac{\text{N}}{\text{m}^3}\right)$	F_1 (N)	F_2 (N)	ϕ (rad)
Values	1	0.5	100	10^4	2	1	$\frac{\pi}{2}$

the response. As shown, higher harmonics, particularly the third harmonic, play a significant role in the response of the system due to the third harmonic of the applied force. Therefore, the effect of higher harmonics on the results of the identification process is investigated.

Due to the nature of the nonlinearity of the system (cubic), only odd harmonics are excited. Figure 6.6 illustrates the ratio between the amplitude of the odd higher harmonics (3^{rd} to 17^{th} harmonics) with respect to the amplitude of the primary harmonic of the response. In other words, it shows the significance of the higher harmonics in the dynamics of the system. It is observed that for the excitation frequency range lower than ω =5.06 rad/s the effect of higher harmonics, particularly the third harmonic, cannot be ignored. Within this frequency band, the response of the system is dominated by the third harmonic. However, the 5^{th}, 7^{th} and even 9^{th} harmonics of the response are also considerable so that the fifth harmonic reaches to almost half of the primary harmonic and the maximum amplitude ratio of the ninth harmonic is greater than 0.6. The contribution of higher harmonics is lower for the excitation frequencies higher than $\omega = 5.06$ rad/s, and it reaches to its lowest value within the frequency range of ω =10 to 13 rad/s. Although the primary harmonic is dominant after ω =5.06 rad/s, a portion of the third harmonic is still considerable in the response. Hence, it is vital to take the effect of higher harmonics into account for identifying the nonlinear model of the system.

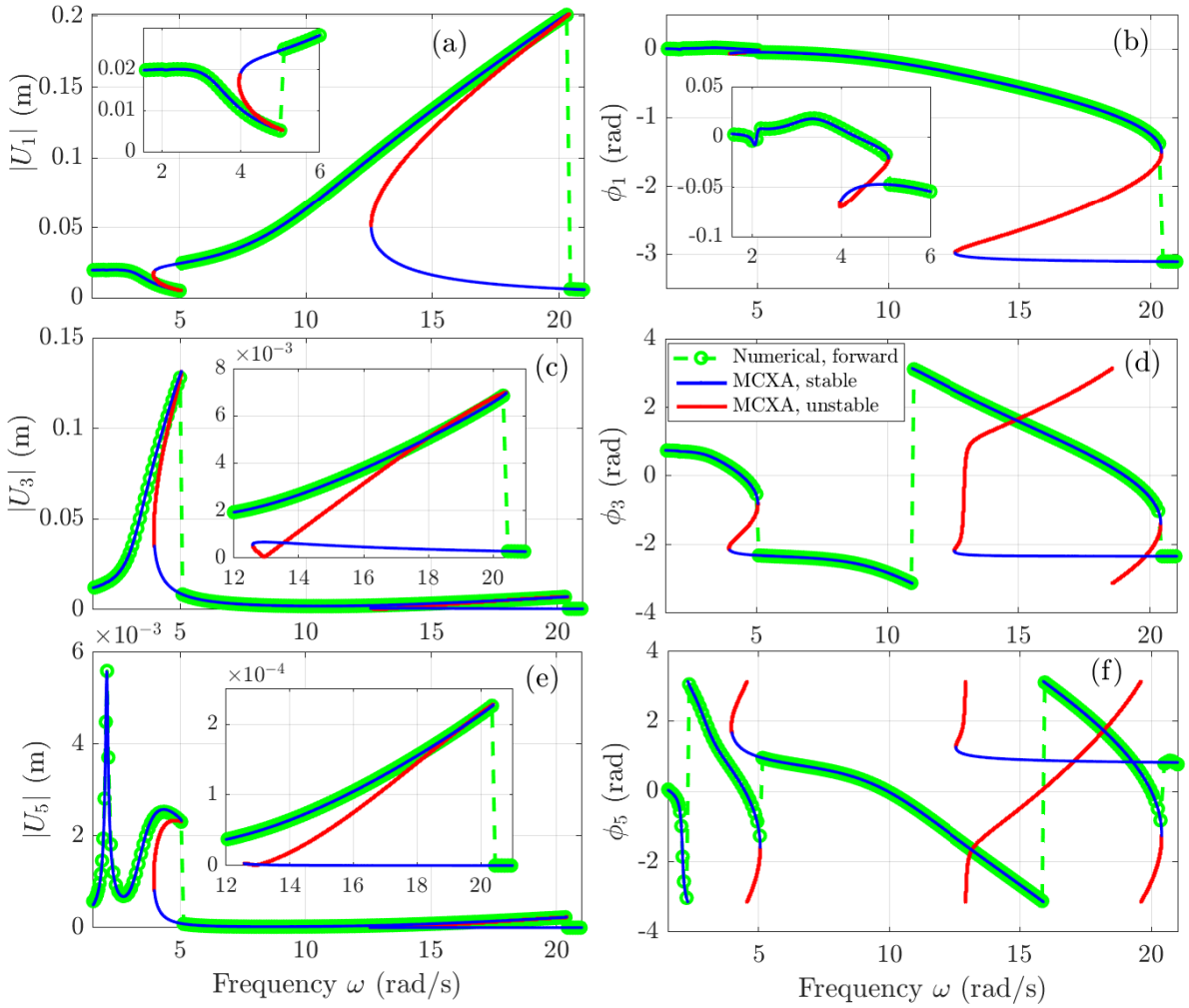

Figure 6.5: Amplitude and phase of the first (a,b), third (c,d), and fifth (e,f) harmonic of the nonlinear response of the system.

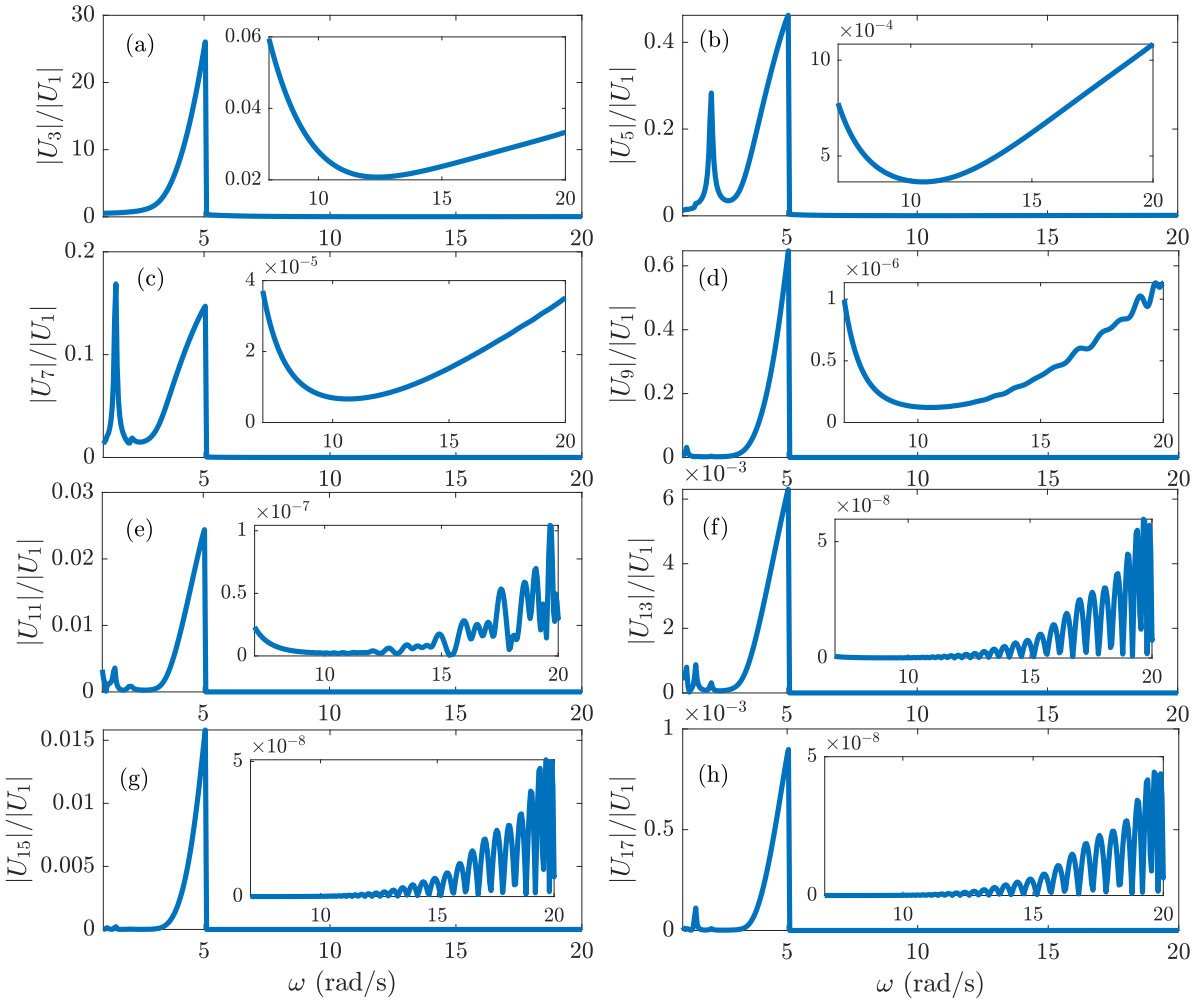

Figure 6.6: The contribution of the odd higher harmonics in the response.

Similar to the previous case in Section 6.3.1, the equation of motion averaged over the first harmonic is utilized to identify the unknown parameter k_2 of the nonlinear force. Applying the EDSM technique, the unknown parameter is obtained using Eq. (6.23) considering only the primary harmonic. Eq. (6.22) is used to determine k_2 through the AHB approach exploiting only the first three harmonics of the response. In order to take the effect of the first five harmonics of the response into account in the AHB method, the unknown parameter is calculated via following equation.

$$k_2 = \frac{\left(\left(F_1 - \left[-m\omega^2 + cj\omega + k_l\right] U_1\right)\right)}{V_1}, \tag{6.28}$$

where V_1 is the complex amplitude of the cubic nonlinear function expanded utilizing five harmonics of the response.

$$\begin{aligned} V_1 = \frac{1}{4}\big(&3U_1^2\bar{U}_1 - 3U_3\bar{U}_1^2 + 3U_2^2\bar{U}_3 - 3U_5\bar{U}_2^2 + 3U_3^2\bar{U}_5 + 6U_1U_2\bar{U}_2 + 6U_1U_3\bar{U}_3 \\ &+ 6U_1U_4\bar{U}_4 + 6U_2U_3\bar{U}_4 + 6U_1U_5\bar{U}_5 + 6U_2U_4\bar{U}_5 - 6U_4\bar{U}_1\bar{U}_2 - 6U_5\bar{U}_1\bar{U}_3 \\ &+ 12jU_0U_2\bar{U}_1 + 12jU_0U_3\bar{U}_2 + 12jU_0U_4\bar{U}_3 + 12jU_0U_5\bar{U}_4\big), \end{aligned} \tag{6.29}$$

The unknown parameter is also estimated using the AFTHB approach. Figures 6.7 and 6.8 compare the estimated k_2 using various approaches, respectively versus the amplitude of the primary harmonic and the excitation frequency. Looking at the results of identification via the EDSM technique and utilizing the single harmonic of the response (neglecting higher harmonics, yellow circles in Figures 6.7 and 6.8 reveals that the largest error in the estimated k_2 occurs at ω =5.06 rad/s where both the third and fifth harmonics have their highest amplitude. On the other hand, as expected, the lowest level of inaccuracy is seen at ω =11 rad/s where the higher harmonics have their lowest amount of contribution. Having the first three harmonics considered for identifying the system may result in a significant reduction in the error. However, still ignoring the contribution of other higher harmonics for the frequencies less than ω <5.06 rad/s gives high levels of inaccuracy. Adding the fifth harmonic to the calculation make the results more accurate, especially for higher excitation frequencies where the 7^{th} to 17^{th} harmonics have low contributions to the dynamics of the system. Nevertheless, ignoring the other higher harmonics causes the identification process not to give its best estimation of k_2. The unknown parameter k_2 is also estimated utilizing the AFTHB approach. The results, shown by red dashed lines, demonstrate a good compatibility with the true value of k_2. In spite of the good accuracy of the AFTHB approach, the excellence of the results of this approach can be improved by increasing the number of measured time points (sampling rate) and accordingly the number of frequency lines. Overall, it can be concluded from the results that neglecting higher harmonics, especially where they play significant role in the response (ω <5.06 rad/s), leads to a high inaccuracy in the identification of the system.

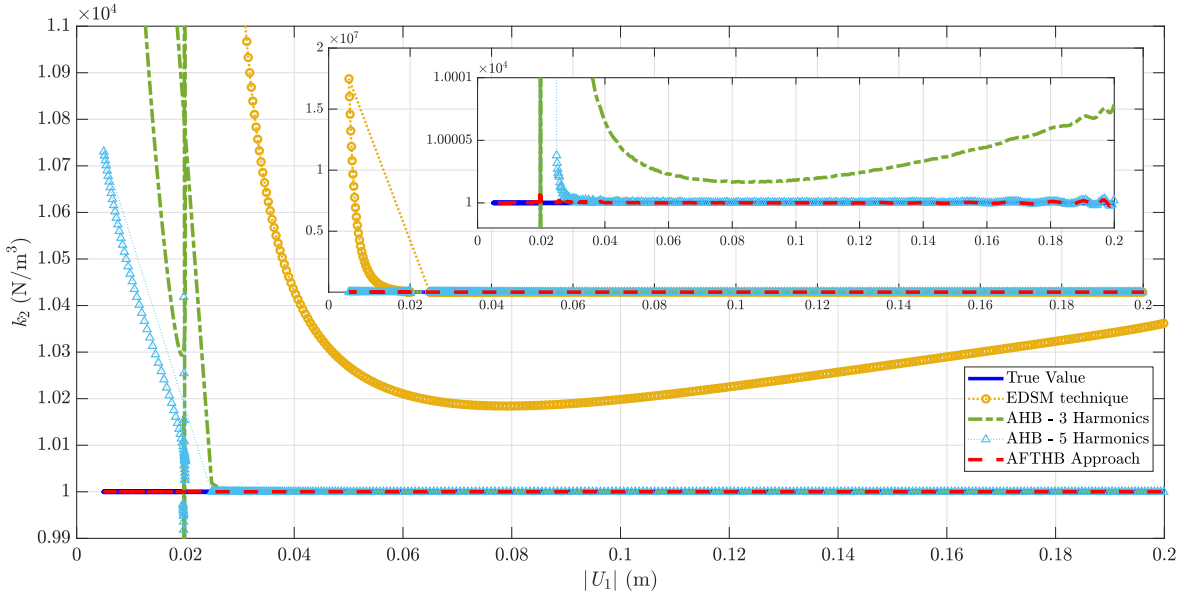

Figure 6.7: Estimated parameter k_2 of the nonlinear force versus the amplitude of the first harmonic.

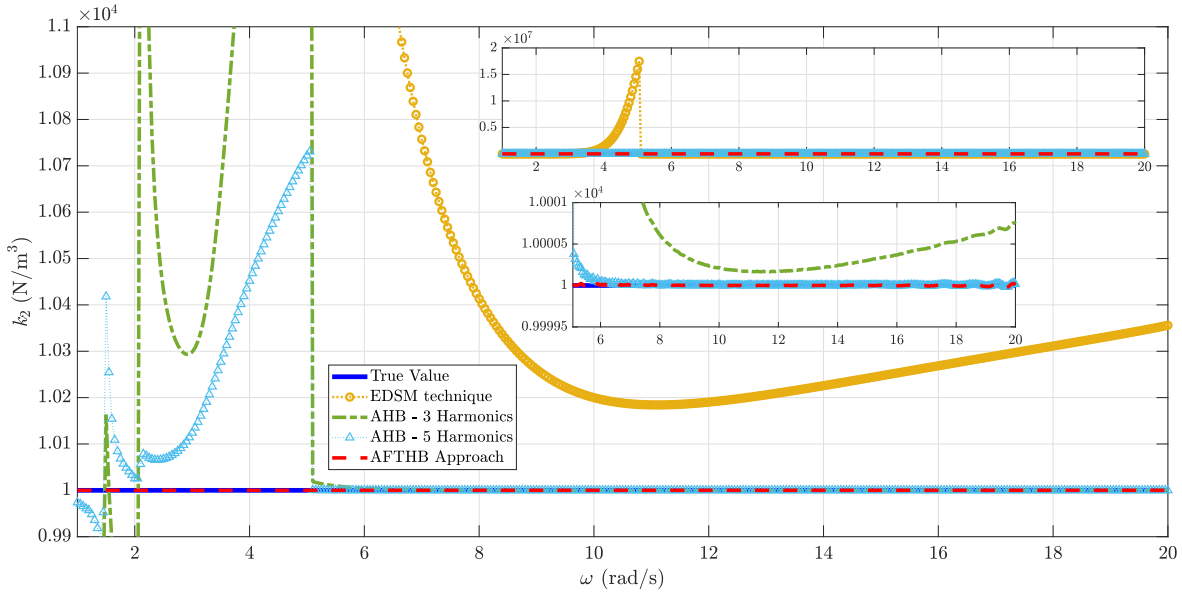

Figure 6.8: Estimated parameter k_2 of the nonlinear force versus the excitation frequency.

6.3.3 Single DOF System with Coulomb Friction

The equation of motion of a single DOF mass-damper-spring oscillator with Coulomb friction is

$$m\ddot{u} + c\dot{u} + ku + F_f \text{sign}(\dot{u}) = F\sin(\omega t), \quad F_f = \mu mg, \tag{6.30}$$

Considering the Coulomb friction as the internal nonlinear force of the system, the nonlinear force is modelled using the sign function in this system as

$$f_{NL} = F_f \text{sign}(\dot{u}), \tag{6.31}$$

Assuming the nonlinear function $g(u, \dot{u})$ as a sign function, the vectors of the parameters and the nonlinear functions are, respectively,

$$\mathbf{A} = a = F_f, \quad \mathbf{g} = g(u, \dot{u}) = \text{sign}(\dot{u}), \tag{6.32}$$

The number of nonlinear functions in this case is $N_g = 1$. Therefore, only the equation of motion averaged over the primary harmonic of $u(t)$ and $g(u, \dot{u})$ is sufficient to find the value of the unknown parameter μ. Utilizing the AHB approach exploiting the single harmonic expansion of Coulomb friction force in the frequency domain, the unknown friction coefficient μ is calculated as

$$\mu = \frac{|U_1|\left(F_1 - (-m\omega^2 + jc\omega + k)\right)}{4jmg}, \tag{6.33}$$

In order to apply the AFTHB approach, the equation of motion is written in the frequency domain using the frequency content calculated from the simulated response of the system.

$$(-m\omega^2 + jc\omega + k)U_1(\omega) + F_f V_1(\omega) = F_1, \tag{6.34}$$

and μ can be found as,

$$\mu = \frac{F_f}{mg}, \tag{6.35}$$

where

$$F_f = \frac{\left(F_1 - (-m\omega^2 + jc\omega + k)U_1\right)}{V_1}, \tag{6.36}$$

The steady state response of the system is simulated using the parameter values given in Table 6.3.

Figure 6.9 illustrates the steady state dynamics of the system of Eq. (6.30). The steady state dynamics are used to identify the unknown parameter F_f and friction coefficient μ. Figure 6.10 gives a comparison between the primary harmonic of the generated nonlinear function $g(u, \dot{u})$ of the Coulomb

Table 6.3: Parameter values used in the simulation of the system of Eq. (6.30).

Parameters (unit)	m (kg)	c $\left(\frac{\text{N.s}}{\text{m}}\right)$	k $\left(\frac{\text{N}}{\text{m}}\right)$	μ	g $\left(\frac{\text{m}}{\text{s}^2}\right)$	F (N)
Values	1	0.5	16	0.15	9.81	4

friction force using the numerically simulated response $\dot{u}(t)$ and the analytical response obtained from the MCXA technique. Some incompatibility is observed in finding the frequency content (FFT) of $g(u, \dot{u})$ using the two methods. This is due to the fact that the response of the system obtained using the analytical MCXA technique includes only the primary harmonic. This shows why it is necessary to take significant higher harmonics into consideration.

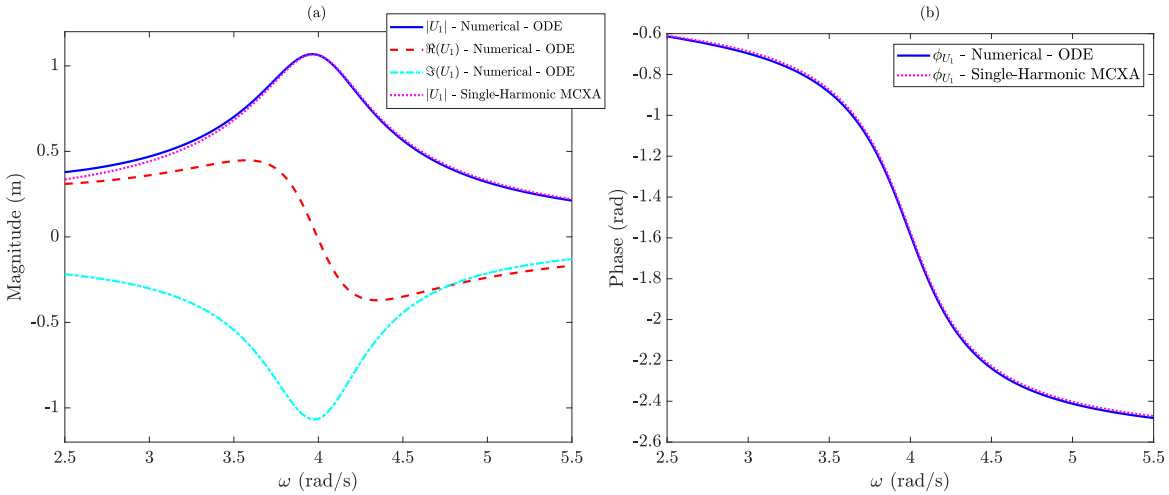

Figure 6.9: Steady state response $u(t)$ of the system with Coulomb friction.

Figures 6.11 and 6.12 compare the identified values of μ separately versus excitation frequency and the amplitude of the primary harmonic of the response. The results show that using the EDSM technique (the AHB approach with only primary harmonic) and neglecting the higher harmonics has led to considerable error, while the identified μ using the AFTHB approach is close to its true value. It is observed in Figure 6.10(b) that in the vicinity of the resonance ($\omega \approx$4 rad/s) the primary harmonic is dominant (higher harmonics do not play a significant role in the dynamics) and hence the inaccuracy of neglecting higher harmonics is reduced. Because of the same reason, the identified value of μ has its lowest error in the neighbourhood of the resonance.

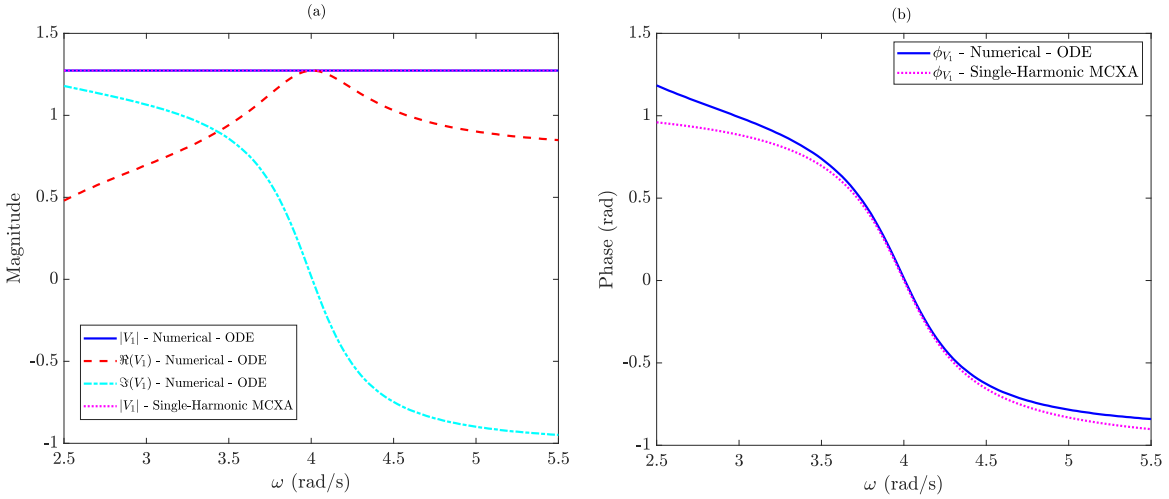

Figure 6.10: Primary harmonic of the generated nonlinear function $g(u, \dot{u})$ for Coulomb friction using the numerically simulated response.

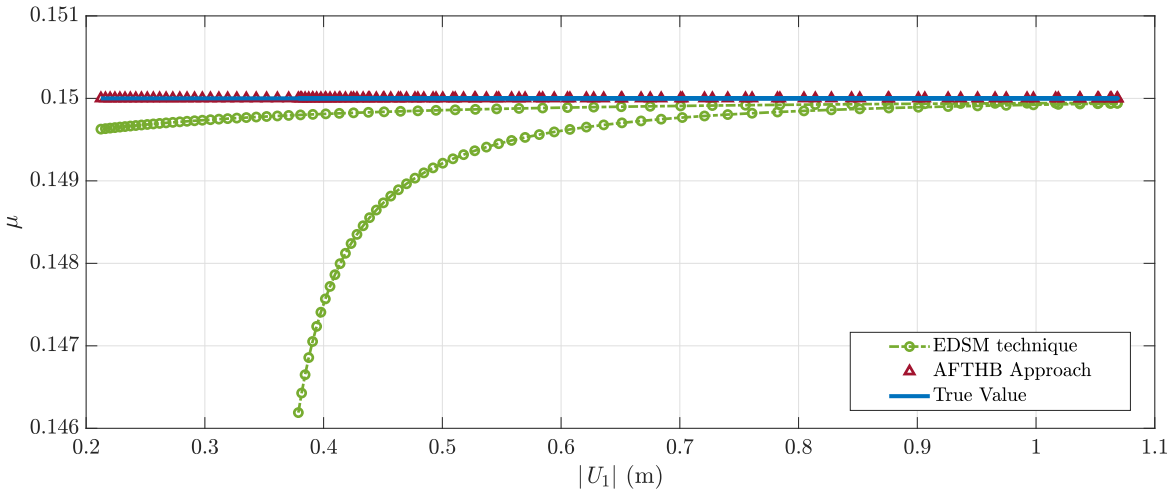

Figure 6.11: Estimated value of μ compared with its true value for different response amplitudes.

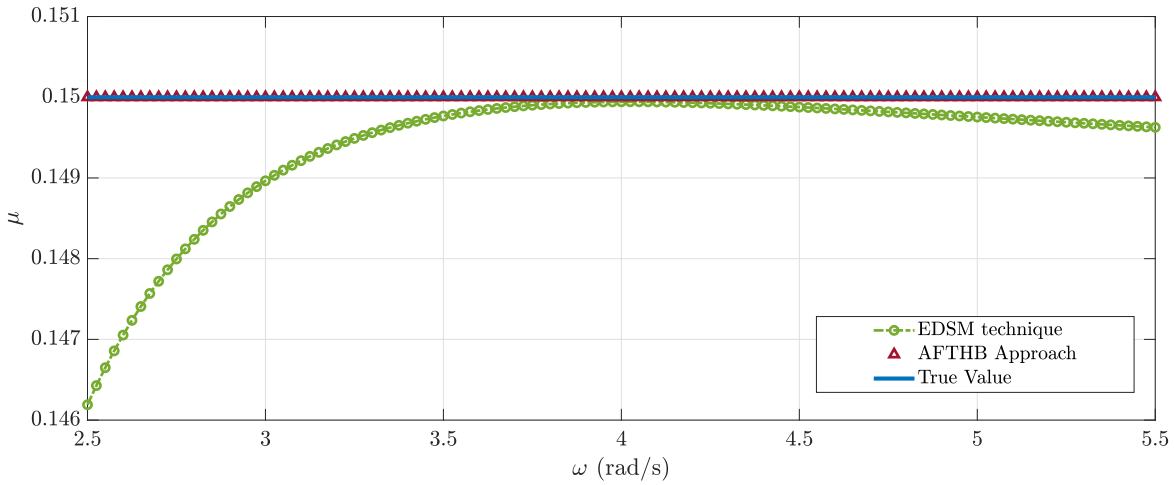

Figure 6.12: Estimated value of μ compared with its true value for different excitation frequencies.

6.3.4 2-DOF Nonlinear System

In order to investigate the efficiency of the presented method for multi-degree-of-freedom systems, a 2 DOF nonlinear system is considered, governed by the following equations of motion,

$$\begin{aligned} m_1\ddot{x}_1 + c_1\dot{x}_1 + k_1x_1 + k_{n_1}x_1^3 + c_3\left(\dot{x}_1 - \dot{x}_2\right) + k_3(x_1 - x_2) + k_{n_3}(x_1 - x_2)^3 \\ = F_1\sin(\omega t + \varphi_1), \\ m_2\ddot{x}_2 + c_2\dot{x}_2 + k_2x_2 + c_{n_2}\dot{x}_2|\dot{x}_2| + c_3(\dot{x}_2 - \dot{x}_1) + k_3(x_2 - x_1) + k_{n_3}(x_2 - x_1)^3 \\ = F_2\sin(\omega t + \varphi_2), \end{aligned} \tag{6.37}$$

The model of the defined system contains three nonlinear functions, and the internal nonlinear force is defined as

$$f_NL = \begin{Bmatrix} k_{n_1}x_1^3 + k_{n_3}(x_1 - x_2)^3 \\ c_{n_2}\dot{x}_2|\dot{x}_2| + k_{n_3}(x_2 - x_1)^3, \end{Bmatrix} \tag{6.38}$$

and hence

$$\mathbf{A} = \begin{bmatrix} k_{n_1} & k_{n_3} & 0 \\ 0 & -k_{n_3} & c_{n_2} \end{bmatrix}, \quad \mathbf{g} = \begin{Bmatrix} g_1 \\ g_2 \\ g_3 \end{Bmatrix} = \begin{Bmatrix} x_1^3 \\ (x_1 - x_2)^3 \\ \dot{x}_2|\dot{x}_2|, \end{Bmatrix} \tag{6.39}$$

The equations of motion can be rewritten in the matrix form as

$$\begin{bmatrix} m_1 & 0 \\ 0 & m_2 \end{bmatrix} \begin{Bmatrix} \ddot{x}_1 \\ \ddot{x}_2 \end{Bmatrix} + \begin{bmatrix} c_1+c_3 & -c_3 \\ -c_3 & c_2+c_3 \end{bmatrix} \begin{Bmatrix} \dot{x}_1 \\ \dot{x}_2 \end{Bmatrix} + \begin{bmatrix} k_1+k_3 & -k_3 \\ -k_3 & k_2+k_3 \end{bmatrix} \begin{Bmatrix} x_1 \\ x_2 \end{Bmatrix} + \begin{bmatrix} k_{n_1} & k_{n_3} & 0 \\ 0 & -k_{n_3} & c_{n_2} \end{bmatrix} \begin{Bmatrix} g_1 \\ g_2 \\ g_3 \end{Bmatrix} = \begin{Bmatrix} F_1 \sin(\omega t + \varphi_2) \\ F_2 \sin(\omega t + \varphi_2) \end{Bmatrix} \tag{6.40}$$

Both the AHB and AFTHB approaches are used to identify the unknown parameters of the nonlinear restoring force. Using the AHB approach, cubic nonlinear functions g_1, g_2 can be determined using multi-harmonic expressions with any number of harmonics. However, it is impossible to find an exact multi-harmonic expression for the nonlinear function $x|\dot{x}|$ in the frequency domain, and hence this function is approximated using only the primary harmonic of the response as

$$V_{1,1_{SH}} = \frac{3}{4} X_{1,1}^2 \bar{X}_{1,1}, \quad V_{2,1_{SH}} = \frac{3}{4} \left(X_{1,1} - X_{2,1}\right)^2 \left(\bar{X}_{1,1} - \bar{X}_{2,1}\right), \quad V_{3,1_{SH}} = \frac{j8\omega^2}{3\pi} \left|X_{2,1}\right| X_{2,1}, \tag{6.41}$$

In contrast, for the AFTHB approach, almost all the significant harmonics of the response are included in the calculation. Keeping the nonlinear force on the left hand side and rearranging Eq. (6.40) for the measured frequency lines, Eq. (6.12) is rewritten for this system as,

$$\begin{bmatrix} V_{1,n}(\omega_1) & V_{2,n}(\omega_1) & V_{3,n}(\omega_1) \\ V_{1,n}(\omega_2) & V_{2,n}(\omega_2) & V_{3,n}(\omega_2) \\ \vdots & \vdots & \vdots \\ V_{1,n}(\omega_{N_\omega}) & V_{2,n}(\omega_{N_\omega}) & V_{3,n}(\omega_{N_\omega}) \end{bmatrix}_{N_\omega \times 3} \begin{bmatrix} k_{n_1} & 0 \\ k_{n_3} & -k_{n_3} \\ 0 & c_{n_2} \end{bmatrix}_{3\times 2} = \begin{bmatrix} V_{1,n}(\omega_1) & V_{2,n}(\omega_1) & \ddots & V_{N_{eq},n}(\omega_1) \\ V_{1,n}(\omega_2) & V_{2,n}(\omega_2) & \ddots & V_{N_{eq},n}(\omega_2) \\ \vdots & \vdots & \vdots & \\ V_{1,n}(\omega_{N_\omega}) & V_{2,n}(\omega_{N_\omega}) & \ddots & V_{N_{eq},n}(\omega_{N_\omega}) \end{bmatrix}_{N_\omega \times N_{eq}}, \quad n = 1, \cdots, H, \tag{6.42}$$

where the unknown parameters are obtained using the calculated frequency content of the measured response and the assumed nonlinear functions utilizing Eq. (6.15).

The steady state time response of the system of Eq. (6.37) is simulated using the parameter values of Table 6.5. Figure 6.13 shows a comparison between the amplitude-frequency response of the primary harmonic of the response of the system obtained by MCXA and direct ODE integration in MATLAB.

Table 6.4: Parameters used for the simulation of the steady state response of the 2 DOF system of Eq. (6.37).

Parameters (unit)	value	Parameters (unit)	value	Parameters (unit)	value
m_1(kg)	1	$k_{l_1}(\frac{\text{N}}{\text{m}})$	150	$k_{n_3}(\frac{\text{N}}{\text{m}^3})$	2000
m_2(kg)	1.5	$k_{l_2}(\frac{\text{N}}{\text{m}})$	100	F_1N	5
$c_1(\frac{\text{N.s}}{\text{m}})$	0.15	$k_{l_3}(\frac{\text{N}}{\text{m}})$	200	F_2N	2
$c_2(\frac{\text{N.s}}{\text{m}})$	0.15	$c_{n_2}(\frac{\text{N.s}^2}{\text{m}^2})$	0.3	$\varphi_1$rad	0
$c_3(\frac{\text{N.s}}{\text{m}})$	0.2	$k_{n_1}(\frac{\text{N}}{\text{m}^3})$	3000	$\varphi_2$rad	$\frac{\pi}{2}$

The response obtained using MCXA is obtained by considering only the primary harmonic, while the response calculated using the ODE includes all harmonics.

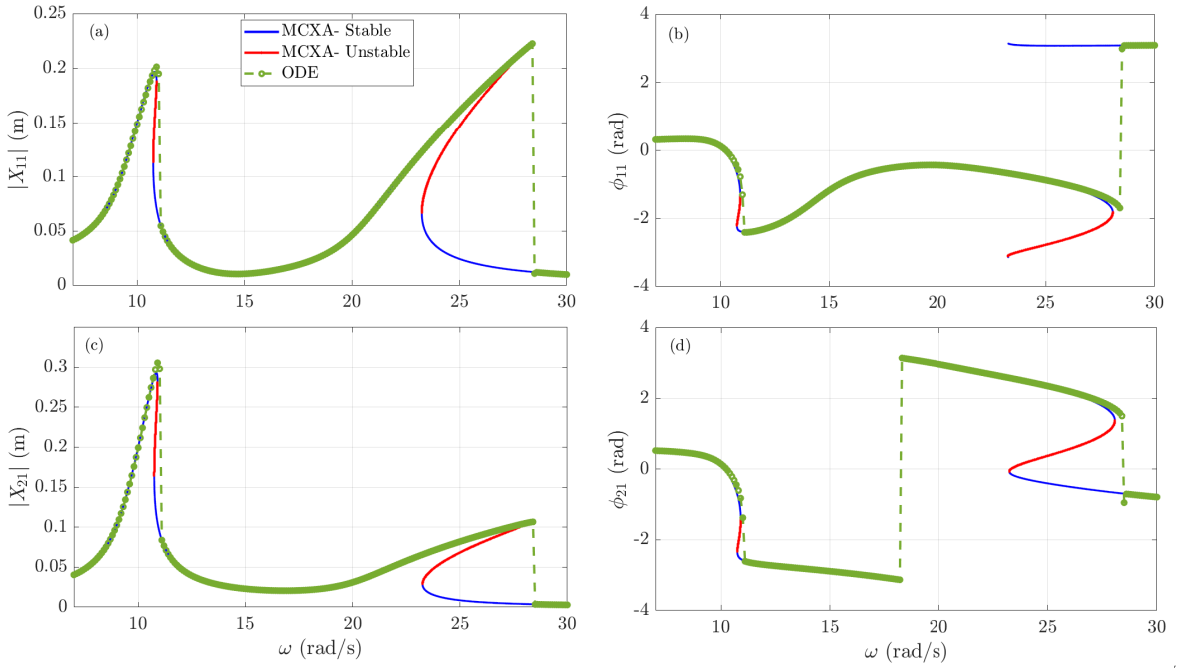

Figure 6.13: Amplitude-frequency diagram of the steady state response of the 2 DOF system of Eq. (6.37) obtained using MCXA and ODE integration in MATLAB.

The simulated steady state responses of the system are utilized to identify the unknown nonlinear restoring force. The results of the identification are shown in Table 6.5 for three different approaches. It is demonstrated that applying the EDSM technique, which exploits only the primary harmonic of the response, results in significant error in the estimated values of the parameters. Using the AHB approach gives the ability to consider the higher harmonics of smooth nonlinear functions such as cubic stiffness. Therefore, utilizing the AHB approach and taking into account the first three harmonics of the response in order to expand the cubic nonlinear functions g_1 and g_2, gives a considerable reduction in error of

Table 6.5: Parameters used for the simulation of the steady state response of the 2 DOF system of Eq. (6.37).

Parameters (unit)	True Value	EDSM Technique		AHB – g_1, g_2 (3H) and g_3 (SH)		AFTHB Approach	
		Identified Value	Error (%)	Identified Value	Error (%)	Identified Value	Error (%)
k_{n_1} $\left(\frac{\mathrm{N}}{\mathrm{m}^3}\right)$	3×10^3	3201.536	6.7179	3000.440	0.0147	2999.963	0.0012
k_{n_3} $\left(\frac{\mathrm{N}}{\mathrm{m}^3}\right)$	2×10^3	1982.197	0.8901	2000.072	0.0036	2000.038	0.0019
c_{n_2} $\left(\frac{\mathrm{N.s}^2}{\mathrm{m}^2}\right)$	0.3	0.034278	88.5741	0.034032	88.6559	0.299997	0.0007

the estimated parameters of the cubic terms. The accuracy of the results can be improved further if more significant harmonics are considered in the AHB approach. On the other hand, it is impossible to provide an exact analytical multi-harmonic expression in the frequency domain for non-smooth nonlinear functions such as Coulomb friction. Hence, using the AHB approach may not be applicable for the systems including non-smooth nonlinearities. The results of the AFTHB approach, on the other hand, shows a very good fit to the true values of the identified parameters. The reason for such low level of error is that, as stated in the theory, the AFTHB approach includes all significant harmonics of the system depending on the sampling rate.

6.3.5 MDOF Simulated Case Study

In this section, the 6-DOF nonlinear discrete system of Figure 6.14 is considered. The system includes various types of grounded or ungrounded nonlinear elements such as Coulomb friction, nonlinear damping, and cubic stiffness. The equation of motion of the system is derived in matrix form as

$$\mathbf{M}\ddot{\mathbf{u}} + \mathbf{C}\dot{\mathbf{u}} + \mathbf{K}\mathbf{u} + \mathbf{f}_{NL}(\mathbf{u}, \dot{\mathbf{u}}) = \mathbf{f}_{ex}(t), \tag{6.43}$$

where $\mathbf{M}$, $\mathbf{C}$, and $\mathbf{K}$ are respectively mass, proportional damping and stiffness matrices.

$$\mathbf{M} = \begin{bmatrix} m_1 & 0 & 0 & 0 & 0 & 0 \\ 0 & m_2 & 0 & 0 & 0 & 0 \\ 0 & 0 & m_3 & 0 & 0 & 0 \\ 0 & 0 & 0 & m_4 & 0 & 0 \\ 0 & 0 & 0 & 0 & m_5 & 0 \\ 0 & 0 & 0 & 0 & 0 & m_6 \end{bmatrix},$$
$$\mathbf{K} = \begin{bmatrix} k_1+k_2 & -k_2 & 0 & 0 & 0 & 0 \\ -k_2 & k_2+k_3 & -k_3 & 0 & 0 & 0 \\ 0 & -k_3 & k_3+k_4 & -k_4 & 0 & 0 \\ 0 & 0 & -k_4 & k_4+k_5 & -k_5 & 0 \\ 0 & 0 & 0 & -k_5 & k_5+k_6 & -k_6 \\ 0 & 0 & 0 & 0 & -k_6 & k_6 \end{bmatrix}, \mathbf{C} = \alpha\mathbf{M} + \beta\mathbf{K}, \tag{6.44}$$

$\mathbf{f}_{NL}$ and $\mathbf{f}_{ex}$ denote the nonlinear force and external force vectors, respectively.

$$\mathbf{f}_{NL} = \begin{Bmatrix} k_{N_1}x_1^3 + \mu m_1 g \frac{\dot{x}_1}{|\dot{x}_1|} \\ k_{N_2}(x_2 - x_3)^3 \\ -k_{N_2}(x_2 - x_3)^3 \\ k_{N_3}x_4^3 + c_N|\dot{x}_4 - \dot{x}_5|(\dot{x}_4 - \dot{x}_5) \\ -c_N|\dot{x}_4 - \dot{x}_5|(\dot{x}_4 - \dot{x}_5) \\ 0 \end{Bmatrix}, \mathbf{f}_{ex} = \begin{Bmatrix} 0 \\ 0 \\ 0 \\ F\sin(\omega t) \\ 0 \\ 0 \end{Bmatrix}, \tag{6.45}$$

μ denotes the friction coefficient, g is the gravitational acceleration, k_{N_1}, k_{N_2}, and k_{N_3} are respectively the coefficients of cubic stiffness, and c_N is the coefficient of nonlinear damping. F and ω denote the amplitude and frequency of the excitation force, respectively. The parameter values of the system are given as

$$\begin{aligned} m_1 =& m_2 = 1\ kg, \quad m_3 = m_4 = m_5 = m_6 = 1.75\ kg \\ k_1 =& 1 \times 10^4\ \frac{N}{m},\ k_2 = 1.2k_1, \quad k_3 = 1.5k_1, \quad k_4 = k_5 = 1.25k_1, \quad k_6 = 2k_1 \\ \alpha =& 0.1, \quad \beta = 2 \times 10^{-5}, \quad \mu = 0.2, \\ k_{N_1} =& 2.5 \times 10^8\ \frac{\mathrm{N}}{\mathrm{m}^3}, \quad k_{N_2} = k_{N_3} = 5 \times 10^8\ \frac{\mathrm{N}}{\mathrm{m}^3}, c_N = 5 \times 10^3\ \frac{\mathrm{N.s}^2}{\mathrm{m}^2} \end{aligned} \tag{6.46}$$

To investigate the applicability of the introduced AFTHB identification method, two different cases of the MDOF system of Figure 6.14 are considered: (a) the system without the friction force applied to m_1; and (b) the system with Coulomb friction applied to m_1.

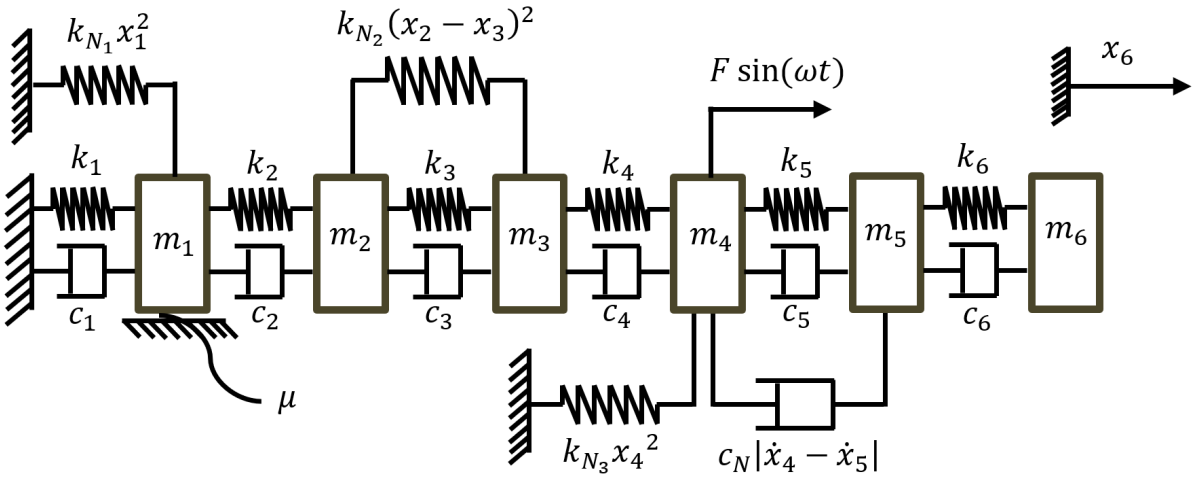

Figure 6.14: Multi degree of freedom nonlinear system.

6.3.5.1 Case I: System without Friction

The simulation of the steady state dynamics of the system of Figure 6.14 is carried out neglecting the friction between the mass m_1 and the ground. The model of the defined system contains three nonlinear functions, and the internal nonlinear force is defined as

$$\mathbf{f}_{NL}=\begin{Bmatrix} k_{N_1}x_1^3 \\ k_{N_2}(x_2-x_3)^3 \\ -k_{N_2}(x_2-x_3)^3 \\ k_{N_3}x_4^3+c_N|\dot{x}_4-\dot{x}_5|(\dot{x}_4-\dot{x}_5) \\ -c_N|\dot{x}_4-\dot{x}_5|(\dot{x}_4-\dot{x}_5) \\ 0 \end{Bmatrix}, \tag{6.47}$$

Defining the matrix of unknown parameters $\mathbf{A}$ and the vector of nonlinear functions $\mathbf{g}$

$$\mathbf{A}=\begin{bmatrix} k_{N_1} & 0 & 0 & 0 \\ 0 & k_{N_2} & 0 & 0 \\ 0 & -k_{N_2} & 0 & 0 \\ 0 & 0 & k_{N_3} & c_N \\ 0 & 0 & 0 & -c_N \\ 0 & 0 & 0 & 0 \end{bmatrix}, \quad \mathbf{g}=\begin{Bmatrix} g_1 \\ g_2 \\ g_3 \\ g_4 \end{Bmatrix}, \tag{6.48}$$

where

$$g_1=x_1^3, \quad g_2=(x_2-x_3)^3, \quad g_3=x_4^3, \quad g_4=|\dot{x}_4-\dot{x}_5|(\dot{x}_4-\dot{x}_5) \tag{6.49}$$

the equation of motion of the system of case I can be written in matrix form as

$$\mathbf{Ag} = \mathbf{f}_{ex} - (\mathbf{M\ddot{u}} + \mathbf{C\dot{u}} + \mathbf{Ku}), \tag{6.50}$$

Using the FFT, the equation of motion of each harmonic H_n $(n = 1, \cdots, N_H)$ is obtained in frequency domain as

$$\mathbf{Ag}(\omega_i) = \mathbf{F}(\omega_i) - (\mathbf{M}H_n^2\omega_i^2 + \mathbf{C}H_n\omega_i j + \mathbf{K}), \quad i = 1, \cdots, N_\omega, \tag{6.51}$$

The unknown parameters are calculated simply by solving Eq. (6.51).

The simulation of the dynamics of the system is carried out for the frequency range of $\omega = 20 - 26$ rad/s with a frequency step of $d\omega$=0.05, using four different levels of excitation F=2,10,20, and 50 N. At each frequency point, the dynamics of the system is simulated for 600 cycles, taking 2^{10} data points at each cycle (i.e. the time step used for the simulation is $dt = 2\pi/(2^{10}\omega)$). It should be noted that considering a large number of data points for each cycle may lead to a significant increase in the computational costs. Indeed, the proper sampling frequency depends on the frequency content of the dynamic response of the system. In other words, if the system under investigation behaves with a multi-frequency or multi-harmonic response (i.e., a large number of harmonics contribute to the response), a relatively high sampling frequency is required to capture all contributing harmonics of the response. The first 300 cycles of the response at each frequency point are discarded to make sure the steady state dynamics are measured. Then, the AFTHB method is applied to the last 300 cycles of the time history of the simulated steady state response of the system to identify the parameters of the nonlinear forces. Figure 6.15 shows the time history and phase diagram of the steady state response of the system at excitation frequency ω=24 rad/s in response to the excitation level of F=20 N. As explained in Section 6.2, the Fast Fourier Transform (FFT) is used to calculate the dynamic response of the system in the frequency domain. Figure 6.16 illustrates the frequency content of the time history of the response shown in Figure 6.15, calculated using the FFT. Performing the same procedure for the simulated steady state response at each excitation frequency, the amplitude-frequency response of the system is obtained. Figure 6.15 illustrates the amplitude-frequency diagram of the 1^{st}, 3^{rd}, 5^{th}, 7^{th}, and 9^{th} harmonics of the steady state dynamics of the system in response to the excitation force level F=20 N. The amplitude frequency diagram of DOF1 of the system is shown in Figure 6.18 for different levels of excitation within the excitation frequency range ω=20-26 rad/s. The resulting response in the frequency domain illustrates the significant contribution of the higher harmonics in the steady state dynamics of the system. Applying the AFTHB identification approach to the simulated results gives the identified values of the unknown parameters of the nonlinear forces. The identified values of the parameters of the nonlinear forces of the system of Case (a) are given in Table 6.6 in comparison with

the true values of the parameters. The comparison indicates the very high accuracy of the introduced AFTHB nonlinear identification approach.

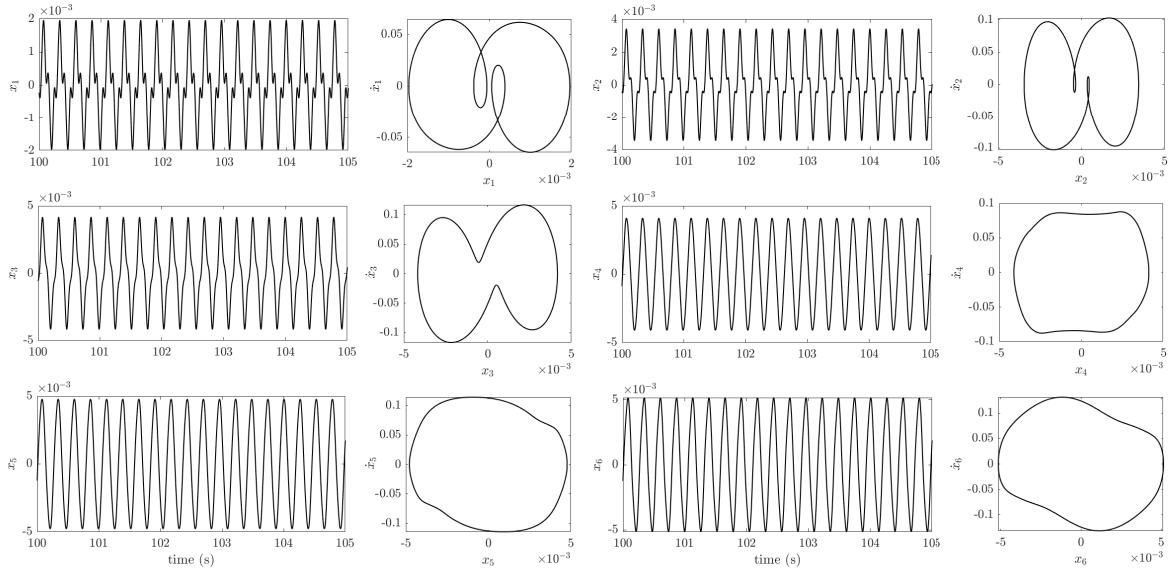

Figure 6.15: Time history and phase diagram of the steady state dynamic response of the system at the excitation frequency ω=24 rad/s in response to the force level of F=20 N.

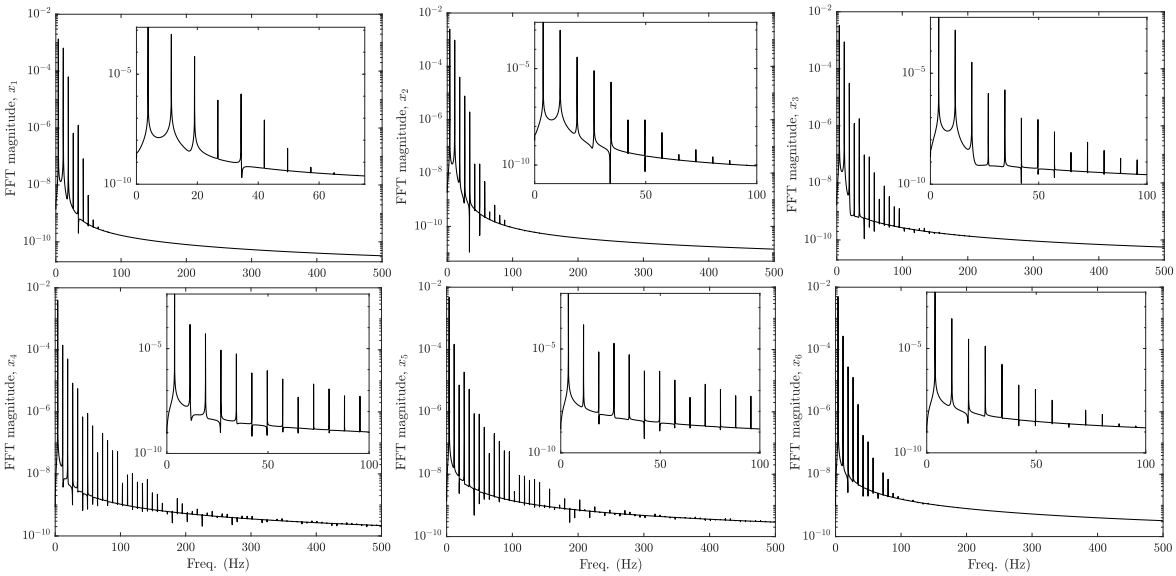

Figure 6.16: Frequency content of the steady state response of the system shown in Figure 6.15 obtained using the FFT.

The identification assumes knowledge of the form of the nonlinear restoring force so that the parameters may be identified. In practice the nonlinear function will not be known with certainty, leading to a model error in the identification process. Here the effect of model error on the performance

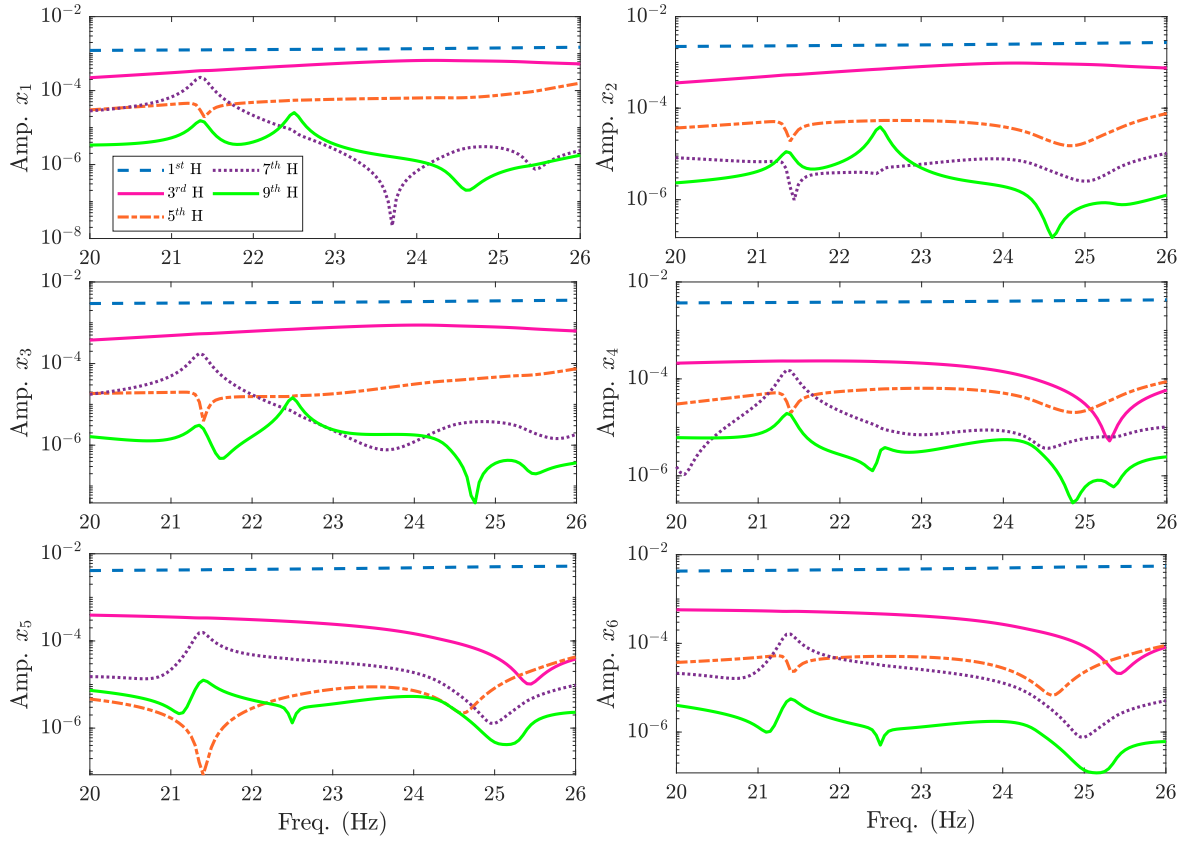

Figure 6.17: Amplitude-frequency diagram of the system in response to the excitation force level F=20 N. Amplitude of the 1^{st}, 3^{rd}, 5^{th}, 7^{th}, and 9^{th} harmonics of the steady state response are shown.

Table 6.6: Comparison between the true and identified parameter values of Eq. (6.48).

Parameters Units	k_{N_1} $\left(\frac{\text{MN}}{\text{m}^3}\right)$	k_{N_2} $\left(\frac{\text{MN}}{\text{m}^3}\right)$	k_{N_3} $\left(\frac{\text{MN}}{\text{m}^3}\right)$	c_N $\left(\frac{\text{kN.s}^2}{\text{m}^2}\right)$
True values	250	500	500	5
Identified values	249.9946	499.983	499.9947	4.99983

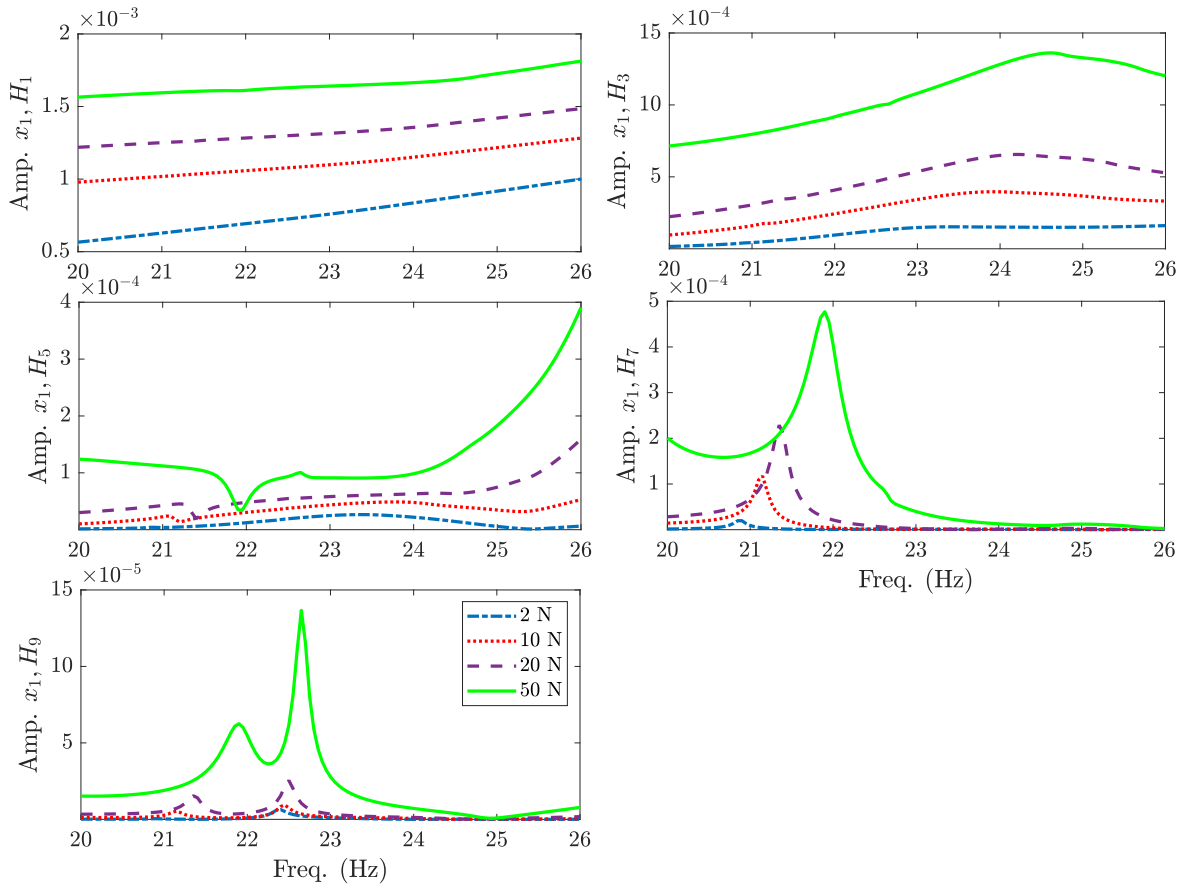

Figure 6.18: Amplitude-frequency diagram of the 1^{st}, 3^{rd}, 5^{th}, 7^{th}, and 9^{th} harmonics of the steady state response x_1 of the first degree of freedom are shown for various levels of excitation.

of the AFTHB approach to identify nonlinear forces is studied by assuming the incorrect forms of nonlinear forces. *Model Error I-* As Model I, an incorrect form is assumed for the nonlinear damping between m_4 and m_5. In order to study the performance of the AFTHB approach in identifying nonlinear forces without pre-knowledge about the type of nonlinearity, an equivalent nonlinear force is considered for the ungrounded nonlinear damping between m_4 and m_5. To this end, a polynomial function with odd terms is considered as

$$f_{N_d} = \sum_{q=1}^{N_q} c_{nl_{2q-1}} (\dot{x}_4 - \dot{x}_5)^{2q-1}, \tag{6.52}$$

where f_{N_d} is the nonlinear force equivalent to nonlinear damping $c_N|\dot{x}_4 - \dot{x}_5|(\dot{x}_4 - \dot{x}_5)$. $c_{nl_{2q-1}}$ are the unknown coefficients of the equivalent nonlinear force to be identified. Considering four terms (i.e. N_q=4), f_{N_d} is composed of a linear damping, a cubic, a fifth order, and a seventh order nonlinear damping term. Accordingly, the matrix of unknown parameters $\mathbf{A}$ of the nonlinear force, and the vector of nonlinear functions $\mathbf{g}$ are given as

$$\mathbf{A} = \begin{bmatrix} k_{N_1} & 0 & 0 & 0 & 0 & 0 & 0 \\ 0 & k_{N_2} & 0 & 0 & 0 & 0 & 0 \\ 0 & -k_{N_2} & 0 & 0 & 0 & 0 & 0 \\ 0 & 0 & k_{N_3} & c_{nl_1} & c_{nl_2} & c_{nl_3} & c_{nl_4} \\ 0 & 0 & 0 & -c_{nl_1} & -c_{nl_2} & -c_{nl_3} & -c_{nl_4} \\ 0 & 0 & 0 & 0 & 0 & 0 & 0 \end{bmatrix},$$
$$\mathbf{g} = \begin{Bmatrix} g_1 & g_2 & g_3 & g_4 & g_5 & g_6 & g_7 \end{Bmatrix}^T,$$
$$g_1 = x_1^3, \quad g_2 = (x_2 - x_3)^3, \quad g_3 = x_4^3, \quad g_4 = (\dot{x}_4 - \dot{x}_5),$$
$$g_5 = (\dot{x}_4 - \dot{x}_5)^3, \quad g_6 = (\dot{x}_4 - \dot{x}_5)^5, \quad g_7 = (\dot{x}_4 - \dot{x}_5)^7, \tag{6.53}$$

The equation of motion of Eq. (6.50) is rewritten accordingly. Then, the AFTHB approach is applied to the simulated response of the system to identify the vector $\mathbf{A}$ of unknown parameters given in Eq. (6.53). Table 6.7 gives the identified values of the unknown parameters of the system considering nonlinear damping of Eq. (6.52). The results show that in case of Model I, the stiffness parameters are estimated accurately. To verify the accuracy of the results of the identification process, the parameters set of Table 6.7 is used to regenerate the simulated response of the system of Eq. (6.50). Figure 6.19 gives a comparison between the time history and phase diagram of the steady state response obtained using the original and equivalent model of the system of Case I. The results show very good compatibility with two sets of simulated responses. The FFT of the responses shown in Figure 6.19 are compared in Figure 6.20. The comparisons show the capability of the identified equivalent model of the system Case I in regenerating the response of the exact model.

Table 6.7: Parameter values identified using the equivalent nonlinear damping model of Eq. (6.52).

Parameters Units	k_{N_1} $\left(\frac{\text{MN}}{\text{m}^3}\right)$	k_{N_2} $\left(\frac{\text{MN}}{\text{m}^3}\right)$	k_{N_3} $\left(\frac{\text{MN}}{\text{m}^3}\right)$	c_{nl_1} $\left(\frac{\text{N}}{\text{m}}\right)$	c_{nl_2} $\left(\frac{\text{kN.s}^3}{\text{m}^3}\right)$	c_{nl_3} $\left(\frac{\text{N.s}^5}{\text{m}^5}\right)$	c_{nl_4} $\left(\frac{\text{mN.s}^7}{\text{m}^7}\right)$
True values	250	500	500	–	–	–	–
Identified (Model I)	249.986	499.947	499.996	18.6977	191.852	47.7547	6.8203

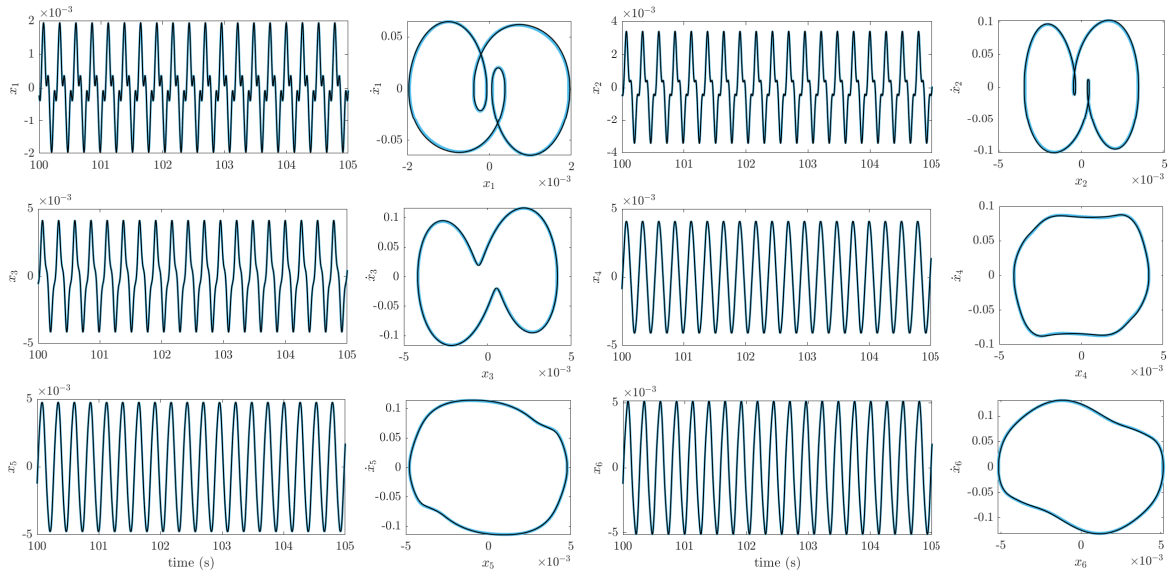

Figure 6.19: Time history and phase diagram of the identified model of the system using the equivalent nonlinear damping model of Eq. (6.52) in comparison with the response obtained using the exact model.

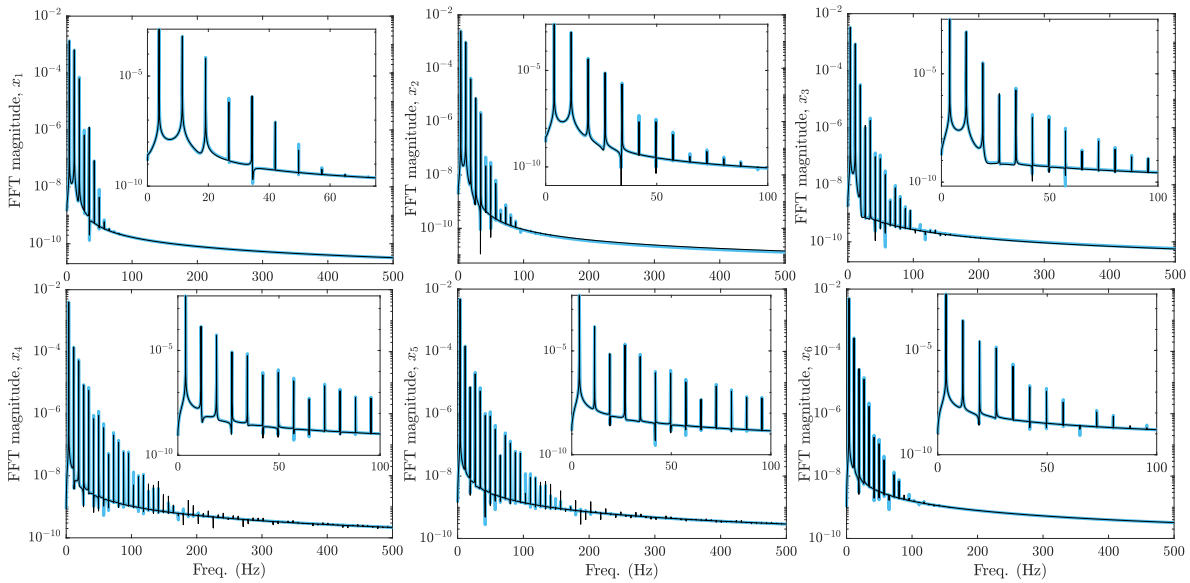

Figure 6.20: Comparison between the frequency content of the responses of the equivalent and exact models shown in Figure 6.19.

Table 6.8: Simulated and estimated parameters for the MDOF system without friction but with modelling error.

Parameters Units	k_{N_1} $\left(\frac{\text{MN}}{\text{m}^3}\right)$	k_{N_2} $\left(\frac{\text{MN}}{\text{m}^3}\right)$	k_{N_3} $\left(\frac{\text{MN}}{\text{m}^3}\right)$	c_N $\left(\frac{\text{kN.s}^2}{\text{m}^2}\right)$
True values	250	500	500	5
Identified (Model II)	249.9657	499.7854	–	11.82

Model Error II- In Model II, a more critical model error is considered. In this case, parameters of the system are identified considering a modelling error so that the grounded cubic stiffness attached to the oscillator m_4 is neglected. Therefore, the matrix of unknown parameters $\mathbf{A}$ for Model II is now

$$\mathbf{A} = \begin{bmatrix} k_{N_1} & 0 & 0 & 0 \\ 0 & k_{N_2} & 0 & 0 \\ 0 & -k_{N_2} & 0 & 0 \\ 0 & 0 & 0 & c_N \\ 0 & 0 & 0 & -c_N \\ 0 & 0 & 0 & 0 \end{bmatrix}, \tag{6.54}$$

where the vector of nonlinear functions $\mathbf{g}$ is the same as Eq. (6.48).

The AFTHB approach is now applied using the simulated response of the original nonlinear functions and Model Error II defined by Eqs. (6.54) for the identification. Table 6.8 gives the identified parameters for Model II. According to the results, stiffness parameters k_{N_1} and k_{N_2} are identified accurately in the presence of Model Error II, while the identified value of the nonlinear damping c_N shows significant error with respect to its true value. To verify the accuracy of the results of the identification process, the parameter set of Table 6.8 is used to regenerate the simulated response of the system. Figure 6.21 compares the phase diagrams and the spectra of the steady state response obtained using the original and equivalent models of the system for x_4. The results of Figures 6.21(a) and 6.21(b) show very good compatibility between the simulated reconstructed responses using the identified parameters of Model I. On the other hand, Figures 6.21(c) and 6.21(d) illustrate that the modelling error due to neglecting the cubic stiffness k_{N_3} led to significant error in the results of identification.

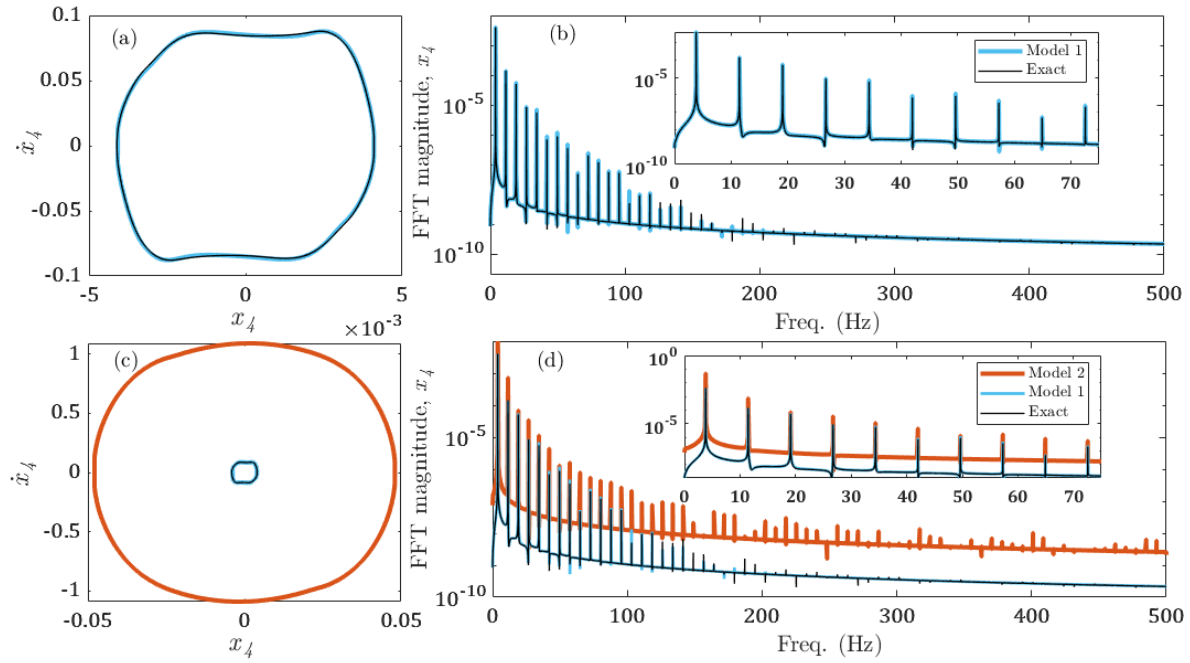

Figure 6.21: Comparison of the phase diagrams and spectra of the steady state dynamic response for x_4 at excitation frequency ω=24 rad/s and force level F=20 N. Model I: (a) and (b), Model 2: (c) and (d); Black is the simulated data and blue and orange are the reconstructed data from the identified Models I and II of Eqs. (6.53) and (6.54), respectively.

6.3.5.2 Case II: System with Coulomb Friction

The system of Figure 6.14 is considered with the dry friction between the mass m_1 and the ground. The vector of nonlinear internal force can be written as

$$\mathbf{f}_{NL} = \begin{Bmatrix} k_{N_1} x_1^3 + \mu m_1 g \left(\frac{\dot{x}_1}{|\dot{x}_1|} \right) \\ k_{N_2} (x_2 - x_3)^3 \\ -k_{N_2} (x_2 - x_3)^3 \\ k_{N_3} x_4^3 + c_N |\dot{x}_4 - \dot{x}_5| (\dot{x}_4 - \dot{x}_5) \\ -c_N |\dot{x}_4 - \dot{x}_5| (\dot{x}_4 - \dot{x}_5) \\ 0 \end{Bmatrix}, \tag{6.55}$$

The equation of motion of the system of Case II can be written in the same matrix form of Eq. (6.45), given the matrix $\mathbf{A}$ of the unknown parameters and the vector $\mathbf{g}$ of nonlinear functions as

$$\mathbf{A} = \begin{bmatrix} k_{N_1} & c_f & 0 & 0 & 0 \\ 0 & 0 & k_{N_2} & 0 & 0 \\ 0 & 0 & -k_{N_2} & 0 & 0 \\ 0 & 0 & 0 & k_{N_3} & c_N \\ 0 & 0 & 0 & 0 & -c_N \\ 0 & 0 & 0 & 0 & 0 \end{bmatrix}, \quad \mathbf{g} = \begin{Bmatrix} g_1 \\ g_2 \\ g_3 \\ g_4 \\ g_5 \end{Bmatrix}, \tag{6.56}$$

where

$$g_1 = x_1^3, \quad g_2 = \frac{\dot{x}_1}{|\dot{x}_1|}, \quad g_3 = (x_2 - x_3)^3, \quad g_4 = x_4^3, \\ g_5 = |\dot{x}_4 - \dot{x}_5|(\dot{x}_4 - \dot{x}_5) \tag{6.57}$$

and $c_f = \mu m_1 g$ denotes the coefficient of friction force.

The same simulation procedure with the same time and frequency steps is carried out to obtain the steady state dynamics of the system of Case II. As in Case I, the same four levels of excitation are used to simulate the response of the system. To examine the applicability of the presented AFTHB approach in identifying the nonlinear systems in the presence of noise in the measured data, the simulated response of the system is polluted with 2% of normally distributed noise. The clean and noisy time history and phase diagram of the steady state dynamic response of the system are shown in Figure 6.22 at excitation frequency ω=23.4 rad/s in response to the force level of F=20 N. Figure 6.23 illustrates the frequency content of the time history of the steady state response shown in Figure 6.22.

Also, a worse case is taken into account to examine the effect of measurement noise on the applicability of the proposed AFTHB identification approach. To this end, the simulated data is contaminated with 5% normally distributed noise. The clean and noisy spectra of the steady state dynamic response of x_1 are shown in Figure 6.24 for excitation frequency ω=23.4 rad/s and force level F=20 N. Including Coulomb friction in the dynamics of the system has increased the number of harmonics contributing to the response of the system. The measurement noise has produced a noise floor that limits the number of harmonics that are useful for the identification.

Applying the AFTHB approach to both the clean and noisy responses of the system, the unknown parameters of Eq. (6.56) are identified utilizing the first five odd harmonics (1, 3, 5, 7, 9). Table 6.9 gives a comparison between the true values of the parameters and their identified values exploiting clean and noisy simulated data. The comparison shows the excellent performance of the presented method in identifying the nonlinear systems even in the presence of noise in the measured/simulated data.

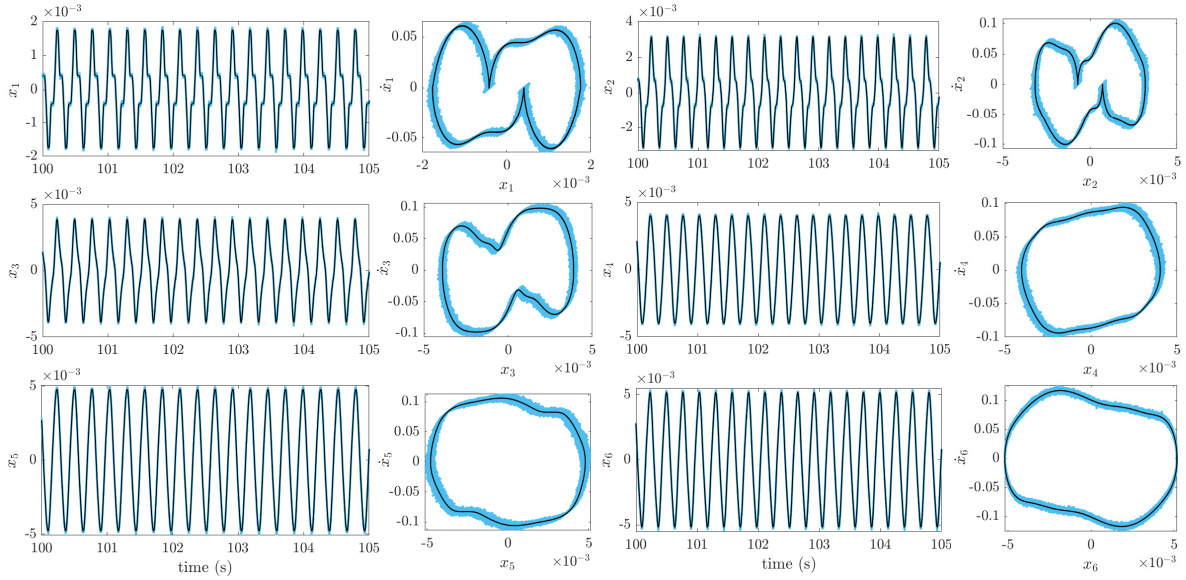

Figure 6.22: Comparison between the time history and phase diagram of the clean and noisy steady state dynamics of the system at the excitation frequency ω=23.4 rad/s in response to the force level of F=20 N. Black and blue colours denote clean and noisy data, respectively.

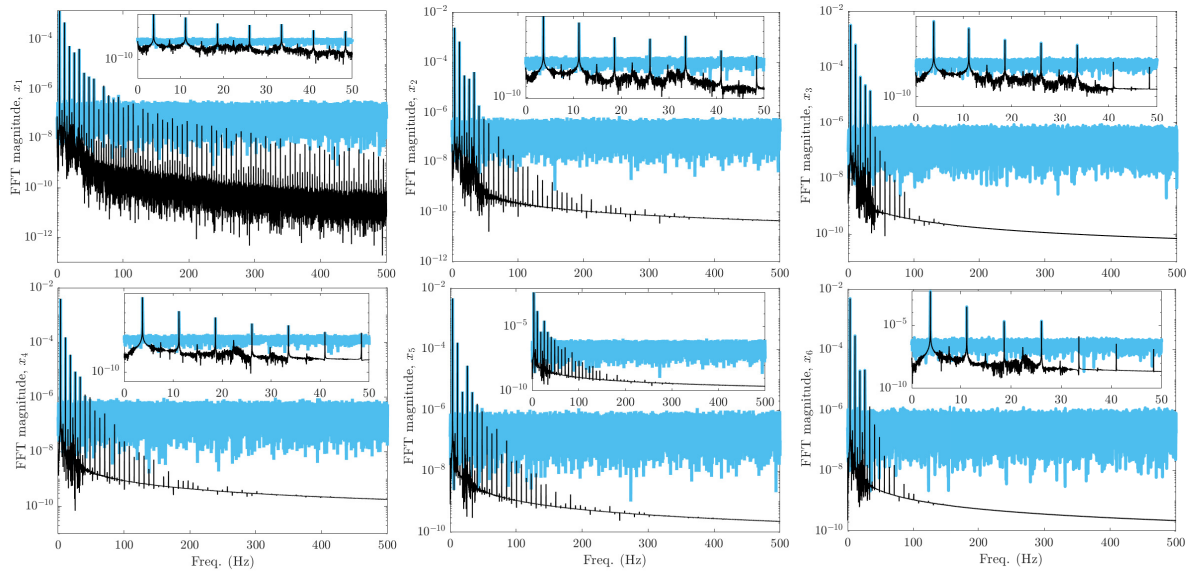

Figure 6.23: Comparison between the FFT of the clean and noisy steady response of the system at the excitation frequency ω=23.4 rad/s under the excitation level F=20 N. Black and blue colours denote clean and noisy data, respectively.

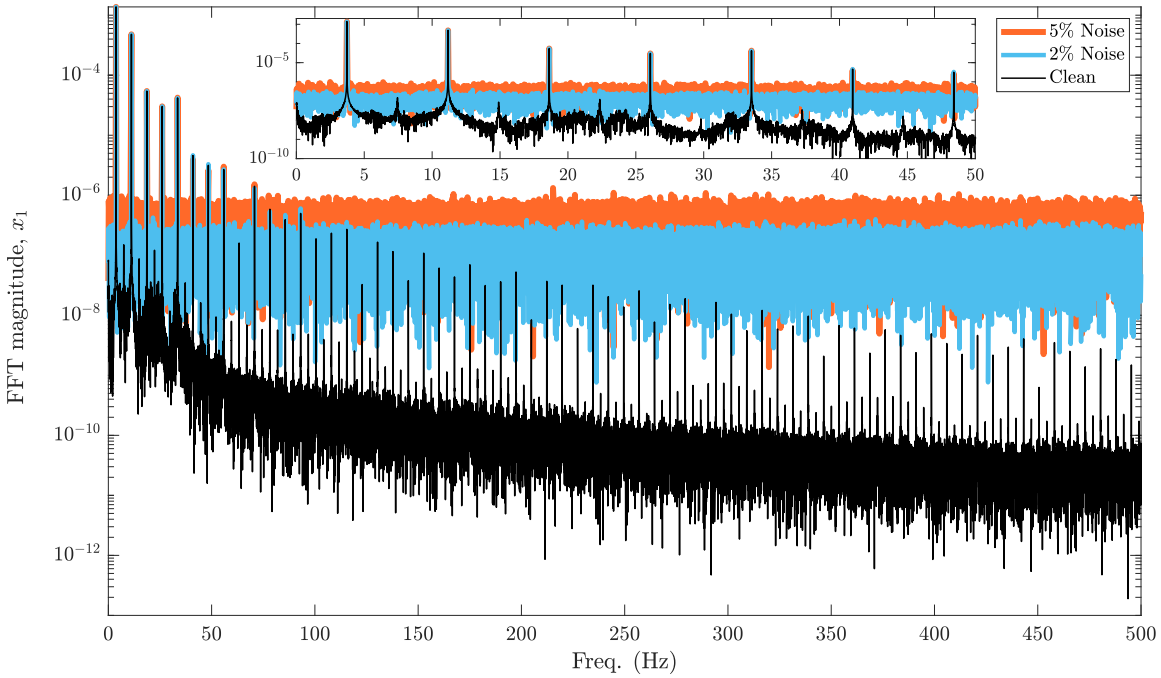

Figure 6.24: The spectra of the clean and noisy steady response of x_1 at excitation frequency ω=23.4 rad/s and force level F=20 N. Black, blue, and orange denote clean, noisy data (2%), and noisy data (5%), respectively.

Table 6.9: Simulated and estimated parameters for the MDOF system with friction, and with and without measurement noise.

Parameters (unit)	$k_{N_1}\left(\frac{\text{MN}}{\text{m}^3}\right)$	μ	$k_{N_2}\left(\frac{\text{MN}}{\text{m}^3}\right)$	$k_{N_3}\left(\frac{\text{MN}}{\text{m}^3}\right)$	$c_N\left(\frac{\text{kN.s}^2}{\text{m}^2}\right)$
Simulated	250	0.2	500	500	5
Identified using clean data	249.758	0.2002	499.957	499.974	4.99561
Error (%)	-0.0968	0.1	-0.0086	-0.0052	-0.0878
Identified using noisy data (2%)	247.863	0.2055	484.658	499.34	4.96470
Error (%)	-0.8548	2.75	-3.0684	-0.132	-0.706
Identified using noisy data (5%)	238.637	0.1812	430.814	496.50	4.6058
Error (%)	-4.5452	-9.4	-13.8372	-0.7	-7.884

6.4 Closure

This study proposes an identification method that exploits the multi-harmonic response and force signals of the structure measured from a multi-input/multi-output vibration test in both the time and frequency domains. Two different approaches are used in this method: the Analytical Frequency Domain (AHB) approach and the Alternative Numerical Time-Frequency (AFTHB) approach. In the AHB approach, the proposed method utilizes the expanded nonlinear functions in the frequency domain obtained from analytical methods such as Fourier Integral (FI), the Complex Averaging (CXA) technique or the Harmonic Balance Method (HBM). In the AFTHB approach, the Fourier Transform of the measured time response is calculated to expand the nonlinear functions in frequency domain. The AHB approach is shown to be very accurate in identifying nonlinear systems if all significant harmonics are considered in the analytical expansion of the nonlinear functions. Nevertheless, it is often cumbersome to include all significant harmonics of the response in the analytical expansion. Besides, it would be difficult to apply the AHB approach to structures with complex forms of nonlinearities such as Coulomb friction and also to multi-degree of freedom nonlinear systems. Therefore, the AFTHB approach is developed. The great advantage of AFTHB is that it can be applied to all forms of nonlinear function. In addition, almost all significant harmonics of the response are included in this approach. In addition, the introduced identification method requires prior-knowledge or appropriate estimation of the type of system nonlinearities. Hence, great engineering insight is necessary to make proper estimation of the type of nonlinear elements. The method with both approaches is applied to four simulated nonlinear vibration systems with single and multi-degrees of freedom and various types of nonlinearities including cubic stiffness, Coulomb friction, and quadratic damping. Comparison has been given between the results of two different approaches of the introduced method. It is shown that the method with both approaches is able to accurately identify the nonlinear terms in the model if all significant harmonics of the response are considered. The results of the AHB approach also show that neglecting the higher harmonics leads to inaccurate identification of the nonlinear system, especially when the higher harmonics have significant contribution in the excitation and responses.

Chapter 7

Application of the AFTHB Approach to Two Experimental Case Studies

7.1 Introduction

This chapter investigates the practical performance of the AFTHB identification approach presented in Chapter 6. To this end, the method is applied to measured data from two experimental case studies. The results are shown and discussed.

7.2 First Experimental Case Study

The experimental set-up shown in Figure 7.1(a) is considered to have nominal parameters of Table 7.1. The system is composed of a cantilever beam subject to a point force supplied by a shaker, as shown. Two permanent magnets attached to the tip of the beam along with two electromagnets located on both sides of the permanent magnets apply nonlinear electromagnetic force on the tip of the beam. Three accelerometers are located on the beam (with distances of 5, 15, and 25 cm from the clamped end of cantilever) to measure the response of the system. The applied force is measured by using a force transducer at a location 5 cm away from the clamped end. The equation of motion of the system is derived using Euler-Bernoulli beam theory and the Finite Element (FE) method. The FE model of the cantilever beam is created using 6 two-noded beam elements whose degrees of freedom are the displacements and slopes at the two nodes. The schematic finite element model of the system is illustrated in Figure 7.1(b). All degrees of freedom of the FE model are shown in the schematic of the system. The effect of all point masses (accelerometers, force transducer, and permanent magnets attached to the beam) is considered in the FE model of the system. Also, to model the interaction

between the shaker and the structure, a linear spring-dashpot model is used. However, in a more detailed investigation of the behaviour of the shaker, a more complicated model can be considered to include other parts of the shaker other than the stinger. The stiffness k_{sh} and damping c_{sh} of the stinger are included in the FE model of the system.

$$\mathbf{M}\ddot{\mathbf{w}} + \mathbf{C}\dot{\mathbf{w}} + \mathbf{K}\mathbf{w} + \mathbf{f}_{NL}(\mathbf{w}, \dot{\mathbf{w}}) = \mathbf{f}_{ex}(t), \tag{7.1}$$

where $\mathbf{M}, \mathbf{C}, \mathbf{K} \in \mathbb{R}^{12\times 12}$ are the mass, damping, and stiffness matrices of the underlying linear FE model of the system, respectively. $\mathbf{w}$ denotes the generalised displacements of the beam and $\mathbf{f}_{ex} \in \mathbb{R}^{12\times 1}$ is the vector of the external force applied to the cantilever beam. As the shaker force is the only excitation force applied to the system at DOF1, the vector of external force is

$$\mathbf{f}_{ex}(t) = \begin{Bmatrix} f_{sh}(t) \\ 0 \\ \vdots \\ 0 \end{Bmatrix}, \tag{7.2}$$

where $f_{sh}(t)$ is the force applied by the shaker and measured by the force transducer. $\mathbf{f}_{NL}(\mathbf{w}, \dot{\mathbf{w}}) \in \mathbb{R}^{12\times 1}$ is the vector of nonlinear restoring force. In order to model the vector of nonlinear restoring force, the nonlinear electromagnetic force is assumed to be localized and be a function of the transverse deflection of the beam at DOF11. Based on this assumption, the nonlinear electromagnetic force of the experimental set-up is modelled using the five models given in Table 7.2 including different types of nonlinear functions ranging from linear stiffness and damping to quadratic, cubic, and fifth order stiffness. It was shown in Chapter 5 that for a perfectly symmetric assembly of the system, the nonlinear electromagnetic restoring force will only include odd terms. Hence, the first four models are composed of only odd nonlinear functions. But it is impossible to control the symmetry of the structure in real experiments, and in practice, the system may include some asymmetry. Therefore, a quadratic nonlinear stiffness is assumed in Model 5 to consider such asymmetry in the nonlinear electromagnetic force. However, the effect of the quadratic nonlinearity is expected to be low. The vector $\mathbf{g}(\mathbf{w}, \dot{\mathbf{w}})$ of nonlinear functions and the matrix of unknown parameters $\mathbf{A}$ is given using the nonlinear force Model 5 as

$$\mathbf{A} = \begin{bmatrix} 0 & 0 & 0 & 0 & 0 \\ \vdots & \vdots & \vdots & \vdots & \vdots \\ 0 & 0 & 0 & 0 & 0 \\ c_{l_1} & k_{l_1} & k_{n_2} & k_{n_3} & k_{n_5} \\ 0 & 0 & 0 & 0 & 0 \end{bmatrix}_{12\times 5}, \quad \mathbf{g} = \begin{Bmatrix} g_1 \\ g_2 \\ g_3 \\ g_4 \\ g_5 \end{Bmatrix} = \begin{Bmatrix} \dot{w}_{11} \\ w_{11} \\ w_{11}^2 \\ w_{11}^3 \\ w_{11}^5 \end{Bmatrix}, \tag{7.3}$$

Table 7.1: Geometry and material properties of the experimental setup of Figure 7.1.

Parameters (unit)	Values
Length of cantilever beam, l (m)	0.3
Width of cantilever beam, d (m)	0.0285
Thickness of cantilever beam, t (m)	0.00145
Density of cantilever beam, ρ $\left(\frac{\text{kg}}{\text{m}^3}\right)$	7800
Modulus of elasticity of cantilever beam, E (GPa)	210
Mass of each accelerometer, (g)	8
Mass of force transducer, (g)	26
Mass of each permanent magnet, (g)	4
Strength of N42 Neodymium permanent magnets (kg pull strength)	2
Electromagnets (kg pull strength)	25
Applied voltage to electromagnets (V)	20
Initial gap between electromagnets and permanent magnets (cm)	4

where w_{11} and $\dot{w}_{11}$ are transverse deflection and velocity at DOF11 (the location of electromagnetic force at the tip of the beam). Two types of vibration test are carried out to identify the nonlinear model of the system. First, a random test is performed to measure the linear response of the system. Exploiting the measured linear response and using linear updating methods, the underlying linear model of the system is first updated. Secondly, a stepped-sine vibration test is carried out to obtain the steady state nonlinear response of the structure at various frequencies. Then the presented ANTF approach is applied to the measured nonlinear response of the system to identify the unknown nonlinear internal force of the system. Figure 7.2 shows the experimental results including linear response obtained from the low amplitude random test, the first three harmonics of the nonlinear response obtained from the stepped-sine vibration test, and three harmonics of the applied force used in the stepped-sine test. In Figure 7.2, $F_{1,1}$ and $W_{i,H}$ denote, respectively, the amplitude of the primary harmonic of the measured excitation force signal and the amplitude of Hth harmonic of the response at DOF-i in the frequency domain. It is observed that in spite of significant higher harmonic amplitude of the force signal, the higher harmonics do not have significant contributions to the nonlinear response of the system. The maximum contribution of the higher harmonics is related to the second harmonic at DOF1 which is about 1% of the primary harmonic. Therefore, in contrast with the simulated examples, this experimental example addresses the identification of a nonlinear system in the presence of higher harmonics of force.

Table 7.3 includes the parameters used to update the underlying linear system of the experimental set-up of Figure 7.1 and their optimized values. The linear frequency response functions (FRF) of the nonlinear cantilever beam system is shown in Figure 7.3. $H_{1,1}$, $H_{5,1}$, and $H_{9,1}$ in Figure 7.3 denote the linear FRFs at DOFs 1, 5, and 9, respectively. The experimental linear FRF is compared with the analytical FRF obtained from the updated underlying linear model for a frequency range including the

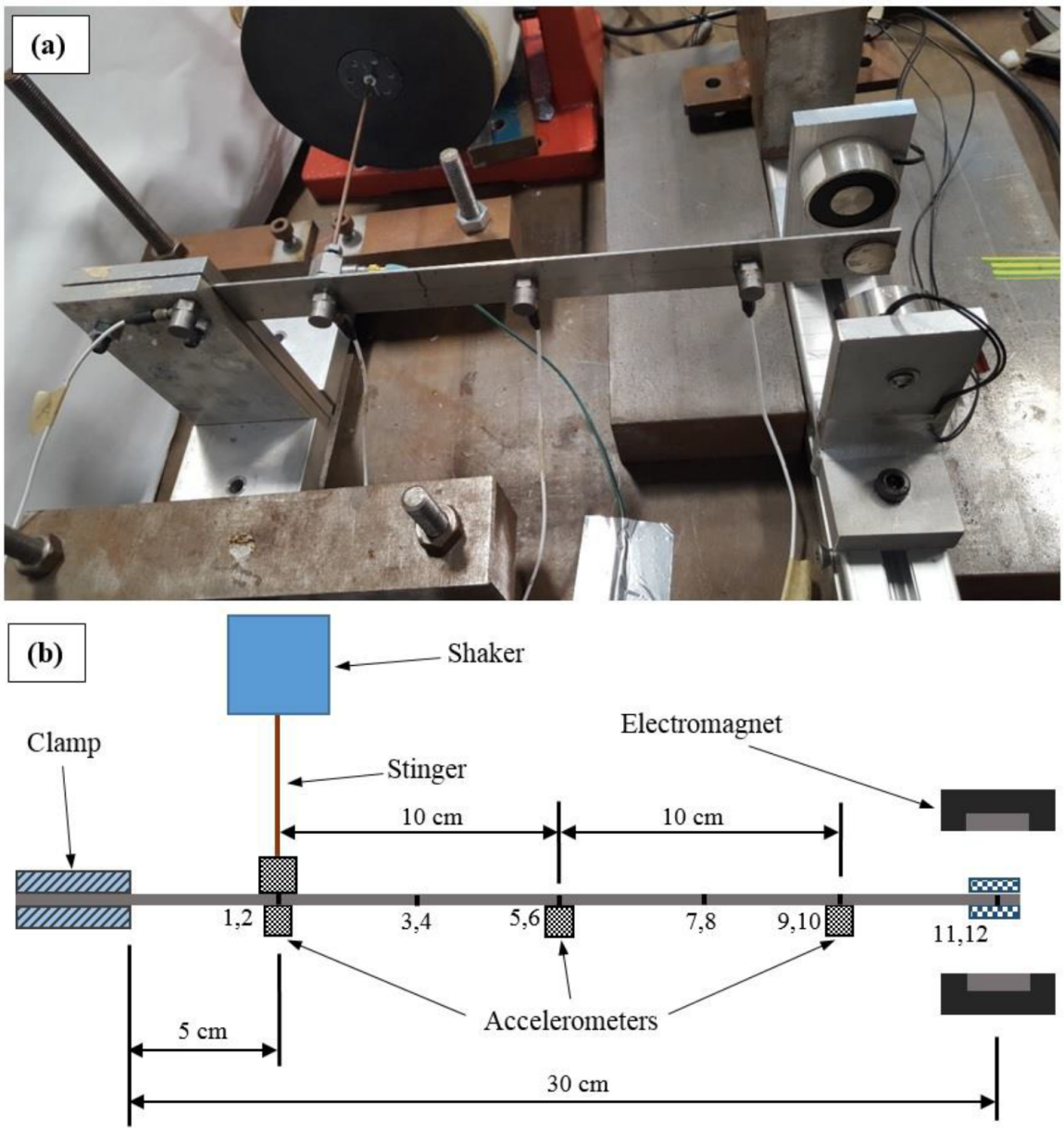

Figure 7.1: Experimental set-up (a) and its schematic with finite element model (b).

Table 7.2: Identified Models of the nonlinear electromagnetic force of the system of Figure 7.1.

Nonlinear Force Models	$f_{NL_{11}}$
Model 1	$f_{NL_{11}} = k_{n_3} w_{11}^3$
Model 2	$f_{NL_{11}} = k_{l_1} w_{11} + k_{n_3} w_{11}^3$
Model 3	$f_{NL_{11}} = c_{l_1} \dot{w}_{11} + k_{l_1} w_{11} + k_{n_3} w_{11}^3$
Model 4	$f_{NL_{11}} = c_{l_1} \dot{w}_{11} + k_{l_1} w_{11} + k_{n_3} w_{11}^3 + k_{n_5} w_{11}^5$
Model 5	$f_{NL_{11}} = c_{l_1} \dot{w}_{11} + k_{l_1} w_{11} + k_{n_2} w_{11}^2 + k_{n_3} w_{11}^3 + k_{n_5} w_{11}^5$

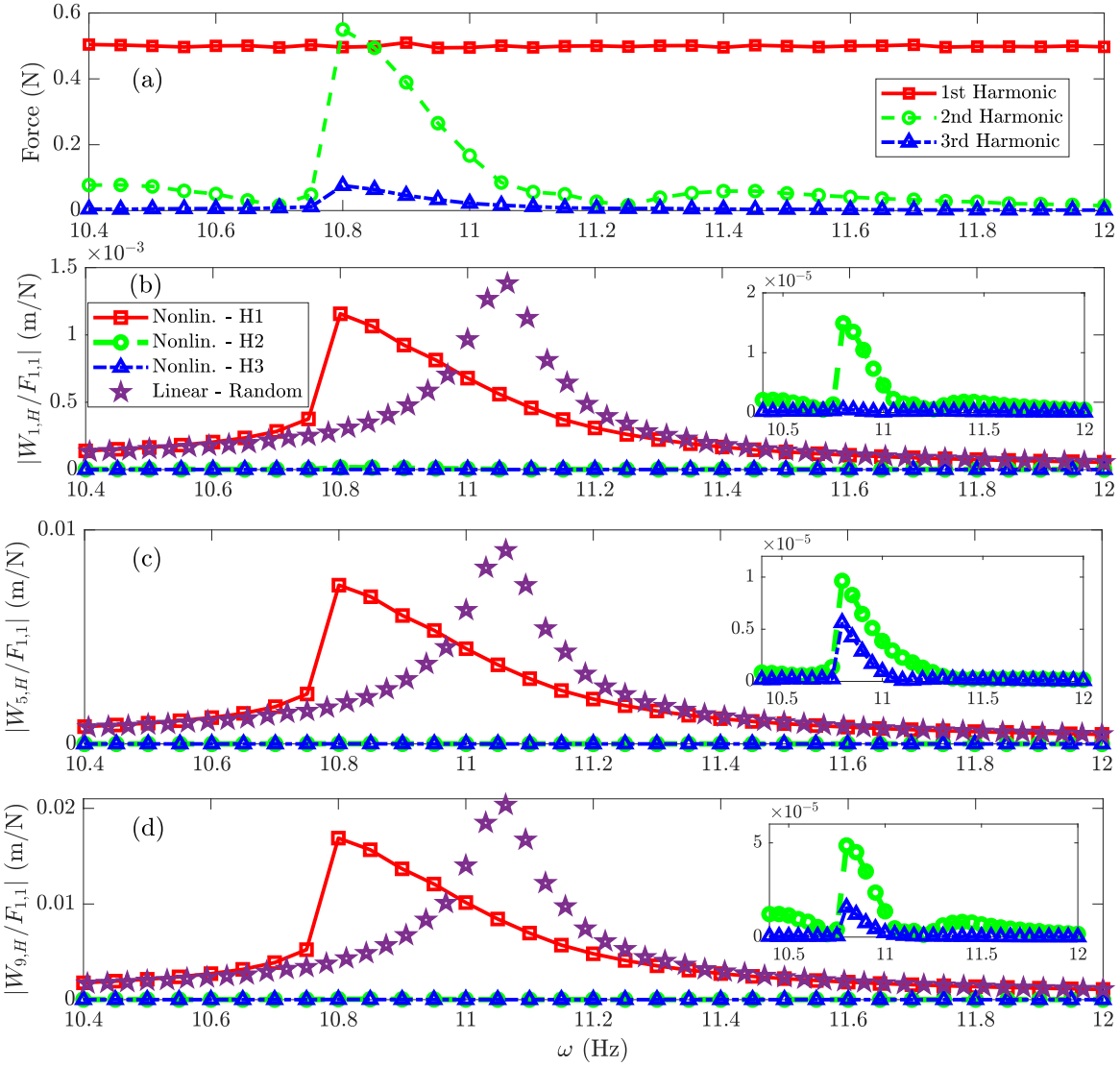

Figure 7.2: Force signal for stepped-sine test (a). Linear (random excitation) and nonlinear (stepped-sine test, first three harmonics) experimental results at DOFs 1 (b), 5 (c), and 9 (d).

Table 7.3: Parameters of the updated underlying linear model.

Parameters (unit)	Initial Values	Updated Values
Flexural Stiffness, $EI\ (\text{Pa.m}^4)$	1.52	1.56
Mass per unit length, $\rho A\ \left(\frac{\text{kg}}{\text{m}}\right)$	0.32	0.29
Proportional Damping Coefficient, α	1	0.75
Proportional Damping Coefficient, β	1×10^{-5}	4×10^{-5}
Point mass at DOF 1 (accelerometer and force transducer) (g)	0.034	0.045
Point mass at DOF 5 (accelerometer) (g)	0.008	0.01155
Point mass at DOF 9 (accelerometer) (g)	0.008	0.0085
Stiffness of the stinger, $k_s\ \left(\frac{\text{N}}{\text{m}}\right)$	5×10^2	1.012×10^2
Damping of the stinger, $c_s\ \left(\frac{\text{N.s}}{\text{m}}\right)$	0.1	0.05

first resonance of the system. The underlying linear system is then utilized to identify the nonlinear model of the system using the AFTHB approach presented in this study.

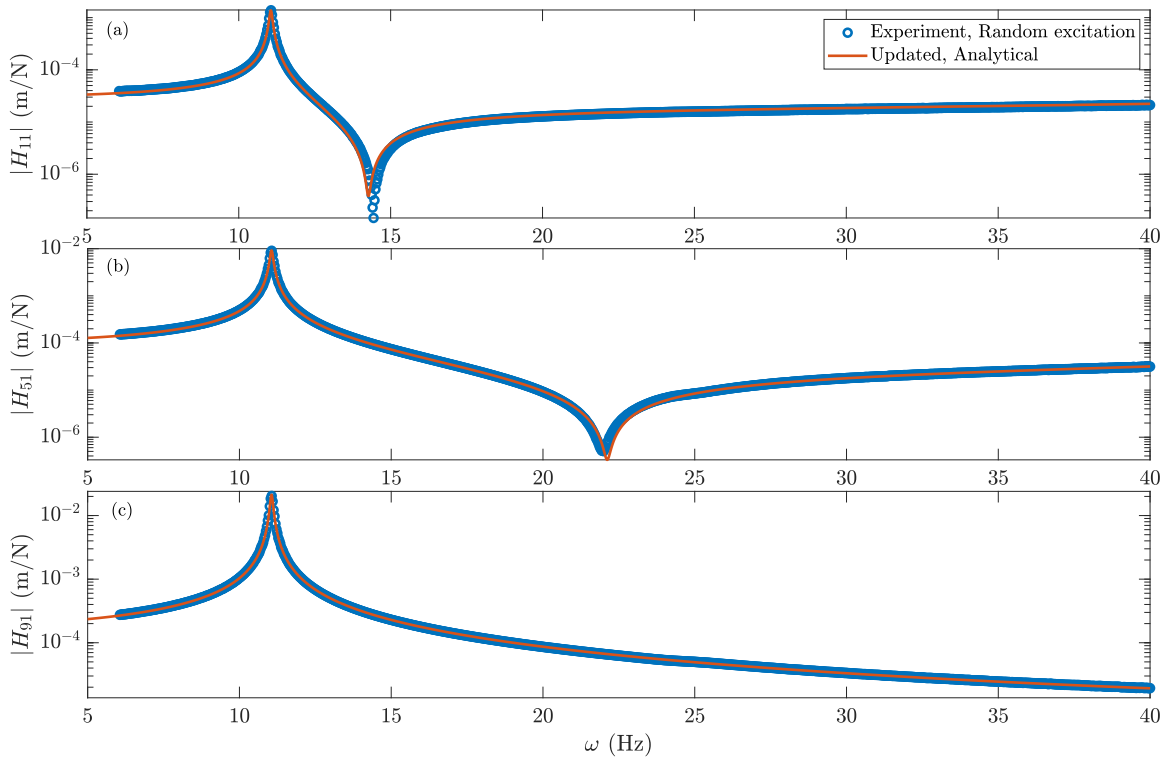

Figure 7.3: Frequency response function of the underlying linear system at three different locations. (a) DOF1, (b) DOF5, (c) DOF9.

The identified models of the nonlinear electromagnetic force are given in Table 7.4. w_{11} in the defined models of Table 7.4 denotes the transverse displacement of DOF11 at the beam tip. Optimized parameters of the various models of nonlinear force are used to regenerate the experimentally measured response of the system. First, a very small fraction (e.g. $\frac{1}{10}$) of the measured time-domain force signal

Table 7.4: Identified Models of the nonlinear electromagnetic force of the system of Figure 7.1.

Nonlinear Functions $g_p(w, \dot{w})$	w_{11}	w_{11}^2	w_{11}^3	w_{11}^5	$\dot{w}_{11}$
Parameters	$k_{l_1}\left(\frac{\mathrm{N}}{\mathrm{m}}\right)$	$k_{n_2}\left(\frac{\mathrm{N}}{\mathrm{m}^2}\right)$	$k_{n_3}\left(\frac{\mathrm{kN}}{\mathrm{m}^3}\right)$	$k_{n_5}\left(\frac{\mathrm{MN}}{\mathrm{m}^5}\right)$	$c_{l_1}\left(\frac{\mathrm{mN.s}}{\mathrm{m}}\right)$
Model 1	-	-	-174.122	-	-
Model 2	-3.21933	-	-41.7534	-	-
Model 3	-2.19748	-	-63.1847	-	2.164
Model 4	-3.05142	-	-51.7534	-3.68403	2.783
Model 5	-2.71924	-90.2361	-59.1892	-8.51754	2.891

obtained from the stepped-sine vibration test of the cantilever beam is applied to the identified nonlinear model of the system. Then the measured force signal is used to estimate the nonlinear response of the system using various forms of identified nonlinear force given in Table 7.4.

Figure 7.4 gives the comparison between the experimentally measured, updated analytical and the numerically simulated FRF of the system. It demonstrates a good prediction of the linear FRF of the using identified nonlinear model excited by a very low amplitude excitation force. The nonlinear responses obtained using various identified models are compared with the measured response in Figure 7.5. As shown, models 3, 4 and 5 give better predictions of the nonlinear response. However, there is still some inaccuracy in the estimated response compared with the measured one. This amount of error can arise from different sources such as the expansion methods used to estimate the unmeasured degrees of freedom. As explained, the quadratic stiffness is added in Model 5 to consider the asymmetry of the nonlinear electromagnetic force. However, it is expected that the quadratic nonlinearity has a low effect in the steady state response of the system. Apparently, this does not make a significant change in the primary harmonic of the response. But looking at the comparison between the second and third harmonics of the response given in Figure 7.6 demonstrates that adding the quadratic term will guarantee the prediction of second harmonic of the response. Although adding the quadratic term makes Model 5 able to predict the second harmonic of the response, Model 4 works better than Model 5 in predicting the response in some cases. The reason is that the quadratic term in Model 5, which is added to predict the second harmonic, causes the performance of Model 5 to be reduced in some cases.

7.3 Second Experimental Case Study

In this section, the AFTHB method is applied to an experimental case study and the results are presented. To this end, the experimental test data provided by Shaw et al. [161] is used to identify the structure. Figure 7.7 shows the test rig for this experimental study. The structure is a stainless-steel cantilever beam that is connected to a grounded nonlinear stiffness attachment at the tip of the beam. Figure 7.7(a) illustrates the geometry of the cantilever, while the schematic of the grounded nonlinear

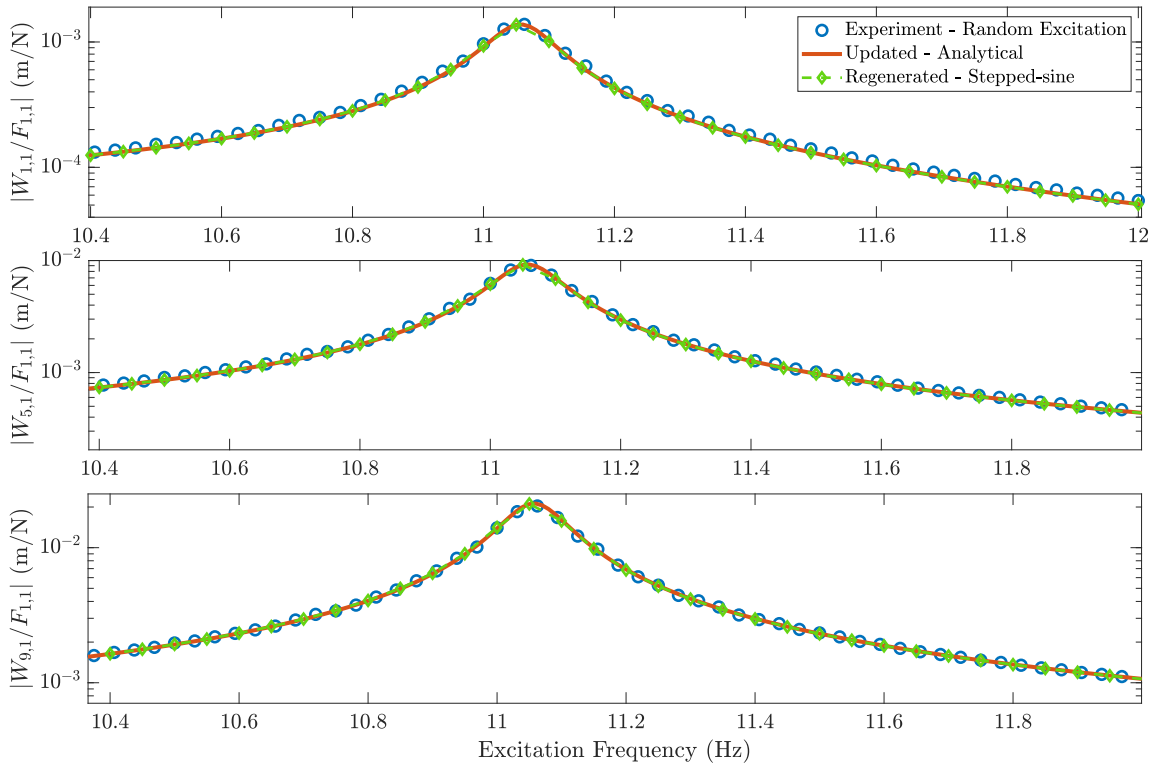

Figure 7.4: Comparison between the experimentally measured, updated, and numerically regenerated linear frequency response function of the beam at three locations along the beam. (a) DOF1, (b) DOF5, (c) DOF9.

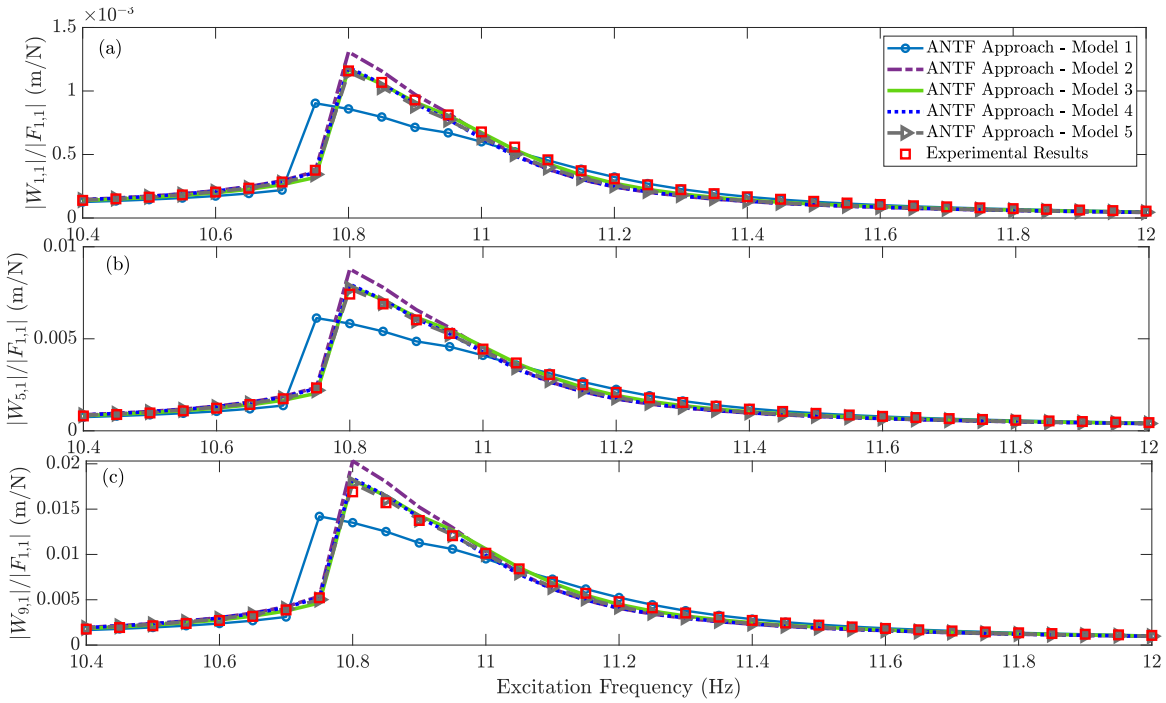

Figure 7.5: Comparison between the experimentally measured and numerically regenerated nonlinear response of the system at three locations along the beam. (a) DOF1, (b) DOF5, (c) DOF9.

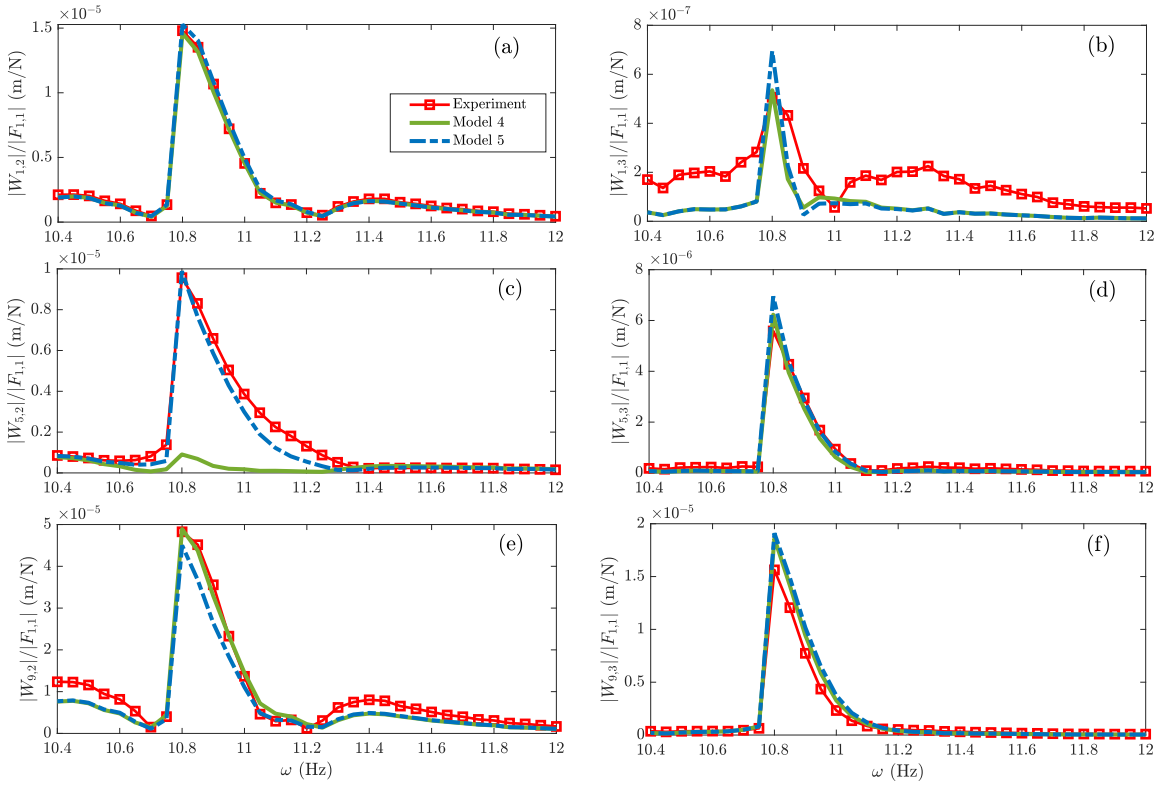

Figure 7.6: Second and third harmonics of the nonlinear response of the system obtained using Models 4 and 5 compared with the experimental results.

stiffness attachment and the test rig are shown respectively in Figures 7.7(b) and 7.7(c). A Data Physics GW-V4 electrodynamic shaker is attached to the beam at x_1 to excite the structure through a 1 mm wire stinger. The applied force is measured using a PCB 208 C03 force transducer, while three PCB 352 C03 piezoelectric accelerometers are attached to the beam to measure the response at x_1, x_2, and x_3 along the beam. Figures 7.7(d) and 7.7(e) show the configuration of the grounded nonlinear stiffness and the experimental test rig, respectively.

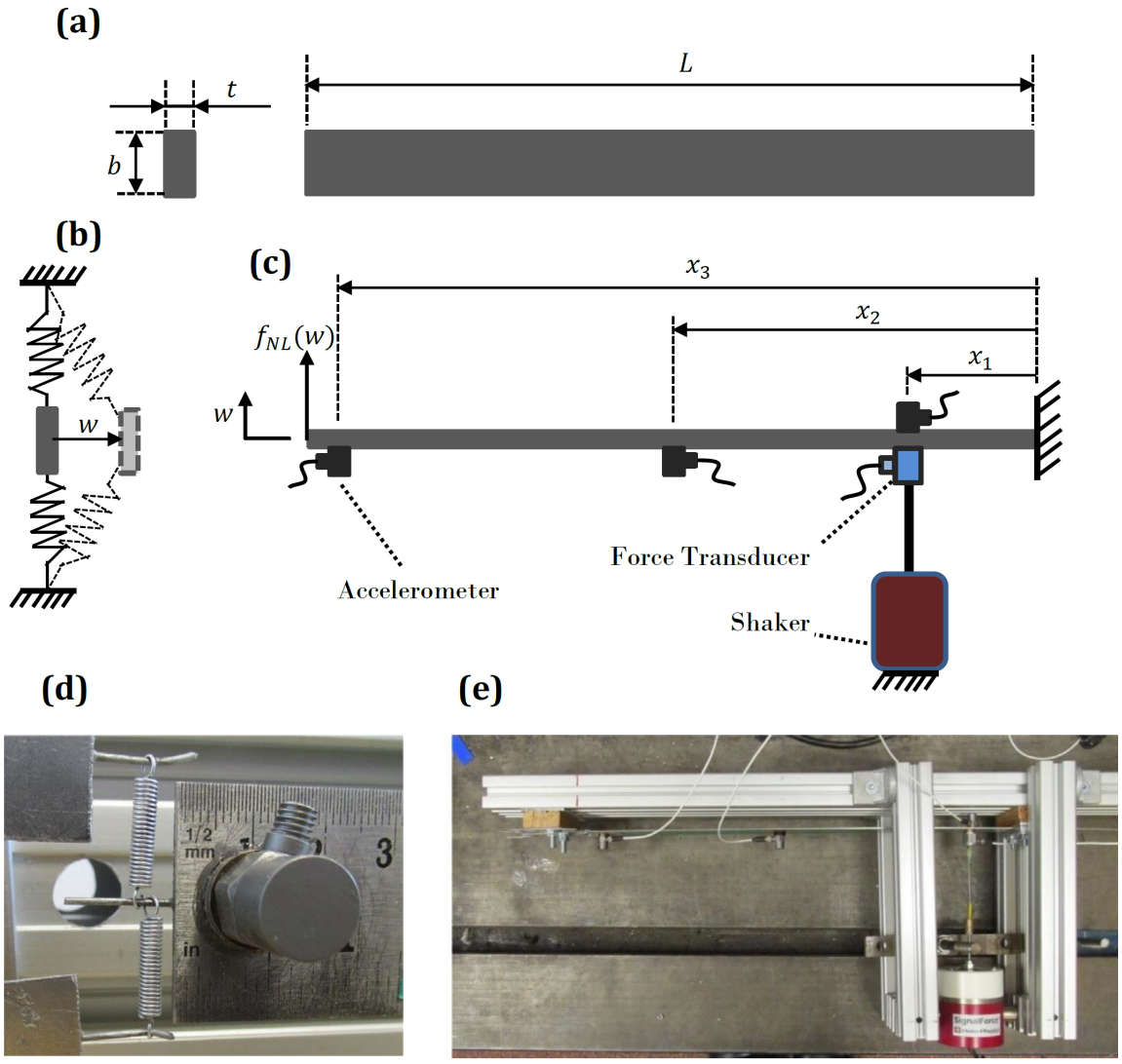

Figure 7.7: (a) Dimensions of the beam; (b) Schematic of the grounded nonlinear stiffness; (c) Schematic of the test rig; (d) and (e) photo of the configuration of nonlinear stiffness and the experimental test rig.

In order to model the structure, the nonlinear restoring force that is applied to the tip of the beam has to be modelled. According to the geometrical configuration of the nonlinear spring setup, the

nonlinear force applied to the tip of the beam can be ideally obtained as

$$f_{nl}\big|_{x=L} = 2kw_L\left(1 - \frac{l_0}{\sqrt{w_L^2 + d^2}}\right), \tag{7.4}$$

where $w_L = w(L,t)$ represent the deflection of the tip of the beam, k denotes the linear stiffness of the springs, l_0 is the free length of the springs, and $2d$ denote the distance between the fixed ends of the two springs. However, due to the asymmetry of the spring configuration, Eq. (7.4) may not accurately generate the exact nonlinear force, although the cubic nonlinearity is the most important term in the Taylor extension of the force. Therefore, the unknown nonlinear force of the grounded nonlinear stiffness is assumed to be of the form

$$f_{nl}\big|_{x=L} = k_l w_L + k_n w_L^3, \tag{7.5}$$

The stinger attached to the beam at x_1 is modelled as a spring with linear stiffness of k_s, and the effect of all point masses (three accelerometers and the force transducer) is considered in the model of the system. Considering the nonlinear force of Eq. (7.5), and assuming proportional damping for the beam, the equation of motion of the system is derived using Euler-Bernoulli beam theory. Thus

$$\begin{aligned}\rho A\left(\frac{\partial^2 w}{\partial t^2}\right) + \sum_{p=1}^{3}\left[m_p\left(\frac{\partial^2 w}{\partial t^2}\right)\delta(x-x_p)\right] + \alpha\left(\frac{\partial w}{\partial t}\right) + \beta\left(\frac{\partial^5 w}{\partial x^4 \partial t}\right) \\ + EI\left(\frac{\partial^4 w}{\partial x^4}\right) + k_s w\delta(x-x_1) + (k_l w + k_n w^3)\delta(x-L) \\ = F\sin(\omega t)\delta(x-x_1),\end{aligned} \tag{7.6}$$

where δ denotes the Dirac delta function, m_1 is the total mass of the force transducer and the accelerometer located at x_1, and m_2, m_3 are the masses of the two other accelerometers respectively located at x_2 and x_3. ρ and E denote the density and elastic modulus of the beam, A and I are the area and the second moment of area of the beam cross section, α, β denote the coefficients of the proportional damping, and F and ω are the amplitude and frequency of the excitation force. Measured natural frequencies are used to update the underlying linear system. The fixed geometrical dimensions and material properties of the structure are given in Table 7.5. Through linear model updating, parameters including point masses m_p of the force transducer and the accelerometers, the linear stiffness k_s of the stinger, and the linear stiffness k_l of the nonlinear grounded spring are updated. The force transducer has a mass of 26 g and the three accelerometers have equal masses of 8 g. However, considering the cabling of all these sensors, the point masses m_p need to be updated. The remaining unknowns are the proportional damping coefficients α, β and the coefficient k_n of the cubic stiffness, and these parameters are identified

utilizing the AFTHB approach. Accordingly, assuming the response as

$$w(x,t) = \sum_{i=1}^{N_m} \varphi_i(x) q_i(t), \tag{7.7}$$

and applying the Galerkin method, the modal equation of motion of the system is obtained in matrix form as

$$\mathbf{M}\ddot{\mathbf{q}} + \mathbf{M}\mathbf{q} + \mathbf{f}_{NL}(\mathbf{q}, \dot{\mathbf{q}}) = \mathbf{f}_{ex}, \tag{7.8}$$

where the elements of the mass and stiffness matrices and the forces are given by

$$\begin{aligned}
M_{ij} =& \rho A \int_0^L \varphi_i \varphi_j dx + \sum_{p=1}^{3} \left[m_p \varphi_i(x_p) \sum_{j=1}^{N-m} \left[\varphi_j(x_p) \right] \right], \quad i,j = 1, \cdots, N_m \\
K_{ij} =& EI \int_0^L \varphi_i \varphi_j^{IV} dx + k_s \varphi_i(x_1) \varphi_j(x_1) + k_l \varphi_i(L) \varphi_j(L), \quad i,j = 1, \cdots, N_m \\
f_{NL_i}(\mathbf{q}, \dot{\mathbf{q}}) =& \alpha \sum_{j=1}^{N_m} \left[\dot{q}_j \int_0^L \varphi_i \varphi_j dx \right] + \beta \sum_{j=1}^{N_m} \left[\dot{q}_j \int_0^L \varphi_i \varphi_j^{IV} dx \right] + \\
& + k_n \varphi_i(L) \left(\sum_{j=1}^{N_m} q_j \varphi_j(L) \right)^3, \quad i = 1, \cdots, N_m, \\
f_i =& \varphi_i(L) F \sin(\omega t), \quad i,j = 1, \cdots, N_m,
\end{aligned} \tag{7.9}$$

and N_m is the total number of modes considered in the mathematical model. The functions $g_{1,i}$, $g_{2,i}$, and $g_{3,i}$ of the unknown internal force are defined as

$$\begin{aligned}
g_{1,i} =& \sum_{j=1}^{N-m} \left[\dot{q}_j \int_0^L \varphi_i \varphi_j dx \right] g_{2,i} = \sum_{j=1}^{N_m} \left[\dot{q}_j \int_0^L \varphi_i \varphi_j^{IV} dx \right] + \\
g_{3,i} =& \varphi_i(L) \left(\sum_{j=1}^{N_m} q_j \varphi_j(L) \right)^3, \quad i = 1, \cdots, N_m,
\end{aligned} \tag{7.10}$$

Separating the unknown parameters α, β, and k_n from the functions $g_{1,i}$, $g_{2,i}$, and $g_{3,i}$, and rewriting the unknown force f_{NL} in matrix form, Eq. (7.9) is rewritten as

$$\begin{bmatrix} g_{1,1} & g_{2,1} & g_{3,1} \\ \vdots & \vdots & \vdots \\ g_{1,N_m} & g_{2,N_m} & g_{3,N_m} \end{bmatrix} \begin{Bmatrix} \alpha \\ \beta \\ k_n \end{Bmatrix} = \left\{ \mathbf{f}_{ex} - \mathbf{M}\ddot{\mathbf{q}} - \mathbf{M}\mathbf{q} \right\}, \tag{7.11}$$

Table 7.6 shows the updated parameters of the underlying linear system of the cantilever beam and gives the comparison between the experimental and updated natural frequencies. The updated values of

Table 7.5: Geometry and material properties of the experimental setup.

Parameters (Units)	Values
Length of cantilever beam, L (m)	0.38
Width of cantilever beam, b (m)	0.03
Thickness of cantilever beam, t (m)	0.001
Density of cantilever beam, $\rho\left(\frac{\text{kg}}{\text{m}^3}\right)$	7850
Modulus of elasticity of cantilever beam, E (GPa)	210
x_1 (m)	0.04
x_2 (m)	0.15
x_3 (m)	0.37

Table 7.6: Results of the linear model updating.

Parameters (Units)	Natural Frequencies $\left(\frac{\text{rad}}{\text{s}}\right)$			m_1 (g)	m_2 (g)	m_3 (g)	k_s $\left(\frac{\text{kN}}{\text{m}}\right)$	k_l $\left(\frac{\text{N}}{\text{m}}\right)$
	ω_{n_1}	ω_{n_2}	ω_{n_3}					
Experimental Values	55.92	199.18	551.04	-	-	-	-	-
Updated Values	56.34	197.53	552.53	39.4	9.3	11.6	14.9	75.68

the parameters given in Table 7.6, along with the nonlinear experimental results, is used in the AFTHB approach to identify the unknown parameters α, β, and k_n.

The experimental steady state dynamics of the structure was measured in sweep-sine tests in the vicinity of the first natural frequency. Figure 7.8 illustrates the controlled force signal applied to the structure and the displacement of the structure at three locations along the beam measured from the backward sweep-sine vibration test within the frequency range of 9 to 12 Hz with an excitation level of 4 N. The sweep-sine test was carried out using 151 frequency points (df=0.02 Hz). The response at each frequency was measured after the structure had settled to its steady state. The signals shown in Figure 7.8 were created using three cycles of the force and displacement signals from the steady state response at each frequency.

Sweep-sine tests were carried out for five different levels of excitation (1.6,2.4,3.2,3.6,4.0 N) to measure the nonlinear response of the system. Figure 7.9 shows the amplitude-frequency diagram of the first and third harmonics of the force signal and the displacement of the beam at the three measured locations. Both forward and backward sweep-sine tests were carried out to obtain jumps and drops in the nonlinear response of the system. The experimental results of Figure 7.9 show the significant contribution of the third harmonic, as well as the primary harmonic, in the dynamic behaviour of the system. Figure 7.10 shows the time history of the force signal and multi-harmonic steady state response of the beam at measurement locations x_1, x_2, and x_3 along the beam in response to the excitation force of level 1.6 N at the excitation frequency 10.6 Hz. Two stable solutions of the system with different amplitudes were

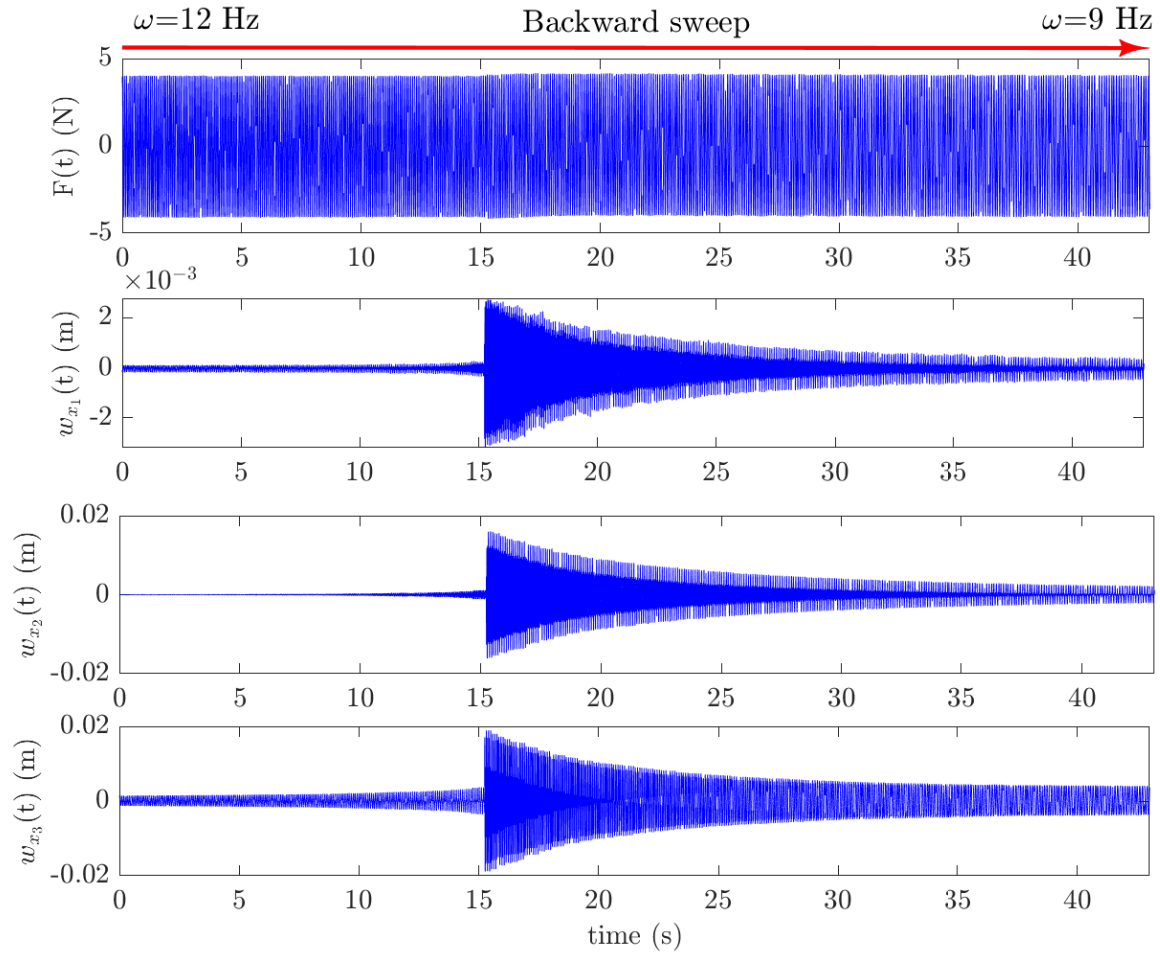

Figure 7.8: Time history of the force signal and displacement of the beam at x_1, x_2 and x_3 in response to the backward sweep-sine vibration test with force amplitude of 4 N.

measured in response to the same force level using forward (upper branch solution) and backward (lower branch solution) sweep-sine vibration tests.

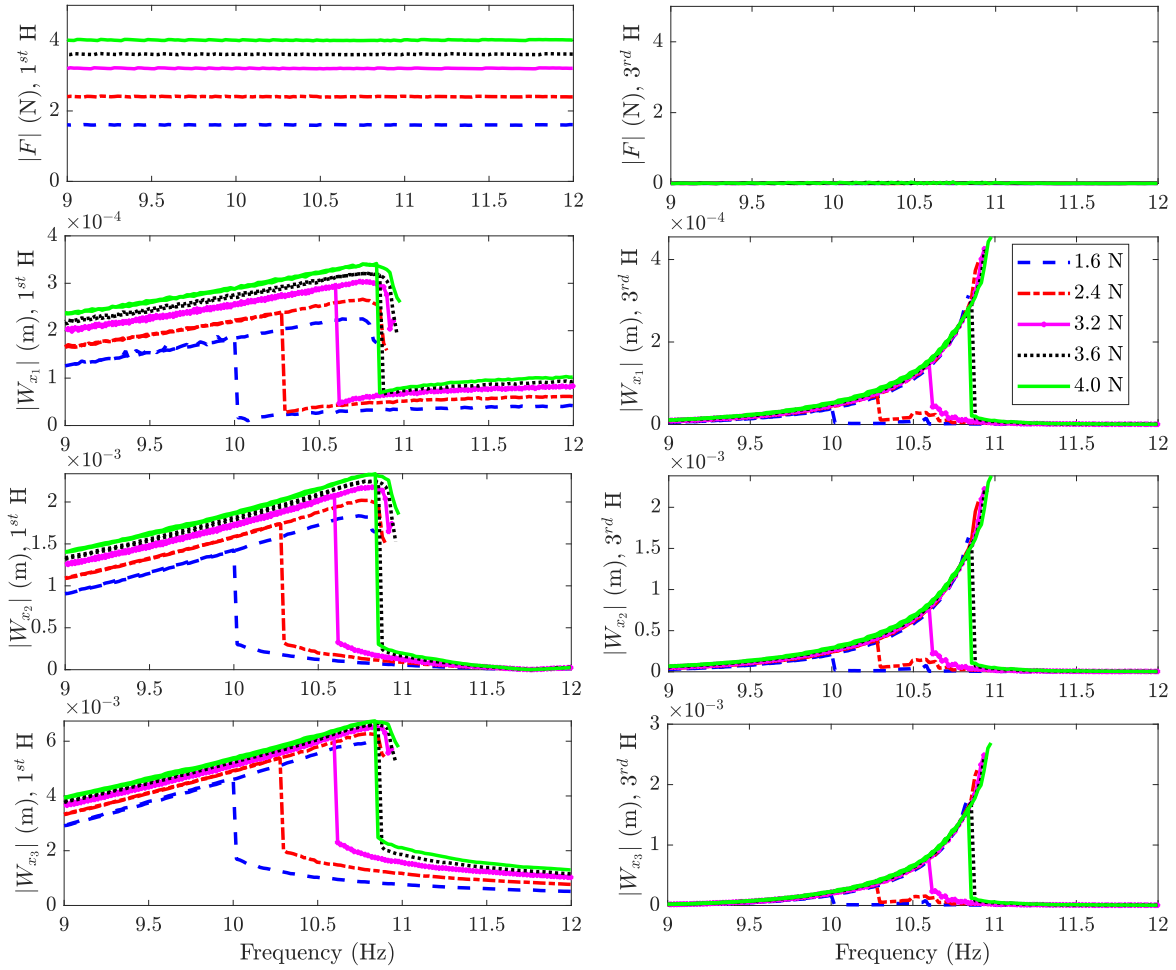

Figure 7.9: First and third harmonics of the force signal and the displacement of the beam in response to the sweep-sine vibrations tests with five different excitation levels.

The experimental data were used to identify the unknown nonlinear force of Eq. (7.11). The identification process results in the identified values of the parameters of nonlinear force of Eq. (7.9) as

$$\alpha = 0.075 \ \frac{\text{N.s}}{\text{m}^2}, \quad \beta = 8.45 \times 10^{-5} \ \text{N.s.m}^2, \quad k_n = 2.152 \times 10^6 \ \frac{\text{N}}{\text{m}^3}, \tag{7.12}$$

The identified nonlinear model of the structure is used to regenerate the experimental response of the beam. Figure 7.11 compares the experimental and the simulated response of the system for an excitation level of 4 N in the neighbourhood of the first natural frequency. The isolated response of the system is measured for three different excitation levels through controlled forward and backward sweep-sine vibration tests. To this end, a sudden excitation force with high enough level was applied to the structure

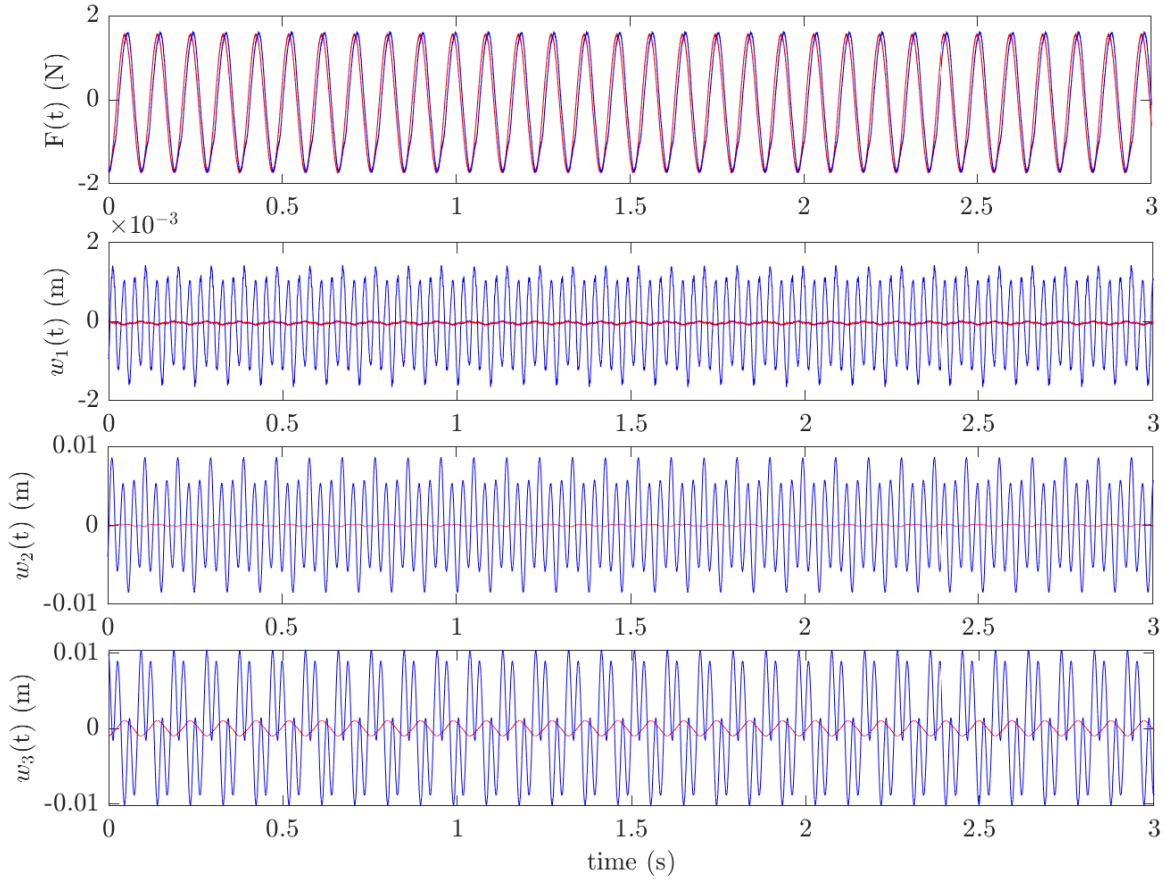

Figure 7.10: Time history of the force signal and the steady state displacements of the beam in response to the excitation force level of 1.6N at frequency 10.6 Hz. Blue and red colours respectively show the response at upper and lower stable branches.

at ω=13 Hz and the force was controlled at the desired level until the system settled to its steady state response. Forward and backward sweep-sine tests were carried out within frequency ranges of 13 to 16 Hz and 13 to 10 Hz, respectively. Detailed explanations of the experiments are given in [161]. Figure 7.12 illustrates the amplitude and phase of the first and third harmonics of the displacement of the beam at x_3 in response to the forward and backward sweep-sine vibration tests with three different excitation levels, capturing the isolated nonlinear response of the system.

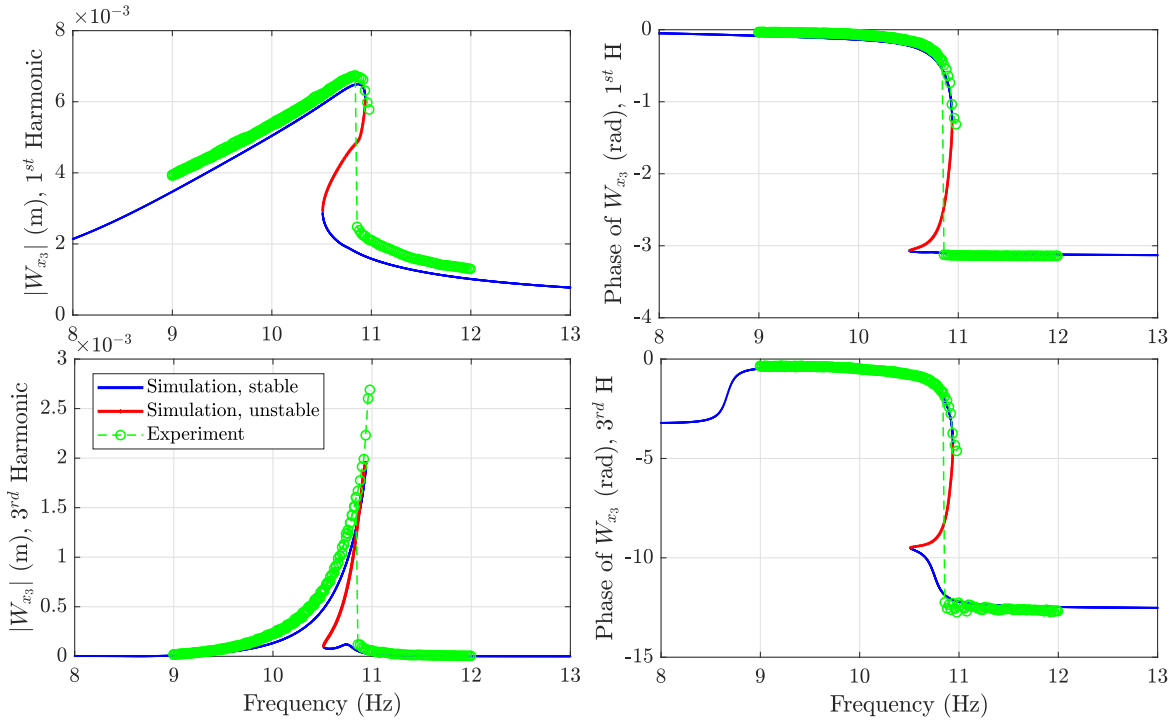

Figure 7.11: Comparison between the first and third harmonics of the experimental and simulated response obtained for excitation level of 4 N.

The identified nonlinear model of the experimental test rig is utilized to regenerate the nonlinear response of the beam under an excitation level of 1.6 N. The simulation was carried out to predict the isolated response of the structure. Figure 7.13 gives a comparison between the amplitude and phase of the experimental and simulated nonlinear response of the cantilever beam of the test rig under the excitation level of 1.6 N. An important factor for an accurate identified model of a nonlinear structure is that the model is valid for different working conditions and various excitation levels. This shows how reliable the identified model is to predict the response of the system under study. The results given in Figure 7.13 shows that the identified model of the structure is able to predict the response at a different level of excitation (1.6 N) than the excitation level at which the model is identified (4 N). The results show that the identified nonlinear model of the structure is capable of regenerating not only the primary harmonic of the experimental response, but also it can predict the third harmonics of the vibration.

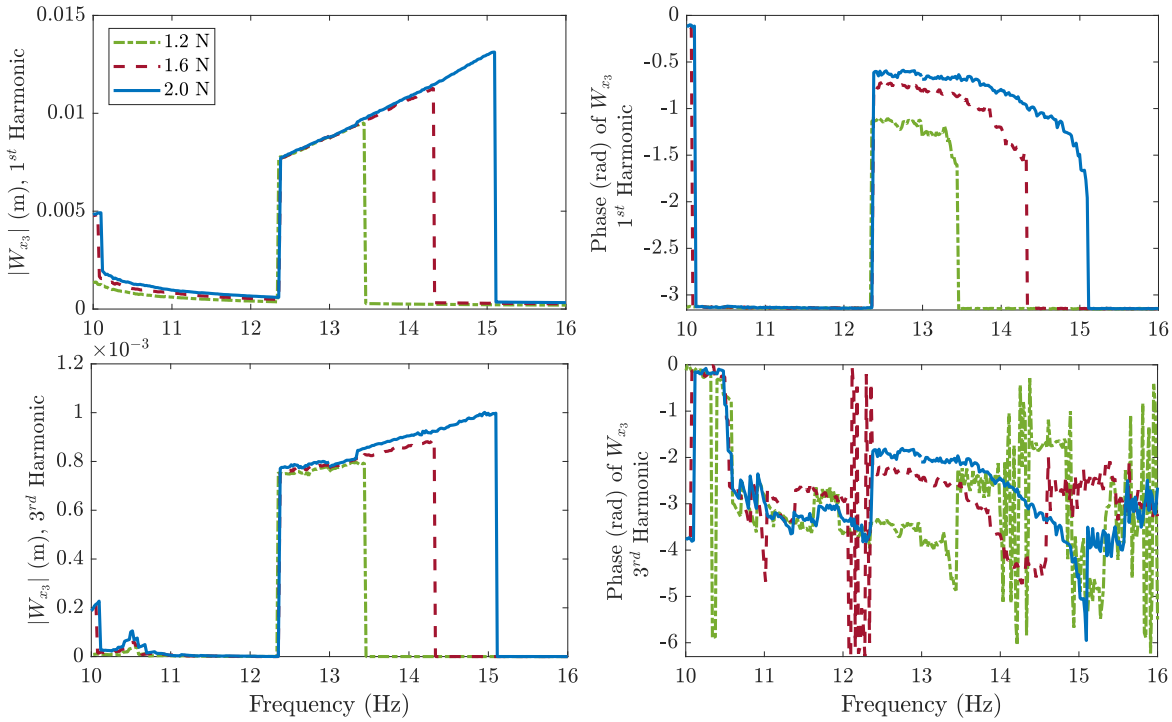

Figure 7.12: Amplitude and phase of the first and third harmonics of the displacement of the beam at x_3 in response to the sweep-sine vibrations tests with three different excitation levels, capturing the isolated nonlinear response of the system.

Furthermore, the identified model is able to regenerate the isolated response, as well as the non-isolated response, for both primary and third harmonics, with good accuracy. According to these results, it is expected that the identified model is robust enough against changes in the working condition of the structure such as the excitation level.

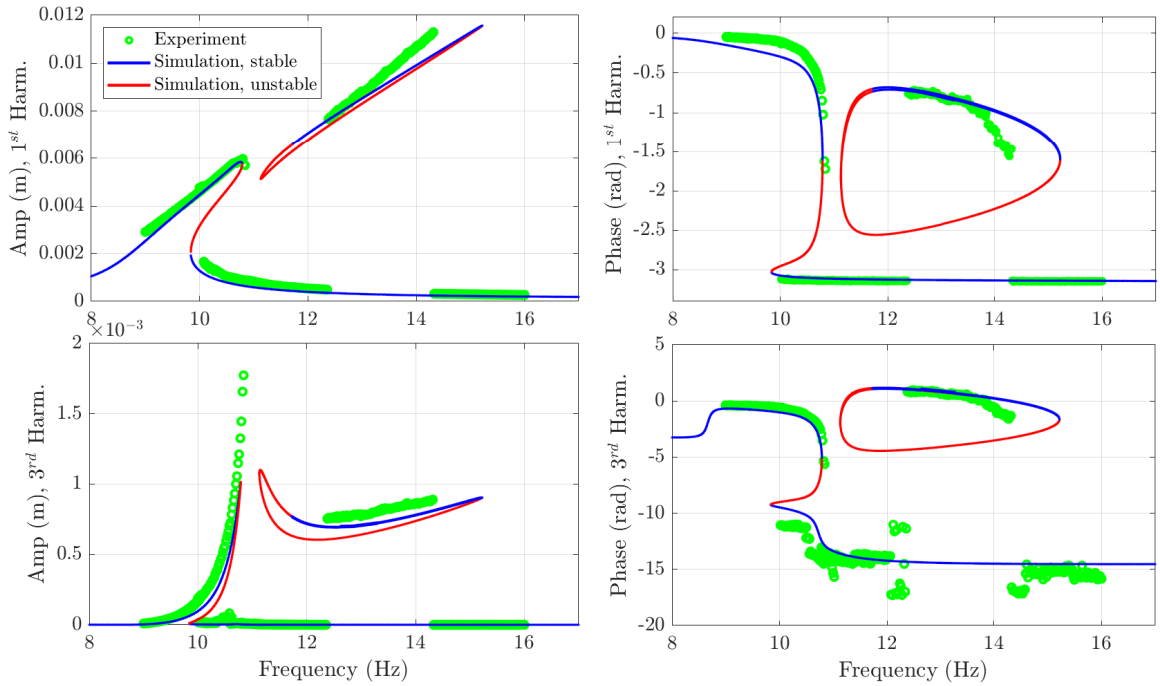

Figure 7.13: Comparison between the first and third harmonics of the experimental and simulated response obtained for excitation level of 1.6 N.

7.4 Closure

In this chapter, the applicability of the AFTHB identification approach presented in Chapter 6 has been investigated via experimental studies. To this end, the AFTHB approach was applied to two experimental cases: a stainless-steel cantilever beam with nonlinear electromagnetic restoring forces applied to the tip of the beam, and a stainless-steel cantilever beam with a grounded cubic nonlinear force on the tip. In the first case, the measured force signal is multi-harmonic, while the measured response is single harmonic. Indeed, the amplitude of the higher harmonics of the response are insignificant with respect to its primary harmonic. In the second case, in contrast, the force applied to the structure is controlled to be single-harmonic. However, the response of the structure in this case is a multi-harmonic response. The multi-harmonic response of this structure is due to the internal resonance of the system. This chapter has investigated the performance of the proposed AFTHB approach in identifying nonlinear structures in the presence of multi-harmonics either in the response or in the measured force signals.

Therefore, the AFTHB approach was applied to both cases to identify the unknown nonlinear parameters of the systems. The nonlinear responses of two experimental cases were estimated using the identified nonlinear models and compared with the experimentally measured nonlinear responses. The results show good performance of the proposed method.

Chapter 8

Conclusions and Future Work

8.1 Conclusions

This chapter concludes and highlights a summary of the main findings of this study given in previous chapters.

This study was focused on nonlinear model updating in structural dynamics. In the first chapter of the thesis, some required background was given. Then, a literature review was carried out in Chapter 2 on model identification in structural dynamics. Through the literature review, it was noticed that there is a gap within the literature associated with the examination of the effect of various sources of inaccuracy on the results of identification. Therefore, the first objective of this study was to investigate the sensitivity of identification methods to various sources of inaccuracy and developing an optimization-based method to deal with this problem. The complexity and relatively high computational cost of model selection approaches is another drawback that affect non-parametric methods. In addition, using a pool of candidate basis functions may lead to ignore some possible nonlinear functions out of the candidate pool or give a physically meaningless model for the structure. To deal with problem, an optimization-based framework is developed with a model-selection procedure benefiting from experienced engineering insight. Using a set of basis nonlinear functions as candidates for the model of the nonlinear force may be used when no experienced engineering insight is available. However, this may increase the computational costs expected. In addition, many of identification methods suffer from at least one of the following drawbacks: high computational costs, complexity of application, low accuracy, being unable to deal with complex nonlinearities, or other limitations such as the implicit regularization bias or neglecting higher harmonics. Hence, the other objective of this study was to introduce an identification method that can merge the simplicity of application with low computational cost and significantly high accuracy to deal

with a wide range of complex nonlinear functions considering the effect of higher harmonics. To this end, the AFTHB method was developed.

Localization of nonlinear elements is one of the early stages of identification processes in nonlinear structural dynamics. On the other hand, using point-force vibration tests via stingers adds some extra properties to the structure and make it more difficult to detect the location of nonlinear elements. Accordingly, the first step of this study in Chapter 3 was focused on the detection of localized structural nonlinearities utilizing the results obtained from base excitation experiments. A localization method was modified and applied to two nonlinear systems in order to localize their nonlinear elements: an experimental case study composed of a cantilever beam subjected to an electromagnetic nonlinear force applied to the tip, and a numerical case of a nonlinear restoring force acting at the tip of a cantilever beam. The results of the localization demonstrate the capability of the method utilized to detect the location of nonlinear elements in both the numerical and experimental cases.

The effect of various types of measurement noise and modelling error on the outcome of the identification methods was examined in Chapter 4 of this thesis. To this end, the Equivalent Dynamic Stiffness Mapping (EDSM) technique was considered as an identification method that works accurately in the absence of any measurement noise or modelling error. The EDSM technique also assumes that the response of the system under study is dominated by the primary harmonic. The effect of four different sources of inaccuracy were examined on the accuracy of the EDSM technique, among them were the noise in the measured data, modelling error, the error from the reduction/expansion methods, and the error that resulted by ignoring the higher harmonics. According to the results, noise-polluted experimental data affects the accuracy and reliability of the identified model by increasing the uncertainty of the measured response. The results show that exploiting the conventional linear reduction/expansion methods such as SEREP gave erroneous results in the process of nonlinear identifications. It was demonstrated that modelling error (e.g. inaccurate pre-known parameters such as density or modulus of elasticity, or assuming wrong nonlinear model) may lead to an inaccurate nonlinear model. It was also illustrated that neglecting the effect of higher harmonics may be one of the reasons for inaccurate identification in the case of nonlinear systems with multi-frequency response or force signals.

In Chapter 5, an optimization-based framework was developed for identification of nonlinear structures. The objective was to eliminate the effect of different factors of inaccuracy discussed in Chapter 4. In the presented framework, a Taylor series expansion was used to describe the nonlinear element/force. Different candidate models were chosen to take various possible models into account. The unknown parameters of the candidate models were estimated utilizing an optimization-based method. The objective function of this optimization is the difference between the predicted nonlinear response and the experimental response. By comparing the predicted responses from the identified models with the experimental results, the most appropriate model can be chosen from the candidates. The proposed

framework was applied to an experimental test case composed of a steel cantilever beam with a nonlinear electromagnetic force applied to the tip. The cantilever beam was modelled using Euler-Bernoulli beam theory. A mass-spring model was used to model the effect of the clamp support of the beam. It was found that the linear model of the support is needed to predict the anti-resonances of the linear experimental responses. Four candidate models (using Taylor series expansion) were assumed for the nonlinear electromagnetic force. Different orders of nonlinearity in the stiffness and damping terms were considered in the assumed models. The proposed optimization-based method was applied to the candidate models in order to identify the unknown parameters exploiting the measured nonlinear responses. The best nonlinear model providing excellent agreement between the predicted responses and the corresponding measured responses was selected.

Chapter 6 developed a harmonic-balance-based identification method for identifying nonlinear systems with multi-harmonic response and force signals. The proposed method exploits the response of the structure measured from a multi-input/multi-output vibration test in both the time and frequency domains. The introduced method utilizes two different approaches: the Analytical Frequency Domain (AHB) approach and the Alternative Numerical Time-Frequency (AFTHB) approach. The AHB approach exploits the expanded nonlinear functions in the frequency domain. To this end, various analytical methods such as the Complex Averaging (CXA) technique, Fourier Integral (FI), or the Harmonic Balance Method (HBM) can be used. In the AFTHB approach, the expanded nonlinear functions in the frequency domain are obtained via the Fourier Transform of the measured time response. The high accuracy of the AHB approach is shown to require the inclusion of all significant harmonics in the analytical expansion of the nonlinear functions. However, in practice, it is very complicated to take all significant harmonics into account in the analytical expansions. In addition, the difficulty of applying the AHB approach to structures with complex forms of nonlinearities such as Coulomb friction and also to multi-degree of freedom nonlinear systems may be considered as another drawback of this approach. The AFTHB approach, on the other hand, can be applied to all forms of nonlinear function. It also includes almost all significant harmonics of the response. Prior-knowledge or appropriate assumption of the nonlinear models are required in the proposed method. Therefore, great engineering insight is necessary to make proper estimation of the type of nonlinear elements. Four simulated case studies with single and multi-degrees of freedom were considered. The proposed method was applied to identify these nonlinear systems with different types of smooth/non-smooth nonlinear elements including cubic stiffness, Coulomb friction, and quadratic damping. It is shown that the method with both approaches is able to accurately identify nonlinear structures if all significant harmonics of the response are considered. The results of the AHB approach also show that neglecting the higher harmonics leads to inaccurate identification of the nonlinear system, especially when the higher harmonics have significant contribution in the excitation and responses.

To investigate the applicability of the AFTHB approach in practical cases, it was applied to two experimental test cases: a stainless-steel cantilever beam with nonlinear electromagnetic restoring forces applied to the tip of the beam, and a stainless-steel cantilever beam with grounded linear springs attached to the tip which cause geometric cubic nonlinearity as they deform. The results of this study are given in Chapter 7 of the thesis. For the case of the cantilever beam, the measured force signal includes considerable contributions of the higher harmonics, particularly the second harmonic, in the vicinity of the resonance. However, these higher harmonics in the force signal did not generate significant amplitudes of higher harmonics in the response of the system. On the other hand, the cantilever beam with grounded cubic nonlinear force was subjected to a controlled force so that the higher harmonics did not contribute significantly to the force signal. However, the higher harmonics of the response of the structure were excited due to the internal resonance of the system. The AFTHB approach was applied to both cases to identify the unknown nonlinear parameters of the systems. The nonlinear responses of two experimental cases were estimated using the identified nonlinear models and compared with the experimentally measured nonlinear responses. The results show good performance of the proposed method.

The main findings of the present thesis can be listed as below:

- It has been demonstrated that there are various sources of inaccuracy such as noisy data, modelling error, expansion/reduction error, and neglecting higher harmonics that may result in significant errors in the model of the identified nonlinear system.
- The proposed optimization-based framework can be used to eliminate or reduce the effect of different sources of inaccuracy.
- The AHB and AFTHB approaches were introduced to tackle the multi-harmonic response and force signals in nonlinear structure identification.
- Despite its high accuracy in the presence all significant harmonics, the AHB was shown to be very cumbersome to use, particularly in structures with complex nonlinearities.
- The accuracy and applicability of the AFTHB approach was demonstrated in both numerical and experimental case studies with various number of DOFs and different types of nonlinearities.

8.2 Future Work

The topics discussed in this thesis introduce possible ideas for future research:

- Most of practical engineering structures include uncertainties or variabilities in their behaviours. Although stochastic excitation tends to linearize the response and so will make identification more

difficult, stochastic nonlinear model updating is used to consider and quantify the uncertainties in the model of such structures. On the other hand, the multi-harmonic signals of response and excitation will make identification even more complicated. Therefore, developing a stochastic nonlinear model identification exploiting multi-harmonic response and force signals can be considered as a promising possibility for research in nonlinear structure identification.

- Spatially incomplete measurement is a problem that may occur due to either lack of enough equipment or difficulty in accessing some parts of the structure under study. On the other hand, as shown by the results in Chapter 4 of the present study, utilizing linear reduction/expansion methods to estimate the unmeasured coordinates or make a reduced order model of a nonlinear model leads to erroneous results. Therefore, it is very important to develop a method to deal with this problem and remove the dependence of the accuracy of the identification process on complete measurements. Although the optimization-based framework introduced in Chapter 4 of this study deals with this problem, the computational costs may be relatively high, particularly for the case of systems with complicated nonlinear functions or high number of nonlinearity. Hence, developing a direct identification approach that deals with the problem of incomplete measurement with no required optimization process is still a challenge in structural dynamics.

- Many practical engineering structures such as rotor systems are subjected to multi-harmonic excitations. The proposed AFTHB method can be applied to various experimental and practical case studies in which higher harmonics play significant role. The AFTHB method can also be utilized for structural health monitoring of such structures.

- The AHB and AFTHB approaches presented in this study assume that the nonlinear functions are explicitly stated in terms of displacement or velocity so that the parameters of the nonlinear functions can be stated in a separate matrix. In case of other complicated nonlinear functions which do not have an explicit form or have a coefficient that cannot be factored, the presented method can be applied using expansion series or polynomial fitting curves. However, developing an identification method to identify and characterize implicit nonlinear functions would be a promising topic for future works.

- Identification of distributed structural nonlinearities rather than localized nonlinear elements are considered less in the literature. Considering the importance of the nonlinear behaviour of mechanical structures in modern engineering applications, this topic can be studied in the future.

- In this study, the interaction between the shaker and the structure under study was modelled using a simple linear model of the stinger. However, the shaker could behave with a nonlinear response and affect the response of the structure in more complicated nonlinear dynamics. Therefore, to

better understand the interaction between the shaker and mechanical structures, particularly in nonlinear systems, it is of interest to model the behaviour of the shaker with a more accurate model in which other parameters of the shaker such as the shaker coil movement are considered.

Appendix A

Analytical Expressions of Nonlinear Functions in the Frequency Domain

In this section, the frequency domain analytical term of a cubic nonlinear function is derived using modified complex averaging (MCXA) technique. To this end, it is assumed that the response of the system is harmonic as

$$\begin{aligned} u(t) =& U_0 + \sum_{n=1}^{N_H} u_n(t), \\ u_n =& \frac{1}{2j}\left(U_n e^{jH_n\omega t} - \bar{U}_n e^{-jH_n\omega t}\right), \end{aligned} \tag{A.1}$$

The nonlinear function is also assumed to be harmonic

$$\begin{aligned} g(u,\dot{u}) =& u^3 = V_0 + \sum_{n=1}^{N_H} v_n(t), \\ v_n(t) =& \frac{1}{2j}\left(V_n e^{jH_n\omega t} - \bar{V}_n e^{-jH_n\omega t}\right), \end{aligned} \tag{A.2}$$

Nonlinear Function with Three Harmonics

Considering three harmonics for the response of the dynamical system $N_H = 3$ (H_n=1,2,3), the response $u(t)$ is rewritten as

$$\begin{aligned} u(t) =& U_0 + \sum_{n=1}^{3} u_n(t) \\ =& U_0 + \frac{1}{2j}\left(U_1 e^{j\omega t} - \bar{U}_1 e^{-j\omega t} + U_2 e^{j2\omega t} - \bar{U}_2 e^{-j2\omega t} + U_3 e^{j3\omega t} - \bar{U}_3 e^{-j3\omega t}\right), \end{aligned} \tag{A.3}$$

Substituting $u(t)$ from Eq. A.3 into the nonlinear function of Eq. A.2, the nonlinear function $g(u,\dot{u})$ is obtained in terms of U_n as

$$\begin{aligned} g(u,\dot{u}) =& V_0 + \sum_{n=1}^{3} v_n(t) = u^3 \\ =& \left[U_0 + \frac{1}{2j}\left(U_1 e^{j\omega t} - \bar{U}_1 e^{-j\omega t} + U_2 e^{j2\omega t} - \bar{U}_2 e^{-j2\omega t} + U_3 e^{j3\omega t} - \bar{U}_3 e^{-j3\omega t}\right)\right]^3, \end{aligned} \tag{A.4}$$

Expanding two sides of Eq. A.4 gives

$$\begin{aligned} V_0 +& \frac{1}{2j}\left(V_1 e^{j\omega t} - \bar{V}_1 e^{-j\omega t} + V_2 e^{j2\omega t} - \bar{V}_2 e^{-j2\omega t} + V_3 e^{j3\omega t} - \bar{V}_3 e^{-j3\omega t}\right) \\ =& \frac{1}{8j}\left(3U_1^2\bar{U}_2 - 3U_2\bar{U}_1^2 + 8jU_0^3 + 6U_1U_2\bar{U}_3 - 6U_3\bar{U}_1\bar{U}_2 + 12jU_0U_1\bar{U}_1\right. \\ &\left. + 12jU_0U_2\bar{U}_2 + 12jU_0U_3\bar{U}_3\right) \\ &+ \frac{1}{2j}\left[\frac{1}{4}\left(3U_1^2\bar{U}_1 + 6U_1U_2\bar{U}_2 + 6U_1U_3\bar{U}_3 + 3\bar{U}_3U_2^2 - 3U_3\bar{U}_1^2\right.\right. \\ &\left.\left. + 12U_0^2U_1 + 12jU_0U_2\bar{U}_1 + 12jU_0U_3\bar{U}_2\right)\right] e^{j\omega t} \\ &+ \frac{1}{2j}\left[\frac{1}{4}\left(3U_2^2\bar{U}_2 + 6U_2U_1\bar{U}_1 + 6U_2U_3\bar{U}_3 + 6U_1U_3\bar{U}_2\right.\right. \\ &\left.\left. + 12U_0^2U_2 - 6jU_0U_1^2 + 12jU_0U_3\bar{U}_1\right)\right] e^{j2\omega t} \\ &+ \frac{1}{2j}\left[\frac{1}{4}\left(-U_1^3 + 6U_3U_1\bar{U}_1 + 6U_3U_2\bar{U}_2 + 3U_3^2\bar{U}_3 + 3\bar{U}_1U_2^2\right.\right. \\ &\left.\left. + 12U_0^2U_3 - 12jU_0U_1U_2\right)\right] e^{j3\omega t} + \cdots, \end{aligned} \tag{A.5}$$

Averaging over each harmonic and equalizing the coefficients of $e^{jn\omega t}$, amplitudes of V_n are derived. For example, the static response V_0 of the nonlinear function $g(u,\dot{u})$ and the amplitude of its first three harmonics, V_1, V_2, V_3, are calculated as

$$\begin{aligned} V_0 =& \frac{1}{8j}\left(3U_1^2\bar{U}_2 - 3U_2\bar{U}_1^2 + 8jU_0^3 + 6U_1U_2\bar{U}_3 - 6U_3\bar{U}_1\bar{U}_2\right. \\ &\left. + 12jU_0U_1\bar{U}_1 + 12jU_0U_2\bar{U}_2 + 12jU_0U_3\bar{U}_3\right) \\ V_1 =& \frac{1}{4}\left(3U_1^2\bar{U}_1 + 6U_1U_2\bar{U}_2 + 6U_1U_3\bar{U}_3 + 3\bar{U}_3U_2^2 - 3U_3\bar{U}_1^2\right. \\ &\left. + 12U_0^2U_1 + 12jU_0U_2\bar{U}_1 + 12jU_0U_3\bar{U}_2\right) \\ V_2 =& \frac{1}{4}\left(3U_2^2\bar{U}_2 + 6U_2U_1\bar{U}_1 + 6U_2U_3\bar{U}_3 + 6U_1U_3\bar{U}_2 + 12U_0^2U_2 - 6jU_0U_1^2 + 12jU_0U_3\bar{U}_1\right) \\ V_3 =& \frac{1}{4}\left(-U_1^3 + 6U_3U_1\bar{U}_1 + 6U_3U_2\bar{U}_2 + 3U_3^2\bar{U}_3 + 3\bar{U}_1U_2^2 + 12U_0^2U_3 - 12jU_0U_1U_2\right), \end{aligned} \tag{A.6}$$

Nonlinear Functions with Five Harmonics

Now five harmonics are included in the response $u(t)$ of the dynamical system and the nonlinear function $g(u,\bar{u})$, $N_H = 5$ ($H_n = 1,\ldots,5$). The response $u(t)$ is rewritten as

$$\begin{aligned} u(t) =& U_0 + \sum_{n=1}^{5} u_n(t) \\ =& U_0 + \frac{1}{2j}\Bigg[\Bigg(U_1 e^{j\omega t} - \bar{U}_1 e^{-j\omega t} + U_2 e^{j2\omega t} - \bar{U}_2 e^{-j2\omega t} + U_3 e^{j3\omega t} - \bar{U}_3 e^{-j3\omega t} \\ &+ U_4 e^{j4\omega t} - \bar{U}_4 e^{-j4\omega t} + U_5 e^{j5\omega t} - \bar{U}_5 e^{-j5\omega t}\Bigg)\Bigg], \end{aligned} \tag{A.7}$$

Substituting $u(t)$ of Eq. A.7 into the nonlinear function of Eq. A.2, the nonlinear function $g(u,\bar{u})$ is obtained in terms of U_n as

$$\begin{aligned} g(u,\dot{u}) =& V_0 + \sum_{n=1}^{5} v_n(t) = u^3 \\ =& \Bigg[U_0 + \frac{1}{2j}\Bigg(U_1 e^{j\omega t} - \bar{U}_1 e^{-j\omega t} + U_2 e^{j2\omega t} - \bar{U}_2 e^{-j2\omega t} + U_3 e^{j3\omega t} - \bar{U}_3 e^{-j3\omega t} \\ &+ U_4 e^{j4\omega t} - \bar{U}_4 e^{-j4\omega t} + U_5 e^{j5\omega t} - \bar{U}_5 e^{-j5\omega t}\Bigg)\Bigg]^3, \end{aligned} \tag{A.8}$$

Expanding two sides of Eq. A.8 gives

$$\begin{aligned} V_0 &+ \frac{1}{2j}\Bigg(V_1 e^{j\omega t} - \bar{V}_1 e^{-j\omega t} + V_2 e^{j2\omega t} - \bar{V}_2 e^{-j2\omega t} + V_3 e^{j3\omega t} \\ &- \bar{V}_3 e^{-j3\omega t} + V_4 e^{j4\omega t} - \bar{V}_4 e^{-j4\omega t} + V_5 e^{j5\omega t} - \bar{V}_5 e^{-j5\omega t}\Bigg) \\ =& \frac{1}{8j}\Bigg(3U_1^2\bar{U}_2 - 3U_2\bar{U}_1^2 + 8jU_0^3 + 6U_1U_2\bar{U}_3 - 6U_3\bar{U}_1\bar{U}_2 + 12jU_0U_1\bar{U}_1 \\ &+ 12jU_0U_2\bar{U}_2 + 12jU_0U_3\bar{U}_3 - 3U_4\bar{U}_2^2 + 3U_2^2\bar{U}_4 + 6U_1U_3\bar{U}_4 + 6U_1U_4\bar{U}_5 + 6U_2U_3\bar{U}_5 \\ &- 6U_4\bar{U}_1\bar{U}_3 - 6U_5\bar{U}_1\bar{U}_4 - 6U_5\bar{U}_2\bar{U}_3 + 12jU_0U_4\bar{U}_4 + 12jU_0U_5\bar{U}_5\Bigg) \\ &+ \frac{1}{8j}\Bigg(3U_1^2\bar{U}_1 + 6U_1U_2\bar{U}_2 + 6U_1U_3\bar{U}_3 + 3\bar{U}_3U_2^2 - 3U_3\bar{U}_1^2 \\ &+ 12U_0^2U_1 + 12jU_0U_2\bar{U}_1 + 12jU_0U_3\bar{U}_2 - 3U_5\bar{U}_2^2 + 3U_3^2\bar{U}_5 + 6U_1U_4\bar{U}_4 + 6U_2U_3\bar{U}_4 \\ &+ 6U_1U_5\bar{U}_5 + 6U_2U_4\bar{U}_5 - 6U_4\bar{U}_1\bar{U}_2 - 6U_5\bar{U}_1\bar{U}_3 + 12jU_0U_4\bar{U}_3 + 12jU_0U_5\bar{U}_4\Bigg)e^{j\omega t} + \cdots \end{aligned} \tag{A.9}$$

Averaging over each harmonic and equalizing the coefficients of $e^{jn\omega t}$, amplitudes of V_n are derived. For example, the static response V_0 of the nonlinear function $g(u,\dot{u})$ and the amplitude of its first

harmonic, V_1, are calculated as

$$\begin{aligned}
V_0 = \frac{1}{8j}\big(&3U_1^2\bar{U}_2 - 3U_2\bar{U}_1^2 + 8jU_0^3 + 6U_1U_2\bar{U}_3 - 6U_3\bar{U}_1\bar{U}_2 + 12jU_0U_1\bar{U}_1 \\
&+ 12jU_0U_2\bar{U}_2 + 12jU_0U_3\bar{U}_3 - 3U_4\bar{U}_2^2 + 3U_2^2\bar{U}_4 + 6U_1U_3\bar{U}_4 + 6U_1U_4\bar{U}_5 + 6U_2U_3\bar{U}_5 \\
&- 6U_4\bar{U}_1\bar{U}_3 - 6U_5\bar{U}_1\bar{U}_4 - 6U_5\bar{U}_2\bar{U}_3 + 12jU_0U_4\bar{U}_4 + 12jU_0U_5\bar{U}_5\big)
\end{aligned} \tag{A.10}$$

$$\begin{aligned}
V_1 = \frac{1}{4}\big(&3U_1^2\bar{U}_1 + 6U_1U_2\bar{U}_2 + 6U_1U_3\bar{U}_3 + 3\bar{U}_3U_2^2 - 3U_3\bar{U}_1^2 + 12U_0^2U_1 \\
&+ 12jU_0U_2\bar{U}_1 + 12jU_0U_3\bar{U}_2 - 3U_5\bar{U}_2^2 + 3U_3^2\bar{U}_5 + 6U_1U_4\bar{U}_4 + 6U_2U_3\bar{U}_4 + 6U_1U_5\bar{U}_5 \\
&+ 6U_2U_4\bar{U}_5 - 6U_4\bar{U}_1\bar{U}_2 - 6U_5\bar{U}_1\bar{U}_3 + 12jU_0U_4\bar{U}_3 + 12jU_0U_5\bar{U}_4\big)
\end{aligned}$$

Bibliography

[1] O.C. Zienkiewicz, R.L. Taylor, *The Finite Element Method, Volume 1: The Basis,*. Fifth edition, Butterworth-Heinemann (2000).

[2] O.C. Zienkiewicz, R.L. Taylor, *The Finite Element Method, Volume 2: Solid Mechanics,*. Fifth edition, Butterworth-Heinemann, (2000).

[3] J.N. Reddy, *Introduction to The Finite Element Method,*. McGraw Hill Professional, Edition 4, (2018).

[4] Kendall Atkinson, Weimin Han, David Stewart, *Numerical Solution of Ordinary Differential Equations*, John Wiley & Sons, (2009).

[5] T.K. Caughey and M.E.J. O'Kelly, Classical normal modes in damped linear dynamic systems, *Transaction of ASME, Journal of Applied Mechanics*, (1965) 32, pp. 583–588.

[6] M. I. Friswell, J. E. Mottershead, *A Finite Element Model Updating in Structural Dynamics*, Springer, Dordrecht, (1995).

[7] S. Adhikari, *Damping models for structural vibration*, Dissertation, University of Cambridge, (2001).

[8] E. Balm‘es New results on the identification of normal modes from experimental complex modes, *Mechanical Systems and Signal Processing*, 11(2) (1997), pp. 229-243.

[9] S. Adhikari, Optimal complex modes and an index of damping non-proportionality, *Mechanical Systems and Signal Processing*, 18 (1) (2004) 1-27.

[10] D.J. Ewins, *Modal Testing: Theory, Practice and Application.* Research Studies Press, Baldock, UK, (2000).

[11] W. Heylen, S. Lammens and P. Sas *Modal Analysis Theory and Testing.* Leuven: KUL Press, (1997).

[12] N.M.M. Maia and J. M.M. Silva *Theoretical and Experimental Modal Analysis.* Taunton: Research Studies Press LTD, (1997).

[13] M.A. Peres, C. Kallmeyer, M.C. Witter, R. Carneiro, F.D. Marques, L.P.R. de Oliveira, Advantages of Multiple-Input Multiple-Output (MIMO) testing using low level excitation systems, *PROCEEDINGS OF ISMA2014 INCLUDING USD2014, DYNAMIC TESTING: METHODS AND INSTRUMENTATION*, (1979) 88, 828-846.

[14] D.L. Brown, R.J. Allemang, R. Zimmerman and M. Mergeay, Parameter Estimation Techniques for Modal Analysis, *SAE Transactions*, (1979) 88, 828-846.

[15] S.R. Ibrahim and E.C. Mikulcik, A time domain modal vibration test technique, *The Shock and Vibration Bulletin*, (1973) 43, 21-37.

[16] S.R. Ibrahim and E.C. Mikulcik, The Experimental Determination of Vibration Parameters From Time Responses, *The Shock and Vibration Bulletin*, (1976) 46(5), 187-196.

[17] P. Van Overschee and B. De Moor *Subspace Identification for Linear Systems: Theory, Implementation, Applications.* Dordrecht: Kluwer Academic Publishers, (1996).

[18] J.N. Juang, R.S. Pappa, An Eigensystem Realization Algorithm for Modal Parameter Identification and Model Reduction *Journal of Guidance, Control, and Dynamics*, Vol. 8, No. 5, 1985, pp. 620-627.

[19] H. Vold, J. Kundrat, G.T. Rocklin, R. Russel, A Multi-Input Modal Estimation Algorithm For Mini-Computers, *SAE Technical Paper Series*, No. 820194, (1982).

[20] H. Vold, G.T. Rocklin, The Numerical Implementation of a Multi-Input Modal Estimation Method for Mini-Computers, *Proceedings of the 1st International Modal Analysis Conference (IMAC I)*, Orlando, Florida, U.S.A., (1982), pp. 542-548.

[21] M.H. Richardson, D.L. Formenti, Parameter Estimation From Frequency Response Measurements Using Rational Fraction Polynomials *Proceedings of the 1st International Modal Analysis Conference (IMAC I)*, Orlando, Florida, U.S.A., (1982), pp. 167-181.

[22] M.H. Richardson, D.L. Formenti, Global Curve-Fitting of Frequency Response Measurements Using the Rational Polynomial Method, *Proceedings of the 3rd International Modal Analysis Conference (IMAC III)*, Orlando, Florida, U.S.A., (1985), pp. 390-397.

[23] M. Link, A. Vollan, Identification of Structural System Parameters From Dynamic Response Data. *Z. Flugwiss. Weltraumforsch*, Vol.2, No. 3, (1978), pp. 165-174.

[24] D.C. Kammer, Test-analysis-model development using an exact modal reduction, *The International Journal of Analytical and Experimental Modal Analysis*, Vol. 2, No. 4, pp. 174-179, (1987).

[25] J.C. O'Callahan, P. Avitabile, R. Riemer, System equivalent reduction expansion process (SEREP), *Proceedings of the 7th International Modal Analysis Conference*, Las Vegas, pp. 29-37, (1989).

[26] J.R.R. Craig, M.C.C Bampton, Coupling of substructures for dynamic analyses, *AIAA journal*, 6.7 (1968): 1313-1319.

[27] A.F. Vakakis, O.V. Gendelman, G. Kerschen, L.A. Bergman, D.M. McFarland, Y.S. Lee, *Nonlinear Targeted Energy Transfer in Mechanical and Structural Systems, I and II*, Springer, Berlin and New York, (2008).

[28] A.H. Nayfeh, D.T. Mook, *Nonlinear Oscillations*, John Wiley & Sons, New York (1979).

[29] R.E. Mickens, *Truly nonlinear oscillations: harmonic balance, parameter expansions, iteration, and averaging methods*, World Scientific, (2010).

[30] H.H. Khodaparast, H. Madinei, M.I. Friswell, S. Adhikari, S. Coggon, J.E. Cooper, An extended harmonic balance method based on incremental nonlinear control parameters, *Mechanical Systems and Signal Processing*, 85 (2017) 716–729.

[31] L. Jezequel, C.H. Lamarque, Analysis of nonlinear dynamic systems by the normal form theory, *Journal of Sound and Vibration*, 149 (3) (1991) 429–459.

[32] J. Taghipour, M. Dardel, Steady state dynamics and robustness of a harmonically excited essentially nonlinear oscillator coupled with a two-DOF nonlinear energy sink, *Mechanical Systems and Signal Processing*, Vol. 62-63, (2015), pp. 164-182.

[33] J. Taghipour, M. Dardel, M.H. Pashaei, Vibration mitigation of a nonlinear rotor system with linear and nonlinear vibration absorbers, *Mechanism and Machine Theory*, (2018) 128, 586-615.

[34] K. Worden, G. Tomlinson, *Nonlinearity in Structural Dynamics: Detection, Identification and Modelling*, Philadelphia, IOP Publishing Ltd., Bristol (2001).

[35] D. Göge, M. Sinapius, U. Füllekrug, M. Link, Detection and description of non-linear phenomena in experimental modal analysis via linearity plots, *International Journal of Non-Linear Mechanics*, (2005) 40, 27–48.

[36] R.M. Lin, D.J. Ewins, Location of localized stiffness nonlinearity using measured modal data, *Mechanical Systems and Signal Processing*, (1995) 9(3), 329–339.

[37] P. Cresta, O. Allix, C. Rey, S. Guinard, Nonlinear localization strategies for domain decomposition methods: Application to post-buckling analyses, *Computer Methods in Applied Mechanics and Engineering*, (2007) 196, 1436–1446.

[38] V. Ondra, I.A. Sever, C.W. Schwingshackl, A method for detection and characterisation of structural nonlinearities using the Hilbert transform and neural networks, *Mechanical Systems and Signal Processing*, (2017) 83, 210–227.

[39] A. Koyuncu, E. Cigeroglu, H.N. Özgüven, Localization and identification of structural nonlinearities using cascaded optimization and neural networks, *Mechanical Systems and Signal Processing*, 95 (2017) 219–238.

[40] X. Wang, H.H. Khodaparast, A.D. Shaw, M.I. Friswell, G. Zheng, Localisation of local nonlinearities in structural dynamics using spatially incomplete measured data, *Mechanical Systems and Signal Processing*, Vol. 99, (2018), pp. 364-383.

[41] M.B. Özer, H.N. Özgüven, A new method for localization and identification of non-linearities in structures, *in: Proceedings of the 6th ASME Biennial Conference on Engineering Systems Design and Analysis (ESDA)*, Istanbul, Turkey, 2002.

[42] G. Kerschen, K. Worden, A.F. Vakakis, J. Golinval, Past, present and future of nonlinear system identification in structural dynamics, *Mechanical Systems and Signal Processing*, Vol. 20, No. 3, (2006), pp. 505-592.

[43] J.P. Noël, G. Kerschen, Nonlinear system identification in structural dynamics: 10 more years of progress, *Mechanical Systems and Signal Processing*, Vol. 83, (2017), pp. 2-35.

[44] C.M. Cheng, Z.K. Peng, W.M. Zhang, G. Meng, Volterra-series-based nonlinear system modeling and its engineering applications: A state-of-the-art review, *Mechanical Systems and Signal Processing*, Vol. 87, (2017), pp. 340-364.

[45] Z.C. Wang, W.X. Ren, G. Chen, Time–frequency analysis and applications in time-varying/nonlinear structural systems: A state-of-the-art review, *Advances in Structural Engineering*, (2018) Vol.21, No.10, pp.1562-1584.

[46] A. Carrella, D.J. Ewins, Identifying and quantifying structural nonlinearities in engineering applications from measured frequency response functions, *Mechanical Systems and Signal Processing*, 25 (2011) 1011–1027.

[47] A. Carrella, Nonlinear identifications using transmissibility: dynamic characterization of Anti Vibration Mounts (AVMs) with standard approach, *International Journal of Mechanical Sciences*, 63 (2012) 74–85.

[48] J.R. Wright, M.F. Platten, J.E. Cooper, M. Sarmast, Identification of multi-degree-of-freedom weakly non-linear systems using a model based in modal space, *in: Proceedings of the International Conference on Structural System Identification,*, Kassel, Germany, 2001.

[49] M. Link, M. Boeswald, S. Laborde, M. Weiland, A. Calvi, An approach to nonlinear experimental modal analysis, *in: Proceedings of the 28th International Modal Analysis Conference (IMAC)*, Jacksonville, FL, USA, 2010.

[50] Z. Yang, G. Dimitriadis, G.A. Vio, J.E. Cooper, J.R. Wright, Identification of structural free-play nonlinearities using the non-linear resonant decay method, *in: Proceedings of the International Seminar on Modal Analysis (ISMA)*, Leuven, Belgium, 2006.

[51] M.F. Platten, J.R. Wright, G. Dimitriadis, J.E. Cooper, Identification of multi-degree of freedom non-linear system using an extended modal space model, *Mechanical Systems and Signal Processing*, 23 (2009) 8–29.

[52] M.F. Platten, J.R. Wright, J.E. Cooper, G. Dimitriadis, Identification of a nonlinear wing structure using an extended modal model, *AIAA Journal of Aircraft*, 46 (5) (2009) 1614–1626.

[53] J.M. Londono, J.E. Cooper, Experimental identification of a system containing geometric nonlinearities, *in: Proceedings of the 32th International Modal Analysis Conference (IMAC)*, Orlando, FL, USA, 2014.

[54] U. Fuellekrug, D. Goege, Identification of weak nonlinearities within complex aerospace structures, *Aerospace Science and Technology*, 23 (2012) 53–62.

[55] R.M. Rosenberg, The normal modes of nonlinear n-degree-of-freedom systems, *Journal of Applied Mechanics*, 29 (1962) 7–14.

[56] A.F. Vakakis, L.I. Manevitch, Y.V. Mikhlin, V.N. Pilipchuk, A.A. Zevin, *Normal Modes and Localization in Nonlinear Systems*, John Wiley & Sons, New York, NY, 1996.

[57] M. Peeters, G. Kerschen, J.C. Golinval, Dynamic testing of nonlinear vibrating structures using nonlinear normal modes, *Journal of Sound and Vibration*, 330 (2011) 486–509.

[58] M. Peeters, G. Kerschen, J.C. Golinval, Modal testing of nonlinear vibrating structures based on nonlinear normal modes: experimental demonstration, *Mechanical System and Signal Processing*, 25 (2011) 1227–1247.

[59] J.L. Zapico-Valle, M. Garcia-Dieguez, R. Alonso-Camblor, Nonlinear modal identification of a steel frame, *Engineering Structures*, 56 (2013) 246–259.

[60] D.A. Ehrhardt, R.B. Harris, M.S. Allen, Numerical and experimental determination of nonlinear normal modes of a circular perforated plate, *in: Proceedings of the 32nd International Modal Analysis Conference (IMAC)*, Orlando, FL, USA, 2014.

[61] D.A. Ehrhardt, M.S. Allen, Measurement of nonlinear normal modes using multi-harmonic stepped force appropriation and free decay, *Mechanical System and Signal Processing*, 76–77 (2016) 612–633.

[62] J.M. Londono, S.A. Neild, J.E. Cooper, Identification of backbone curves of nonlinear systems from resonance decay responses, *Journal of Sound and Vibration*, 348 (2015) 224–238.

[63] L. Renson, A. Gonzalez-Buelga, D.A.W. Barton, S.A. Neild, Robust identification of backbone curves using control-based continuation, *Journal of Sound and Vibration*, 367 (2016) 145–158.

[64] E.F. Crawley, A.C. Aubert, Identification of nonlinear structural elements by force-state mapping, *AIAA Journal*, Vol. 24, No. 1, (1986), pp. 155-162.

[65] E.F. Crawley, K.J. O'Donnell, Force-state mapping identification of nonlinear joints, *AIAA Journal*, Vol. 25, No. 7, (1987), pp. 1003-1010.

[66] G. Kerschen, J.C. Golinval, K. Worden, Theoretical and experimental identifcation of a nonlinear beam, *Journal of Sound and Vibration*, Vol. 244, No. 4, (2001), pp. 597-613.

[67] G.E.P. Box, G.M. Jenkins, *Time Series Analysis, Forecasting and Control,*. Holden-Day, San Francisco, 1970 (Section 3.2).

[68] I.J. Leontaritis, S.A. Billings, Input-output parametric models for nonlinear systems, part I: deterministic nonlinear systems, *International Journal of Control*, 41 (1985) 303–328 (Sections 3.2, 6.3).

[69] I.J. Leontaritis, S.A. Billings, Input-output parametric models for nonlinear systems, part II: stochastic nonlinear systems, *International Journal of Control*, 41 (1985) 329–344 (Sections 3.2, 6.3).

[70] S.A. Billings, S. Chen, R.J. Backhouse, Identification of linear and nonlinear models of a turbocharged automotive diesel engine, *Mechanical Systems and Signal Processing*, 3 (1989) 123–142 (Sections 3.2, 6.3).

[71] M. Korenberg, S.A. Billings, Y.P. Liu, P.J. McIlroy, An orthogonal parameter estimation algorithm for nonlinear stochastic systems, *International Journal of Control*, 48 (1988) 193–210 (Sections 3.2, 6.3).

[72] S.A. Billings, H.B. Jamaluddin, S. Chen, Properties of neural networks with applications to modelling non-linear dynamical systems, *International Journal of Control*, 55 (1991) 193–224 (Sections 3.2, 3.6, 6.3).

[73] M. Feldman, Nonparametric identification of asymmetric nonlinear vibration systems with the Hilbert transform, *Journal of Sound and Vibration*, Vol. 331, No. 14, (2012), pp. 3386-3396.

[74] M. Feldman, Hilbert transform methods for nonparametric identification of nonlinear time varying vibration systems, *Mechanical Systems and Signal Processing*, Vol. 47, No. 1, (2014), pp. 66-77.

[75] K. Worden, J.J. Hensman, Parameter estimation and model selection for a class of hysteretic systems using Bayesian inference, *Mechanical Systems and Signal Processing*, Vol. 32, (2012), pp. 153-169.

[76] P.L. Green, Bayesian system identification of a nonlinear dynamical system using a novel variant of Simulated Annealing, *Mechanical Systems and Signal Processing*, Vol. 52-53, (2015), pp. 133-146.

[77] P.L. Green, E.J. Cross, K. Worden, Bayesian system identification of dynamical systems using highly informative training data, *Mechanical Systems and Signal Processing*, 56-57 (2015) 109–122.

[78] M. Feldman, S. Braun, Nonlinear vibrating system identification via Hilbert decomposition, *Mechanical Systems and Signal Processing*, 84 (2017) 65–96.

[79] V. Lenaerts, G. Kerschen, J.C. Golinval, Identification of a continuous structure with a geometrical non-linearity. Part II: Proper orthogonal decomposition, *Journal of Sound and Vibration*, 262 (2003) 907–919.

[80] G. Kerschen, V. Lenaerts, J.C. Golinval, Identification of a continuous structure with a geometrical non-linearity. Part I: Conditioned reverse path method, *Journal of Sound and Vibration*, 262 (2003) 889–906.

[81] S.F. Masri, T.K. Caughey, A Nonparametric Identification Technique for Nonlinear Dynamic Problems, *Journal of Applied Mechanics*, June 1979, Vol. 46, 433-447.

[82] M.A. AL-Hadid, J.R. Wright, Developments in The Force-State Mapping Technique for Non-Linear Systems and The Extension to The Location of Non-Linear Elements in a Lumped-Parameter System, *Mechanical Systems and Signal Processing*, (1989) 3(3), 269-290.

[83] K. Yasuda, S. Kawamura, K. Watanabe, Identification of Nonlinear Multi-Degree-of-Freedom Systems : Identification Under Noisy Measurements, *JSME international journal, Ser. 3, Vibration, control engineering, engineering for industry*, Vol. 31, No. 3, (1988), pp. 502-509.

[84] M. Feldman, Nonlinear System Vibration Analysis Using Hilbert Transform-II. Forced Vibration Analysis Method "FORCEVIB", *Mechanical Systems and Signal Processing*, (1994) 8(3), pp. 309-318.

[85] S. Marchesiello, A. Fasana, L. Garibaldi, Modal contributions and effects of spurious poles in nonlinear subspace identification, *Mechanical Systems and Signal Processing*, 74 (2016) 111–132.

[86] S. Marchesiello, L. Garibaldi, A time domain approach for identifying nonlinear vibrating structures by subspace methods, *Mechanical Systems and Signal Processing*, 22 (2008) 81–101.

[87] S. Marchesiello, L. Garibaldi, Identification of clearance type nonlinearities, *Mechanical Systems and Signal Processing*, 22 (2008) 1133–1145.

[88] M.D. Narayanan, S. Narayanan, C. Padmanabhan, Parametric identification of nonlinear systems usingmultiple trials, *Nonlinear Dynamics*, 48 (2007) 341–360.

[89] C.M. Richards, R. Singh, Identification of multi-degree-of-freedom nonlinear systems under random excitations by the "Reverse Path" spectral method, *Journal of Sound and Vibration*, (1998) 213(4), 673-708.

[90] S. Marchesiello, Application of the conditioned reverse path method, *Mechanical Systems and Signal Processing*, (2003) 17(1), 183–188.

[91] G. Kerschen, J.C. Golinval, Generation of Accurate Finite Element Models of Nonlinear Systems – Application to an Aeroplane-Like Structure, *Nonlinear Dynamics*, (2005) 39: 129–142.

[92] M. Magnevall, A. Josefsson, K. Ahlin, G. Broman, Nonlinear structural identification by the "Reverse Path" spectral method, *Journal of Sound and Vibration*, 331 (2012) 938–946.

[93] P. Muhamad, N.D. Sims, K. Worden, On the orthogonalised reverse path method for nonlinear system identification, *Journal of Sound and Vibration*, 331 (2012) 4488–4503.

[94] J.P. Noël, G. Kerschen, A new subspace-based approach to identify nonlinear mechanical structures in the frequency domain, *16th IFAC Symposium on System Identification, The International Federation of Automatic Control*, Brussels, Belgium, July 11-13, 2012.

[95] J.P. Noël, G. Kerschen, Frequency-domain subspace identification for nonlinear mechanical systems, *Mechanical Systems and Signal Processing*, 40 (2013) 701–717.

[96] T.L. Hill, A. Cammarano, S.A. Neild, D.J. Wagg, Interpreting the forced response of a two-degree-of-freedom nonlinear oscillator using backbone curves, *Journal of Sound and Vibration*, 349 (2015) 276–288.

[97] J.M. Londoño, J.E. Cooper, S.A. Neild, Identification of systems containing nonlinear stiffnesses using backbone curves, *Mechanical Systems and Signal Processing*, 84 (2017) 116–135.

[98] Ö. Arslan, M. Aykan, H.N. Özgüven, Parametric identification of structural nonlinearities from measured frequency response data, *Mechanical Systems and Signal Processing*, 25 (2011) 1112–1125.

[99] X. Wang, T.L. Hill, S.A. Neild, A.D. Shaw, H. Haddad Khodaparast, M.I. Friswell, Model updating strategy for structures with localised nonlinearities using frequency response measurements, *Mechanical Systems and Signal Processing*, Vol. 100, (2018), pp. 940-961.

[100] Z.J. Yang, S. Sanada, Frequency Domain Subspace Identification with the Aid of the w-Operator, *Electrical Engineering in Japan*, Vol. 132, No. 1, 2000, Translated from Denki Gakkai Ronbunshi, Vol. 119-C, No. 3, March 1999, pp. 326–334.

[101] D.E. Adams, R.J. Allemang, A frequency domain method for estimating the parameters of a nonlinear structural dynamic model through feedback, *Mechanical Systems and Signal Processing*, 14 (2000) 637–656.

[102] M. Schetzen, *The Volterra and Wiener Theories of Nonlinear Systems,*. John Wiley & Sons, NewYork, NY, USA, 1980.

[103] J.A. Vazquez Feijoo, K. Worden, R. Stanway, Analysis of time-invariant systems in the time and frequency domain by associated linear equations (ALEs), *Mechanical Systems and Signal Processing*, 20 (2006) 896–919.

[104] S. da Silva, S. Cogan, E. Foltête, Nonlinear identification in structural dynamics based on Wiener series and Kautz filters, *Mechanical Systems and Signal Processing*, 24 (2010) 52–58.

[105] A. Chatterjee, Structural damage assessment in a cantilever beam with a breathing crack using higher order frequency response functions, *Journal of Sound and Vibration*, 329 (2010) 3325–3334.

[106] Z.K. Peng, Z.Q. Lang, S.A. Billings, Linear parameter estimation for multi-degree-of-freedom nonlinear systems using nonlinear output frequency response functions, *Mechanical Systems and Signal Processing*, 21 (2007) 3108–3122.

[107] Z.K. Peng, Z.Q. Lang, S.A. Billings, Nonlinear parameter estimation for multi-degree-of-freedom nonlinear systems using nonlinear output frequency response functions, *Mechanical Systems and Signal Processing*, 22 (2008) 1582–1594.

[108] Z.K. Peng, Z.Q. Lang, S.A. Billings, Non-linear output frequency response functions of mdof systems with multiple non-linear components, *International Journal of Nonlinear Mechanics*, 42 (2007) 941–958.42 (2007) 941–958.

[109] R.S. Bayma, Y. Zhu, Z.Q. Lang, The analysis of nonlinear systems in the frequency domain using Nonlinear Output Frequency Response Functions, *Automatica*, 94 (2018) 452–457.

[110] Z.Q. Lang, S.A. Billings, Energy transfer properties of non-linear systems in the frequency domain, *International Journal of Control*, 78 (2005) 345–362.

[111] M. Haroon, D.E. Adams, Y.W. Luk, A.A. Ferri, A time and frequency domain approach for identifying nonlinear mechanical system models in the absence of an input measurement, *Journal of Sound and Vibration*, Vol 283, No. 3, (2005), pp. 1137-1155.

[112] J. Prawin, A.R.M. Rao, Nonlinear identification of MDOF systems using Volterra series approximation, *Mechanical Systems and Signal Processing*, Vol. 84, (2017), pp. 58-77.

[113] J.P. Noël, S. Marchesiello, G. Kerschen, Subspace-based identification of a nonlinear spacecraft in the time and frequency domains, *Mechanical Systems and Signal Processing*, 43 (2014) 217–236.

[114] S. Marchesiello, L. Garibaldi, A time domain approach for identifying nonlinear vibrating structures by subspace methods, *Mechanical Systems and Signal Processing*, 22 (2008) 81–101.

[115] S.L. Lacy, D.S. Bernstein, Subspace identification for non-linear systems with measured-input nonlinearities, *International Journal of Control*, 78 (12) (2005) 906–926.

[116] G. Kerschen, V. Lenaerts, S. Marchesiello, A. Fasana, A Frequency Domain Versus a Time Domain Identification Technique for Nonlinear Parameters Applied to Wire Rope Isolators, *Journal of Dynamic Systems, Measurement, and Control*, December 2001, Vol. 123, 645-650.

[117] M.D. Narayanan, S. Narayanan, C. Padmanabhan, Multi harmonic excitation for nonlinear system identification, *Journal of Sound and Vibration*, 311 (2008) 707–728.

[118] M. Feldman, Time-varying vibration decomposition and analysis based on the Hilbert transform, *Journal of Sound and Vibration*, 295 (2006) 518–530.

[119] M. Feldman, Considering high harmonics for identification of non-linear system by Hilbert transform, *Mechanical Systems and Signal Processing*, 21 (2007) 943–958.

[120] N.E. Huang, Z. Shen, S.R. Long, M.C. Wu, H.H. Shih, Q. Zheng, N.C. Yen, C.C. Tung, H.H. Liu, The empirical mode decomposition and the Hilbert spectrum for nonlinear and non-stationary time series analysis, *Proceedings of the Royal Society of London A*, 454 (1998) 903–995.

[121] R. Pintelon, J.Schoukens, *System Identification: A Frequency Domain Approach*, IEEE Press, Piscataway, NJ, USA, 2001.

[122] L. Ljung, *System Identification – Theory for the User,*. Prentice Hall, Upper Saddle River, NY, USA, 1999.

[123] M.B. Özer, H.N. Özgüven, T.J. Royston, Identification of structural non-linearities using describing functions and the Sherman–Morrison method, *Mechanical Systems and Signal Processing*, 23 (2009) 30–44.

[124] M. Aykan, H.N. Özgüven, Parametric identification of nonlinearity in structural systems using describing function inversion, *Mechanical Systems and Signal Processing*, 40 (2013) 356–376.

[125] X. Wang, G.T. Zheng, Equivalent Dynamic Stiffness Mapping technique for identifying nonlinear structural elements from frequency response functions, *Mechanical Systems and Signal Processing*, 68–69 (2016) 394–415.

[126] J. Schoukens, M. Vaes, R. Pintelon, Linear system identification in a nonlinear setting: nonparametric analysis of the nonlinear distortions and their impact on the best linear approximation, *IEEE Control Systems*, 36(3) (2016) 38–69.

[127] E. Zhang, J. Antoni, R. Pintelon, J. Schoukens, Fast detection of system nonlinearity using nonstationary signals, *Mechanical Systems and Signal Processing*, 24 (2010) 2065–2075.

[128] W.D. Widanage, J. Stoev, A. Van Mulders, J. Schoukens, G. Pinte, Nonlinear system identification of the filling phase of a wet-clutch system, *Control Engineering Practice*, 19 (2011) 1506–1516.

[129] M. Vaes, J. Schoukens, B. Peeters, J. Debille, T. Dossogne, J.P. Noël, G. Kerschen, Nonlinear ground vibration identification of an F-16 aircraft. Part I: fast nonparametric analysis of distortions in FRF measurements, *in: Proceedings of the 16th International Forum on Aeroelasticity and Structural Dynamics (IFASD)*, Saint Petersburg, Russia, 2015.

[130] P. Grange, D. Clair, L. Baillet, M. Fogli, Brake squeal analysis by coupling spectral linearization and modal identification methods, *Mechanical Systems and Signal Processing*, 23 (2009) 2575–2589.

[131] M.W. Sracic, M.S. Allen, Method for identifying models of nonlinear systems using linear time periodic approximations, *Mechanical Systems and Signal Processing*, 25 (2011) 2705–2721.

[132] M.W. Sracic, M.S. Allen, Identifying parameters of multi-degree-of-freedom nonlinear structural dynamic systems using linear time periodic approximations, *Mechanical Systems and Signal Processing*, 46 (2014) 325–343.

[133] B. Moaveni, E. Asgarieh, Deterministic-stochastic subspace identification method for identification of nonlinear structures as time-varying linear systems, *Mechanical Systems and Signal Processing*, 31 (2012) 40–55.

[134] T.S. Jang, Non-parametric simultaneous identification of both the nonlinear damping and restoring characteristics of nonlinear systems whose dampings depend on velocity alone, *Mechanical Systems and Signal Processing*, 25 (2011) 1159–1173.

[135] T. Karaağaçlı, H.N. Özgüven, A frequency domain nonparametric identification method for nonlinear structures: Describing surface method, *Mechanical Systems and Signal Processing*, 144 (2020) 106872.

[136] S.A. Billings, *Nonlinear System Identification: NARMAX Methods in the Time, Frequency and Spatio-Temporal Domains*, Wiley, 2013.

[137] S.A. Billings, *Engineering Vibrations*, Fourth Edition, Pearson, 2013.

[138] M. Platten, J. Wright, K. Worden, G. Dimitriadis, J. Cooper, Non-linear identification in modal space using a genetic algorithm approach for model selection, *International Journal of Applied Mathematics and Mechanics*, 3 (1) (2007) 72–89.

[139] P. Gluzmann, D. Panigo, Global search regression: a new automatic model-selection technique for cross-section, time-series, and panel-data regressions, *Stata Journal*, 15 (2) (2015) 325–349.

[140] F. Mezghani, A.F. del Rincón, M.A. Ben Souf, P. G. Fernandez, F. Chaari, F.V. Rueda, M. Haddar, Alternating Frequency Time Domains identification technique: Parameters determination for nonlinear system from measured transmissibility data, *European Journal of Mechanics / A Solids*, 80 (2020) 103886.

[141] R. Fuentes, R. Nayek, P. Gardner, N. Dervilis, T. Rogers, K. Worden, E.J. Cross, Equation discovery for nonlinear dynamical systems: A Bayesian viewpoint, *Mechanical Systems and Signal Processing*, 154 (2021) 107528.

[142] S.L. Brunton, J.L. Proctor, J.N. Kutz, Discovering governing equations from data by sparse identification of nonlinear dynamical systems, *Proceedings of the National Academy of Sciences USA*, 113 (2016) 3932–3937.

[143] A.B. Abdessalem, N. Dervilis, D. Wagg, K. Worden, Model selection and parameter estimation in structural dynamics using approximate bayesian computation, *Mechanical Systems and Signal Processing*, 99 (2018) 306–325.

[144] D. Lisitano, E. Bonisoli, Direct identification of nonlinear damping: application to a magnetic damped system, *Mechanical Systems and Signal Processing*, 146 (2021) 107038.

[145] S. Safari, J.M. Londoño Monsalve, Direct optimisation based model selection and parameter estimation using time-domain data for identifying localised nonlinearities, *Journal of Sound and Vibration*, 501 (2021) 116056.

[146] J. Paduart, L. Lauwers, J. Swevers, K. Smolders, J. Schoukens, R. Pintelon, Identification of nonlinear systems using polynomial nonlinear state space models, *Automatica*, 46 (4) (2010) 647–657.

[147] A.D. Carri, B. Weekes, D. DiMaio, D.J. Ewins, Extending modal testing technology for model validation of engineering structures with sparse nonlinearities: a first case study, *Mechanical Systems and Signal Processing*, 84 (B) (2017) 97–115.

[148] K.J. Moore, M. Kurt, M. Eriten, D.M. McFarland, L.A. Bergman, A.F. Vakakis, Time-series-based nonlinear system identification of strongly nonlinear attachments, *Journal of Sound and Vibration*, 438 (2019) 13-32.

[149] S. Le Guisquet, M. Amabili, Identification by means of a genetic algorithm of nonlinear damping and stiffness of continuous structures subjected to large-amplitude vibrations. Part I: single-degree-of-freedom responses, *Mechanical Systems and Signal Processing*, 153 (2021) 107470.

[150] J.E. Mottershead, M. Link, M.I. Friswell, The sensitivity method in finite element model updating: a tutorial, *Mechanical Systems and Signal Processing*, 25 (7) (2011) 2275–2296.

[151] https://www.first4magnets.com/tech-centre-i61/information-and-articles-i70/how-is-the-strength-of-a-magnet-measured-i81 .

[152] A.C. Gondhalekar, *Strategies for Non-Linear System Identification,*. Imperial College, London, 2009.

[153] M. Belhaq, A. Bichri, J. Der Hogapian, J. Mahfoud, Effect of electromagnetic actuations on the dynamics of a harmonically excited cantilever beam, *International Journal of Non-Linear Mechanics*, 46 (2011) 828–833.

[154] H. Madinei, H. Haddad Khodaparast, S. Adhikari, M.I. Friswell, Design of MEMS piezoelectric harvesters with electrostatically adjustable resonance frequency, *Mechanical Systems and Signal Processing*, 81 (2016) 360–374.

[155] S.S. Rao, *Mechanical Vibrations,*. 5th edition, Pearson, 2011.

[156] M. Claeys, J.J. Sinou, J.P. Lambelin, B. Alcoverro, Multi-harmonic measurements and numerical simulations of nonlinear vibrations of a beam with non-ideal boundary conditions, *Communications in Nonlinear Science and Numerical Simulation, Elsevier*, (2014), 19 (12), pp.4196-4212.

[157] G.B. Zhang, C.P. Zang, M.I. Friswell, Measurement of Multivalued Response Curves of a Strongly Nonlinear System by Exploiting Exciter Dynamics, *MMechanical Systems and Signal Processing,*, 140, June 2020, paper 106474.

[158] T.C. Yuan, J. Yang, L.Q. Chen, Nonlinear vibration analysis of a circular composite plate harvester via harmonic balance, *Acta Mechanica Sinica*, (2019) 35(4):912-925.

[159] T.M. Cameron, J.H. Griffin, An alternating frequency/time domain method for calculating the steady- state response of nonlinear dynamic systems, *Journal of Applied Mechanics*, (1989) 56 149-154.

[160] A. Cardona, A. Lerusse, M. Gearadin, Fast Fourier nonlinear vibration analysis, *Computational Mechanics*, 22 (2) (1998) 128–142.

[161] A.D. Shaw, T.L. Hill, S.A. Neild, M.I. Friswell, Periodic responses of a structure with 3:1 internal resonance, *Mechanical System and Signal Processing*, 81 (2016), 19–34.